Controlling the Functionality of Block Copolymer Bicontinuous Nanospheres.

Olivia Rose Monaghan

A thesis submitted to the University of Kent in partial

fulfilment of the requirements for the degree of

Doctor of Philosophy

University of Kent
Canterbury
Kent
CT2 7NZ

17th December 2015

I dedicate this thesis to the loving memory of my grandad

James William Steele Pithie

9th January 1932 – 18th December 2013

"Happiness can be found even in the darkest of times, if one only remembers to turn on the light"

J.K. Rowling

Acknowledgements

I would like to thank my supervisor Dr Simon Holder firstly for giving me the opportunity to do this PhD, also for the guidance and support throughout my PhD and undergraduate studies, but in particular his support in the final year of my PhD and I really appreciate the time he gave. I would also like to thank our collaborators at Eindhoven University of Technology, Professor Nico Sommerdijk and Paul Bomans for the opportunity to visit and work with their cryo-TEM. The training, knowledge and help to obtain the cryo-TEM images within this thesis was invaluable.

I would like to thank Ian Brown for his help and guidance using the TEM and also the technical staff in SPS for their help throughout the past three years.

Thanks goes to my fellow PhD students in Lab 310 and our ever changing office number. Chrissie, Katy, Nanami, Kate and Marc for being Mum and Dad when I first started, in particular the help Kate has given me over the years, Alex and Yarry for tormenting me with elastic bands etc., Christina who started this journey with me and we encouraged each other throughout, Aaron (for the keys), Francesco for the serious and not so serious conversations, Ollie for helping make demonstrating bearable and Trev whose help particularly over the past year has really helped me push forward with this thesis and for reading my thesis.

Thank you to Laurie for making the past 6 months as fun as possible and for all the support and advice during my writing up, which was invaluable.

Thanks goes to Tom I genuinely wouldn't have been able to complete this without your support and understanding.

I would like to thank my family (mum, Callum and Grandma) for their endless encouragement and in helping me achieve my goals, particularly my mum for her constant support. My final thanks goes to my Grandad who was one of the the most intelligent people I know, thank you for always taking the time and interest in everything I did.

Declaration

I declare that this thesis is my own work and effort, and has been written in my own words. Due care has been taken to properly reference the work of others wherever necessary.

Olivia Monaghan
17th December 2015

Abstract

Amphiphilic block copolymers (BCPs) form self-assembled aggregates in solution with a range of morphologies including spherical micelles, cylindrical micelles, vesicles (polymersomes) and bicontinuous nanospheres. This research focuses on the formation of bicontinuous nanospheres using a number of different BCPs for use in thermo-responsive drug delivery.

It has been shown previously that PEO-*b*-PODMA (poly(ethylene oxide)-*block*-poly(octadecyl methacrylate)) forms semi-crystalline bicontinuous nanospheres with a phase transition temperature (T_m) of 21.8°C. This corresponds to the melting transition of the semi-crystalline PODMA block. To increase the T_m, while maintaining all other properties, the hydrophobic monomer ODMA, was replaced with docosyl methacrylate (DSMA), which has a higher melting point. Upon self-assembly the PEO-*b*-PDSMA (25 wt % PEO) formed bicontinuous nanospheres. Analysis using differential scanning calorimetry (DSC) revealed the T_m of PEO-*b*-PDSMA in bulk and aggregate solution to be 41.3°C and 41.1°C respectively.

To further demonstrate the control achieved over the T_m, random copolymers of ODMA and DSMA using a PEO macroinitiator were synthesised at varying wt % ratios of PODMA:PDSMA. DSC analysis of these polymers showed that an increase in PDSMA led to an increase in the T_m for the bulk and self-assembled samples. The controlled release of Ibuprofen from these bicontinuous nanospheres was investigated to determine the rate of release and the optimum temperature for release following a previously used method. The concentration of release was then analysed using HPLC.

To incorporate acid functionality into the bicontinuous nanospheres PMAA-*b*-PODMA (poly(methacrylic acid)-*block*-poly(octadecyl methacrylate)) was synthesised (via ATRP) with hydrophilic wt % of 20 %. The self-assembled solution of PMAA-*b*-PODMA was analysed using cryo-TEM which revealed the presence of bicontinuous nanospheres. Another approach to incorporate acid functionality into bicontinuous nanospheres was the self-assembled of PEO-*b*-PS and PEO-*b*-PODMA followed by the alkaline hydrolysis of PEO to leave an acid end group.

Abbreviations

AFM	Atomic Force Microscopy
AGET-ATRP	Activator Generated by Electron Transfer-Atom Transfer Radical Polymerisation
ATRP	Atom Transfer Radical Polymerisation
BCP	Block Copoylmer
BDE	Bond Dissociation Energy
BN	Bicontinuous Nanopsheres
BPN	Bicontinous Polymeric Nanospheres
CMC	Critical Micelle Concentration
C-NMR	Carbon- Nuclear Magnetic Resonance
CRP	Controlled Radical polymersiation
Cu(I)Br	Copper (I) Bromide
Cu(I)Cl	Copper (I) Chloride
Cu(II)Br	Copper (II) Bromide
Cu(II)Cl	Copper (II) Chloride
DLS	Dynamic Light Scattering
DMF	Dimethylformamide
DMSO	Dimethyl Sulfoxide
DP	Degree of Polymerisation
DSC	Differential Scanning Calorimetry

DSMA	Docosyl Methacrylate
FT-IR	Fourier Tranfsorm-Infrared Spectroscopy
GO_x	Glucose oxide
GPC	Gel Permeation Chromatography
HCl	Hydrochloric acid
H-NMR	Proton Nucelar Magnetic Resonance
HPLC	High Perfomance Liquid Chromatography
LCST	Lower Critical Solution Temperature
MBrP	methyl 2- bromopropionate
MCM	Multi Compartmental Micelles
MCV	Multi Compartmental Vesicles
MIP	methyl 2- iodopropionate
M_n	Number average molecular weight
M_w	Weight average molecular weight
NMP	nitroxide-mediated LRP
P2VP	poly(2-vinylpyridine)
P3HT	poly(3-hexylthiophene)-
P4VP-Mel	Poly(4- vinylpyridinium methyl iodide)
PAA	Poly(acrylic acid)
PBD	polybutadiene
PBMA	Poly(butyl methacrylate)
PDEAM	poly(N,N-diethylacrylamide)

Đ	dispersity index
PDSMA	Poly(docosyl methacrylate)
PEE	poly ethyl ethylene
PEG	Poly(ethylene glycol)
PEO	Poly(ethylene oxide)
PFS	poly(ferrocenylsilane)-
PGA	poly(L-glutamic acid)
PIB	propargyl 2-bromoisobutryrate,
PMA	Poly (methyl acrylate)
PMAA	Poly (methacrylic acid)
PMMA	Poly(methyl methacrylate)
PMVE	poly(*N*,*N*- methylvinylether)
PNIPAAm	Poly(N-isopropylacrylamide)
PNVCl	poly(*N*-vinylcaprolactam)
PODMA	Poly(octadecyl methacrylate)
POEGMA	Poly[oligo(ethylene glycol) methyl ether methacrylate]
PPO	Poly(p-phenylene oxide)
PS	Poly(styrene)
PTMC	poly(trimethylene carbonate)-
PDMS	Poly(dimethyl siloxane)
RAFT	Radical Additon-Fragmentation Chain Transfer
RMM	Relative Molar Mass

SCM	Spherical Compound Micelles
SET-LRP	Single Electron Transfer-Living Radical Poylmerisation
TEM	Transmission Electron Microscopy
TFA	Trifluoroacetic acid
THF	Tetrahydrofuran
T_m	Melting transition

Table of Contents

List of Figures

List of Tables

List of Equations

Chapter 1. Introduction

1.1 Polymers

A polymer is a macromolecular compound made up of a large number of covalently bonded small molecular units.[1] These units are known as monomers, monomers are required to have two or more bonding sites (monomer functionality) in order to polymerise.[2] Monomers with two bonding sites are known to be bifunctional, monomers with more than two bonding sites are known as polyfunctional. This increased functionality of the monomer allows more complex polymer chains to be synthesised. The key factors that need to be established when analysing a polymer chain are the degree of polymerisation (DP), the molecular weight and the dispersity (Đ). The DP is depicted with the symbol *n*, this is representative of the number of repeating units (monomers) in the polymer chain.[3] The molecular weight of the polymer is relative to the DP. Polythene (or polyethylene) is a very well-known example of a polymer[1] (Figure 1.1) in this example *n* is the number of CH_2CH_2 (ethane) units in the polymer chain.

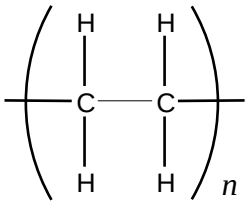

Figure 1.1: Poly(ethylene) repeating unit

The molecular weight (M_n) is calculated by multiplying the molecular weight of one ethane unit by the value of *n*, therefore increasing the DP will increase the molecular weight of the polymer. The molecular weight of the polymer is measured using two different parameters the M_n and the M_w. M_n is the number average molecular weight, where the average number of chains (*n*) is established and multiplied by the RMM of the repeating unit (monomer).[1] The M_w is the weight average molecular weight, it takes into account the molecular weight of all the chains not just the average number of repeating units.[1] A low distribution of molecular weight amongst the chains is desirable to ensure the properties are consistent for further synthesis or applications. To determine the molecular weight distribution, the ratio of M_w/M_n is used, this is known as the dispersity index (Đ).[3] An acceptable Đ depends on the

synthesis method, in the case of the method used in this research, below 1.3 is deemed acceptable.

The polymers properties are highly dependable on the structure of the polymer chain along with other factors which are mentioned later. The most common polymer chains produced are linear chains due to the bonds in the chain being covalent (strong) and directional. However branched[4], cross-linked, combed[5] and star chains[6, 7] can also be produced a few examples are shown in figure 1.2. Although these polymers may have been polymerised using the same monomer, the structure of the chain may alter the polymer properties.

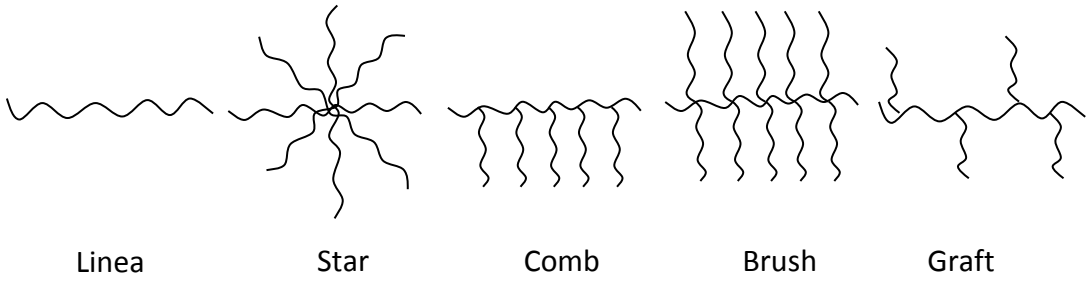

Figure 1.2: Examples of different polymer topologies that can be produced.

The structure of the polymer chain is not the only factor that has an effect on the polymers properties. Polymer properties can be altered using a number of different methods including cold-drawing, the addition of a plasticizer or copolymerisations. Copolymerisation has been used extensively in research to alter the polymer properties. It has its advantage over other methods due to the fact a number of properties can be altered in a controlled way.

1.1.1 Copolymer

A copolymer is made up of more than one monomer unit. They can be synthesised to produce a number of different topologies including random, graft, alternating and block copolymers which can be seen in Figure 1.3.[2]

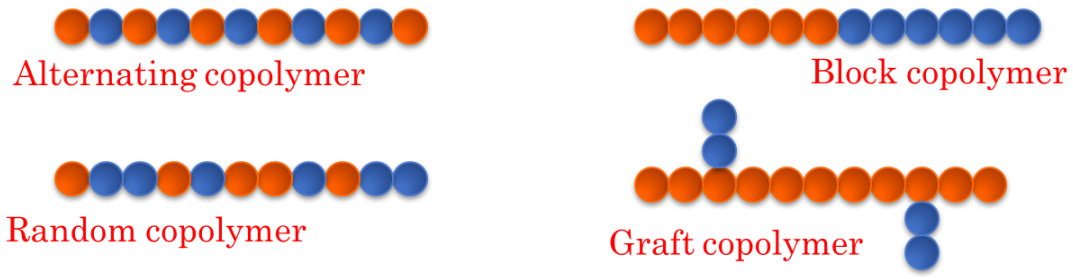

Figure 1.3: The different topologies of block copolymers.

Homopolymers are at a disadvantage as it is hard to change or improve their properties. Copolymers have the advantage as they are produced to give improved properties such as flexibility, heat resistance, processability and higher melting points.[1] Also generally the copolymers produced will have a combination of the best properties of each monomer.

Random copolymers are best at displaying a combination of properties from each monomer added, where the addition at alternating ratios can vary the properties.. This is the same for alternating copolymers, however these are almost impossible to produce using the favoured free radical route and are therefore not commonly used. Block copolymers and Graft copolymers will produce new properties not necessarily seen in their contributing monomers.[2] They also allow regions within the polymer to demonstrate different properties, such as a hydrophobic and hydrophilic region. This becomes extremely valuable when applied to self-assembly of polymer chains.

1.1.2 Block Copolymers

Block copolymers are made up of two or more sequences of monomer units. Diblock copolymers are made using two different monomer units. The first block (A) is polymerised and the second block (B) is polymerised using the active end of block A. The blocks are bonded together via a covalent bond or a junction block, which is a non-repeating subunit, i.e. not a polymer.[1] The structure of a block copolymer can be seen in figure 1.3 above. There are a number of different sequences of block copolymers, diblock copolymers are made up of two different monomer blocks. Triblock copolymers are made up of three monomer blocks with the possibility of two different sequences, this can be seen in figure 1.4. Block copolymers can be synthesised using controlled living radical polymerisation as the reaction can be controlled, this will be further discussed in the next section.

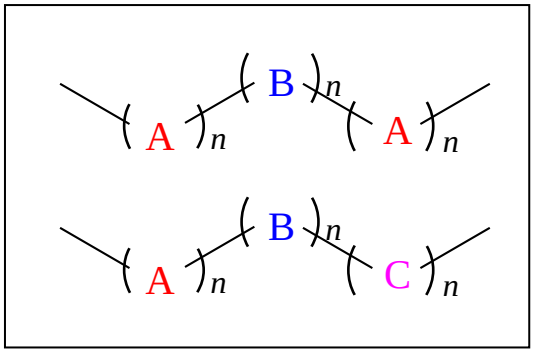

Figure 1.4: Example of triblock copolymers ABA and ABC

Block copolymers are very useful due to the ability to combine a number of key properties from individual polymers into one macromolecule. Generally the different blocks are incompatible due to their different properties, this allows them to self-assemble resulting in a well-defined structure. Block Copolymers can be prepared by a number of different controlled polymerisation techniques, including atom transfer radical polymerisation (ATRP), reverse addition fragmentation transfer polymerisation (RAFT) and catalytic chain transfer polymerisation (CCTP). The BCPs in this thesis were synthesised using ATRP as the method was well defined in the literature for the monomers used.

1.1.3 Random Copolymers

Random copolymers are usually prepared by free-radical polymerisation, however to achieve a more controlled polymerisation with low dispersity ATRP can be used with great success. They are formed due to irregular propagation of the polymer chain, where the two different monomer units join the chain randomly.[2] Usually in block copolymers the component monomer units supply different properties to the copolymer, random copolymers are particularly useful at combining the properties of the component monomer units. This can be done by varying the ratio of the component monomers to obtain the optimum desired properties.[1] However a problem can arise with this method of copolymerisation. The activity of the two or more monomer units during polymerisation can have an effect on the composition of the copolymer, with the chains growing unevenly and the ratio of monomer units differing each time the reaction is attempted, meaning there is less control over the reaction. To overcome this, controlled radical polymerisation techniques can be used, the chains grow at the same rate making the resultant copolymers composition to be consistent, however the monomer sequence along the chain can vary.[2]

1.2 Controlled Living Radical Polymerisation

Controlled living Radical Polymerisation (CRP) is a form of addition polymerisation where polymer chain terminations are supressed leaving an active end group.[8] This means there is little to no chain termination/chain transfer reactions.[9] CRP can be used on a large range of monomers[10], producing a number of topologies of copolymers (Figure 1.3) with a predetermined molecular weight and low dispersities[11-13] and functionalised end groups[14-17] (Figure 1.5).

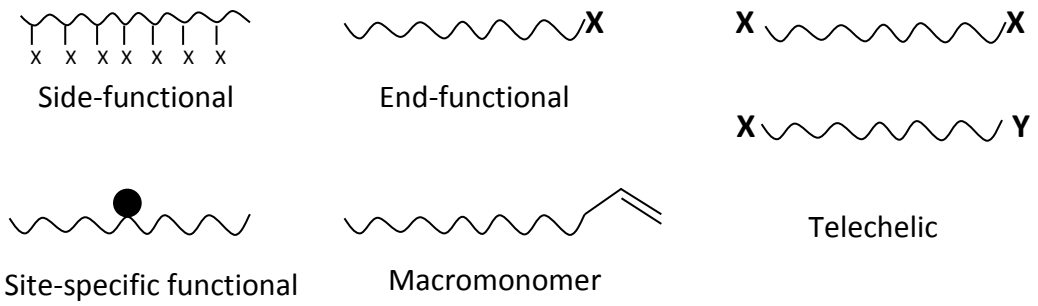

Figure 1.5: Polymers exhibiting different functionalities

Controlled living radical polymerisation has first-order kinetic behaviour[18], this means the polymerisation rate (Rp) is a linear function of time, taking into account the monomer concentration ([M]).[19] This is because the active propagating species concentration ([P*]) is constant. Figure 1.6 displays the effect on time of changing [P*]. A constant [P*] will have a linear plot, this is kept constant by a balance between the rates of activation and deactivation. A plot with an upward curvature signifies that the [P*] has increased due to a slow initiation. A decrease in [P*] will result in a downward curvature, this may be due to increasing terminations or side reactions.

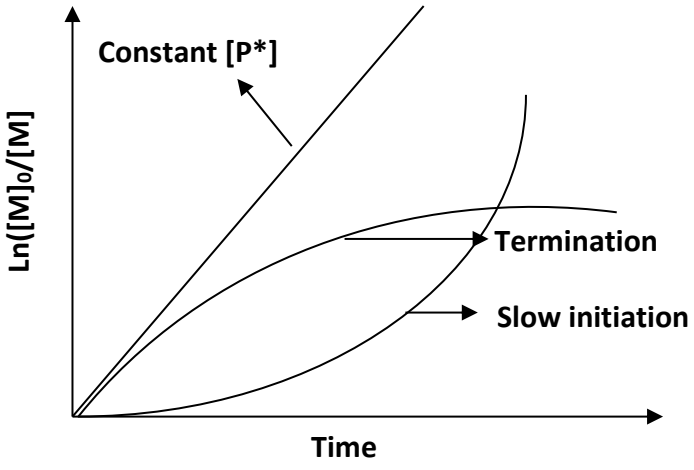

Figure 1.6: The dependence of $\ln([M]_0/[M])$ on time

The use of CRP allows the synthesis of a polymer with a predetermined degree of polymerisation, this in turn means the M_n value is predetermined.[12, 13, 20] The M_n is a linear function of monomer conversion which is displayed in Figure 1.7. This linear plot is achieved by keeping the number of polymer chains constant throughout the reaction, this is done by having a fast initiation, and a lack of chain-transfer reactions which increase the total number of chains.

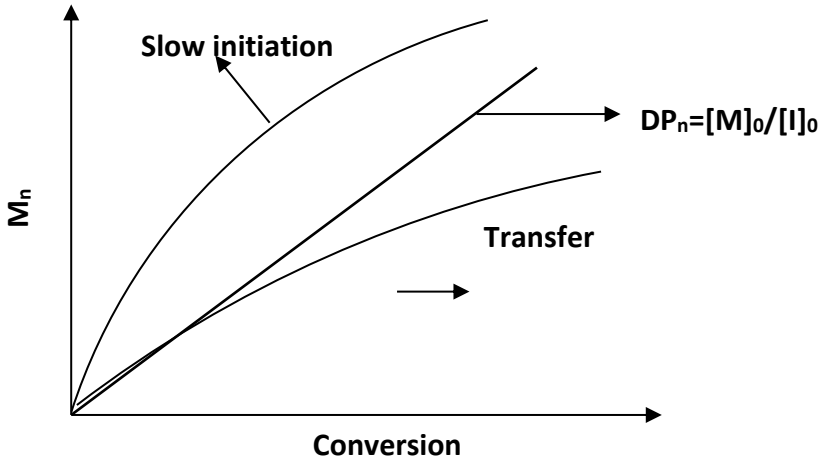

Figure 1.7: The dependency of molecular weight on conversion.

CRP is used to synthesise polymers with a low dispersity, i.e. below 1.3.[13, 18, 20, 21] This means that the polymers will have a narrow molecular weight distribution. In order for this to happen the rate of chain initiation needs to be greater than the rate of chain propagation (reactive intermediate continuously growing).There also must be no chain transfers or terminations.

Controlled radical polymerisation can be used for the preparation of a number of different polymers including copolymers. Its advantages over regular radical polymerisation are that the DP and Molecular weight is pre-determined,[13] the dispersity is low[20] and there is control over the functionality of the end groups[17] leading to the ability to synthesise copolymers.[15, 22]

There are a number of living radical polymerisation (LRP) techniques that have been developed including nitroxide-mediated LRP (NMP),[23] reversible addition/fragmentation transfer polymerization (RAFT),[24] atom-transfer radical polymerization (ATRP),[25] and single-electron transfer mediated LRP (SET-LRP).[26] This research will focus on the synthesis of BCPs *via* ATRP.

1.2.1 Atom Transfer Radical Polymerisation

Atom transfer radical polymerisation (ATRP) is a type of living polymerisation. It was first discovered in 1995 by Matyjaszewski[27] and Sawamoto[9] independently. It is used to form a carbon-carbon bond through a transition metal catalyst (Cu(I)Br) and ligand. The use of ATRP allows the control over the compositions, functionalities and topologies of the polymer chains produced. It also allows the use of a number of different initiators and macroinitiators that have a halogen atom (i.e. the active site), which is activated during the reaction. The rate of polymerisation can also be controlled, this is done by controlling the rate of propagating radicals by differing the amount and activity of the catalyst.[28]

Mechanism

For an ATRP reaction to take place a number of components and conditions are needed. A dormant alkyl halide initiator is activated by a reversible redox process, where the catalyst is a transition metal complex (e.g. Cu(I)Br/Ligand). The chain is then grown by the repetitive addition of the monomer. This is further illustrated in the mechanism for ATRP in Scheme 1.[29]

The initiator is activated by the homolytic fission of the carbon-halide bond (P_n-X). This halide then oxidises the catalyst to a higher oxidation number. The initiator radical then causes the homolysis of the pi bond in the monomer creating a new radical. Equilibrium is set up between the dormant and propagating species as seen in scheme 1.1, where the propagating radical (P_n*) then reacts with the halogen atom from the oxidised transition metal, reforming the alkyl halide and the catalyst to its original oxidation state. [30, 31]

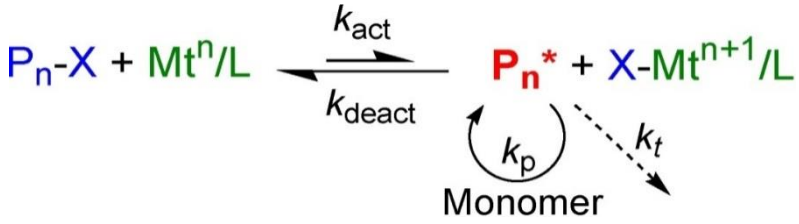

Scheme 1.1: General Mechanism for an ATRP reaction. Reproduced from ref.[30]

The rate of ATRP is dependent on the k_{ATRP} (equilibrium constant) where k_{ATRP} = k_{act}/k_{deact}. The rate of k_{act} and k_{deact} controls the equilibrium, the rate of the k_{deact}

needs to be greater than k_{act} to ensure the equilibrium lies to the left (dormant species). This keeps the radical concentration low meaning only a few monomer units are incorporated at each exchange, resulting in a well-controlled process with radical termination supressed.[32] If the k_{act} is greater than k_{deact} then terminations can take place due to a large concentration of propagating radicals. This can be overcome by use of a deactivator species such as Cu^{II}.[33]

Components of ATRP:

There are a number of key components and reaction conditions needed to undertake ATRP. The components are an alkyl halide that acts as the initiator, a transition metal catalyst (in its lower oxidation state), a ligand, a monomer and an appropriate solvent. The reaction conditions that need to be taken into consideration are the temperature and the reaction time, the optimal reaction time can be analysed by sampling the reaction at timed intervals. This next section will discuss in more detail the roles of the key components and conditions.

Monomer:

ATRP is an excellent technique for the polymerisation of many vinyl monomers including acrylates,[34] methacrylates, styrenes, acrylonitrile and dienes.[18] (Figure 8) These monomers work well in ATRP because they are molecules with stabilising substituents, for example in methacrylates they have an electron-withdrawing group that stabilises the propagating radical.[35] In the ATRP synthesis the initiator, once initialised, will attack the vinyl bond in the monomer breaking it and producing a new radical. Hydroxy derivatives can also be polymerised via ATRP such as hydroxyethyl acrylate.[36]

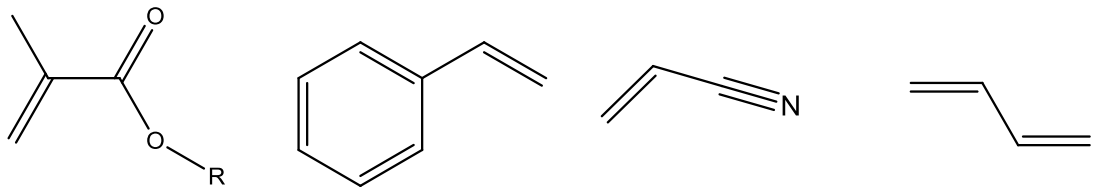

Figure 1.8: Structure of methacrylate, styrene, acrylonitrile and diene monomers.

Monomers that are less reactive such as ethylene, vinyl chloride and vinyl acetate cannot be polymerised via ATRP due to the instability of the radicals they produce. Acids such as methacrylic acid and acrylic acid also struggle to be polymerised using

ATRP as Cu^{II} carboxylates are formed which act as deactivators. However they are inefficient deactivators and are unable to reduce to Cu^{I}.[16] They can however be successfully polymerised using a protecting group such as t-butyl which is then removed post-polymerisation using a strong acid such as TFA or HCl.[7, 37]

***Initiator*:**

The initiator determines the number of growing polymer chains and therefore the DP this in turn determines the molecular weight. A faster rate of initiation leads to fewer terminations and transfers. With a fast initiation the number of growing chains is constant and equal to the starting initiator concentration.[35] This means the DP can be determined based on the initial initiator concentration and the monomer conversion.

There are a number of factors to consider when choosing an initiator, firstly are there enough functionalised end groups for the intended reaction, an initiator can be either mono or bifunctional where propagation can occur at one end or both.[25] To determine a good initiator the ratio of the apparent initiation rate constant (k_i^{app}) to the apparent propagation rate constant (k_p^{app}) must be considered. If $k_i^{app} << k_p^{app}$ then the initiation is not complete, this will give too high molecular weights and dispersity. If $k_i^{app} >> k_p^{app}$ then the concentration of free radicals is too high, this means the reaction is no longer controlled, and it will terminate before it reaches the desired DP. [16, 35] It is best to use less reactive radicals which are formed with relatively higher efficiency than growing radicals.

Research was undertaken by Tang *et al.* on the effect initiator structure has on the equilibrium constants.[38] All conditions were kept the same with a change in initiator each time. They found a number of factors that affect the initiator efficiency including the leaving group, whether it is primary, secondary or tertiary, and the stability of the radical formed. They found that the initiator leaving group contributes to the activity of the initiator with alkyl bromides being more active than alkyl chlorides so have a higher K_{ATRP} in comparison to the corresponding alkyl chloride.[39] This correlates with the differences in the bond dissociation energy (BDE) of the carbon-halide bonds, with the C-Br bond being much weaker than the C-Cl bond.[31] The C-I bond is the most active due to the C-I bond being the weakest, which is evident from

its low BDE. A comparison of the affect an alkyl iodide has on K_{atrp} in comparison to an alkyl bromide was observed by Tang *et al.* with the alkyl halides MIP and MBrP. They reported that there was not much difference between the K_{act} with MIP being slightly more active, but that the K_{ATRP} of MIP was found to be 15 times smaller than that of MBrP due to the resultant Cu^{II}-I bond being very unstable.[38] As well as considering the BDE of the alkyl halides, the association of the halide to the copper species must also be taken into consideration[40] and the reason for the small amount of difference in K_{act} between MIP and MBrP is due to iodides much weaker affinity towards the Cu.[41]

Whether the alkyl halide is primary, secondary of tertiary will have an effect on the K_{act}, it was found that ester initiators K_{act} and K_{ATRP} decrease in the following order 3° > 2°> 1°. For K_{act} the difference between primary and secondary and secondary and tertiary are very similar, however the difference in K_{ATRP} between a secondary ester and primary ester was small whereas the K_{ATRP} for tertiary esters is 30 times larger than for secondary esters.[38]

During the initiation step radicals are formed that need to be stabilised to ensure no termination reactions take place. This radical stabilisation can be achieved by using an appropriate substituent, with the substituent stability increasing in this order; ester < cyano < phenyl. The substituents also have a stabilising effect on the C-X bond which increases with an increase in electron donating ability in this order; cyano < ester < phenyl.[38, 41] The relative activity of the alkyl halides tested by Tang *et al*. are displayed in Figure 1.9.

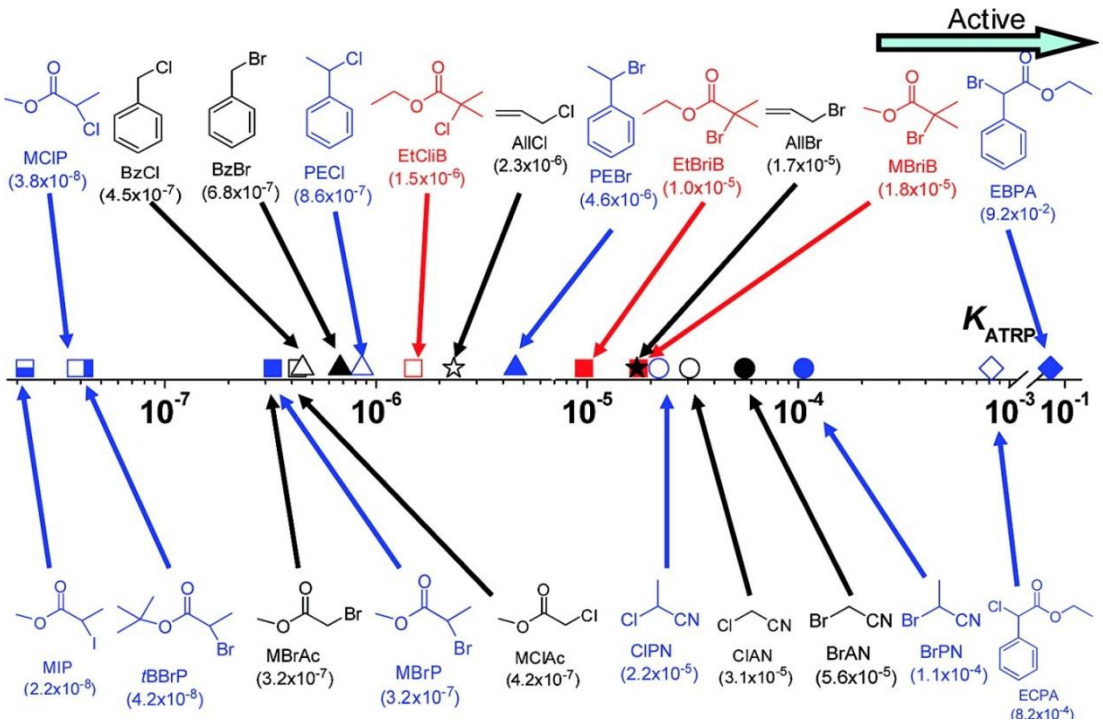

Figure 1.9: ATRP equilibrium constants for various initiators with $Cu^{I}X$/TPMA (X = Br, Cl) in MeCN at 22 °C. Colour key: (red) 3°; (blue) 2°; (black) 1°. Symbol key: (solid) R−Br; (open) R−Cl; (bottom-half-solid) R−I; (△) phenyl; (□) ester; (°) nitrile; (◇) phenyl ester; (☆) allyl. Reproduced from ref.[38]

It is not only low molar mass molecules that can be used as an initiator, macromolecules can be used, which can be functionalised in two ways, firstly by synthesising the polymer using ATRP, so it will have an active end, or to end-functionalise the desired polymer using an alkyl halide group. This makes it possible to synthesise block and graft copolymers.

Catalyst/ligand:

The catalyst plays an important role in the ATRP reaction, it provides the equilibrium between the active (propagating) and inactive (dormant) polymer. The dormant state is preferred as it suppresses side reactions. The equilibrium decreases the concentration of propagating radicals and therefore suppresses unintentional terminations and controls the molecular weight. The equilibrium constant also controls the rate of reaction, a small equilibrium (low k_{eq}) gives a slow rate of polymerisation, whereas a large equilibrium constant will result in a high dispersity.

The halide group moves quickly between the transition metal and the propagating polymer chain. It has been found that the best halides for this, are bromine and

chlorine, as the carbon-fluorine bond is too strong and iodine, although a good leaving group, causes side reactions.[35] There are a number of transition metals that can be used for ATRP including nickel,[42] palladium[43] and titanium.[44] The use of iron has been documented and has its advantages such as the catalyst can be easily washed away by an aqueous wash and reusable iron catalysts have been developed.[45] The disadvantage of using an iron based catalyst is that they have low activity and can interact with polar monomers.[46] Copper halides have been found to be more efficient and have been well investigated for use in ATRP.

The catalyst is required to have high selectivity towards the atom transfer process and to have a high lability towards X-Mt^{n+1} species. The catalyst needs to have a high affinity for the halide group so as to drive the atom transfer process,[35] and a low affinity for the propagating alkyl radicals so as to avoid the formation of organometallic derivatives which reduce the selectivity of propagation and the 'livingness' of the reaction.

As mentioned previously the ATRP process has an activator (X-Mt^{n}) and a deactivator (X-Mt^{n+1}). The deactivator is made in the process by the addition of a halide radical increasing the metals oxidation state. The K_{deact} needs to be higher to ensure a low dispersity and low terminations.[31] Using a highly pure catalyst will result in a polymer with high dispersity due to a high molecular weight fraction being formed at the initial stages. This can be overcome by the use of a deactivator. Increasing the concentration of the deactivator manually will drive the equilibrium position in the direction of K_{deact}. This will reduce the rate of polymerisation and therefore the dispersity will decrease. An increase in deactivator concentration will see a decrease in dispersity. However the concentration of deactivator needs to be well balanced as if not it can cause side reactions. The lability of the X-Mt bond is also an important factor, the more labile $CuBr_2$ makes a more efficient deactivator giving a lower dispersity than when $CuCl_2$ is used.[16]

There are some disadvantages to using a deactivator such as CuX_2 because it is highly reactive and although it reacts by atom transfer, it may also react by electron-transfer and direct addition to an alkene. It can also cause the cleavage of the C-X bond herterolytically due to its Lewis acid properties. This can be overcome by use of a

nucleophilic ligand which reduces the CuX_2 acidity, choosing the appropriate halide as for example iodides more easily cleave herterolytically, understanding that an electron donating substituent present at the alpha position on the terminal C-atom will speed up the heterolytic cleavage and by use of a non-polar solvents as polar solvents aid the heterolytic cleavage.[16]

The choice of halide can also have an effect upon the rate of propagation. When a mixed halide initiator/catalyst system of benzyl bromide and copper (I) chloride was used, better control over the rate of propagation was observed in comparison to using copper (I) bromide. This is due to the preference of an alkyl chlorine bond forming over an alkyl bromine bond, therefore the propagating radicals would be preferentially terminated with a chlorine. The alkyl chlorine bond is stronger and harder to break, therefore there would be faster initiation with the bromine being the leaving group, and slower propagation due to the strong C-Cl bond.[28]

Primarily it was thought the role of the ligand in ATRP was to solubilise the catalyst, however extensive research has now been done that indicates the ligand stabilises the catalyst making it more active. It was found by Tang *et. al.* that a catalyst is more active when stabilised by a ligand. They investigated the activity of Cu^{I} complexes with various ligands while keeping all other reaction conditions consistent. As seen in figure 10, the activity of copper complexes were found to decrease, when using a variety of ligands, in this order: alkyl amine ≈ pyridine > alkyl imine >> aryl imine > aryl amine. The activity is also affected by the number of nitrogen atoms present on the ligand, as the number of nitrogen atoms on the ligand decreases so does the activity. This means that bidentate and tridentate ligands produce the least active catalyst complex. The more reducing the complex the better the catalyst, however if the catalyst is too active then a higher proportion of radicals will be formed leading to a higher percentage of termination reactions. [38, 47]

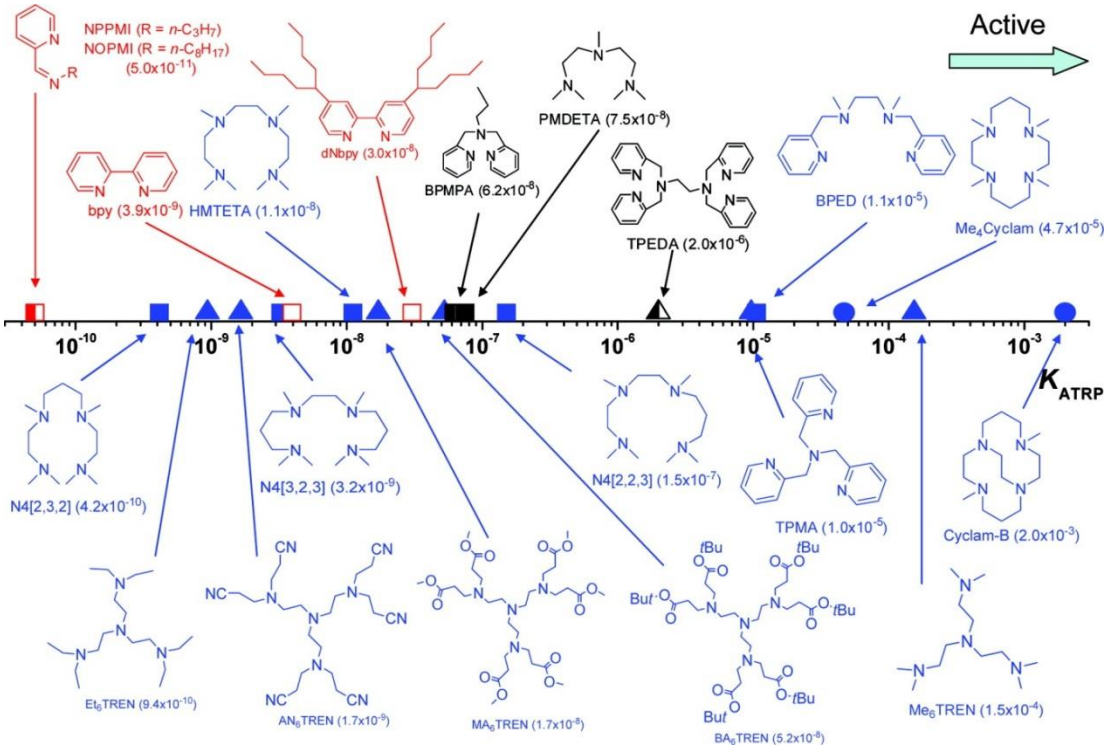

Figure 1.10: ATRP equilibrium constants K_{ATRP} for various N-based ligands with the initiator EtBriB in the presence of Cu^{I}Br in MeCN at 22 °C. Color key: (red) N2; (black) N3 and N6; (blue) N4. Symbol key: (solid) amine/imine; (open) pyridine; (left-half-solid) mixed; (▯) linear; (Δ) branched; (°) cyclic. Reproduced from ref.[47]

Solvent/Temperature:

The solvent has its role in ATRP, generally the solvents used are non-polar (benzene, diphenyl ether), however when a low molecular weight polymer (M_n < 20,000) is being synthesised toluene or xylene can be used. Polar solvents have also been used to some success, such as water,[48] ethylene carbonate or propylene carbonate. The effects of the solvent upon the course of the other componants of the reaction should be considered, for example Matyjaszewski *et al.* reported the ATRP of n-butyl acrylate with Cu(I)Br/bpy with ethylene carbonate as the solvent. It was found that the reaction proceeded much faster than in bulk and was it was suggested this was due to a change in the structure of the catalyst due to the solvent.[49] Water, another polar solvent, has been seen to accelerate the rate of reaction as the water competes with the ligand and halide to complex with the transition metal which changes the equilibrium position.[39] The amount of solvent used can also affect the rate of reaction. For example, as ATRP is first order, diluting the reaction by 50 % will lead to a four times slower rate of reaction.[16] Therefore the balance needs to be made between the amount of solvent needed and the rate of reaction required to have a

controlled synthesis. Horn and Matyjaszewski reported the effects of 14 different solvents on the activation rate constant in ATRP. They found that the activation rate increased with an increase in the solvents polarity.[50] The reaction is also sensitive to oxygen, the catalyst, which is present at a higher concentration than the propagating radicals, will react with the oxygen which reduces the concentration of the catalyst and may cause deactivation.

The temperature also controls the rate of polymerisation, the rate of propagation increases with an increase in temperature which increases on increasing temperature, as the equilibrium constant and the radical propagation rate constants will be increased.[35] At higher temperatures the reaction is better controlled. However the optimum temperature needs to be established as too high a temperature will lead to side reactions giving high dispersities and low of functionality.[51]

ATRP has proven to be a very useful technique for the synthesis of polymers with a number of different topologies, including block, alternating, graft and random copolymers. It has also been used to make functionalised polymers as the halogen end group can be altered with other functional end groups once the polymerisation has taken place. As mentioned throughout this section the important components to take into account when synthesising using ATRP are finding a radical stabilising monomer, the reactivity and structure of the initiator, the concentration of catalyst used in the reaction to find the balance between propagating radicals and dormant polymer chains, the halogen end-group used (generally bromine or chlorine), the solvent volume and finally the optimum temperature.

1.2.2 Activator Generated by Electron Transfer-ATRP and Single Electron Transfer-Living Radical Polymerisation

The use of the high concentrations of copper in ATRP is one of its major drawbacks as it hinders the system from being biocompatible and the copper can sometimes be hard to remove after polymerisation due to its strong interaction with the ligand. The use of activator generated by electron transfer ATRP (AGET-ATRP) can be used to overcome the issues of high copper concentrations. AGET ATRP works by using Cu^{II} initially instead of Cu^{I}. A reducing agent is then employed to reduce the Cu^{II} to Cu^{I} forming the activator. This reducing agent must not be radical forming so as not to disrupt the reaction process. The newer technique of activator regenerated by electron transfer ATRP (ARGET ATRP) works in the same way as AGET ATRP with the added bonus that the reducing agents used constantly regenerate the activator (Cu^{I}) so that concentrations of Cu^{II} as low as ppm amounts can be used.[52] AGET and ARGET ATRP also have the added advantage of the reducing agent also removes any dissolved oxygen which can terminate the reaction.[53] Examples of reducing agents employed for ARGET ATRP are tin^{II} 2-ethylhexanoate ($Sn(EH)_2$),[54] glucose,[54] ascorbic acid,[55] hydrazine and phenyl hydrazine.[56] The mechanism for ARGET-ATRP is given in Figure 1.11.

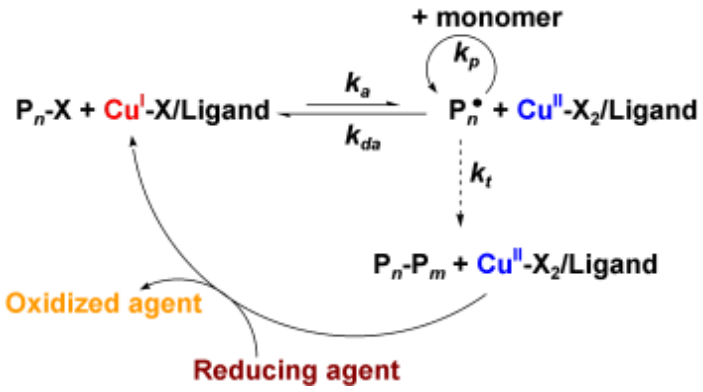

Figure 1.11: ARGET-ATRP reaction scheme. Reproduced from ref.[54]

The problems that arise in the use of ATRP, such as chain end termination can be overcome with the use of single electron transfer living radical polymerisation (SET-LRP). SET-LRP rapidly synthesises functional polymers with a control over the molecular weight and the dispersity while maintaining excellent chain end fidelity.[26] It can be also used at lower temperatures than ATRP. The major differences between

SET-LRP and ATRP are that the catalyst used in SET is Cu^0 as opposed to an oxidised M-X catalyst. Also the initiation step is thought to be single electron transfer from the catalyst (electron donor) to the initiator electron acceptor, rather than atom transfer. Cu^I is formed in this step which goes on to disproportionate into Cu^0 and Cu^{II}.[26] The Cu^{II} acts, as it does in ATRP, as the radical deactivator. SET-LRP has been adapted for a wide variety of monomers[57] but is not yet as widely versed as ATRP.

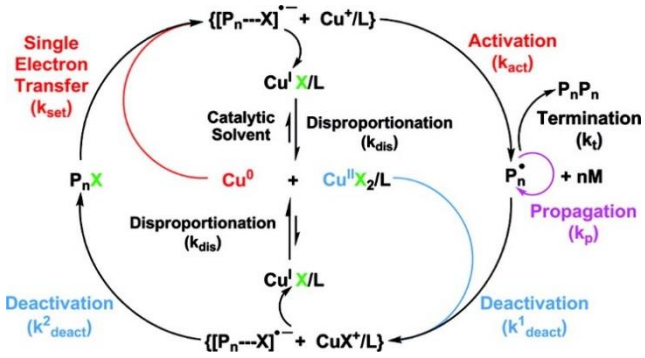

Figure 1.12: Mechanism of SET-LRP. Reproduced from ref.[58]

1.3 Self-Assembly of Amphiphilic Block Copolymers

The self-assembly of block copolymers (BCPs) has been widely investigated with a range of applications such as drug delivery[6], reversible transport for drug delivery[59], thin films[60] and as nanocarriers[59]. The BCPs act as amphiphiles in solution yielding ordered structures with different morphologies depending on the relative ratios of the hydrophobic and hydrophilic blocks and the molecular weight, along with other factors. The more common morphologies include micelles, cylindrical micelles and vesicles[61] (polymersomes).[62] However the use of BCP's in self-assembly has the potential to produce more complex aggregates for use as nano- to micro-sized carriers for active compounds, for inorganic materials templating and for controlled release of encapsulated compounds.[6]

The aim of the work outlined in this report is to produce aggregates with bicontinuous micellar morphology. Bicontinuous micelles is thought to be a complex morphology, they are multi-compartment micelles. While simple vesicles have been used to encapsulate both hydrophobic and hydrophilic materials as they exhibit both

a hydrophilic cavity and a hydrophobic core, multi-compartment micelles have the ability to encapsulate two different hydrophobic materials. This is due to the fact that upon assembly of the copolymer the hydrophobic core of the aggregates will form segregated areas. For this reason, there has been great interest in the research into the self-assembly of copolymers with the notion for use in drug delivery and templating.[63]

1.3.1 Factors that affect polymer self-assembly

For thermodynamically stable aggregates to form BCPs there are three contributing factors to the free energy of the system. These are the degree of stretching of the core forming block (generally the hydrophobic block), the interfacial tension between the core and the solvent outside the core (i.e. the hydrophobe-water interaction) and the repulsive interactions among the corona forming chains.[62, 64] The morphology of the resultant polymer aggregates are controlled by factors that affect these three contributions, for example the polymer composition, preparation techniques, polymer concentration etc. This section will discuss the factors that affect the aggregation of BCPs.

1.3.1.1 Polymer Aggregate Preparation

A number of factors affect the formation of polymer aggregates; these include the preparation method, the polymer composition and the polymer concentration. There are a number of methods that could be utilized for the preparation of polymer aggregates include micro-fluidic techniques[65], layer-by-layer assembly[66], electroformation[67] and more recently formation of aggregates during synthesis of the BCPs in solution.[68] There are two main methods used for the preparation of polymer aggregates, the direct dissolution method and the dialysis method. The choice of which, depends largely on the polymers solubility in water. Direct dissolution is when the polymer is dissolved directly in water, and therefore this method can only be used for a polymer that has high enough water solubility. The dialysis method is used for BCPs when one or all of the blocks are not easily soluble in water. A common organic solvent, one that dissolves both blocks, is used to dissolve the BCP, this solvent must be miscible with water. The solution is then dialysed against water to remove the organic solvent and induce micellisation. With

crew-cut aggregates, where the core forming block of the polymer is longer than the corona forming block,[69] water is first added slowly to the solvated polymer to induce aggregation before dialysing against distilled water to remove the organic solvent. Schematics of the methods are shown in Figure 1.13. Another method used for the self-assembly of polymers is the evaporation method where the polymer is dissolved in an organic solvent, the solvent is evaporated off and the polymer is then re-suspended in aqueous solution. The evaporation method is also used when the polymer has low water solubility although the dialysis method is more commonly employed.[70]

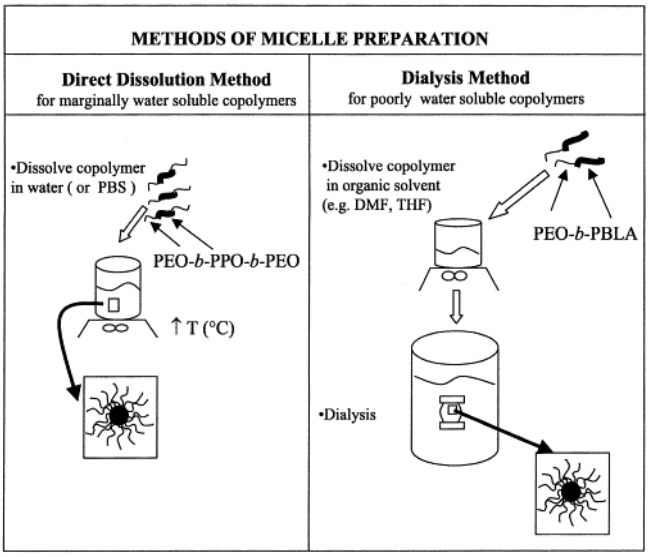

Figure 1.13: Schematic of the direct dissolution and dialysis methods for the self-assembly of block copolymers. Reproduced from reference.[71]

The direct dissolution method has been employed for a number of polymer systems and after the direct dissolution the solution is left to anneal by standing or the annealing happens by thermal treatment,[72] Thermal annealing to reach an equilibrium structure is a lengthy process typically taking several days, this can be significantly reduced as seen by Yabu *et al.*[73] They found that microwave annealing of a hydrophobic block copolymer nanoparticles in water lead to stable structures within a few minutes that retain their spherical shape and that the internal morphology could be controlled by controlling the microwave annealing temperature.

With use of the dialysis method the size and morphology of the resultant polymer aggregates can be controlled with a choice in the organic solvent used but also the

volume of solvent used.[74] Eisenberg *et al.*[75] investigated the effect a change in wt % of the common solvent dioxane has on the resultant morphology of PAA-*b*-PS aggregates. It was found that upon a decrease in wt % of dioxane the morphology changed from spheres to rods and then finally vesicles. Nagarajan proposed a theory that changing the solvent content of the core of the aggregates can change the aggregate morphology. This was later shown experimentally by Eisenberg *et al*.[76] They discovered that a change in common solvent not only changes the dimensions of the core due to increased degree of swelling, but may also cause repulsion between the corona chains due to solvent polymer interactions. PS-*b*-PAA BCPs were prepared with various mol % of PAA, it was found that in DMF all the BCPs produced spherical micelles. Changing the solvent to THF increased the degree of swelling of the core forming PS block and spheres, vesicles and large compound micelles were observed. With the use of dioxane which again increase the degree of swelling of the PS core resultant in spherical micelles, cylinders, vesicles and large compound micelles depending on the relevant PAA mol %. The solubility of the core forming and corona forming blocks in the common solvent explains the influence of the solvent on the resultant morphologies. This was established by Holder *et al.*[77] where a BCP of PEO-*b*-PBMA (17 wt % PEO) was self-assembled in THF and produced bicontinuous nanospheres. A dispersion of the same polymer this time in dioxane instead of THF, resulted in multi-lamellar vesicles, flattened bilayers and internal twisted lamellar structures. When the solubility parameters of the two blocks were compared to those of the solvents it showed that the hydrophilic PBMA block was better solubilised by THF and that PEO was better solubilised by dioxane, this meant that the PEO hydrophilic head group had an increased degree of swelling, i.e. increase volume which supressed the inverse curvature of the BCP that was seen for bicontinuous nanospheres to form. As already mentioned the repulsion between the corona forming chains also affects the aggregate formation and can drive the self-assembly towards a particular morphology by altering the molecular structure. The strength of the repulsion depends on the coil dimension and the charge density of the chains, these factors depend on the interactions between the chosen solvent and the corona forming block (hydrophilic block).[78] The effect a solvent may have upon the corona forming block is assessed by the dielectric constant, therefore the effect

can be easily altered by tuning the dielectric constant of the common solvent by solvent mixing.[79]

1.3.1.2 Packing Parameter

The block copolymers have both hydrophilic and hydrophobic domains which, in aqueous solution they self-assemble to minimise the energetically unfavourable hydrophobe-water interactions.[80] It is thought that the molecular curvature of the block copolymers is in part responsible for the particular morphologies of the aggregates formed, along with the relative ratio of different blocks[6]. When the molecular curvature of the BCP is a cylinder then a membrane morphology will form, when the curvature is a wedge a rod-like structure will form and when the curvature is a cone spherical morphologies will be present.[81] This curvature, and therefore the morphology, can be estimated by calculating the block copolymers packing parameter, *p*. This is outlined in Equation 1.1.

Equation 1.1: Calculation of the packing parameter for block copolymers

$$p = \frac{v}{al}$$

Where *p*= packing parameter, v= hydrophobic volume, a= optimal area of the head group and l= length of the hydrophobic tail. This calculation has been used to successfully predict the morphology of aggregates formed by Israelachvili *et al.*, when taking into account the following guidelines; when p= 1/3 spherical micelles will form, when p=1/2 cylindrical micelles will form, and when p=1 vesicles (polymersomes) will form (Figure 1.14).[80, 82] However this is a general rule and is not always accurate, given the wide range of morphologies that can be formed such as toroidal, disk like and bicontinuous micelles.[6] Other physical and chemical factors will affect the morphology of the aggregates. These include changing the chemical structure or properties of the polymers, the hydrophilic/hydrophobic ratio, and as already discussed tweaking the preparation technique such as polymer concentration or solvent properties, will result in a change in aggregate morphology.

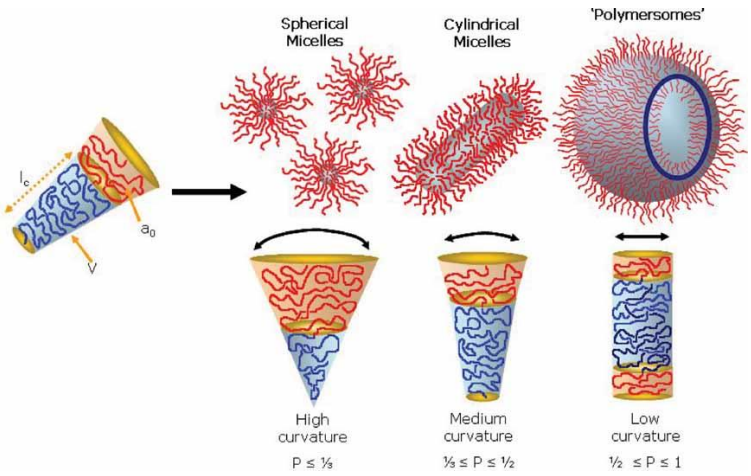

Figure 1.14: The different aggregates formed by self-assembly of block copolymers. The aggregate morphology is predicted from the inherent curvature of the molecule, which is estimated from the block copolymers packing parameter, p. Re-produced from reference.[80]

As mentioned previously, the relative ratios of the hydrophobic to hydrophilic blocks will have an effect on the aggregate morphologies. Generally, when the copolymer hydrophilic/hydrophobic ratio is greater than 1:1 micelles will form, a ratio less than 1:2 will see vesicles forming and copolymers with a ratio less than 1:3 may produce vesicles, inverted microstructures and other complex vesicles such as bicontinuous nanospheres and toroidal micelles.[63] In addition other research has indicated that the hydrophilic block is the region that drives the self-assembly, this research has shown that at a hydrophilic weight percentage of: 35 % ± 10 % it is expected that vesicles (polymersomes) will form; < 50 % will see the formation of cylindrical micelles; > 45 % micelles may form; and ,25 % it is expected that inverted micelles will be present.[74,62] There are obviously exceptions that are observed and the various other factors mentioned previously will affect these guidelines. Not only can the morphology be controlled, to some extent, the size of the aggregates formed can also be controlled via the alteration of the block copolymer chain lengths and the solvent/water ratio, the hydrophobic/hydrophilic ratio also plays a part in controlling the aggregates size.[78, 83]

1.3.1.3 Critical Micelle Concentration

The polymer concentration can affect the resultant polymer aggregate morphology as demonstrated by Eisenberg *et al.*[84] for the BCP PS_{190}-*b*-PAA_{20} where an increase in polymer concentration led to a morphological change from spheres to rods to

vesicles when the polymer was self-assembled in DMF-water mixtures. A change in morphology upon a change in polymer concentration has been seen before in the literature.[85]

Whether a polymer will form aggregates or not is dependent upon the critical micelle concentration (CMC). The CMC is the minimum concentration of polymer required for aggregates such as micelles to form.[86] Below this concentration the number of polymer chains is insufficient to induce self-assembly. The chains are dispersed throughout the solution, absorbed at the air-water interface and the solvent-water interface. As the concentration increases the interface and the bulk solution became saturated above which aggregate formation takes place. The reason for the formation of aggregates at this point is to reduce the interfacial free energy, the major mechanism for the reduction in free energy is in the unfavourable hydrophobe-water interactions in aqueous solution, known as the "hydrophobic effect".[87]

1.3.2 Morphologies of Block Copolymer Aggregates

1.3.2.1 Micelles

As previously discussed micelle formation of amphiphilic block copolymers occurs to reduce the interfacial free energy of the polymer-water system.[86] The major mechanism for this is minimising the undesirable hydrophobe-water interactions otherwise known as the "hydrophobic effect".[88] Micelles self-assemble with the hydrophobic block chains forming the core and the hydrophilic head group forming the corona. Micelles can be both spherical or cylindrical, inverse micelles are also possible where the hydrophobic chain forms the corona, this is possible when the BCP is self-assembled in a good organic solvent that solubilises the hydrophobic block.[64, 89] The hydrophilic corona of BCP micelles not only offers the micelle its solubility in water but also, depending on the choice of hydrophilic block, can also protect the core from external influences.[90] For example, PEO is the most commonly employed corona forming block, PEO is known to resist external influences such as protein adsorption and cellular adhesion.[91] The hydrophobic core allows micelles to be used for a number of applications including the encapsulation of hydrophobic drugs.[92, 93]

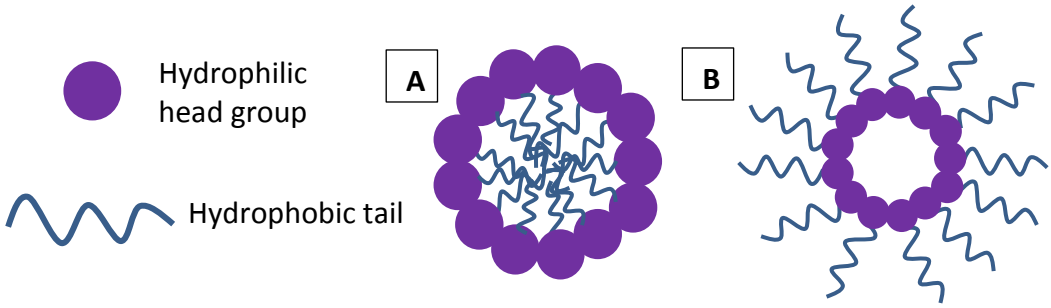

Figure 1.15: Schematic of **A)** micelles and **B)** inverse micelles.

There are two types of spherical micelles, crew cut and star micelles. These micelle types are distinguishable by the relative lengths of the two blocks. When the hydrophobic block is much longer than the hydrophilic segment the micelles are known as "crew cut" and have a much smaller corona compared to the core. "Star-like" micelles are when the corona is much larger than the core.[94] Crew-cut BCPs can form aggregates of a number of different morphologies not just spherical micelles.[95] The size of the micelles is determined by the relative volumes of the –B- concentration, pH, ionic strength and the temperature.[86] The size is also affected by the choice and volume of solvent used along with other preparation parameters as previously discussed.[64, 89]

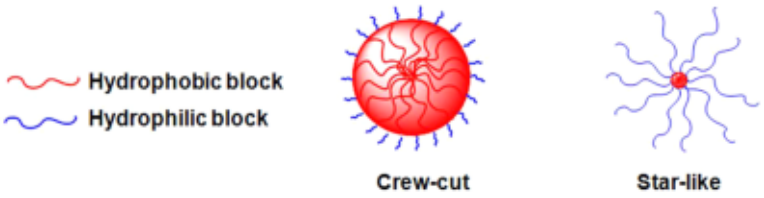

Figure 1.16: Schematic of crew-cut and star-like micelles. Reproduced from ref.[96]

Star-like micelles can be prepared by the direct dissolution method as the corona forming block (largest block) is easily solvated in water. Crew-cut micelles are nto easily prepared by the direct dissolution method due to their large hydrophobic region, instead a selective or common organic solvent is first used followed by the addition of water.[95]

Examples of crew-cut micelles include PAA_{25}-*b*-PS_{410},[64] poly(styrene-*b*-4-vinylpyridinium methyl iodide) (PS_{933}-*b*-P4VP-Mel_{82})[69, 95] and PS_{240}-*b*-PEO_{15}.[97] More recently Borsali *et al.* reported the transition of star-like micelles to crew-cut micelles. When PS-*b*-PMMA star-like micelles (self-assembled in a selective solvent)

were exposed to UV light, it caused the cross-linking of the core PS chains and degradation of the corona forming PMMA chains, this caused the transition to crew-cut micelles (Figure 1.17).[98]

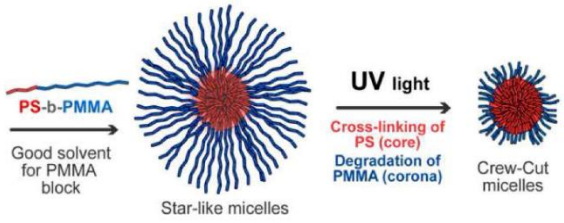

Figure 1.17: Schematic for the transition of PS-*b*-PMMA star-like micelles to crew-cut micelles.

Cylindrical micelles, like spherical micelles have a hydrophobic core surrounded by a hydrophilic corona. They have similar diameters as spherical micelles (ca. 30 nm), however their length can be as large as 10s of micrometres.[62] Cylindrical micelles can form from diblock copolymers but are not as commonly observed as spherical micelles.[99] The length of the cylindrical micelles can be controlled as reported by Wang *et al*. They reported the formation of cylindrical micelles from a PFS_{53}-*b*-PI_{320} (poly(ferrocenylsilane)-*block*-poly(isoprene)) BCP. Upon addition of more of the BCP to the cylindrical micelle solution, the length of the micelle increased almost proportionally with an increase in polymer concentration (Figure 1.18).[100] This control has been observed more recently with the use of a "seed" micelle of poly(3-hexylthiophene)-*b*-poly-(dimethylsiloxane) (P3HT-*b*-PDMS) prepared by sonication of a solution of larger cylindrical micelles. A P3HT unimer was then added at increasing concentrations to increase the cylindrical micelles length.[101]

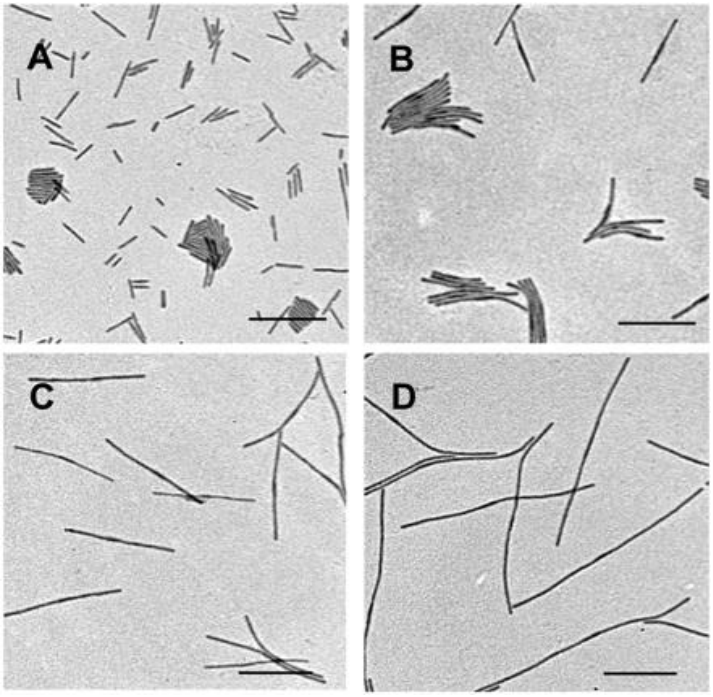

Figure 1.18: TEM images for (**A**) sonicated PFS_{53}-PI_{320} micelles in hexane (0.5 mg/mL); (**B** to **D**) elongated micelles after adding 0.5 mg (B), 1 mg (C), and 2 mg (D) of PFS_{53}-PI_{320} in THF (0.1 mL) to 1.0-mL solutions of (A). Scale bars, 500 nm.

To allow the cylindrical micelle to have uniform curvature across the aggregate, theoretically infinitely long cylinders would be the most stable arrangement. This would be more energetically favourable over short cylinders.[80] The cylinders can be closed off by end caps (Figure 1.19) whose formation is driven by the molecular frustration and are stabilised by an increase in the entropy.[102] Other terminals for cylindrical micelles have been observed such as branch points which are less energetically favourable than end caps,[102, 103] Y-junctions [104] (Figure 1.19) and worm-like micellar networks.[105]

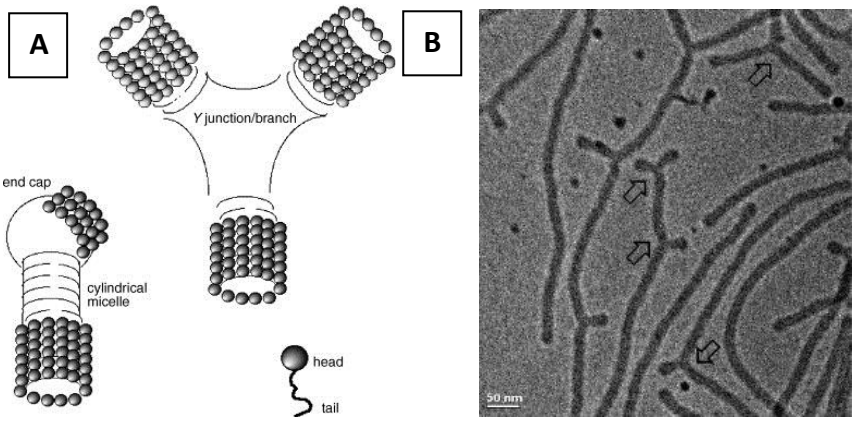

Figure 1.19: A) Defects in cylindrical micelles showing end-caps and *Y*-branch points. **B)** TEM image showing cylindrical micelles with Y-junctions (arrows).

Cylindrical micelles have been used for the solubilisation of hydrophobic compounds. They also have potential for use in alignment of metal, superconductor and magnetic nanoparticles.

1.3.2.2 Vesicles (Polymersomes)

Liposomes are vesicles that form from naturally occurring and synthetic lipids. Polymer vesicles also known as polymersomes exhibit superior mechanical and physical properties when compared to liposomes.[80, 106] This was determined by analysing the amount of higher tension and area strain the vesicles can undergo before rupturing. This was much higher for vesicles than liposomes.[62] The closing of a membrane (lamellae) to form the polymer vesicles is due to thermodynamic curvature stabilisation mechanism. The curvature of the polymer chains is stabilised due to repulsions between the exterior hydrophobic chains and the water molecules.[62] BCP vesicles are hollow spheres with internal and external hydrophilic coronas and a hydrophobic wall (Figure 1.20). The general rule for the formation of polymer vesicles is that the packing parameter, p, should be close to 1[82] and that the weight fraction of the hydrophilic block should be 30 % ± 10 %.[74]

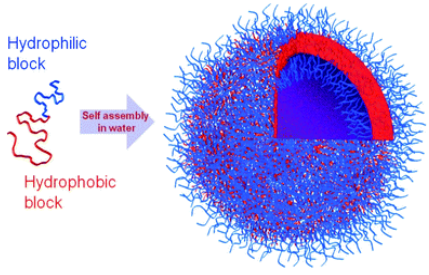

Figure 1.20: Schematic of a polymer vesicle. Reproduced from ref.[107]

The first observation of polymer vesicles was reported by Eisenberg *et al.* with the self-assembly of poly(styrene)-*block*-poly(acrylic acid) (PS-*b*-PAA) BCP.[64] A few more examples of a simple vesicles system are PEO-*b*-PEE (PEE- poly ethyl ethylene),[108] PEO-b-PBD (PBD- polybutadiene)[108] and PEO-*b*-poly(methylphenylsilane).[109]

Vesicles can be utilised and modified for a number of different applications. As previously mentioned PEO is a biocompatible polymer and can be used as the corona of a vesicle used within the body. The corona can be modified an example of which is the attachment of antibodies that allow targeted delivery of pharmaceuticals. Hydrophobic compounds amongst others can be easily incorporated into the vesicles wall and carried within the body along with hydrophilic compounds encapsulated within the core of the vesicle. The vesicles can be modified to have one or more stimuli-responsiveness which provides the vesicle with the ability to have controlled release of active compounds. Stimuli-responsive polymers will be discussed in more detail later in this chapter.

The size of the vesicles formed is greatly affected by the preparation method. The electro formation method usually produces vesicles that are microns in size, however use of the film rehydration method produces vesicles that are one or two magnitudes smaller. The wall thickness (hydrophobic blocks) is controlled by the molecular weight of the copolymer and more importantly the DP of the wall forming block with the wall thickening with an increase in DP.[62]

The deformation of vesicles is often observed by TEM with slight indentations, stomatocytes[110] or fully collapsed “kippah” structures are observed (Figure 1.21).[111] When an organic solvent is used in the preparation of vesicles deformation can take place due to the difference in water concentrations between the interior and exterior of the vesicle. This causes the organic solvent to diffuse to the exterior and water to diffuse to the interior, the rate of diffusion of the organic solvent is greater than the rate of diffusion of the water causing this collapse. When a glassy hydrophobic polymer is used such as PS the collapsed shape is frozen and the vesicular shape cannot be reformed.[112]

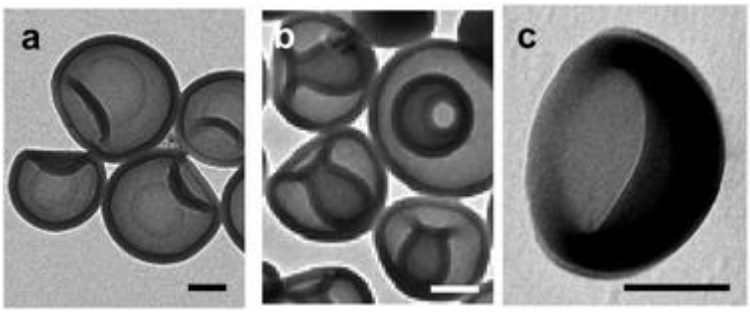

Figure 1.21: Deformation of vesicles. (a) Slight indentations. (b) Stomatocytes. (c) Fully collapsed "kippah" structure; kippah is a Hebrew word for both dome and the traditional skullcapReproduced from ref.[62]

1.3.2.3 Multi-compartmental Micelles

When an ABC triblock copolymer is self-assembled in aqueous solution phase separation can occur between the two hydrophobic domains (B and C). The product of this is known as a multi-compartmental micelle, where the corona forming block is hydrophilic and there are two separate hydrophobic internal regions.[113] The use of multi-compartmental micelles as nanocarriers is of particular interest as two or more incompatible hydrophobic compounds may be encapsulated within the separate hydrophobic domains.[6, 114] The most simple example of a multi-compartmental micelle is a core-shell-corona morphology. These micelles are commonly formed from linear ABC ter-block copolymers and have an "onion-like arrangement" of the three different polymer domains in a spherical formation. There is both a disadvantage and advantage to this arrangement for use as a nanocarriers. The inner hydrophobic domain is not directly accessible to the exterior of the micelle so the encapsulated active compound would have to pass through the second hydrophobic domain first, however this would allow a slower release time in comparison to the compound encapsulated in the B domain.[113] Stimuli-responsive blocks can be incorporated into the copolymer design. Jerome *et al.* reported the self-assembly of poly(styrene)-*block*-poly(2-vinylpyridine)-*block*-poly(ethylene oxide) (PS-*b*-P2VP-*b*-PEO), which self-assembled to form a core-shell-corona micelles. The P2VP block was responsive to changes in pH where the shell reversibly contracted and expanded.[115] Although the common external shape of these core-shell-corona micelles are spherical, cylindrical and spiral like core-shell-corona micelles have also been observed (Figure 1.22).[116]

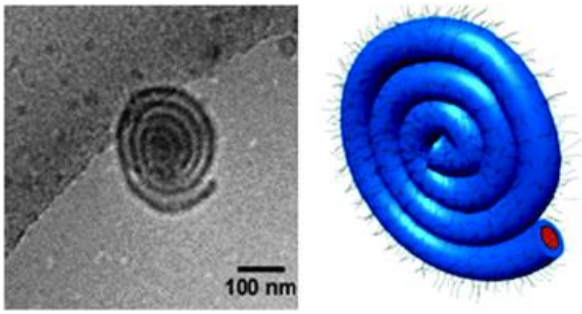

Figure 1.22: Cryo-TEM picture of a spiral-like micellar aggregates from the poly(ODFOx$_{23}$-*b*-EPOx$_{28}$-*b*-EtOx$_{49}$) triblock terpolymer in water. Right: schematic representation of a potential spiral-like aggregate made by the poly(ODFOx$_{23}$-*b*-EPOx$_{28}$-*b*-EtOx$_{49}$) triblock terpolymer in water (EtOx in black, EPOx in blue and ODFOx in orange).

Other more complex multi-compartmental aggregates have been observed by Du *et al.* They investigated the effect of a terminal alkynyl end group upon the self-assembly of a fully hydrophilic homopolymer such as PNIPAAm and POEGMA. It was found that the alkynyl end group can drive the self-assembly of the homopolymer into a variety of different morphologies. When using the polymer system PIB-*b*-PNIPAAm-Br, where the alkynyl end group PIB is propargyl 2-bromoisobutryrate, an increase in the DP of the PNIPAAm resulted in multicompartment vesicles, then spherical compound micelles and finally flower-like complex particles (Figure 1.23).[117]

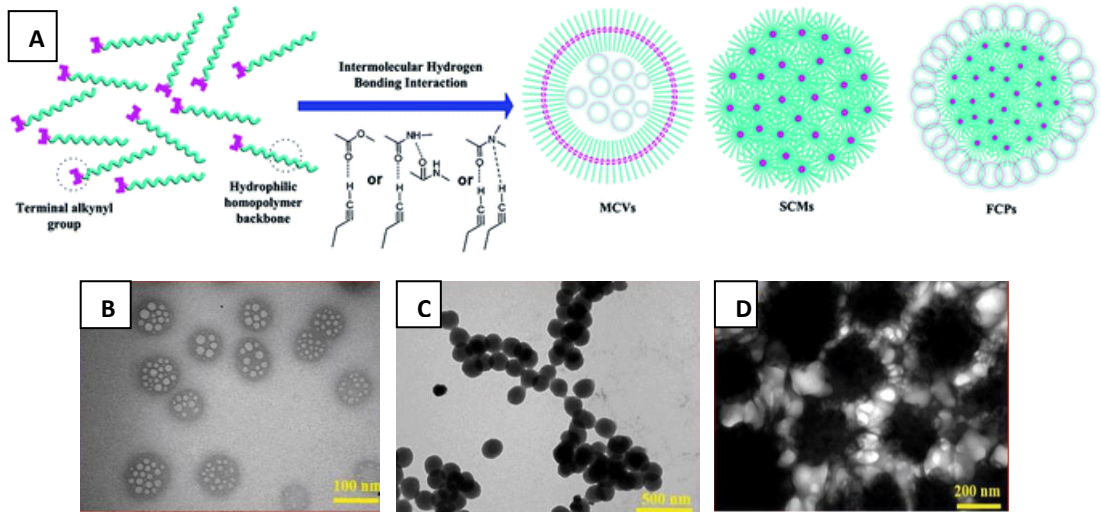

Figure 1.23: A) Schematic for the formation of multicompartment vesicles, spherical compound micelles and flower-like complex particles formed form PNIPAAm homopolymer with a terminal alkynyl group. **B)** TEM image of MCV's **C)** TEM image of SCMs **D)** TEM images of FCPs.

Self-assembly of a linear ABC block copolymer where one of the blocks is fluorinated can produce a variety of different compartmentalised aggregates that are more complex than core-shell-corona micelles. Feng *et al.* investigated the effects of CO_2 upon the resultant morphologies of a PEO-*b*-poly(2,2,3,4,4,4,-hexafluorobutyl methacrylate)-*b*-poly(2-(diethylamino)ethyl methacrylate) block copolymer. In the absence of CO_2 the polymer self-assembled to form spherical aggregates. After exposure to CO_2 a number of more complex morphologies were observed with segregated micro domains. These included hamburgers (a lamellar region sandwiched between other regions), reverse hamburgers, clovers and footballs (Figure 1.24). The reason for the fluorinated block and the hydrocarbon blocks segregation is due to the incompatibility between the two blocks.[118]

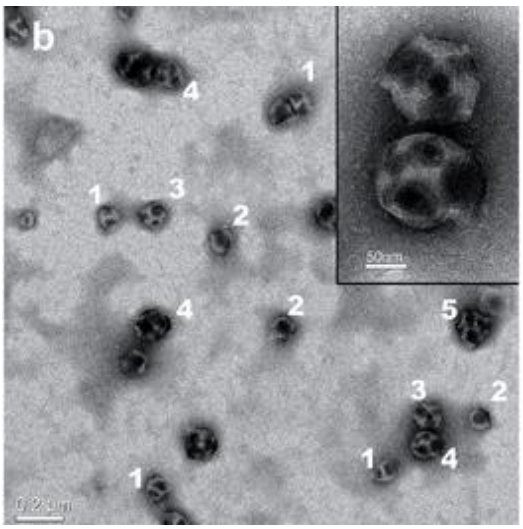

Figure 1.24: TEM images of compartmentalised aggregates formed from PEO-*b*-poly(2,2,3,4,4,4,-hexafluorobutyl methacrylate)-*b*-poly(2-(diethylamino)ethyl methacrylate) block copolymer after bubbling CO_2; the different numbers distinguish between different types of MCMs: “hamburgers” (1), “reverse hamburgers” (2), “clovers” (3), “footballs” (4) and more complex structures (5).

Other multi-compartmental aggregate structures include segmented cylindrical micelles (hydrophobic regions alternate along the length of the micelle), raspberry micelles (spherical shapes of one region embedded in the matrix of another) and blackberry-type capsules (large core vesicles with a layer of smaller vesicles and micelles deposited upon the surface).[119]

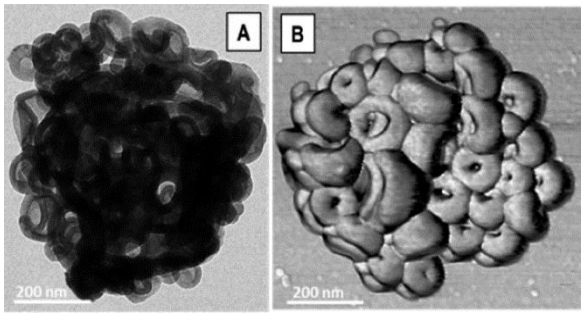

Figure 1.25: A) TEM image and B) AFM image of blackberry-like capsules of PS_{297}-*b*-$P4VP_{30}$ vesicles surrounded by PS_{190}-*b*-PAA_{34} vesicles in solution.

1.3.2.4 Bicontinuous Nanospheres

Amphiphilic block copolymers can self-assemble to form bicontinuous nanospheres that consist of a twisted network of the hydrophobic phase interconnected with the hydrated hydrophilic moieties.[120] The first amphiphilic block copolymer to exhibit a bicontinuous structure in aqueous solution was observed by Eisenberg *et al.* (1996).[97] It was formed from a 4.3 % PS_{190}-*b*-PAA_{20} solution in a 8.5 % DMF-water mixture. Eisenberg *et al.* analysed the aggregates with TEM (Figure 1.26) and describes the morphology as a three dimensional structure of interconnected rods. Further investigation and characterisation of the morphology was not conducted. Bicontinuous nanospheres were later observed by Wooley *et al.*[121] for the aggregates of ABC block copolymer PAA_{99}-*b*-PMA_{73}-*b*-PS_{203}. PAA_{99}-*b*-PMA_{73}-*b*-PS_{203} formed bicontinuous aggregates when self-assembled in a water-THF mixture (1:0.2) in the presence of EDDA. Increasing the water content to 1:0.8 saw a morphological change from bicontinuous to multi-lamellar. This was suggested to be due to the water increasing the volume of the PAA chains via swelling and effecting the interfaces within the aggregate and therefore the molecular curvature.

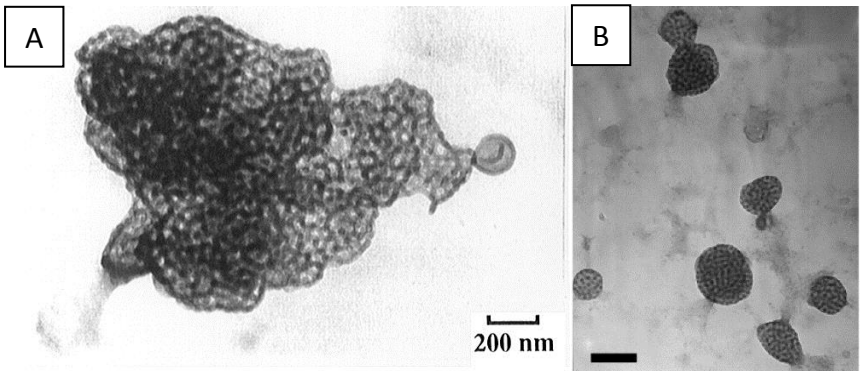

Figure 1.26: A) TEM micrograph of a bicontinuous aggregate formed from PS-*b*-PAA in a DMF-water mix. Reproduced from ref.[97] **B)** TEM micrograph of bicontinuous nanospheres formed from PAA-*b*-PMA-*b*-PS and EDDA in THF/water; scale bar = 200 nm. Reproduced from ref.[121]

Parry *et al.*[120] reported the first example of bicontinuous aggregates formed in the absence of an additive. They were formed by the slow addition of water to a solution of amphiphilic polynorborene based double comb diblock polymer of a tripeptide glycine-leucine-phenylalanine and oligo(ethylene glycol) methyl ether (OEGME) in DSMO, followed by the removal of the solvent *via* dialysis against pure water. The internal morphology was modified by changing the amino acid sequence of the peptide to produce worm-like micelles (Figure 1.27).

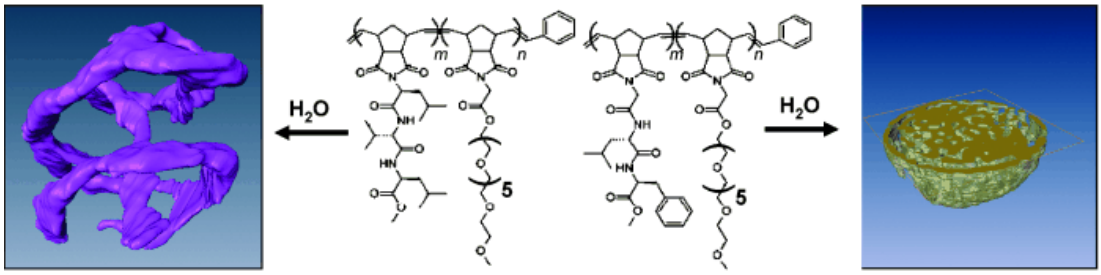

Figure 1.27: Amphiphilic norbornene-based double-comb diblock polymers with peptide and oligo(ethylene oxide) side chains aggregate in water to form unprecedented complex morphologies depending on the amino acid sequence of the peptide. The internal structures of the aggregates observed by cryo electron tomography show densely folded and highly branched wormlike micelles (left) and spherical aggregates with a bicontinuous architecture (right). Reproduced from ref.[120]

The internal structure of these bicontinuous nanospheres was investigated for the first time by Parry *et al.* with use of cryo-ET, with the structure being described as a branched network of worm-like hydrophobic peptide-containing segments segregated from channels of hydrated OEGME moieties.

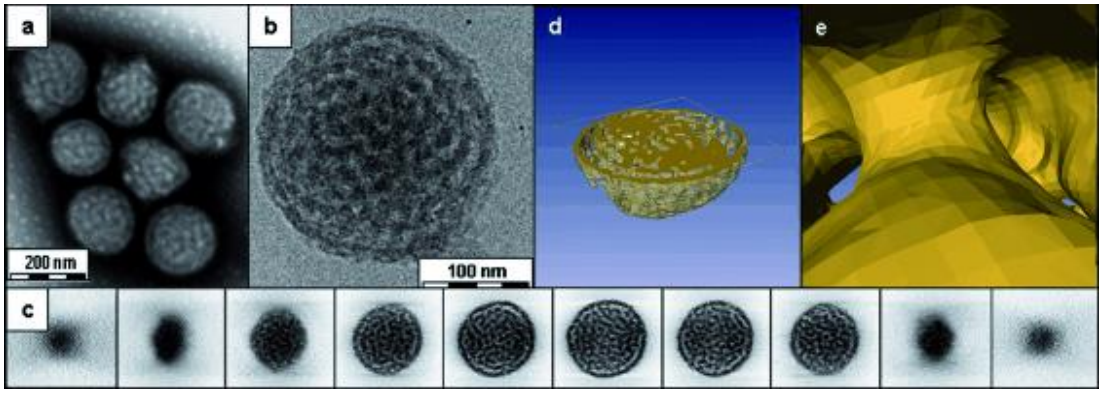

Figure 1.28: TEM analysis of aggregates of PNOEG–PNGLF (**1**). a) Conventional TEM using negative staining; b) cryoTEM image of a vitrified film; c) gallery of *z* slices showing different cross sections of a 3D SIRT (simultaneous iterative reconstruction technique) reconstruction of a tomographic series recorded from the vitrified film in (b); d,e) visualization of the segmented volume showing d) a cross section of the aggregate and e) a view from within the hydrated channels. Reproduced from ref. [120]

McKenzie *et al.*[122] reported the formation of bicontinuous nanospheres from semi-crystalline BCP PEO_{39}-*b*-$PODMA_{17}$ by dissolving it in THF followed by the slow addition of water at 35°C. The THF was later removed via dialysis against pure water at 35°C. It was found that an increase in the concentration of the BCP resulted in the increase in particle size, with a 0.1 wt % and 0.5 wt % solutions giving diameters of 275 and 350 nm respectively as determined by DLS. This polymer system is also temperature responsive due to the melting transition (T_m) of the semi-crystalline octadecyl chains upon the PODMA backbone. When heated above this melting transition the nanospheres undergoing an order-disorder transition of the microphase separated domains when heated above this melting transition. The morphology switches to planar oblate spheroids whose internal ordered microphase separated domains become disordered. This was established by vitrification of the nanospheres at 4 and 45°C followed by analysis with cryo-TEM (Figure 1.29).

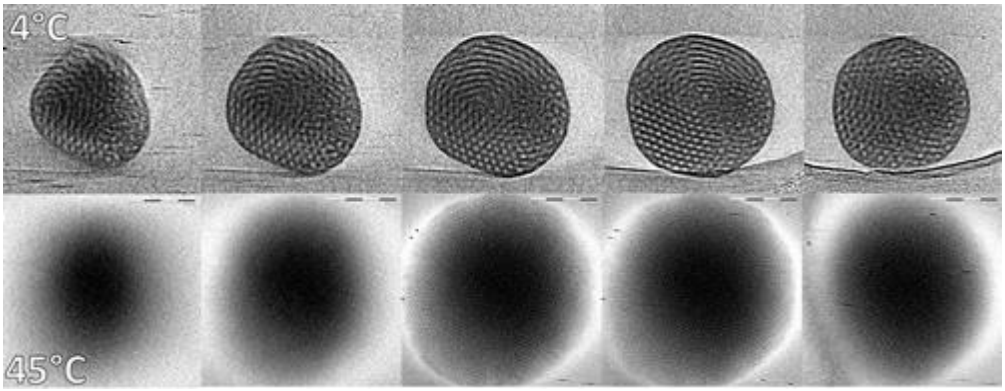

Figure 1.29: Gallery of z slices showing different cross sections of a bicontinuous nanosphere vitrified at 4 and 45°C.

The temperature-responsive nature of these nanospheres presented a promising possibility for their use in thermo-responsive drug delivery systems. Holder *et al.*[123] investigated the thermo-responsive controlled release of pyrene from these PEO-*b*-PODMA bicontinuous nanospheres. It was found that the bicontinuous nanospheres displayed controlled release of the pyrene and furthermore the release rate significantly increases when the measurement temperature was increased above PODMA's T_m (20-25°C) (Figure 1.30).

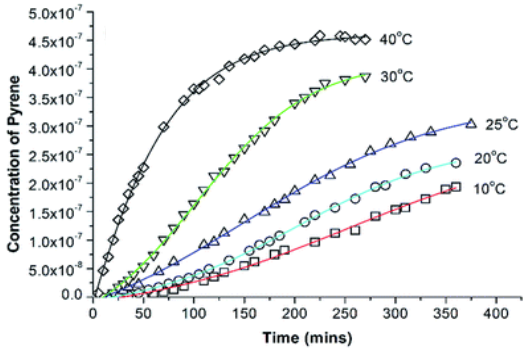

Figure 1.30: Release of pyrene from bicontinuous nanospheres formed from PEO_{45}-*b*-$PODMA_{20}$. Reproduced from ref.[123]

We recently reported the criteria for bicontinuous nanosphere (BN) formation via the construction of a phase diagram.[124] It was found that BNs will form from copolymers with molecular weights of <17 kDa and a hydrophilic weight fraction of ≤ 25 %. It was also established that size of the nanospheres could be tailored by altering the initial volume of THF used to dissolve the copolymer. Control of the internal pore sizes could be achieved simply by changing the initial volume of THF used to dissolve the copolymer. Control of the internal pore sizes was also observed with a decrease in pore size observed upon a decrease in the hydrophilic weight fraction.

1.3.3 Stimuli-responsive polymers for the controlled delivery of drugs

Stimuli-responsive polymers undergo a significant and abrupt change in their physical and/or chemical properties in response to an external stimulus. External stimulus such as pH, temperature, light, electric/magnetic fields or a bioresponsive stimuli such as glucose. Encapsulation of pharmaceuticals, in particular hydrophobic drugs, within these stimuli-responsive polymers allows the transport of hydrophobic drugs that have low water solubility. It also allows higher drug concentrations to be transported as encapsulation of the hydrophobic drugs within the hydrophobic core greatly increase their solubility. [91] The use of as stimuli-responsive polymer system as a nanocarriers allows control over the release of encapsulated active compounds.

1.3.3.1 pH-Responsive Polymers

Due to changes in pH throughout the body (Table 1.1), release of a pharmaceutical drug from a pH-responsive polymer system can be targeted to a certain tissue or cellular compartment.[125]

Table 1.1: pH in various tissues and cellular compartments. (reproduced from ref[125])

Tissue/Cellular Compartment	pH
Blood	7.35-7.45
Stomach	1.0-3.0
Duodenum	4.8-8.2
Colon	7.0-7.5
Early endosome	6.0-6.5
Late endosome	5.0-6.0
Lysosome	4.5-5.0
Golgi	6.4
Tumour	7.2-6.5

All pH-responsive polymers contain either weak acidic groups (e.g. carboxylic acids) and/or weak basic groups (e.g. ammonium salts). In response to an environmental change in pH these groups undergo protonation or deprotonation. Rapid change in the overall charge of the groups cause a change in the molecular structure of the polymer. As previously discussed it is the molecular structure that drives the

morphology. The functional groups along the polymer backbone undergo ionisation under specific pH conditions, this leads to a change in the polymer conformation resulting in swelling or dissolution of the polymer.[126] The most commonly used pH responsive acidic polymers are poly (acrylic acid) and poly (methacrylic acid).

Eisenberg and Lui reported the rapid pH triggered vesicle corona switching of triblock copolymer PAA-b-PS-b-P4VP in DMF/THF/H_2O mixtures. At pH 1, vesicles were present with the p4VP chains forming the corona. The PS and PAA (which were protonated and water insoluble) formed the core. As the pH increased the morphology changed from vesicles to solid spherical aggregates and back to vesicles at a pH of 14. At pH 14 the vesicles corona forming block was made up of the PAA chains which were now negatively charger and water soluble. The core therefore was made up of the P4VP and PS chains (Figure 1.31).[127]

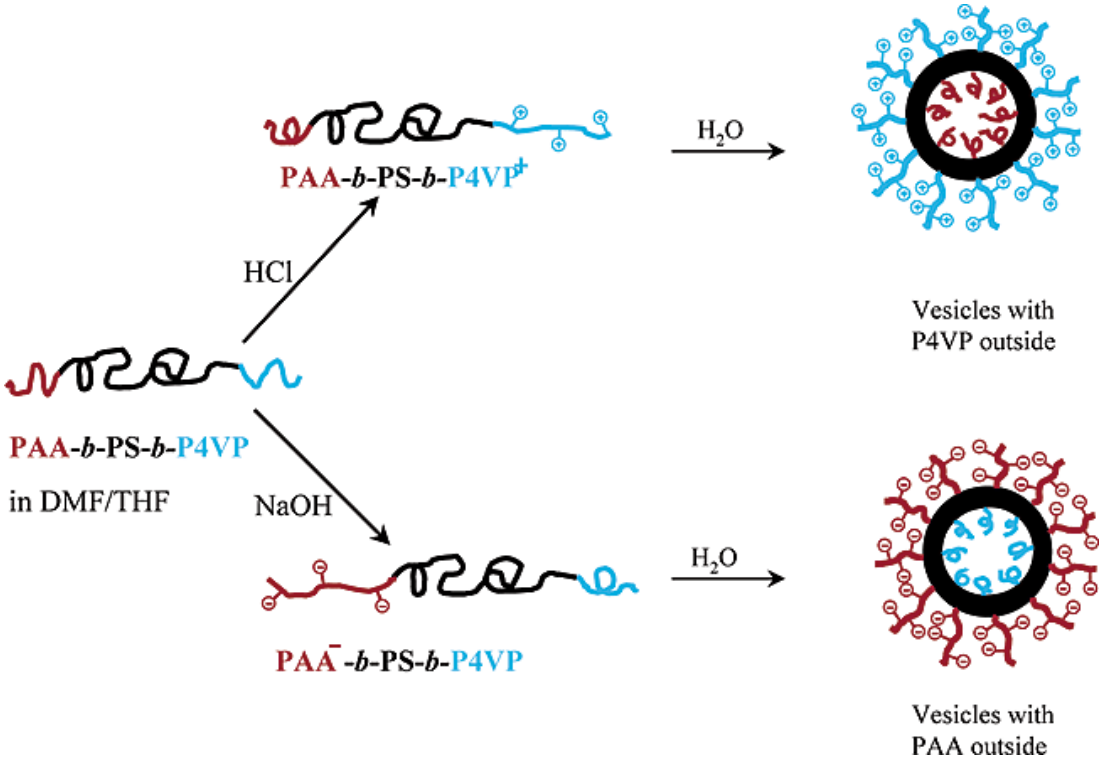

Figure 1.31: Schematic of the preparation of the two types of PAA-*b*-PS-*b*-P4VP vesicles. Reproduced from ref.[127]

pH-responsive polymer nanospheres have been used extensively in recent years for the encapsulation and subsequent release of active compounds.[128-130] In the case of polymer micelles this has been achieved by protonation of the hydrophobic core, this causes the micelle to disassemble, releasing the drug.[131] This behaviour has been

observed with polymer micelles of poly(ethylene glycol)-*b*-poly(alkyl acrylate-*co*-methacrylic acid) (PEG-*b*-P(AlA-*co*-MAA)). The carboxylic acid groups were deprotonated by increasing the pH causing the hydrophobic core to become hydrophilic, this resulted in dissociation of the assemblies and rapid release of the encapsulated hydrophobic progesterone.[132] Another response polymer nanoparticles have to pH is a change in membrane permeability upon a change in pH, as seen by Armes *et al.* with poly(ethylene oxide)-b-poly[2-(diethylamino)ethyl methacrylate-*s*-3-(trimethoxysilyl)propyl methacrylate] (PEO-*b*-P(DEA-*s*-TMSPMA)) vesicles where a decrease in pH resulted in increased permeability due to the PDEA being protonated and therefore becoming protonated. The process was reversible upon an increase in pH. [133]

1.3.3.2 Temperature responsive polymers

Drug delivery can be triggered by a change in temperature either by an increase in body temperature due to disease or by a modulated external temperature.[125] Temperature-responsive polymers are one of the most studied stimuli for biomedical applications.[134] The most common property related to temperature responsive polymers is their LCST and UCST. The LCST is the critical point below which (lower critical solution temperature) the polymer and solvent are miscible. When the polymer solution is heated above the LCST they become immiscible. The Upper Critical solution temperature is the critical point where an immiscible polymer solution becomes miscible (Figure 1.32).[129]

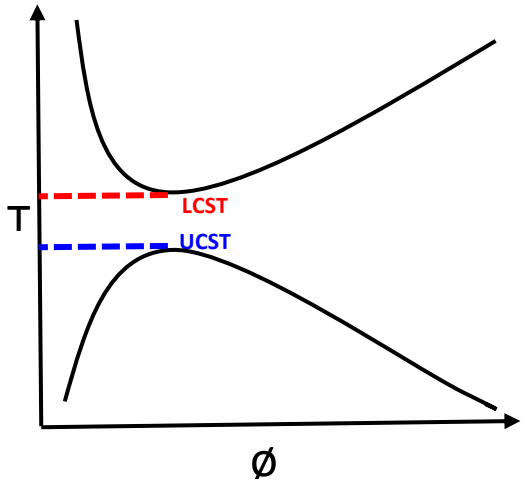

Figure 1.32: Temperature v ø (polymer volume fraction) phase diagram of polymer solutions LCST and UCST behaviour.

The thermo-responsive nature of the polymers can trigger drug release but may also be a trigger for the formation of the aggregates. The most commonly used polymer that presents an LCST is poly(*N*-isopropylacrylamide) (PNIPAAm) due to its LCST occurring around body temperature (32°C)[135] and that the LCST can be easily adjusted to an appropriate temperature. PNIPAAms LCST has been adjusted by copolymerisation with hydrophobic or hydrophilic monomers. The incorporation of a hydrophobic monomer will decrease the LCST and inclusion of a hydrophilic monomer will increase it. This was seen by Kuckling *et al.*[136] with the copolymer P(NIPAAm-*co*-C_nAAm) where an increase in the hydrophilic comonomer (C_nAAm) content (mol %) resulted in a decrease in the phase transition temperature of PNIPAAm, with phase transition temperatures obtained from 10 to 32°C. When a solution of a hydrophilic-hydrophilic BCP (one of the block being PNIPAAm) is heated above PNIPAAms LCST the thermo-responsive block becomes hydrophobic, causing the BCP to act as an amphiphile and self-assemble. This process is reversible with a decrease in solution temperature below the LCST.[137] The LCST is also dependent upon the molecular weight and architecture of the polymer. [138]

An example of the use of PNIPAAm as a thermo-responsive block in a hydrophilic-hydrophilic BCP was reported by Qin *et al*. with the BCP PEO-*b*-PNIPAAm. When the BCP was heated above PNIPAAms LCST vesicles formed with the encapsulation of the hydrophilic anticancer drug doxorubicin and inclusion of a hydrophobic fluorescent dye into their membranes, due to PNIPAAm becoming hydrophobic. When the vesicles were cooled below the LCST PNIPAAm becomes hydrophilic and the vesicles disassembled to release the dye (Figure 1.33).[139]

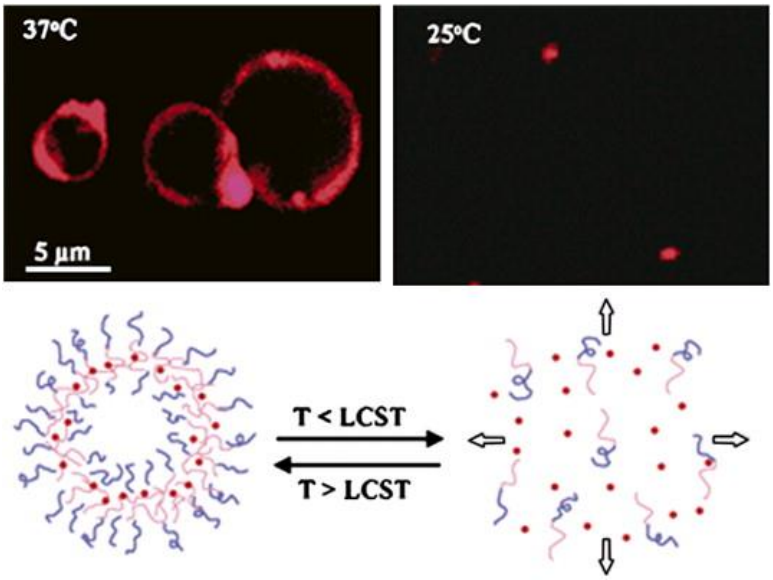

Figure 1.33: Narrow-dispersity thermoresponsive block copolymers of poly(ethylene oxide)-*block*-poly(*N*-isopropylacrylamide) self-assemble into vesicles at temperatures above 32 °C. The vesicles integrate a hydrophobic fluorescent dye into their membranes and encapsulate the hydrophilic anticancer drug doxorubicin. Temperature-controlled release of the dye through disintegration of the vesicles takes place at temperatures below 32 °C, as shown in the figure. Reproduced from ref.[139]

The opposite effect was observed for the PNIPAAm-*b*-PMMA polymer system. Below PNIPAAms LCST the BCP formed micelles due to the PNIPAAm being hydrophilic and the PMMA block being hydrophobic. Upon an increase in temperature above the LCST the PNIPAAm block became hydrophobic dispersing the polymer chains and releasing the encapsulated anti-inflammatory drug (Figure 1.34).[140]

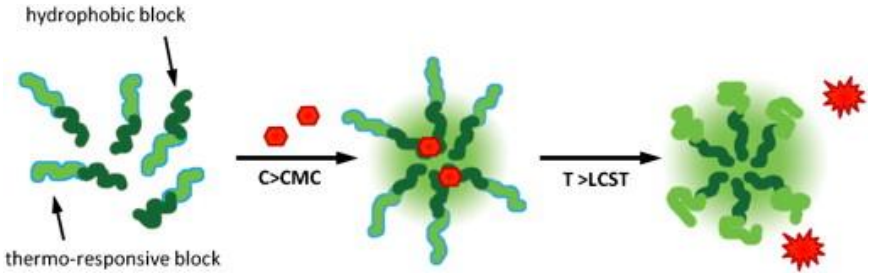

Figure 1.34: Drug encapsulation and release from a thermo-responsive polymer micelle. Reproduced from ref.[131]

Other typical ΔT responsive polymers are poly(N,N-diethylacrylamide) (PDEAM),[141] poly(*N*,*N*- methylvinylether) (PMVE), and poly(*N*-vinylcaprolactam) (PNVCl)[142] and poly(ethylene oxide)-*block*-poly(p-phenylene oxide) (PEO-*b*-PPO).[143] In these

examples the LCST's lie between 30-37°C with the exception of PEO-*b*-PPO which has a large range in LCST of 20-80°C.[129]

The LCST is not the only property of polymers that will produce a response to a change in temperature. The melting transition of one of the blocks in BCPs can be employed to produce a response. An example of this is with the BCP poly(trimethylene carbonate)-*b*-poly(L-glutamic acid) (PTMC-*b*-PGA). PTMC-*b*-PGA was self-assembled to encapsulate the anti-cancer drug doxorubicin. Release profiles of the drug were obtained at various temperatures and showed an increased rate of release with a temperature above the T_m of the PTMC. This was due to an increase in the membrane permeability of the vesicles.[144] Another thermo-responsive polymer that exhibits its responsiveness due to the polymers T_m is PEO-*b*-PODMA which self-assembled to form bicontinuous nanospheres. The PODMA block exhibits a melting transition due to the crystallinity of the long alkyl side chains attached to the methacrylate backbone. As previously discussed the release of pyrene from these bicontinuous nanospheres increases significantly when the polymer is heated above PODMA's T_m.[123] Unlike the linear T_m responsive PTMC, the use of semi-crystalline side chains offers the opportunity to control the thermo-responsive nature of the polymer system by manipulation of the T_m with a change in alkyl side chain length.

1.3.3.3 Other Responsive Polymers

Bio-responsive polymer systems are becoming increasingly more important for use as nanocarriers. The main advantage is that they respond to the stimuli present in the body (i.e. natural stimuli).[145] The response of a polymer system to glucose is not normally a direct one. The incorporation of glucose oxidase (GOx) in the polymer system leads to enzymatic oxidation of glucose, this produces gluconic acid and H_2O_2. A pH responsive polymer is typically used that reacts to the change in pH due to the production of gluconic acid.[146] An example of this is the covalent modification of a cellulose film to include GOx conjugated with PAA. As the levels of glucose in the blood rise the GOx causes the glucose to be converted to gluconic acid and this in turn causes the protonation of the PAA releasing insulin (Figure 1.35).[147] Glucose

responsiveness has also been seen in hydrogel systems where a combination of pH, glucose an temperature responses were used.[148]

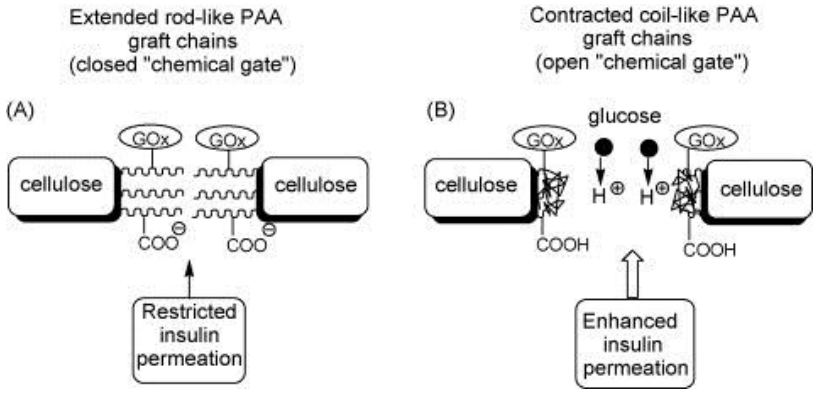

Figure 1.35: (A) In the absence of glucose, the PAA chains are extended which lowers the permeability of the membrane. (B) Addition of glucose leads to a lowering of local pH and chain collapse due to a reduction in electrostatic repulsion. Reproduced from ref.[147]

Light-responsive polymer micelles can be used for the transport of drugs. The light response is usually by use of a linker that will be cleaved upon irradiation with light of a certain wavelength. The advantages of a light-responsive carrier is that the release of a drug can be controlled so that an early release or activation is avoided as the drug is only being release once irradiated with light from outside the body. An example of a light sensitive nanocarriers was reported by Jiang *et al.* where the BCP PEO-*b*-PMA with an attached pyrene derivative was irradiated with UV light. The pyrene groups were cleaved and turned the hydrophobic core hydrophilic causing the dissolution of the micelle and release of Nile red.[149]

Other responsive polymer nanocarriers include ultrasonic-responsive,[150] magnetic field-responsive,[151] electrical field-responsive[152] and ion-responsive[153] who release their encapsulated drug after the stimuli has been applied.

1.4 Instrumentation

1.4.1 Dynamic Light Scattering

Dynamic Light Scattering (DLS) measurements were obtained on a Malvern High Performance Particle Sizer (Nano Zetasizer HPPS HPP5001) with a laser at a wavelength of 633 nm. The measurements were taken using a clean quartz cuvette containing a 1 mL sample. Measurements were taken at both 15 and 35°C, the temperature was set and the machine was left to settle at this temperature for 10 minutes, after this 10 measurements were taken and an average was obtained.

Dynamic light scattering (DLS) is used to establish particle, molecular size, the distribution of the particles and the relaxations in complex fluids. DLS is a good technique because it is non-invasive/destructive, it only requires a small sample quantity, it can detect low concentrations and detect particles from submicron to as small as 1nm.

The Brownian motion of particles causes the laser light to be scattered at different intensities, which yields the velocity of Brownian motion. This can then be used to establish the particle size using Stokes-Einstein relationship, where D_h is the hydrodynamic diameter (particle size), D_t is the diffusion coefficient, k_B is the Boltzmann constant, T is thermodynamic temperature and η is the dynamic viscosity.[154]

$$D_h = \frac{k_B T}{3\pi \eta D_t}$$

Equation 1.2: Stokes-Einstein relationship

DLS uses the data gathered from the scattering of a laser on a microsecond timescale to determine the hydrodynamic diameter. The light from the laser illuminates the sample and the light scatter is detected using the right angle detector (90°) or the backscatter detector (173°) or both. The advantage of the backscatter detector is that it has a wider measurement volume and can measure a larger concentration range, therefore it can be used to measure a more concentrated sample. The right angle detector is more sensitive to larger particles.

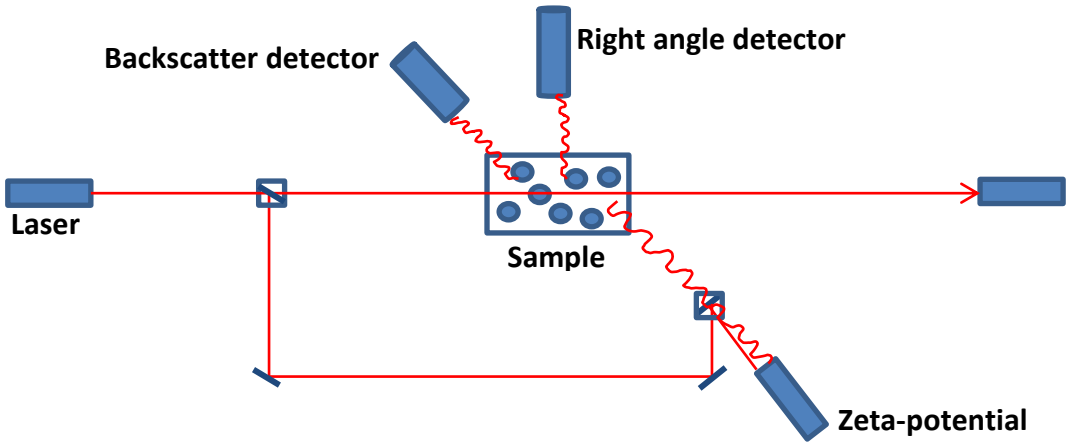

Figure 1.36: Dynamic Light Scattering Schematic

An optical signal is given which has random fluctuations due to the position of the particles changing inconsistently. The signal is then interpreted in terms of an autocorrelation function (ACF). The autocorrelation function pinpoints repeating patterns within the signal, for example when a periodic signal is being obscured by noise. The incoming data is processed in real time, producing the autocorrelation function as a function of delay time, τ. The faster the decay the smaller the particles are. This is because larger particles move slower through solution.[154]

A different calculation is done when the particles are all the same size compared with a mix of particle sizes. For a sample with particles of equal size the decay of the ACF is used to determine particle size in the following way.

$$C = \exp(-2\Gamma\tau)$$

Equation 1.3: Exponential decay of autocorrelation function

C is the baseline subtracted autocorrelation function, Γ is the decay constant which is derived from applying a curve fit to the experimental data as seen in figure 1.37 below.

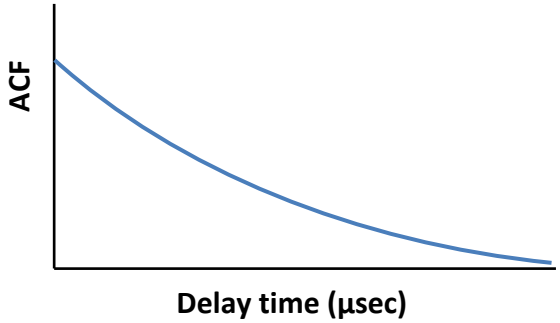

Figure 1.37: The decay of the autocorrelation function

Once the decay constant has been established the diffusion coefficient, D_t, can be calculated using equation 1.4.

$$\Gamma = D_t q^2$$

Equation 1.4: Relationship between diffusion coefficient and the decay constant.

The scattering vector, q, can be defined using equation 4 describes the wavelength of the laser light used, λ, the scattering angle, θ and takes into account the refractive index of the solvent. The particle size (hydrodynamic diameter) can then be determined by inserting the calculated diffusion coefficient into the Stokes-Einstein equation (equation 1.5).

$$q = (\frac{4\pi n}{\lambda}) \sin(\frac{\theta}{2})$$

Equation 1.5: Defining the scattering vector

Where there is a sample with a distribution of particle sizes the exponential decay is rewritten so that the linear decay constant is proportional to the average diffusion coefficient this is then interpreted to establish the average particle size. What is different is that particle size is a weighted mean size known as the z-average, this means that the DLS actually calculates the intensity weighted diffusion coefficient which means that the particle size can be thought as intensity weighted harmonic mean size. As the z-average increases this is directly proportional to the particle size.

1.4.2 Differential Scanning Calorimetry

DSC is a thermo-analytical technique that measures the phase transitions of a sample. In this case the sample to be measured and the reference are sealed in an aluminium crucible and placed on individual thermoelectric disks. The sample and reference are heated and a linear rate as a function of time. The heat capacity of the sample leads to a difference in temperature between the samples and the reference pans. More or less heat is needed to maintain the reference and the sample pan at the same temperature. This difference is recorded and the heat flow can then be determined using the thermal equivalent of Ohm's law:

$$q = \frac{\Delta T}{R}$$

Equation 1.6: Ohm's law to determine heat flow

Where q is the heat flow of the sample, ΔT is the difference in temperature between the sample and the reference and R is the resistance of the thermoelectric disk. The enthalpy of the phase transition can also be measured using the following equation:

$$\Delta H = kA$$

Equation 1.7: Equation for the change in enthalpy of the phase transition.

Where *k* is the calorimetric constant and A is the area under the curve.

1.4.3 Transmission Electron Microscopy

Conventional TEM has been widely used for the imaging of polymer particles. The polymer aggregate solution is dried onto a carbon coated grid (the substrate) and a beam of electrons is transmitted through the specimen. A contrast between the substrate and the particles is needed for a clear image and this can be obtained when there is either a difference in the number of scattered electrons or from changes of the phase of the electron waves. For particles to be observed the sample should scatter more electrons than the carbon coating. The carbon coating is typically around 40 nm thick this means that there will be little contrast between a carbon based polymer particle that is around 40 nm in size and the substrate.[155] Therefore for imaging of polymer particles with conventional TEM staining the sample with a high atomic number compound such as uranyl acetate is necessary, this will selectively bind to the grid giving an enhanced contrast between the grid and the particle (negative staining) or bind to the amorphous regions of the polymer (positive staining).[156]

Analysis of the polymer particles with TEM in the dry state is preferred due to the fact that TEMs operate with internal pressure of < 10^{-10} Pa.[155] The downside with conventional staining TEM is the removal of water from the sample when the sample is dried onto the grid, this can cause a collapse of the structure and means that the particles morphology is not viewed in its natural solvated environment.[157] The use of negative staining can conceal the complex internal morphologies of the polymer

particles[158] and/or interact with the polymer causing deformations or a change in morphology.[159, 160] The use of cryo-TEM can overcome these issues seen with conventional TEM. Cryo-TEM allows the sample to be analysed in situ and can prevent any deformation of the sample through vitrification of the sample.[161]

The polymer aggregate solution is applied to a TEM grid. The grid is then blotted with filter paper to create a thin film.[155] The sample is plunge-frozen into a cryogen solvent (normally liquid ethane at -183°C), this traps the particles in a thin layer of ice which is transparent to the electron beam.[157] Figure 1.37 shows a schematic of the cryo-TEM sample preparation. Once the vitrified sample has been prepared it must be kept at cryogenic temperatures for imaging, this prevents the formation of cubic or hexagonal ice that can obscure the image of the particles.[162]

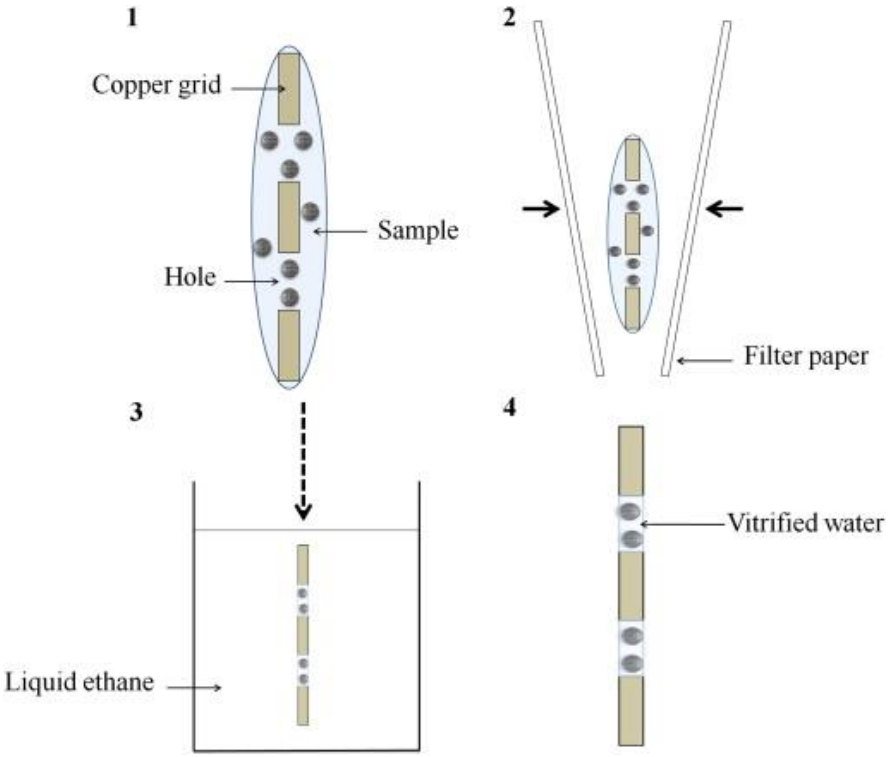

Figure 1.37: Schematic of cryo-TEM sample preparation. Reproduced from ref.[158]

Although cryo-TEM has great advantages over conventional negatively stained TEM it does have the disadvantage that the images obtained are 2D images of 3D objects. Therefore the internal features may be overlapping obscuring the overall morphology and may lead to false interpretations.[163] To overcome this disadvantage,

cryogenic transmission electron tomography (cryo-ET) has been employed to obtain structural information in 3D.[157] In Cryo-ET, a series of TEM images are acquired at different tilt angles. These images are then combined and the 3D particle is reconstructed.[157] Cryo-ET can be used therefore to investigate the internal structure of polymer nanospheres. The first example of this was carried out by Parry *et al.* where cryo-ET was used to reconstruct the internal morphology of a PNOEG-*b*-PNGLF bicontinuous nanospheres (Figure 1.38).[120] Cryo-ET is not yet widely used for investigations into the internal structures of polymer nanospheres which is most likely due to its complex nature and extensive analysis time, however it is a promising emerging technique.

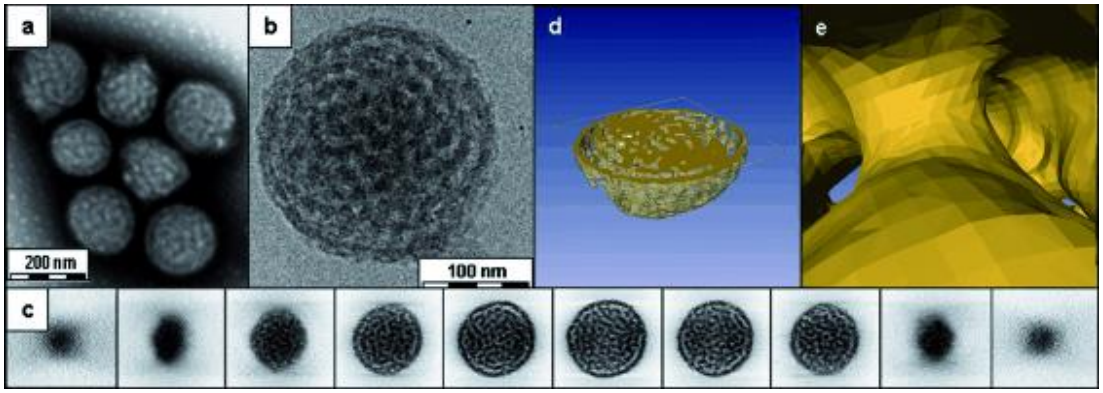

Figure 1.38: TEM analysis of aggregates of PNOEG–PNGLF (1). **a)** Conventional TEM using negative staining; **b)** cryoTEM image of a vitrified film; **c)** gallery of *z* slices showing different cross sections of a 3D SIRT (simultaneous iterative reconstruction technique) reconstruction of a tomographic series recorded from the vitrified film in (b); **d,e)** visualization of the segmented volume showing d) a cross section of the aggregate and e) a view from within the hydrated channels Reproduced from ref.[120]

1.5 References

1. D. Walton, P. L., *Polymers*. Oxford University Press: United States of America, 2000.

2. J.M.G. Cowie, V. A., *Polymers: Chemistry and Physics of Modern Materials*. CRC Press: United States of America, 2008.

3. Fried, J. R., *Polymer Science and Technology*. Prentice Hall Professional Technical Reference: United States of America, 2003.

4. Shenoi, R. A.; Narayanannair, J. K.; Hamilton, J. L.; Lai, B. F. L.; Horte, S.; Kainthan, R. K.; Varghese, J. P.; Rajeev, K. G.; Manoharan, M.; Kizhakkedathu, J. N., Branched Multifunctional Polyether Polyketals: Variation of Ketal Group Structure Enables Unprecedented Control over Polymer Degradation in Solution and within Cells. *Journal of the American Chemical Society* **2012,** *134* (36), 14945-14957.

5. Snijkers, F.; Vlassopoulos, D.; Ianniruberto, G.; Marrucci, G.; Lee, H.; Yang, J.; Chang, T., Double Stress Overshoot in Start-Up of Simple Shear Flow of Entangled Comb Polymers. *ACS Macro Letters* **2013,** *2* (7), 601-604.

6. Holder, S. J.; Sommerdijk, N., New micellar morphologies from amphiphilic block copolymers: disks, toroids and bicontinuous micelles. *Polymer Chemistry* **2011,** *2* (5), 1018-1028.

7. He, E.; Yue, C. Y.; Tam, K. C., Association Behavior of Star-Shaped pH-Responsive Block Copolymer: Four-Arm Poly(ethylene oxide)-b-Poly(methacrylic acid) in Aqueous Medium. *Langmuir* **2009,** *25* (9), 4892-4899.

8. Greszta, D.; Mardare, D.; Matyjaszewski, K., Living Radical Polymerization .1. Possibilities And Limitations. *Macromolecules* **1994,** *27* (3), 638-644.

9. Kato, M.; Kamigaito, M.; Sawamoto, M.; Higashimura, T., Polymerization of Methyl-Methacrylate with the Carbon-Tetrachloride Dichlorotris(Triphenylphosphine)Ruthenium(Ii) Methylaluminum Bis(2,6-Di-Tert-

Butylphenoxide) Initiating System - Possibility of Living Radical Polymerization. *Macromolecules* **1995,** *28* (5), 1721-1723.

10. Matyjaszewski, K.; Spanswick, J., Controlled/living radical polymerization. *Materials Today* **2005,** *8* (3), 26-33.

11. Matyjaszewski, K.; Xia, J. H., Atom transfer radical polymerization. *Chemical Reviews* **2001,** *101* (9), 2921-2990.

12. Wang, J. S.; Matyjaszewski, K., Living Controlled Radical Polymerization - Transition-Metal-Catalyzed Atom-Transfer Radical Polymerization In the Presence of a Conventional Radical Initiator. *Macromolecules* **1995,** *28* (22), 7572-7573.

13. Wang, J. S.; Matyjaszewski, K., Controlled Living Radical Polymerization - Atom-Transfer Radical Polymerization In the Presence of Transition-Metal Complexes. *Journal of the American Chemical Society* **1995,** *117* (20), 5614-5615.

14. Qiu, J.; Charleux, B.; Matyjaszewski, K., Progress in controlled/living polymerization in aqueous media Part I. Principles and methods. *Polimery* **2001,** *46* (7-8), 453-460.

15. Sawamoto, M.; Kamigaito, M., Living radical polymerization based on transition metal complexes. *Trends in Polymer Science* **1996,** *4* (11), 371-377.

16. Matyjaszewski, K., Mechanistic and synthetic aspects of atom transfer radical polymerization. *Journal of Macromolecular Science-Pure and Applied Chemistry* **1997,** *A34* (10), 1785-1801.

17. Braunecker, W. A.; Matyjaszewski, K., Controlled/living radical polymerization: Features, developments, and perspectives. *Progress in Polymer Science* **2007,** *32* (1), 93-146.

18. Matyjaszewski, K., Controlled radical polymerization. *Current Opinion in Solid State & Materials Science* **1996,** *1* (6), 769-776.

19. Tsarevsky, N. V.; Sumerlin, B. S., *Fundamentals of Controlled/Living Radical Polymerization.* Royal Society of Chemistry: 2012.

20. Wang, J. S.; Matyjaszewski, K., Controlled Living Radical Polymerization - Halogen Atom-Transfer Radical Polymerization Promoted by A Cu(I)Cu(Ii) Redox Process. *Macromolecules* **1995,** *28* (23), 7901-7910.

21. Gaynor, S. G.; Wang, J. S.; Matyjaszewski, K., Controlled Radical Polymerization by Degenerative Transfer - Effect of the Structure of the Transfer Agent. *Macromolecules* **1995,** *28* (24), 8051-8056.

22. Qiu, J.; Charleux, B.; Matyjaszewski, K., Progress in controlled/living polymerization in aqueous media. Part I. Principles and methods. *Polimery (Warsaw, Pol.)* **2001,** *46* (Copyright (C) 2014 American Chemical Society (ACS). All Rights Reserved.), 453-460.

23. Nicolas, J.; Guillaneuf, Y.; Lefay, C.; Bertin, D.; Gigmes, D.; Charleux, B., Nitroxide-mediated polymerization. *Progress in Polymer Science* **2013,** *38* (1), 63-235.

24. Keddie, D. J., A guide to the synthesis of block copolymers using reversible-addition fragmentation chain transfer (RAFT) polymerization. *Chemical Society Reviews* **2014,** *43* (2), 496-505.

25. Matyjaszewski, K.; Tsarevsky, N. V., Macromolecular Engineering by Atom Transfer Radical Polymerization. *Journal of the American Chemical Society* **2014,** *136* (18), 6513-6533.

26. Percec, V.; Guliashvili, T.; Ladislaw, J. S.; Wistrand, A.; Stjerndahl, A.; Sienkowska, M. J.; Monteiro, M. J.; Sahoo, S., Ultrafast Synthesis of Ultrahigh Molar Mass Polymers by Metal-Catalyzed Living Radical Polymerization of Acrylates, Methacrylates, and Vinyl Chloride Mediated by SET at 25 °C. *Journal of the American Chemical Society* **2006,** *128* (43), 14156-14165.

27. Wang, J.-S.; Matyjaszewski, K., Controlled/"Living" Radical Polymerization. Halogen Atom Transfer Radical Polymerization Promoted by a Cu(I)/Cu(II) Redox Process. *Macromolecules* **1995,** *28* (23), 7901-7910.

28. Matyjaszewski, K.; Shipp, D. A.; Wang, J.-L.; Grimaud, T.; Patten, T. E., Utilizing Halide Exchange To Improve Control of Atom Transfer Radical Polymerization. *Macromolecules* **1998,** *31* (20), 6836-6840.

29. Wang, Y.; Kwak, Y.; Buback, J.; Buback, M.; Matyjaszewski, K., Determination of ATRP Equilibrium Constants under Polymerization Conditions. *ACS Macro Letters* **2012,** *1* (12), 1367-1370.

30. Braunecker, W. A.; Matyjaszewski, K., Recent mechanistic developments in atom transfer radical polymerization. *Journal of Molecular Catalysis A: Chemical* **2006,** *254* (1–2), 155-164.

31. Matyjaszewski, K., Atom Transfer Radical Polymerization (ATRP): Current Status and Future Perspectives. *Macromolecules* **2012,** *45* (10), 4015-4039.

32. Patten, T. E.; Matyjaszewski, K., Atom transfer radical polymerization and the synthesis of polymeric materials. *Advanced Materials* **1998,** *10* (12), 901-+.

33. Matyjaszewski, K.; Nanda, A. K.; Tang, W., Effect of [CuII] on the Rate of Activation in ATRP. *Macromolecules* **2005,** *38* (5), 2015-2018.

34. Coca, S.; Jasieczek, C. B.; Beers, K. L.; Matyjaszewski, K., Polymerization of acrylates by atom transfer radical polymerization. Homopolymerization of 2-hydroxyethyl acrylate. *Journal of Polymer Science Part A: Polymer Chemistry* **1998,** *36* (9), 1417-1424.

35. Matyjaszewski, K.; Xia, J., Atom Transfer Radical Polymerization. *Chemical Reviews* **2001,** *101* (9), 2921-2990.

36. Muñoz-Bonilla, A.; León, O.; Cerrada, M. L.; Rodríguez-Hernández, J.; Sánchez-Chaves, M.; Fernández-García, M., Chemical modification of block copolymers based on 2-hydroxyethyl acrylate to obtain amphiphilic glycopolymers. *European Polymer Journal* **2015,** *62*, 167-178.

37. Zhang, X.; Xia, J.; Matyjaszewski, K., Atom transfer radical polymerization of protected methacrylic acids. *Polym. Prepr. (Americal Chemical Society, Division Polymer Chemistry)* **1999,** *40* (2), 440-441.

38. Tang, W.; Kwak, Y.; Braunecker, W.; Tsarevsky, N. V.; Coote, M. L.; Matyjaszewski, K., Understanding Atom Transfer Radical Polymerization: Effect of Ligand and Initiator Structures on the Equilibrium Constants. *Journal of the American Chemical Society* **2008,** *130* (32), 10702-10713.

39. Ayres, N., Atom Transfer Radical Polymerization: A Robust and Versatile Route for Polymer Synthesis. *Polymer Reviews* **2011,** *51* (2), 138-162.

40. Gillies, M. B.; Matyjaszewski, K.; Norrby, P.-O.; Pintauer, T.; Poli, R.; Richard, P., A DFT Study of R−X Bond Dissociation Enthalpies of Relevance to the Initiation Process of Atom Transfer Radical Polymerization. *Macromolecules* **2003,** *36* (22), 8551-8559.

41. Tang, W.; Matyjaszewski, K., Effects of Initiator Structure on Activation Rate Constants in ATRP. *Macromolecules* **2007,** *40* (6), 1858-1863.

42. Granel, C.; Dubois, P.; Jérôme, R.; Teyssié, P., Controlled Radical Polymerization of Methacrylic Monomers in the Presence of a Bis(ortho-chelated) Arylnickel(II) Complex and Different Activated Alkyl Halides. *Macromolecules* **1996,** *29* (27), 8576-8582.

43. Lecomte, P.; Drapier, I.; Dubois, P.; Teyssié, P.; Jérôme, R., Controlled Radical Polymerization of Methyl Methacrylate in the Presence of Palladium Acetate, Triphenylphosphine, and Carbon Tetrachloride. *Macromolecules* **1997,** *30* (24), 7631-7633.

44. Kabachii, Y. A.; Kochev, S. Y.; Bronstein, L. M.; Blagodatskikh, I. B.; Valetsky, P. M., Atom Transfer Radical Polymerization with Ti(III) Halides and Alkoxides. *Polymer Bulletin* **2003,** *50* (4), 271-278.

45. Niibayashi, S.; Hayakawa, H.; Jin, R.-H.; Nagashima, H., Reusable and environmentally friendly ionic trinuclear iron complex catalyst for atom transfer radical polymerization. *Chemical Communications* **2007,** (18), 1855-1857.

46. Ishio, M.; Katsube, M.; Ouchi, M.; Sawamoto, M.; Inoue, Y., Active, Versatile, and Removable Iron Catalysts with Phosphazenium Salts for Living Radical Polymerization of Methacrylates(1). *Macromolecules* **2009,** *42* (1), 188-193.

47. Tang, W.; Matyjaszewski, K., Effect of Ligand Structure on Activation Rate Constants in ATRP. *Macromolecules* **2006,** *39* (15), 4953-4959.

48. Konkolewicz, D.; Magenau, A. J. D.; Averick, S. E.; Simakova, A.; He, H.; Matyjaszewski, K., ICAR ATRP with ppm Cu Catalyst in Water. *Macromolecules* **2012,** *45* (11), 4461-4468.

49. Matyjaszewski, K.; Nakagawa, Y.; Jasieczek, C. B., Polymerization of n-Butyl Acrylate by Atom Transfer Radical Polymerization. Remarkable Effect of Ethylene Carbonate and Other Solvents. *Macromolecules* **1998,** *31* (5), 1535-1541.

50. Horn, M.; Matyjaszewski, K., Solvent Effects on the Activation Rate Constant in Atom Transfer Radical Polymerization. *Macromolecules* **2013,** *46* (9), 3350-3357.

51. Matyjaszewski, K., Inner sphere and outer sphere electron transfer reactions in atom transfer radical polymerization. *Macromolecular Symposia* **1998,** *134* (1), 105-118.

52. Jakubowski, W.; Min, K.; Matyjaszewski, K., Activators Regenerated by Electron Transfer for Atom Transfer Radical Polymerization of Styrene. *Macromolecules* **2006,** *39* (1), 39-45.

53. Jakubowski, W.; Matyjaszewski, K., Activator Generated by Electron Transfer for Atom Transfer Radical Polymerization. *Macromolecules* **2005,** *38* (10), 4139-4146.

54. Jakubowski, W.; Matyjaszewski, K., Activators Regenerated by Electron Transfer for Atom-Transfer Radical Polymerization of (Meth)acrylates and Related Block Copolymers. *Angewandte Chemie International Edition* **2006,** *45* (27), 4482-4486.

55. Min, K.; Gao, H.; Matyjaszewski, K., Use of Ascorbic Acid as Reducing Agent for Synthesis of Well-Defined Polymers by ARGET ATRP. *Macromolecules* **2007,** *40* (6), 1789-1791.

56. Matyjaszewski, K.; Jakubowski, W.; Min, K.; Tang, W.; Huang, J.; Braunecker, W. A.; Tsarevsky, N. V., Diminishing catalyst concentration in atom transfer radical polymerization with reducing agents. *Proceedings of the National Academy of Sciences* **2006,** *103* (42), 15309-15314.

57. Samanta, S. R.; Anastasaki, A.; Waldron, C.; Haddleton, D. M.; Percec, V., SET-LRP of methacrylates in fluorinated alcohols. *Polymer Chemistry* **2013,** *4* (22), 5563-5569.

58. Rosen, B. M.; Percec, V., Single-Electron Transfer and Single-Electron Transfer Degenerative Chain Transfer Living Radical Polymerization. *Chemical Reviews* **2009,** *109* (11), 5069-5119.

59. Bai, Z.; Lodge, T. P., Polymersomes with Ionic Liquid Interiors Dispersed in Water. *Journal of the American Chemical Society* **2010,** *132* (45), 16265-16270.

60. Albert, J. N. L.; Epps, T. H., Self-assembly of block copolymer thin films. *Materials Today* **2010,** *13* (6), 24-33.

61. Discher, B. M.; Hammer, D. A.; Bates, F. S.; Discher, D. E., Polymer vesicles in various media. *Current Opinion in Colloid & Interface Science* **2000,** *5* (1–2), 125-131.

62. Mai, Y.; Eisenberg, A., Self-assembly of block copolymers. *Chemical Society Reviews* **2012,** *41* (18), 5969-5985.

63. Du, J.; O'Reilly, R. K., Advances and challenges in smart and functional polymer vesicles. *Soft Matter* **2009,** *5* (19), 3544-3561.

64. Zhang, L.; Eisenberg, A., Multiple Morphologies of "Crew-Cut" Aggregates of Polystyrene-b-poly(acrylic acid) Block Copolymers. *Science* **1995,** *268* (5218), 1728-1731.

65. Shum, H. C.; Kim, J.-W.; Weitz, D. A., Microfluidic Fabrication of Monodisperse Biocompatible and Biodegradable Polymersomes with Controlled Permeability. *Journal of the American Chemical Society* **2008,** *130* (29), 9543-9549.

66. Decher, G., Fuzzy nanoassemblies: toward layered polymeric multicomposites. *Science (Washington, D. C.)* **1997,** *277* (5330), 1232-1237.

67. Menger, F. M.; Angelova, M. I., Giant Vesicles: Imitating the Cytological Processes of Cell Membranes. *Accounts of Chemical Research* **1998,** *31* (12), 789-797.

68. Warren, N. J.; Armes, S. P., Polymerization-Induced Self-Assembly of Block Copolymer Nano-objects via RAFT Aqueous Dispersion Polymerization. *Journal of the American Chemical Society* **2014,** *136* (29), 10174-10185.

69. Gao, Z.; Varshney, S. K.; Wong, S.; Eisenberg, A., Block Copolymer "Crew-Cut" Micelles in Water. *Macromolecules* **1994,** *27* (26), 7923-7927.

70. Mishra, A. K., *Nanomedicine for Drug Delivery and Therapeutics*. Wiley: 2013.

71. Allen, C.; Maysinger, D.; Eisenberg, A., Nano-engineering block copolymer aggregates for drug delivery. *Colloids and Surfaces B: Biointerfaces* **1999,** *16* (1–4), 3-27.

72. Riess, G., Micellization of block copolymers. *Progress in Polymer Science* **2003,** *28* (7), 1107-1170.

73. Higuchi, T.; Shimomura, M.; Yabu, H., Reorientation of Microphase-Separated Structures in Water-Suspended Block Copolymer Nanoparticles through Microwave Annealing. *Macromolecules* **2013,** *46* (10), 4064-4068.

74. Discher, D. E.; Eisenberg, A., Polymer vesicles. *Science* **2002,** *297* (5583), 967-973.

75. Shen, H.; Eisenberg, A., Morphological Phase Diagram for a Ternary System of Block Copolymer PS310-b-PAA52/Dioxane/H2O. *The Journal of Physical Chemistry B* **1999,** *103* (44), 9473-9487.

76. Yu, Y.; Eisenberg, A., Control of Morphology through Polymer-Solvent Interactions in Crew-Cut Aggregates of Amphiphilic Block Copolymers. *Journal of the American Chemical Society* **1997,** *119* (35), 8383-8384.

77. McKenzie, B. E.; de Visser, J. F.; Friedrich, H.; Wirix, M. J. M.; Bomans, P. H. H.; de With, G.; Holder, S. J.; Sommerdijk, N. A. J. M., Bicontinuous Nanospheres from Simple Amorphous Amphiphilic Diblock Copolymers. *Macromolecules* **2013,** *46* (24), 9845-9848.

78. Yu, Y.; Zhang, L.; Eisenberg, A., Morphogenic Effect of Solvent on Crew-Cut Aggregates of Apmphiphilic Diblock Copolymers. *Macromolecules* **1998,** *31* (4), 1144-1154.

79. Bhargava, P.; Zheng, J. X.; Li, P.; Quirk, R. P.; Harris, F. W.; Cheng, S. Z. D., Self-Assembled Polystyrene-block-poly(ethylene oxide) Micelle Morphologies in Solution. *Macromolecules* **2006,** *39* (14), 4880-4888.

80. Blanazs, A.; Armes, S. P.; Ryan, A. J., Self-Assembled Block Copolymer Aggregates: From Micelles to Vesicles and their Biological Applications. *Macromolecular Rapid Communications* **2009,** *30* (4-5), 267-277.

81. Israelachvili, J. N., 19 - Thermodynamic Principles of Self-Assembly. In *Intermolecular and Surface Forces (Third Edition)*, Israelachvili, J. N., Ed. Academic Press: San Diego, 2011; pp 503-534.

82. Israelachvili, J. N.; Mitchell, D. J.; Ninham, B. W., Theory of self-assembly of hydrocarbon amphiphiles into micelles and bilayers. *Journal of the Chemical Society, Faraday Transactions 2: Molecular and Chemical Physics* **1976,** *72* (0), 1525-1568.

83. Lim Soo, P.; Eisenberg, A., Preparation of block copolymer vesicles in solution. *Journal of Polymer Science Part B: Polymer Physics* **2004,** *42* (6), 923-938.

84. Zhang, L.; Eisenberg, A., Thermodynamic vs Kinetic Aspects in the Formation and Morphological Transitions of Crew-Cut Aggregates Produced by Self-Assembly of Polystyrene-b-poly(acrylic acid) Block Copolymers in Dilute Solution. *Macromolecules* **1999,** *32* (7), 2239-2249.

85. Feng, C.; Lu, G.; Li, Y.; Huang, X., Self-Assembly of Amphiphilic Homopolymers Bearing Ferrocene and Carboxyl Functionalities: Effect of Polymer Concentration, β-Cyclodextrin, and Length of Alkyl Linker. *Langmuir* **2013,** *29* (34), 10922-10931.

86. Owen, S. C.; Chan, D. P. Y.; Shoichet, M. S., Polymeric micelle stability. *Nano Today* **2012,** *7* (1), 53-65.

87. Jordan, J. H.; Gibb, B. C., Molecular containers assembled through the hydrophobic effect. *Chemical Society Reviews* **2015,** *44* (2), 547-585.

88. Maibaum, L.; Dinner, A. R.; Chandler, D., Micelle Formation and the Hydrophobic Effect†. *The Journal of Physical Chemistry B* **2004,** *108* (21), 6778-6781.

89. Choucair, A.; Eisenberg, A., Control of amphiphilic block copolymer morphologies using solution conditions. *The European Physical Journal E* **2003,** *10* (1), 37-44.

90. Yang, L.; Alexandridis, P., Physicochemical aspects of drug delivery and release from polymer-based colloids. *Current Opinion in Colloid & Interface Science* **2000,** *5* (1–2), 132-143.

91. Rösler, A.; Vandermeulen, G. W. M.; Klok, H.-A., Advanced drug delivery devices via self-assembly of amphiphilic block copolymers. *Advanced Drug Delivery Reviews* **2001,** *53* (1), 95-108.

92. Rios-Doria, J.; Carie, A.; Costich, T.; Burke, B.; Skaff, H.; Panicucci, R.; Sill, K., A Versatile Polymer Micelle Drug Delivery System for Encapsulation and In Vivo Stabilization of Hydrophobic Anticancer Drugs. *Journal of Drug Delivery* **2012,** *2012*, 951741.

93. Movassaghian, S.; Merkel, O. M.; Torchilin, V. P., Applications of polymer micelles for imaging and drug delivery. *Wiley Interdisciplinary Reviews: Nanomedicine and Nanobiotechnology* **2015,** *7* (5), 691-707.

94. Zhang, L.; Eisenberg, A., Multiple Morphologies and Characteristics of “Crew-Cut” Micelle-like Aggregates of Polystyrene-b-poly(acrylic acid) Diblock Copolymers in Aqueous Solutions. *Journal of the American Chemical Society* **1996,** *118* (13), 3168-3181.

95. Zhang, L.; Eisenberg, A., Formation of crew-cut aggregates of various morphologies from amphiphilic block copolymers in solution. *Polymers for Advanced Technologies* **1998,** *9* (10-11), 677-699.

96. Topete, A.; Barbosa, S.; Taboada, P., Intelligent micellar polymeric nanocarriers for therapeutics and diagnosis. *Journal of Applied Polymer Science* **2015,** *132* (41), 42650.

97. Yu, K.; Zhang, L.; Eisenberg, A., Novel Morphologies of "Crew-Cut" Aggregates of Amphiphilic Diblock Copolymers in Dilute Solution. *Langmuir* **1996,** *12* (25), 5980-5984.

98. Fayad, S. J.; Minatti, E.; Soldi, V.; Borsali, R., Transition from star-like to crew-cut micelles induced by UV radiation. *Journal of Colloid and Interface Science* **2014,** *416*, 54-58.

99. Zhulina, E. B.; Adam, M.; LaRue, I.; Sheiko, S. S.; Rubinstein, M., Diblock copolymer micelles in a dilute solution. *Macromolecules* **2005,** *38* (12), 5330-5351.

100. Wang, X.; Guerin, G.; Wang, H.; Wang, Y.; Manners, I.; Winnik, M. A., Cylindrical Block Copolymer Micelles and Co-Micelles of Controlled Length and Architecture. *Science* **2007,** *317* (5838), 644-647.

101. Patra, S. K.; Ahmed, R.; Whittell, G. R.; Lunn, D. J.; Dunphy, E. L.; Winnik, M. A.; Manners, I., Cylindrical Micelles of Controlled Length with a π-Conjugated Polythiophene Core via Crystallization-Driven Self-Assembly. *Journal of the American Chemical Society* **2011,** *133* (23), 8842-8845.

102. Dan, N.; Safran, S. A., Junctions and end-caps in self-assembled non-ionic cylindrical micelles. *Advances in Colloid and Interface Science* **2006,** *123–126*, 323-331.

103. Jain, S.; Bates, F. S., Consequences of Nonergodicity in Aqueous Binary PEO−PB Micellar Dispersions. *Macromolecules* **2004,** *37* (4), 1511-1523.

104. Jain, S.; Bates, F. S., On the Origins of Morphological Complexity in Block Copolymer Surfactants. *Science* **2003,** *300* (5618), 460-464.

105. Jain, S.; Gong, X.; Scriven, L. E.; Bates, F. S., Disordered Network State in Hydrated Block-Copolymer Surfactants. *Physical Review Letters* **2006,** *96* (13), 138304.

106. Discher, B. M.; Won, Y.-Y.; Ege, D. S.; Lee, J. C.-M.; Bates, F. S.; Discher, D. E.; Hammer, D. A., Polymersomes: Tough Vesicles Made from Diblock Copolymers. *Science* **1999,** *284* (5417), 1143-1146.

107. LoPresti, C.; Lomas, H.; Massignani, M.; Smart, T.; Battaglia, G., Polymersomes: nature inspired nanometer sized compartments. *Journal of Materials Chemistry* **2009,** *19* (22), 3576-3590.

108. B.M. Discher, Y. Y. W., D.S. Ege, J.C.M. Lee, F.S. Bates, D.E. Dsicher, D.A. Hammer, Polymersomes: tough vesicles made from diblock copolymers. *Science* **1999,** *284*, 1143.

109. J. Holder, S.; A. J. M. Sommerdijk, N.; J. Williams, S.; J. M. Nolte, R.; C. Hiorns, R.; A. J. M. Sommerdijk, N.; G. Jones, R., The first example of a poly(ethylene oxide)-poly(methylphenylsilane) amphiphilic block copolymer: vesicle formation in water. *Chemical Communications* **1998,** (14), 1445-1446.

110. Kim, K. T.; Zhu, J.; Meeuwissen, S. A.; Cornelissen, J. J. L. M.; Pochan, D. J.; Nolte, R. J. M.; van Hest, J. C. M., Polymersome Stomatocytes: Controlled Shape Transformation in Polymer Vesicles. *Journal of the American Chemical Society* **2010,** *132* (Copyright (C) 2015 American Chemical Society (ACS). All Rights Reserved.), 12522-12524.

111. Azzam, T.; Eisenberg, A., Fully Collapsed (Kippah) Vesicles: Preparation and Characterization. *Langmuir* **2010,** *26* (13), 10513-10523.

112. Meeuwissen, S. A.; Kim, K.-T.; Chen, Y.-C.; Pochan, D. J.; van Hest, J. C. M., Controlled Shape Transformation of Polymersome Stomatocytes. *Angewandte Chemie, International Edition* **2011,** *50* (Copyright (C) 2015 American Chemical Society (ACS). All Rights Reserved.), 7070-7073, S7070/1-S7070/14.

113. Moughton, A. O.; Hillmyer, M. A.; Lodge, T. P., Multicompartment Block Polymer Micelles. *Macromolecules (Washington, DC, U. S.)* **2012,** *45* (Copyright (C) 2014 American Chemical Society (ACS). All Rights Reserved.), 2-19.

114. Lodge, T. P.; Rasdal, A.; Li, Z.; Hillmyer, M. A., Simultaneous, Segregated Storage of Two Agents in a Multicompartment Micelle. *Journal of the American Chemical Society* **2005,** *127* (50), 17608-17609.

115. Gohy, J.-F.; Willet, N.; Varshney, S.; Zhang, J.-X.; Jérôme, R., Core–Shell–Corona Micelles with a Responsive Shell. *Angewandte Chemie International Edition* **2001,** *40* (17), 3214-3216.

116. Kempe, K.; Hoogenboom, R.; Hoeppener, S.; Fustin, C.-A.; Gohy, J.-F. o.; Schubert, U. S., Discovering new block terpolymer micellar morphologies. *Chemical Communications* **2010,** *46* (35), 6455-6457.

117. Liu, T.; Tian, W.; Zhu, Y.; Bai, Y.; Yan, H.; Du, J., How does a tiny terminal alkynyl end group drive fully hydrophilic homopolymers to self-assemble into multicompartment vesicles and flower-like complex particles? *Polymer Chemistry* **2014,** *5* (Copyright (C) 2014 American Chemical Society (ACS). All Rights Reserved.), 5077-5088.

118. Liu, H.; Zhao, Y.; Dreiss, C. A.; Feng, Y., CO2-switchable multi-compartment micelles with segregated corona. *Soft Matter* **2014,** *10* (34), 6387-6391.

119. Vyhnalkova, R.; Xiao, L.; Yang, G.; Eisenberg, A., Spherical Blackberry-type Capsules Containing Block Copolymer Aggregates. *Langmuir* **2014,** *30* (Copyright (C) 2014 American Chemical Society (ACS). All Rights Reserved.), 2188-2195.

120. Parry, A. L.; Bomans, P. H. H.; Holder, S. J.; Sommerdijk, N. A. J. M.; Biagini, S. C. G., Cryo Electron Tomography Reveals Confined Complex Morphologies of Tripeptide-Containing Amphiphilic Double-Comb Diblock Copolymers. *Angewandte Chemie International Edition* **2008,** *47* (46), 8859-8862.

121. Hales, K.; Chen, Z.; Wooley, K. L.; Pochan, D. J., Nanoparticles with Tunable Internal Structure from Triblock Copolymers of PAA-b-PMA-b-PS. *Nano Letters* **2008,** *8* (7), 2023-2026.

122. McKenzie, B. E.; Nudelman, F.; Bomans, P. H. H.; Holder, S. J.; Sommerdijk, N., Temperature-Responsive Nanospheres with Bicontinuous Internal Structures from a Semicrystalline Amphiphilic Block Copolymer. *Journal of the American Chemical Society* **2010,** *132* (30), 10256-10259.

123. Holder, S. J.; Woodward, G.; McKenzie, B.; Sommerdijk, N. A. J. M., Semi-crystalline block copolymer bicontinuous nanospheres for thermoresponsive controlled release. *RSC Advances* **2014,** *4* (50), 26354-26358.

124. McKenzie, B. E.; Friedrich, H.; Wirix, M. J. M.; de Visser, J. F.; Monaghan, O. R.; Bomans, P. H. H.; Nudelman, F.; Holder, S. J.; Sommerdijk, N. A. J. M., Controlling Internal Pore Sizes in Bicontinuous Polymeric Nanospheres. *Angewandte Chemie International Edition* **2015,** *54* (8), 2457-2461.

125. Priya, B.; Viness, P.; Yahya, E. C.; Lisa, C. d. T., Stimuli-responsive polymers and their applications in drug delivery. *Biomedical Materials* **2009,** *4* (2), 022001.

126. Chan, A.; Orme, R. P.; Fricker, R. A.; Roach, P., Remote and local control of stimuli responsive materials for therapeutic applications. *Advanced Drug Delivery Reviews* **2013,** *65* (4), 497-514.

127. Liu, F.; Eisenberg, A., Preparation and pH Triggered Inversion of Vesicles from Poly(acrylic Acid)-block-Polystyrene-block-Poly(4-vinyl Pyridine). *Journal of the American Chemical Society* **2003,** *125* (49), 15059-15064.

128. Zhao, Z.; Zhu, F.; Qu, X.; Wu, Q.; Wang, Q.; Zhang, G.; Liang, F., pH-Responsive polymeric Janus containers for controlled drug delivery. *Polymer Chemistry* **2015,** *6* (22), 4144-4153.

129. Schmaljohann, D., Thermo- and pH-responsive polymers in drug delivery. *Advanced Drug Delivery Reviews* **2006,** *58* (15), 1655-1670.

130. Huh, K.; Kang, H.; Lee, Y.; Bae, Y., pH-sensitive polymers for drug delivery. *Macromolecular Research* **2012,** *20* (3), 224-233.

131. Fleige, E.; Quadir, M. A.; Haag, R., Stimuli-responsive polymeric nanocarriers for the controlled transport of active compounds: Concepts and applications. *Advanced Drug Delivery Reviews* **2012,** *64* (9), 866-884.

132. Sant, V. P.; Smith, D.; Leroux, J. C., Novel pH-sensitive supramolecular assemblies for oral delivery of poorly water soluble drugs: Preparation and characterization. *Journal of Controlled Release* **2004,** *97* (2), 301-312.

133. Du, J.; Armes, S. P., pH-Responsive Vesicles Based on a Hydrolytically Self-Cross-Linkable Copolymer. *Journal of the American Chemical Society* **2005,** *127* (37), 12800-12801.

134. Gil, E. S.; Hudson, S. M., Stimuli-reponsive polymers and their bioconjugates. *Progress in Polymer Science* **2004,** *29* (12), 1173-1222.

135. Ward, M. A.; Georgiou, T. K., Thermoresponsive Polymers for Biomedical Applications. *Polymers* **2011**.

136. Kuckling, D.; Adler, H. J. P.; Arndt, K. F.; Ling, L.; Habicher, W. D., Temperature and pH dependent solubility of novel poly(N-isopropylacrylamide) copolymers. *Macromolecular Chemistry and Physics* **2000,** *201* (2), 273-280.

137. Li, M.-H.; Keller, P., Stimuli-responsive polymer vesicles. *Soft Matter* **2009,** *5* (5), 927-937.

138. Ward, M. A.; Georgiou, T. K., Thermoresponsive terpolymers based on methacrylate monomers: Effect of architecture and composition. *Journal of Polymer Science Part A: Polymer Chemistry* **2010,** *48* (4), 775-783.

139. Qin, S.; Geng, Y.; Discher, D. E.; Yang, S., Temperature-Controlled Assembly and Release from Polymer Vesicles of Poly(ethylene oxide)-block- poly(N-isopropylacrylamide). *Advanced Materials* **2006,** *18* (21), 2905-2909.

140. Wei, H.; Zhang, X. Z.; Zhou, Y.; Cheng, S. X.; Zhuo, R. X., Self-assembled thermoresponsive micelles of poly(N-isopropylacrylamide-b- methyl methacrylate). *Biomaterials* **2006,** *27* (9), 2028-2034.

141. Idziak, I.; Avoce, D.; Lessard, D.; Gravel, D.; Zhu, X. X., Thermosensitivity of Aqueous Solutions of Poly(N,N-diethylacrylamide). *Macromolecules* **1999,** *32* (4), 1260-1263.

142. Makhaeva, E. E.; Tenhu, H.; Khokhlov, A. R., Conformational changes of poly(vinylcaprolactam) macromolecules and their complexes with ionic surfactants in aqueous solution. *Macromolecules* **1998,** *31* (18), 6112-6118.

143. Ahn, S.-k.; Kasi, R. M.; Kim, S.-C.; Sharma, N.; Zhou, Y., Stimuli-responsive polymer gels. *Soft Matter* **2008,** *4* (6), 1151-1157.

144. Sanson, C.; Diou, O.; Thevenot, J.; Ibarboure, E.; Soum, A.; Brulet, A.; Miraux, S.; Thiaudiere, E.; Tan, S.; Brisson, A.; Dupuis, V.; Sandre, O.; Lecommandoux, S., Doxorubicin Loaded Magnetic Polymersomes: Theranostic Nanocarriers for MR Imaging and Magneto-Chemotherapy. *ACS Nano* **2011,** *5* (2), 1122-1140.

145. Priya James, H.; John, R.; Alex, A.; Anoop, K. R., Smart polymers for the controlled delivery of drugs – a concise overview. *Acta Pharmaceutica Sinica B* **2014,** *4* (2), 120-127.

146. Roy, D.; Cambre, J. N.; Sumerlin, B. S., Future perspectives and recent advances in stimuli-responsive materials. *Progress in Polymer Science* **2010,** *35* (1–2), 278-301.

147. Ito, Y.; Casolaro, M.; Kono, K.; Imanishi, Y., An insulin-releasing system that is responsive to glucose. *Journal of Controlled Release* **1989,** *10* (2), 195-203.

148. Kotsuchibashi, Y.; Agustin, R. V. C.; Lu, J.-Y.; Hall, D. G.; Narain, R., Temperature, pH, and Glucose Responsive Gels via Simple Mixing of Boroxole- and Glyco-Based Polymers. *ACS Macro Letters* **2013,** *2* (3), 260-264.

149. Jiang, J.; Tong, X.; Zhao, Y., A New Design for Light-Breakable Polymer Micelles. *Journal of the American Chemical Society* **2005,** *127* (23), 8290-8291.

150. Du, L.; Jin, Y.; Zhou, W.; Zhao, J., Ultrasound-Triggered Drug Release and Enhanced Anticancer Effect of Doxorubicin-Loaded Poly(D,L-Lactide-Co-Glycolide)-Methoxy-Poly(Ethylene Glycol) Nanodroplets. *Ultrasound in Medicine and Biology* **2011,** *37* (8), 1252-1258.

151. Lee, K.; Bae, K. H.; Lee, Y.; Lee, S. H.; Ahn, C. H.; Park, T. G., Pluronic/polyethylenimine shell crosslinked nanocapsules with embedded magnetite nanocrystals for magnetically triggered delivery of siRNA. *Macromolecular Bioscience* **2010,** *10* (3), 239-245.

152. Schmidt, D. J.; Moskowitz, J. S.; Hammond, P. T., Electrically triggered release of a small molecule drug from a polyelectrolyte multilayer coating. *Chemistry of Materials* **2010,** *22* (23), 6416-6425.

153. Nishiyama, N.; Yokoyama, M.; Aoyagi, T.; Okano, T.; Sakurai, Y.; Kataoka, K., Preparation and Characterization of Self-Assembled Polymer−Metal Complex Micelle from cis-Dichlorodiammineplatinum(II) and Poly(ethylene glycol)−Poly(α,β-aspartic acid) Block Copolymer in an Aqueous Medium. *Langmuir* **1999,** *15* (2), 377-383.

154. DLS. http://www.horiba.com/uk/scientific/products/particle-characterization/technology/dynamic-light-scattering/.

155. Patterson, J. P.; Robin, M. P.; Chassenieux, C.; Colombani, O.; O'Reilly, R. K., The analysis of solution self-assembled polymeric nanomaterials. *Chemical Society Reviews* **2014,** *43* (8), 2412-2425.

156. Libera, M. R.; Egerton, R. F., Advances in the Transmission Electron Microscopy of Polymers. *Polymer Reviews* **2010,** *50* (3), 321-339.

157. Nudelman, F.; de With, G.; Sommerdijk, N. A. J. M., Cryo-electron tomography: 3-dimensional imaging of soft matter. *Soft Matter* **2011,** *7* (1), 17-24.

158. McKenzie, B. E.; Holder, S. J.; Sommerdijk, N., Assessing internal structure of polymer assemblies from 2D to 3D CryoTEM: Bicontinuous micelles. *Current Opinion in Colloid & Interface Science* **2012,** *17* (6), 343-349.

159. Talmon, Y., Staining and drying-induced artifacts in electron microscopy of surfactant dispersions. *Journal of Colloid and Interface Science* **1983,** *93* (2), 366-382.

160. Danino, D.; Moon, K.-H.; Hinshaw, J. E., Rapid constriction of lipid bilayers by the mechanochemical enzyme dynamin. *Journal of Structural Biology* **2004,** *147* (3), 259-267.

161. Cui, H.; Hodgdon, T. K.; Kaler, E. W.; Abezgauz, L.; Danino, D.; Lubovsky, M.; Talmon, Y.; Pochan, D. J., Elucidating the assembled structure of amphiphiles in solution via cryogenic transmission electron microscopy. *Soft Matter* **2007,** *3* (8), 945-955.

162. Falls, A. H.; Wellinghoff, S. T.; Talmon, Y.; Thomas, E. L., A transmission electron microscopy study of hexagonal ice. *Journal of Materials Science* **1983,** *18* (9), 2752-2764.

163. Loebling, T. I.; Haataja, J. S.; Synatschke, C. V.; Schacher, F. H.; Mueller, M.; Hanisch, A.; Groeschel, A. H.; Mueller, A. H. E., Hidden Structural Features of Multicompartment Micelles Revealed by Cryogenic Transmission Electron Tomography. *ACS Nano* **2014,** *8* (Copyright (C) 2014 American Chemical Society (ACS). All Rights Reserved.), 11330-11340.

Chapter 2 Synthesis and Self-Assembly of Poly(ethylene oxide)-*block*-Poly(octadecyl methacrylate)

2.1 Abstract

This chapter focuses on the synthesis and self-assembly of block copolymer PEO-*b*-PODMA to form bicontinuous nanospheres. Previous work revealed that PEO-*b*-PODMA will from bicontinuous nanospheres when the PEO wt % is < 25 % and an overall M_w of < 17 kDa. The effect of the PEO weight fraction upon the resultant morphology was investigated in this chapter and was consistent with previous work, with PEO 25 wt % resulting in bicontinuous nanospheres and a mixture of morphologies including cylindrical micelles and multi-lamellar particles being observed for PEO 30 wt %. It was also established that the bicontinuous structure was maintined with an increase in poylemr concentration from 0.1 wt % in solution to 5 wt %.

The use of the semi-crystalline PODMA block gives the BCP a thermo-responisve nature. The thermo-responsive properties of both the bulk and aggregate samples of PEO-*b*-PODMA was investigated using DSC, which revealed a T_m of 21.5 and 23.4°C respectively. The degree of crystalisation (D_c) for both samples was also established, with the aggregate sample exhibiting a lower D_c than for the bulk.

2.2 Introduction

Amphiphilic molecules are those that have an affinity for two different types of environment, an example of amphiphilic molecules are lipids and surfactants.[1] Lipids and surfactants have a hydrophilic polar head group connected to a hydrophobic non polar tail. They self-assemble in aqueous media to form bilayers (membranes) and micelles due to the unfavourable hydrophobic water interactions. The advancements in controlled radical polymerisation has led to the synthesis of amphiphilic block copolymers whose composition and molecular weights can be accurately targeted and the polymers can be readily functionalised pre or post synthesis for a specific application.[2] The BCPs can emulate natural surfactants whose self-assembled aggregates are more stable, but also more complex morphologies can be produced.

In this chapter the self-assembly of PEO-*b*-PODMA, synthesised via ATRP, to form bicontinuous nanospheres is investigated. Bicontinuous nanospheres are discrete

aggregates that have a twisted hydrophobic network interconnected with that of the hydrophilic moiety.[3] Bicontinuous nanospheres have been observed before in the literature, where their self-assembly has been aided by an additive.[4-5] The self-assembly of PEO-*b*-PODMA is achieved by use of a cosolvent only and the formation of this complex morphology by the dialysis method has been has been investigated by Holder *et al*.[3] It was found that the weight fraction of the hydrophilic block along with the molecular weight, determined the resultant morphology with a phase diagram that illustrates that bicontinuous nanospheres are present when the hydrophilic wt % is <30 % and the molecular weight is < 17kDa. In this chapter the effect of the weight fraction of the hydrophilic block and the molecular weight is investigated to see if the results are consistent with the PEO-*b*-PODMA phase diagram. Previously bicontinuous nanospheres of PEO-b-PODMA have only been observed at concentrations ≤ 0.5 wt % in solution.[6] In this chapter the effect increasing the concentration up to 5 wt % in solution, has on the ability for stable dispersions to form whilst preserving the bicontinuous internal morphology will be investigated.

These use of a comb-like hydrophobic block such as PODMA gives the bicontinuous nanospheres a temperature-responsive nature. When the nanospheres are heated above the T_m of the PODMA block, or more correctly the T_m of the semi-crystalline alkyl side-chains, the bicontinuity is lost whilst the external spherical structure is maintained.[6] The T_m and degree of crystallinity of the bulk PEO-*b*-PODMA BCP and its 5 wt % BPN dispersion is investigated in this chapter by use of DSC to establish if the temperature-responsive nature of the alkyl side-chains was maintained when the BCP was self-assembled.

The dialysis method is used to self-assemble PEO-*b*-PODMA into BPNs. The BCP is first dissolved in a predetermined volume of THF, water is then added to this solution (kept at a temperature above the T_m) dropwise to make the total volume up to 10 mL. The solution is then dialysed against distilled water (kept at a temperature above the T_m) to remove the THF for 24 hours. It has been found that the BPNs only start to be observed when the aggregate solution is cooled below 20°C and that above the T_m large films were observed.[2] This shows that the dialysis method might not be

crucial for the formation of bicontinuous nanospheres. The dialysis approach is a lengthy process and could be reduced by use of a different procedure. A number of different self-assembly methods will be studied in this chapter to establish a method that significantly reducing the self-assembly procedure time while still producing bicontinuous nanospheres.

2.3 Experimental

2.3.1 Materials and Apparatus for ATRP of poly (ethylene oxide)-*block*-poly(octadecyl methacrylate)

Triethylamine (TEA) (99 %), 2-bromoisobutryl bromide (BIBB) (98 %), 4-dimethylamino pyridine (DMAP) (99 %), poly (ethylene glycol) methyl ether (M_n ca. 2000 and 5000 g/mol) (PEGME), octadecyl methacrylate (ODMA), copper (I) bromide (98 %), N,N,N',N'',N''-pentamethyldiethylenetriamine (PMDETA) (99 %) were all used as received from Sigma-Aldrich. Aluminium oxide (activated, neutral, for column chromatography 50-200µm) and sodium bicarbonate (analytical reagent grade) were purchased from Acros Organics. Tetrahydrofuran (analytical reagent grade), isopropyl alcohol and ethanol (analytical grade) were purchased from Fisher Scientific. Xylene was purchased from BDH Lab Supplies. The deuterated solvent used in ^{1}H-NMR was used as purchased from Cambridge Isotope Laboratories Incorporated. Hydrochloric acid (36 %) was purchased from Fisher Scientific and diluted with distilled water to make a 10 % concentration. Dichloromethane (analytical reagent grade) was purchased from Fisher Scientific and dried and distilled over calcium hydride before use.

All reactions were performed under inert atmosphere using schlenk techniques. The infra-red spectra were recorded using a Shimadzu FT-IR spectrometer. ^{1}H-NMR and ^{13}C-NMR spectra were obtained by dissolving the sample in deuterated chloroform (CDCl3) and recorded on a JEOL ECS-400 spectrometer (400 MHz) at 25°C. Molecular weight averages and dispersity indices were calculated using Size Exclusion Chromatography on a Gel Permeation Chromatography (GPC) using two 5µm mixed C PLgel columns at 40°C. The GPC was calibrated using poly(methyl methacrylate) standards (PMMA). The samples were all dissolved in THF and detected by a refractive index detector.

2.3.2 Materials and Apparatus for the Self-Assembly of Poly(ethylene oxide)-*block*-Poly(octadecyl methacrylate)

The BCPs were used as synthesised. Distilled water was used as obtained. *A* syringe pump (220 Voltz, 0.1 Amps, 50 Hz) was used from Semat technical Limited at 0.085 mL per minute. A 5 mL dialysis cassette was used with dialysis membrane (MWCO-12-14000 Daltons) from MEDICELL international Ltd.

Dynamic Light Scattering

Dynamic Light Scattering (DLS) measurements were obtained on a Malvern High Performance Particle Sizer (Nano Zetasizer HPPS HPP5001) with a laser at a wavelength of 633 nm. The measurements were taken using a clean quartz cuvette containing a 1 mL sample. Measurements were taken at both 15 and 35°C, the temperature was set and the machine was left to settle at this temperature for 10 minutes, after this 10 measurements were taken and an average was obtained.

Transmission Electron Microscopy

Transmission Electron Microscopy (TEM) was carried out on all the self-assembled samples using a JEOL JEM (200-FX) TEM machine (120kV). 10 µl of the sample was pipetted onto a carbon-coated copper grid (200 mesh) and left for 5 minutes and then removed using suction. Using 10 µl of 5 % uranyl acetate the grid was then stained, and removed via suction.

Cryo-Transmission Electron Microscopy

Cryo-Transmission Electron Microscopy (cryo-TEM) was performed on a FEI Cryo-Titan with a field emission gin operating at 300 kV. The sample vitrification process was as follows; 3 µl of the self-assembled solution was pipetted onto a surface plasma treated (Cresington Carbon Coater 208) Quantifoil holey (Cu 200 mesh) grid inside a FEI Vitrobot chamber (set to 100 % humidity at room temperature to prevent sample evaporation). The sample was then blotted and plunged into liquid ethane cooled by liquid nitrogen.

2.3.3 Materials and Apparatus for Differential Scanning Calorimetry

Differential Scanning Calorimetry (DSC) was carried out on the bulk sample of P3 (PEO_{49}-*b*-$PODMA_{16}$), along with the 5 wt % aggregate solution. Thermal analysis was carried out across the range -20°C to 60°C for P3 bulk and 5 to 60°C for the 5 wt % aggregate solution of P3. The samples were heated at a rate of 10°C/min. The samples were heated and cooled three times with the first heating run not taken into account to allow for any artifacts present due to a number of contributing factors such as abrupt changes in heat transfer or temperature fluctuations. The measurements taken from the second heating run are therefore where the values are calculated from. Bulk P3 was measured against an empty aluminium pan as the reference and an aluminium pan filled with water was used as the reference for the 5 wt % solution of P3 to remove any transition seen by the water solvent.

2.3.4 Synthesis of Poly (ethylene oxide) Macroinitiators via esterification (I1-I5)

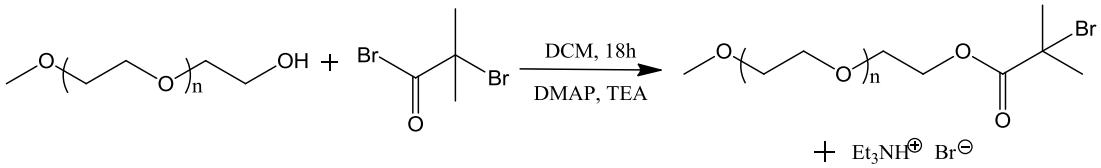

Scheme 2.1: Synthesis of PEO Macroinitiator

A literature method used as the typical procedure for the synthesis of all PEO macrointiators[6]**:** 2-bromoisobutryl bromide (11.50 g, 50 mmol), triethylamine (5.06 g, 50 mmol) and 4-dimethylamino pyridine (6.11 g, 50 mmol) dissolved in anhydrous dichloromethane were added to a round bottom flask and stirred, the flask was then sealed. PEGME (M_n 2000) (50 g, 25 mmol) dissolved in 100 mL of anhydrous dichloromethane was added drop wise to the mixture at 0°C for 1 hour under nitrogen. The mixture was then stirred for a further 18 hours at room temperature. The mixture was filtered to remove the amine salt and half the solvent was evaporated off (rotary evaporator). The mixture was made up to 100 mL with dichloromethane. In a separating funnel the mixture was then washed twice with a saturated sodium bicarbonate solution and then twice with hydrochloric acid (10 %). The organic layer (bottom) was then collected and dried using anhydrous magnesium sulphate for 1 hour. The solution was filtered, the solvent evaporated off (rotary evaporator) and the product was dried in a vacuum oven overnight to produce a white waxy solid. The compound was characterised using ^{1}H-NMR, FT-IR and GPC. I2-I5 were synthesised following this same method using the masses seen in Table 2.1. The GPC and NMR results can be seen in Table 2.3.

(I1) ^{1}H NMR (400 MHz, $CDCl_3$, ppm) δ: 1.94 (singlet, 6H, $(CH_3)_2C$-), 3.38 (singlet, 3H, -OCH_3), 3.65 (broad peak, 4H, -OCH_2CH_2-), 3.82 (triplet, 2H, -CH_2O-), 4.33 (triplet, 2H, $COOCH_2$-)**. (I1) ^{13}C NMR ($CDCl_3$, ppm) δ:** 31.3 (Br-C(**C**$H_3)_2$-), 56.2 (Br-**C**-), 59.5 (**C**H_3-O-), 65.6 (-COO-**C**H_2-CH_2-), 69.2 (-COO-CH_2-**C**H_2-),71.0 (-O-**C**H_2**C**H_2-), 72.4 (CH_3O-**C**H_2-), 172.1 (Br-C($CH_3)_2$-**C**OO-). **(I1) FTIR (cm^{-1}):** 2883 C-H stretch, 1734 C=O stretch, 1465 C-H bend, 1099 C-O stretch, 528 C-Br stretch. I2-I5 gave identical signals.

Table 2.1: Masses of starting materials used for the synthesis of I1-I5 PEO macroinitiators.

Code	PEGME (M_n 2000)	PEGME (M_n 5000)	BIBB	TEA	DMAP	Yield (%)
I1	30 g	N/A	6.91 g	3.05 g	3.60 g	28
I2	50 g	N/A	11.53 g	5.08 g	6.00 g	40
I3	38.5 g	N/A	8.86 g	3.90 g	4.71 g	56
I4	N/A	25 g	2.31 g	1.02 g	1.22 g	51
I5	N/A	50 g	4.61 g	2.03 g	2.44 g	18

2.3.5 Polymerisation of PEO-*b*-PODMA *via* ATRP

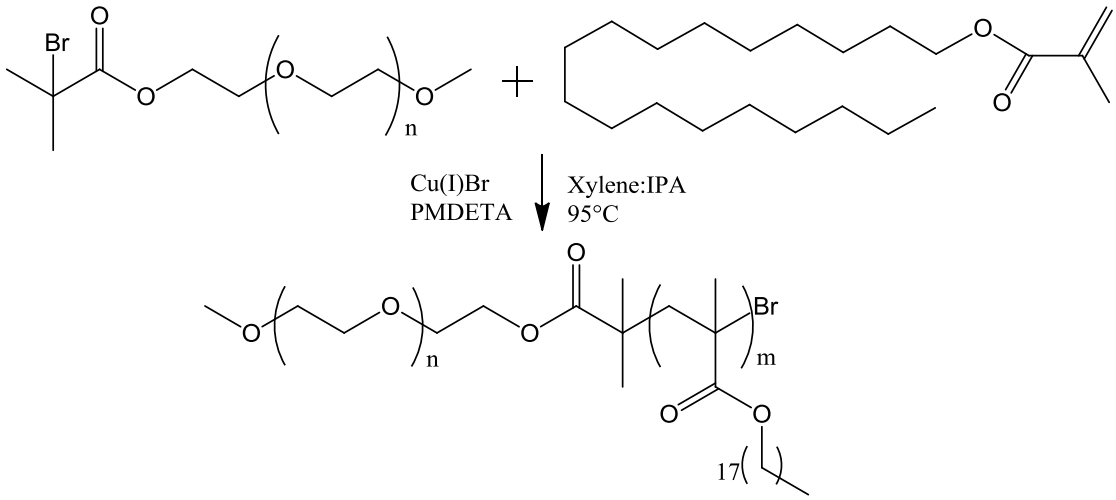

Scheme 2.2: Synthesis of PEO-*b*-PODMA

A literature method was modified and used as the typical procedure for the synthesis of PEO-*b*-PODMA block copolymers[6]. Cu (I) Br (30.12 mg, 0.21 mmoles) was placed in a 25 mL Schlenk tube with a magnetic stirrer. The PEO macroinitiator (1.00 g, 0.42 mmoles) was dissolved in xylene:IPA mixture (9:1) (4 mL) and then added to the Schlenk tube along with PMDETA (72.79 mg, 0.42 mmoles) and ODMA (2.7764 g, 8.2 mmoles). The Schlenk tube was sealed and the mixture was degassed (N_2) at 95°C for 1 hour. The mixture was then stirred at 95°C for 24 hours under nitrogen. After 24 hours the reaction was stopped by exposure to air and diluting with THF. The mixture was run through an alumina column to remove the catalyst and ligand and half the solvent was evaporated off (rotary evaporator). The polymer was precipitated out into ethanol drop wise at 0°C. The block copolymer was characterised using ^{1}H-NMR and GPC. This synthesis was carried out for P3, all other block copolymers were synthesised following the same method, the masses of the starting materials and reaction conditions for all can be seen in Table 2.2.

(P3) ^{1}H NMR (400 MHz, $CDCl_3$, ppm) δ: 0.88 (triplet, 3H, -$(CH_2)_{17}$-C**H_3**), 1.02 (broad peak, 3H, -CH_2-C-C**H_3**), 1.28 (broad peak, 30H, -(C**H_2**$)_{15}$-), 1.60 (broad peak, 2H, -C**H_2**-$(CH_2)_{15}$-), 3.38 (singlet, 3H, C**H_3**O-), 3.64 (triplet, 4H, -O-C**H_2**C**H_2**-O), 3.91 (broad peak, 2H, -COO-C**H_2**-). **(P3) ^{13}C NMR ($CDCl_3$, ppm) δ:** 14.23 (-CH_2CH_2**C**H_3), 22.8 (-CH_2**C**H_2CH_3), 32.04 (-**C**$H_2CH_2CH_3$), 29.5 (-$CH_2(CH_2)_{10}$**C**H_2-), 29.8 (-CH_2(**C**$H_2)_{10}CH_2$-), 26.2

(-COO-CH_2CH_2**C**H_2-), 28.20 (-COO-CH_2**C**H_2CH_2-), 65.1(-COO-**C**$H_2CH_2CH_2$-), 70.65 (-O-**C**H_2**C**H_2O-). **(P3) FTIR (cm^{-1}):** 2916 C-H stretch, 2848 C-H stretch, 1728 C=O stretch, 1465 C-H stretch, 1242 C-C stretch, 1145 C-O stretch, 721 C-H rock.

Table 2.2: Reaction conditions for polymers P1-P9 synthesised *via* the above method.

Code	ODMA	PEO macroinitiator	PMDETA	Cu(I)Br	Cu(I)Cl	Temperature (˚C)	Reaction time (hour)
P1	5.52 g	I3-1.00 g	78 mg	33 mg	-	95	24
P2	3.99 g	I1- 1.00 g	73 mg	30 mg	-	95	24
P3	2.50 g	I1- 1.05 g	0.19 g	22 mg	-	95	24
P4	2.97 g	I2- 1.00 g	80 mg	33 mg	-	95	24
P5	2.97 g	I2- 1.00 g	80 mg	33 mg	-	95	24
P6	2.91 g	I3- 1.00 g	78 mg	33 mg	-	95	24
P7	2.50 g	I1- 1.05 g	0.19 g	23 mg	-	95	24
P8	1.56 g	I2- 1.00 g	73 mg	30 mg	-	95	24
P9	2.50 g	I5- 2.36 g	0.15 g	-	16 mg	95	24

2.3.6 Self-Assembly of PEO-*b*-PODMA

2.3.6.1 Procedure A: Self-Assembly of PEO-b-PODMA via Dialysis

PEO-*b*-PODMA was dissolved in THF (4 m) and left stirring in an oil bath set to 35°C. Deionised water (6 mL) was then added drop-wise to the solution over 70 minutes via a syringe pump. After 70 minutes the solution was transferred to a dialysis chamber, sealed with a dialysis membrane and then left spinning in 3L of deionised water pre-heated to 35°C. The dialysis chamber was left immersed in the deionised water for 24 hours to displace the THF, over the 24 hours the water was changed twice. The self-assembled polymer was then analysed using Dynamic Light Scattering (DLS) and Transmission Electron Microscopy (TEM) to determine the size and dispersity of the aggregates.

2.3.6.2 Procedure B: Self-Assembly of PEO-b-PODMA via evaporation

PEO-*b*-PODMA (40 mg) was dissolved in THF (20 mL) in a round bottom flask equipped with a magnetic stir bar. Distilled water (40 mL) was added and the solution was stirred at 35°C for 2 hours. After 2 hours the THF was removed via rotary evaporation at 60°C and 374 mbar. The size and dispersity of the aggregates was then analysed using DLS and TEM.

2.3.6.3 Procedure C: Self-Assembly of PEO-b-PODMA via slow addition of water and evaporation

PEO-*b*-PODMA (40 mg) was dissolved in THF (20 mL) in a round bottom flask equipped with a magnetic stir bar and heated to 35°C. Distilled water (40 mL) was added dropwise via a syringe pump at a rate of 5.15 mL/hour. The THF was removed via rotary evaporation at 60°C and 374 mbar. The solution was then analysed with DLS and TEM to determine the particle size and dispersity.

2.3.6.4 Procedure D: Self-Assembly of PEO-b-PODMA via emulsification

PEO-*b*-PODMA (10 mg) was placed in a sample vial with deionised water (10 mL) and heated in an oil bath to 40°C. The solid and water solution was then emulsified using an IKA ULTRA-TURRAX T8 disperser. The resultant aggregate solution was analysed with DLS and TEM to determine the particle size and dispersity.

2.4 Results and Discussion

2.4.1 Characterisation of PEO Macroinitiators

PEGME and 2-bromoisobutryl bromide were esterified in dichloromethane under nitrogen, resulting in the PEO Macroinitiator (I1). The product was then washed with hydrochloric acid and sodium bicarbonate solutions to remove any impurities. The solution was then dried over magnesium sulphate and the product obtained. This product was characterised for purity using FT-IR, ^{1}H-NMR and ^{13}C-NMR.

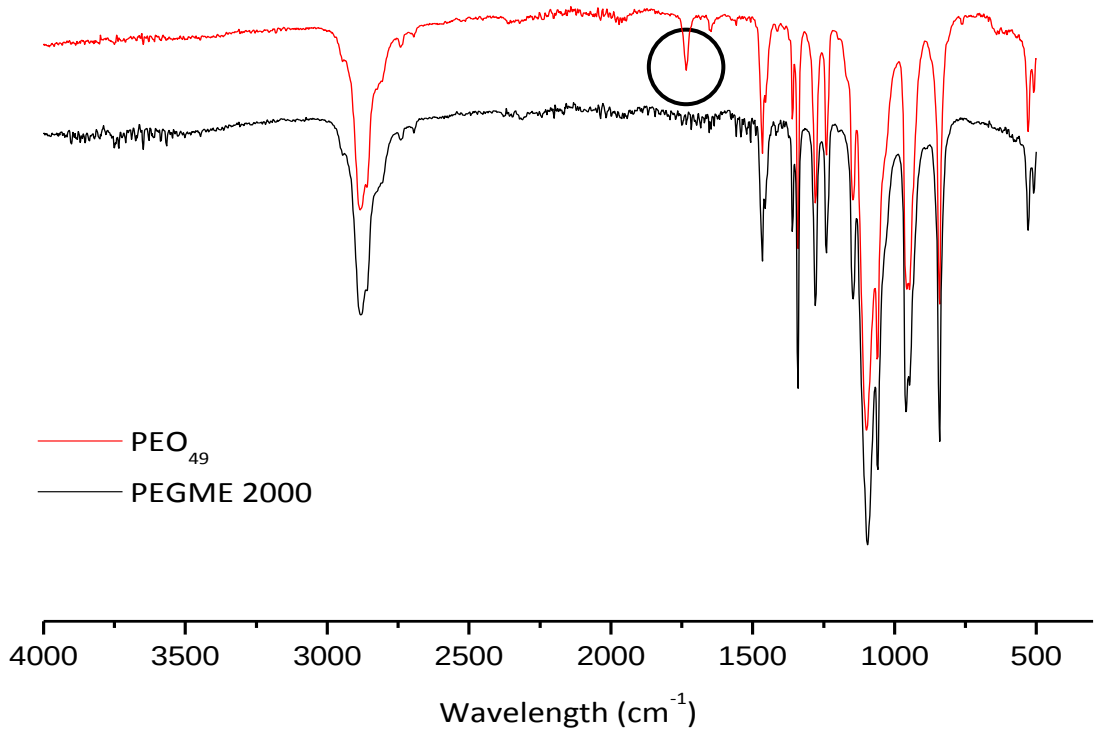

Figure 2.1: FTIR spectra overlay of PEGME (M_n ca. 2000g/mol) and PEO macroinitiator (I1). The peak circled represents the carbonyl group, confirming the formation of an ester bond.

The FT-IR was used to confirm that the ester bond had been made and that the OH bond had been broken. This can be seen in Figure 2.1 the peak at 1734 cm^{-1} (circled), present in the spectrum of I1, represents the C=O bond, confirming that an ester bond has been made as this peak is not present in the spectrum of PEGME 2000. Along with the ^{1}H-NMR spectra, this confirms the reaction was successful in substituting the hydroxyl group with an ester group. Macroinitiators I2-I5 gave the same results when analysed with FT-IR.

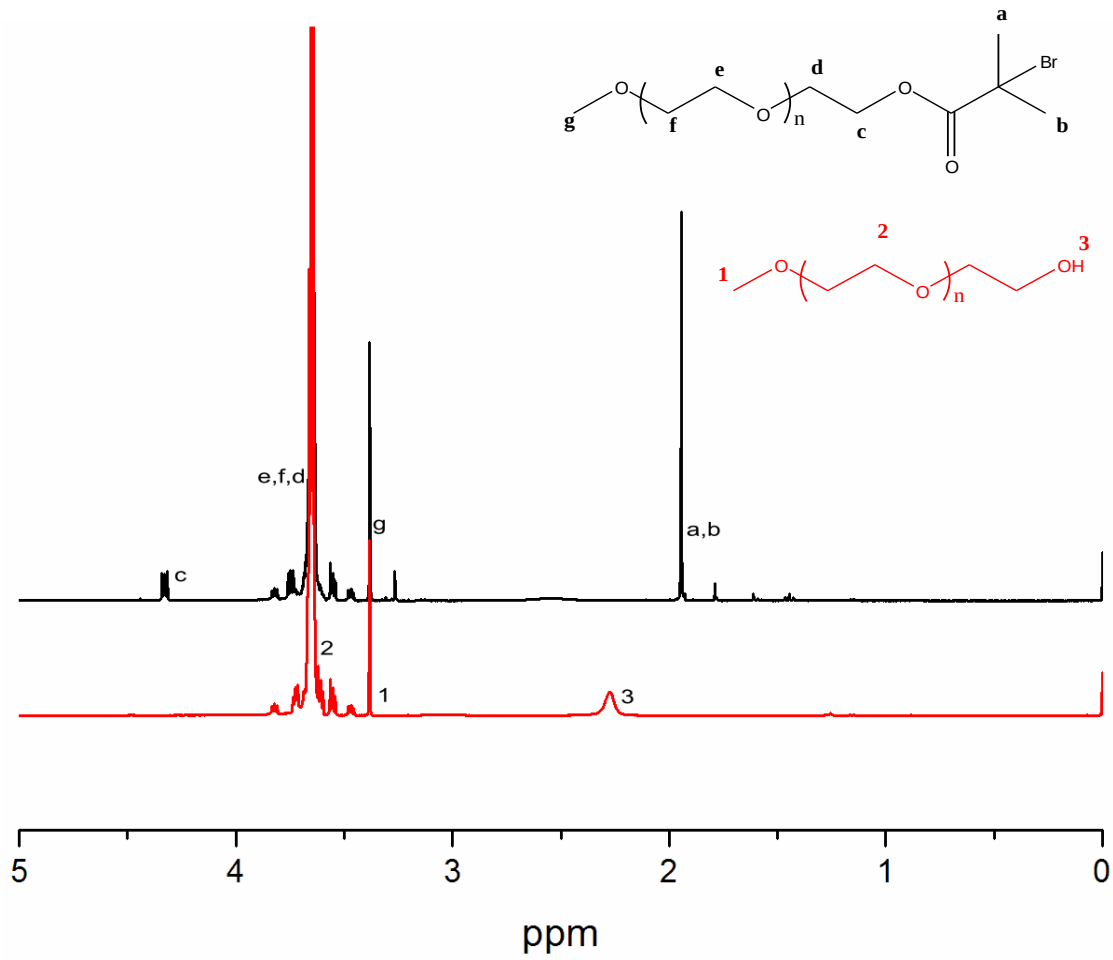

Figure 2.2: ^{1}H-NMR spectra of PEGME (M_n ca. 2000) (bottom) and PEO macroinitiator I1 (top).

Figure 2.2 shows the comparison of the ^{1}H-NMR spectra of PEGME and a PEO Macroinitiator (I1). The spectrum of PEGME shows a singlet at 2.25ppm (peak 3) which confirms the presence of an -OH (3). In the spectra of I1 this peak is absent, confirming what the FT-IR spectrum (Figure 2.1) displayed, that this bond has been broken. Furthermore the ester bonds formation is attested in the spectrum of I1 by the triplet (peak c) at 4.28ppm which is due to the CH_2 group adjacent to the ester bond. A new singlet peak (peak a,b) is also seen at 1.9ppm confirming the structural features of the macroinitiator as can be seen in Figure 2.2.

GPC was used to calculate the molecular weight parameters of the PEO macroinitiators (I1-I5) and these values were compared to the M_n values calculated from ^{1}H-NMR (Table 2.3)The number of ethylene oxide repeating units (*n*) was calculated from ^{1}H-NMR by comparing the integrals of peak g (CH_3) (3.31ppm) and peak e,f (CH_2CH_2O) (Figure 2.2).

I1, I2 and I3 were synthesised using PEGME 2000g/mol on different scales. I4 and I5 were synthesised using PEGME 5000g/mol. Table 1 represents the data collected from both GPC and ^{1}H-NMR. It is evident that there is a difference between the ^{1}H-NMR M_n values and the GPC M_n values. Benoit *et al*.[7] established that GPC separates polymers based on their hydrodynamic volume (radius of gyration). They measured the retention times of polystyrene with known M_w and linear, star and comb-like topologies. Unsurprisingly the branched polymers resulted in a longer retention time. This indicated that the calibration method of plotting log M_w against elution volume does not give a universal calibration curve due to the differences in hydrodynamic volumes of the calibrants and polymers to be tested. The calibrants in this case are PMMA and will therefore have a different hydrodynamic volume to PEO-*b*-PODMA, due to its comb-like structure compared to PMMA's linear structure, this will result in a difference in molecular weight between ^{1}H-NMR and GPC.[8-10] This was taken into account and any following calculations using these results were consistently performed using the M_n^b values. The GPC revealed that all the macroinitiators have a dispersity index of below 1.09 indicating a narrow molecular weight distribution. All the macroinitiators have a DP (degree of polymerisation) value close to that of the relevant PEGME molecule as can be seen in Table 2.3.

Table 2.3: Molecular weight parameters and value of n (number of ethylene oxide units) of PEO macroinitiators calculated using ^{1}H-NMR and GPC.

Code	M_n^a (Da)	M_w^a (Da)	$Đ^a$	M_n^b (Da)	DP^b
PEGME 2000g/mol	***3300***	***3400***	***1.04***	***2030***	***45***
I1	3600	3900	1.06	2380	49
I2	3600	3900	1.08	2160	44
I3	3300	3600	1.09	2200	45
PEGME 5000g/mol	***9700***	***10100***	***1.04***	***5150***	***115***
I4	9500	10200	1.07	5280	115
I5	9000	10100	1.04	5370	117

[a] Calculations from GPC using PMMA standards.
[b] Calculations from ^{1}H-NMR comparing the integrals peak g (CH_3) to peak d,e,f (CH_2CH_2O).

2.4.2 Characterisation of PEO-*b*-PODMA

The block copolymers PEO-*b*-PODMA were synthesised via ATRP using macroinitiators I1-I5. All the block copolymers were characterised using GPC and ^{1}H-NMR to determine the purity, molecular weight parameters and the dispersity. This was vital, as the effect of these parameters on the self-assembly of the block copolymer was later investigated.

The degree of polymerisation of PODMA and molecular weight parameters were determined by the resultant monomer:initiator ratio for each reaction using ^{1}H-NMR, the molecular weight and dispersity were also calculated using GPC. The results of these measurements are displayed in Table 2.4. The dispersity indices (Đ) for all the polymers were below 1.3, this was as expected for an ATRP reaction. The M_n and M_W values obtained via GPC are given in Table 2.4. The degree of polymerisation for each PODMA block was as predicted. The PEO wt % for each block copolymer was calculated using the data obtained from ^{1}H-NMR, with the following equation; (PEO M_n/total copolymer M_n) x 100. The GPC traces and the ^{1}H-NMR spectra were further analysed to identify the block copolymer made and to ensure it was free from impurities.

Table 2.4: Parameters for block copolymers PEO-*b*-PODMA obtained using ^{1}H-NMR and GPC.

Code	Initiator	Structure	M_n[a] (Da)	M_w[a] (Da)	Đ[a]	DP[b]	M_n[b] (Da)	PEO wt %
P1	I3	PEO_{45}-*b*-$PODMA_{36}$	16300	19200	1.18	36	14370	15
P2	I1	PEO_{49}-*b*-$PODMA_{28}$	14100	16900	1.20	28	11840	20
P3	I1	PEO_{49}-*b*-$PODMA_{21}$	15400	19900	1.29	21	9500	25
P4	I2	PEO_{44}-*b*-$PODMA_{19}$	10700	12900	1.20	19	8580	25
P5	I2	PEO_{44}-*b*-$PODMA_{19}$	11100	12800	1.15	19	8580	25
P6	I3	PEO_{45}-*b*-$PODMA_{19}$	10800	13000	1.12	19	8580	25
P7	I1	PEO_{49}-*b*-$PODMA_{16}$	10900	14000	1.28	16	7780	30
P8	I2	PEO_{44}-*b*-$PODMA_{11}$	9982	10700	1.07	11	5880	40
P9	I5	PEO_{117}-*b*-$PODMA_{10}$	15100	17300	1.14	10	8660	60

[a] Calculations from GPC in THF (PMMA Standards)

[b] Calculations from ^{1}H-NMR in $CDCl_3$ by comparing the integrals of peak a to peak f.

The block copolymer P3 was overlaid with the macroinitiator I1 in order to determine if there was any macroinitiator left unreacted. This was done for all synthesised PEO-*b*-PODMA block copolymers, Figure 2.3A represents the GPC traces of P3 overlaid with I1, which is representative of all BCP's synthesised with a I1 initiator. The peak for P3 is monomodal suggesting all the macroinitiator has reacted, also there is <10 % overlap between the two peaks, this was established by the integral analysis of the RI response, therefore the preliminary results suggested there was an insignificant amount of PEO macroinitiator left unreacted in this polymer precipitate, this was also the case of P5 overlaid with I2 (Figure 2.3B). The GPC trace of P9 overlaid with I5 (Figure 2.3C) shows a large amount of overlap between the initiator and the BCP peaks, however a low dispersity was observed for this BCP. However the ^{1}H-NMR spectra were required to confirm this.

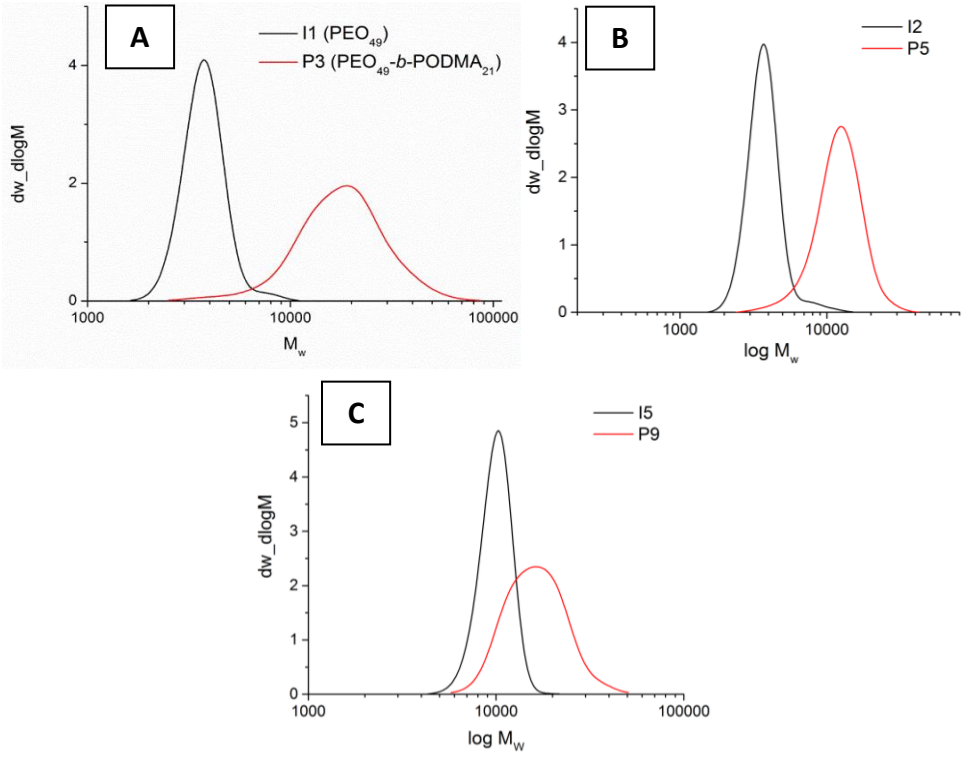

Figure 2.3: GPC traces of **A)** PEO_{49}-*b*-$PODMA_{21}$ (P3) after one precipitation into ethanol, overlaid against macroinitiator PEO_{49} (I1), **B)** PEO_{44}-*b*-$PODMA_{19}$ (P5) after one precipitation into ethanol, overlaid against macroinitiator PEO_{44} (I2) and **C)** PEO_{117}-*b*-$PODMA_{10}$ (P9) after one precipitation into ethanol, overlaid against macroinitiator PEO_{117} (I5)

Figure 2.4 is the ^{1}H-NMR spectrum collected for PEO_{49}-*b*-$PODMA_{21}$ (P3) it is representative for all PEO-*b*-PODMA block copolymers synthesised in this section and used for self-assembly. There is an absence of the methacrylate monomer peaks at 5.5 and 6.1ppm and the macroinitiator peak at 4.3ppm (peak 2) is not present on the spectrum of P3. This confirms the absence of unreacted macroinitiator in sample P3.

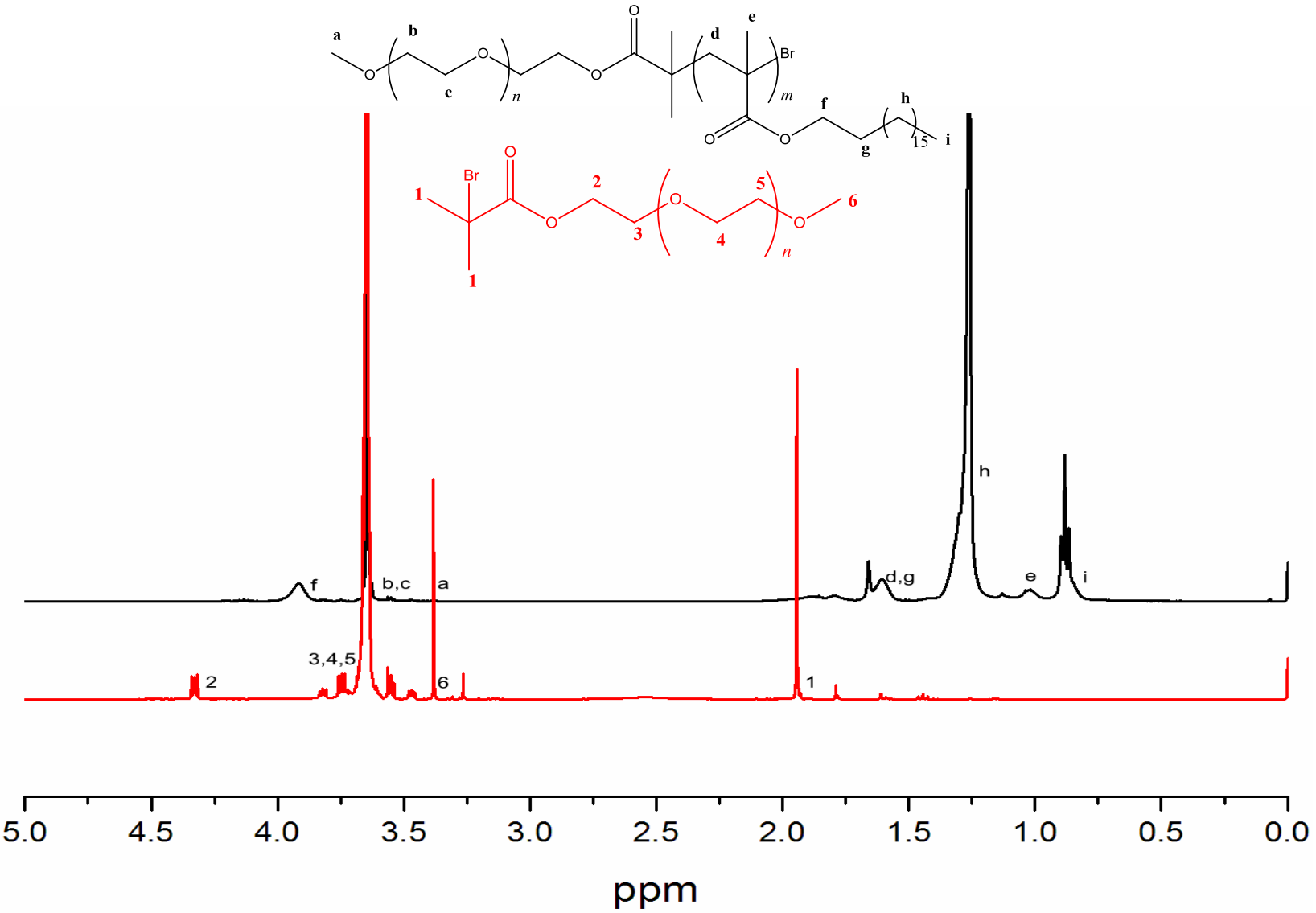

Figure 2.4: ^{1}H-NMR spectra of PEO_{49}-*b*-$PODMA_{21}$ (P3) (top) overlaid with macroinitiator PEO_{49} (I1) (bottom)

2.4.3 Differential Scanning Calorimetry of P3

The ability of the octadecyl side chains to crystallise is what makes this block crucial to form a bicontinuous nanosphere with thermo-responsive properties. Rehberg and Fisher (1948)[11] studied the brittle points of a series of polyacrylates and polymethacrylates and found that these points decrease with an increase in carbons within the alkyl side chain, however above 8 carbons for acrylates and 12 for methacrylates the brittle points increase. This is attributed to the side chains increase in crystallinity and therefore melting point.[12-13] Jordan *et al.* studied the crystallinity of alkyl side chains in poly(*n*-alkyl acrylates), poly(*N*-*n*-alkyl-acrylamides) and poly(vinyl esters), they established via DSC studies that it is only the outer methylene units that contribute to the crystal lattice.[14-15] This was also seen by several other investigators who propose that the 9 methylene units closest to the polymer backbone do not contribute to the side chain crystallinity.[13, 16-17]

It has been well established that poly acrylates and poly methacrylates alkyl side chains pack hexagonally like closed pack cylinders.[18-19] They pack into paraffin-like crystallites.[17] It has also been established that the molecular weight does not have a significant effect on side chain crystallinity, Beiner *et al*. [20] observed this for a series of PODMA homopolymers where an increase in DP of the ODMA monomer sees only a slight increase in D_c (degree of crystallinity). It has been observed that a regular distribution of crystallisable side chains along the backbone is not essential for them to crystallise.[17, 21]

Generally poly(acrylates) have higher T_m than poly(methacrylates) with the same alkyl side chain length. This is due to the extra methyl group on the methacrylate causing the backbone to become stiff.[13, 22-23] Less favourable packing is a result of this reduction in flexibility and the conformational freedom of the side-chain is reduced. Therefore the degree of crystallinity for methacrylates will be lower indicating a lower T_m.[13, 23-24] This has also been seen when styrene and alkyl-styrene are incorporated into the backbone.

It was thought that incorporating docosyl methacrylate into the PODMA block would increase the T_m. It has been seen previously that although the molecular mass does not significantly affect the T_m[25], the increase of longer alkyl chains on the

methacrylate and acrylate backbones does, where an increase in degree of crystallisation and T_m was observed.[25-26] It was also thought that having defined ratios of the two monomers (ODMA and DSMA) within the copolymer would allow us control over the T_m as seen before by Alfrey *et al.* where the T_m for a copolymer of tetradecyl and octadecyl methacrylate was almost midway between the T_m of the individual homopolymers.[13]

A T_m (onset) for bulk PEO-*b*-PODMA has already been established (22°C).[6] The values obtained from the heating run for bulk P3 are consistent with those previously measured, giving a T_m (onset) of 21.3°C, which is attributed to the melting of the semi-crystalline PODMA block. This melting temperature is due to the crystallinity of the octadecyl alkyl side chains on the methacrylate backbone, which gives the PODMA block a comb-like topology. The aggregate solution gave a T_m of 32.4°C an increase of 2°C compared to the bulk sample.

Table 8 displays the temperatures and enthalpies (ΔH) related to the transitions for both the bulk and aggregate samples of P3. To compensate for 95 % (water) of the aggregate solution not contributing to the transition, the enthalpy change was modified to only take into account the 5 % PEO-*b*-PODMA nanospheres (calcualtion in chapter 3). The ΔH for the aggregate sample is lower than the bulk, this could be due to the transition being masked by the water transition, or that the degree of crystallinity for the PODMA chains has decreased on self-assembly of the BCP.

Table 2.5: DSC results for the melting transition of P3 bulk and 5 wt % aggregate solution. All measurements were taken from the second heating run.

Sample	Peak		Peak	Onset	ΔCp	ΔH (KJ/mol)
	Start (°C)	*End* (°C)	(°C)	(°C)	(J/(g*K)	
Bulk P3	13.6	33.9	26.6	21.5	30.93	9.78
P3 5 wt %	22.6	30	24.9	23.4	0.1308	1.03
I1 (PEO)	39.9	66.9	57.8	45.1	147.2	6.48
PODMA	20.2	33.1	27.7	23.7	26.45	8.94

The thermogram for the melting transition of P3 bulk is shown in Figure 2.5. A smooth transition is seen with a wide range from 13.6-33.9°C.

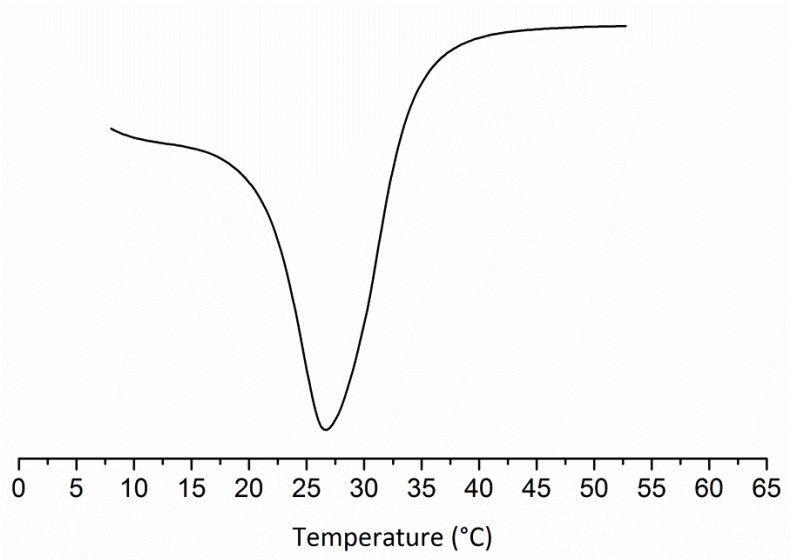

Figure 2.5: DSC thermogram for P3 bulk melting transition. Measurement taken from the second heating run.

The melting transition for P3 5 wt % aggregate solution was not as easy to determine as for the bulk. This was due to the transition of the water the aggregates were suspended in, obscuring the transition (Figure 2.6). A smaller enthalpy was seen for the aggregate as only 5 % of the solution was contributing to the transition. A smaller range was also seen for the transition with it starting at 22°C and ending at 30°C.

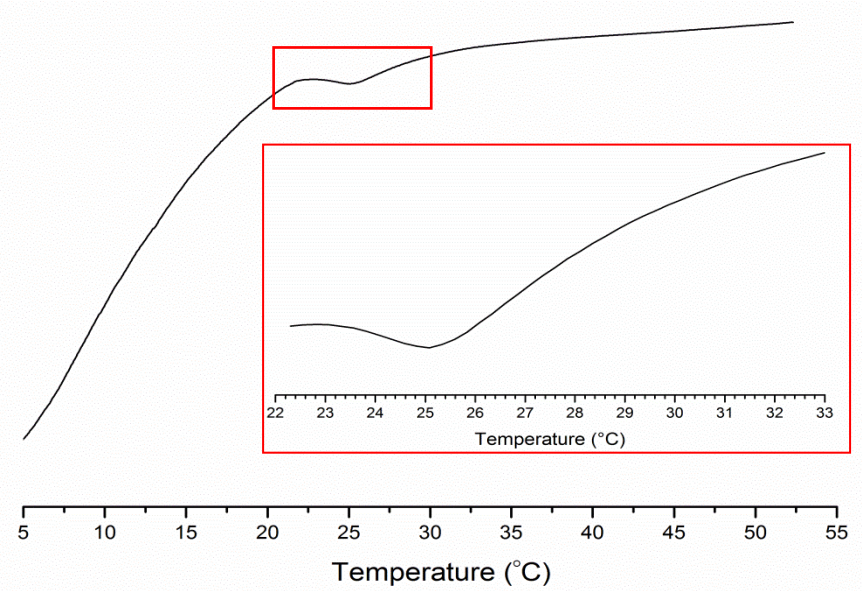

Figure 2.6: DSC thermogram for P3 5 wt % aggregate solution. Inset zoomed in on transition. Measurement taken from second heating run.

2.4.4 Self-Assembly of Poly(ethylene oxide)-*block*-Poly(octadecyl methacrylate)

2.4.4.1 *Effect of hydrophilic weight fraction on morphological changes in PEO-b-PODMA particles*

PEO-*b*-PODMA has been found to form bicontinuous nanospheres when the weight percentage of the hydrophilic block (PEO) is between 11-25 % and the BCP has a M_w of <17kDa. Multi-lamellar vesicles were observed for PEO-*b*-PODMA with 34 PEO wt %.[3] To confirm the requirements for the formation of bicontinuous nanospheres PEO-*b*-PODMA was self-assembled at varying PEO weight fractions using procedure A and the resultant aggregate solutions were analysed using DLS and TEM to compare the particle sizes and morphologies produced. According to Discher and Eisenberg when the hydrophilic weight fraction *f* is at 35 % ± 10 % polymersomes (vesicles) should form. Cylindrical micelles will be present at *f* = <50 %. At *f* = >45 % micelles should be observed and an inverted structure is present at f = <25 %. These predictions were made based on the polymer systems PS_{40}-*b*-poly(isocyano-L-alanine-Lalanine)$_m$, PEO-*b*-PBD (PBD, polybutadiene) and PEO-*b*-PEE (PEE, polyethylethylene) amongst other BCPs.[27] The size of the hydrophobic moiety (in comparison to the hydrophilic block) determines the molecular curvature at the hydrophobic-hydrophilic interface.[28] The molecular curvature is what drives the morphology as determined by Bates *et al.*[29] The packing parameter, p, can also be used to predict the resultant morphology by giving an indication to the molecular curvature of the polymer. The use of the packing parameter to predict polymer aggregate morphology was first introduced by Israelachvili *et al.* and as discussed in chapter 1, the general rule for the three major morphologies are p= 1/3 (spherical), p= ½ (cylindrical) and p=1 (membrane/vesicle).[30] Bicontinuous nanospheres do not fall into these guidelines

To confirm that above 25 wt % the bicontinuous morphology has been lost, studies were carried out on the PEO 30 wt % (P7) and 25 wt % (P3) BCPs for comparison. The BCPs were self-assembled at concentrations of 0.1-5 wt % in solution, to assess whether the morphology persisted with an increase in concentration, and analysed further with DLS, TEM and cryo-TEM.

Varying masses of each polymer were dissolved in THF and water was then added dropwise following dialysis procedure A. The mass of the block copolymer used to make each corresponding weight percentage are seen in Table 2.6.

Table 2.6: Weight percentage and masses used for the self-assembly of all PEO-*b*-PODMA block copolymers.

PEO-*b*-PODMA wt %	Mass (g) (PEO-*b*-PODMA)	THF volume (mL)	Water volume (mL)	Total volume (mL)
0.1	0.01	4	6	10
1	0.1	4	6	10
4	0.4	4	6	10
5	0.5	4	6	10

Dynamic Light Scattering was used to determine the particle size and particle size distribution of the block copolymers in solution. DLS was used on each self-assembled block copolymer at varying weight percentages. Measurements were taken at both 15 and 35°C above and below the calculated transition temperature of PEO-*b*-PODMA. Each measurement consisted of 10 runs with the average of the number mean calculated. The dispersity index in this case represents the size distribution of the particles in solution, this is calculated from the Z-average.

P3- PEO_{49}-*b*-$PODMA_{21}$ (25 PEO wt %)

Block copolymer P3 (PEO_{49}-*b*-$PODMA_{21}$) was synthesised with a ratio of PEO:PODMA at 1:21 giving a PEO wt % of 25 %. It was self-assembled at weight percentages 0.1, 1 and 4 % in 4 mL of THF and 6 mL of deionised water at 35°C. Each sample was then analysed using DLS, at 15 and 35°C, and TEM, the DLS results are shown in Table 2.7. At 35°C the number mean was higher, this was the case for all the concentrations. This increase in N_{ave} suggest the particles are either aggregating together, having been heated above the PODMA T_m (21.3°C), or their internal bicontinuity will have been lost and the particles have expanded, this thermo-response has been previously observed using cryo-TEM by McKenzie *et al.*[6] and will be discussed in more detail in chapter 3. On increase of the polymer concentration in solution a decrease in the particle sizes were observed at both 15 and 35°C, this means that either the size of the particles were decreasing on increase of polymer or that the particles were more

dispersed in solution. There was however an anomaly to this observation. The 1 % solution had a large increase in number mean at 15°C when compared to the 0.1 wt % solution. The dispersity index stayed consistent with the temperature change however it increased drastically with an increase in weight percentage. This suggests that with a lower weight percentage there is a narrow size distribution.

Table 2.7: Number mean values for self–assembled block copolymer P3 (PEO_{49}-*b*-$PODMA_{21}$) with a PEO weight percentage of 25 % calculated from the Z-average using Dynamic Light Scattering.

wt %	T (°C)	N_{ave} (d.nm)	SD (± nm)	Z_{Ave} (d.nm)	SD (± nm)	CONTIN (nm)	Đ
0.1	15	380	44	436	5	484/187	0.15
0.1	35	476	49	524	7	286/686	0.19
1	15	458	37	628	14	400/831	0.37
1	35	482	39	716	12	345/1277	0.36
4	15	344	61	820	30	171/428/1232	0.54
4	35	360	52	759	19	230/803	0.57

The number % calculated from the Z-average was plotted as a line graph for each concentration of P3 at 15 and 35°C. Figure 2.7 illustrates the distribution plots for P3 at 15°C. The plot for the 0.1 % solution is monomodal this indicates a low size distribution, Table 2.7 supports this showing a Đ of 0.15. As discussed earlier the 1 % solution at 15°C did not follow the trend and had an increase in number mean this is seen in Figure 2.7 where a bimodal distribution is evident, a small number % of particles (6.2 %) have formed aggregates within the large range of 750-3000 nm and Peak 1 (350 nm) represents 93.8 % of the polymer particles, which shows that there was in fact a decrease in N_{ave} when compared to the 0.1 wt % solution. A bimodal distribution is also seen for the 4 wt % solution with the highest number of particles being approximately 200 nm in diameter and a small number of larger particles present across the size range 500-1625 nm. The larger particles sizes seen could be due to the particles aggregating together.

When measured at 35°C with DLS a small 9.95 % of particles in the 0.1 % solution have aggregated together giving rise to a slightly higher number mean than when measured at 15°C (Table 3). Above the BCP T_m the bicontinuous nanospheres lose order[6] which would explain the change in particle size. The 1 and 4 % solutions have a higher number % of particles that have aggregated together between 500 and 1600 nm. All the solutions at 35°C have bimodal peaks and therefore this explains why they all have a high dispersity compared to the measurements taken at 15°C.

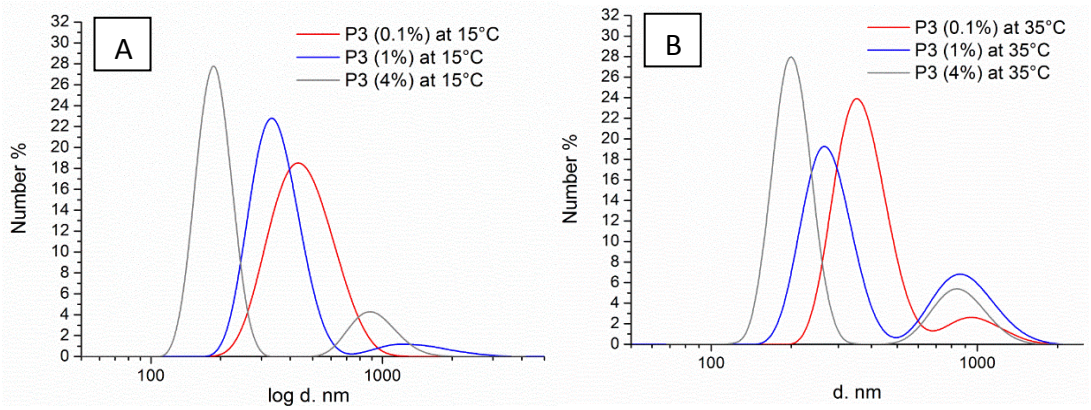

Figure 2.7: DLS distribution plot of P3 (PEO_{49}-*b*-$PODMA_{21}$), wt % 0.1-4 % at 15°C (A) and 35°C (B).

The sizes of the PEO-*b*-PODMA aggregates have already been established using DLS, however this needed to be confirmed by TEM, along with the shape and morphology of the aggregates. TEM alone was not sufficient to determine the morphology so the samples were also analysed using cryo-TEM as it allows the particles to be analysed in their natural environment without staining or dehydration. The sample is pipetted onto a carbon coated grid, plasma treated to remove the top carbon layer leaving a hydrophilic surface, the sample is then vitrified in liquid ethane cooled by liquid nitrogen to prevent the formation of ice crystals.

Table 2.8 shows the number average size (nm) of the polymer aggregates obtained from TEM and the morphologies observed from cryo-TEM. Bicontinuous nanospheres were observed for all three concentrations of P3 (PEO_{49}-*b*-$PODMA_{21}$) (PEO wt % of 25 %) and the number average particle size decreased on increase in polymer concentration in solution, this result was consistent with the sizes observed via DLS measurements. Figure 2.8 shows the TEM and cryo-TEM images of P3 at 0.1

wt %. The TEM images (A) show spherical aggregates with possible bicontinuous morphology with a N_{ave} of 307 nm (calculated from 60 particles). The cryo-TEM images (B) confirm the presence of bicontinuous nanospheres, showing spherical aggregates with a porous internal morphology with a size range of 200-700 nm.

Table 2.8: Size and morphology of P3 (PEO_{49}-*b*-$PODMA_{21}$) (PEO 25 wt %) aggregates obtained from TEM and cryo-TEM.

wt %	N_{ave} (d.nm)	SD (±nm)	Morphology
0.1	307	109	Bicontinuous nanospheres
1	222	125	Bicontinuous nanospheres
4	194	80	Bicontinuous nanospheres, lamellar

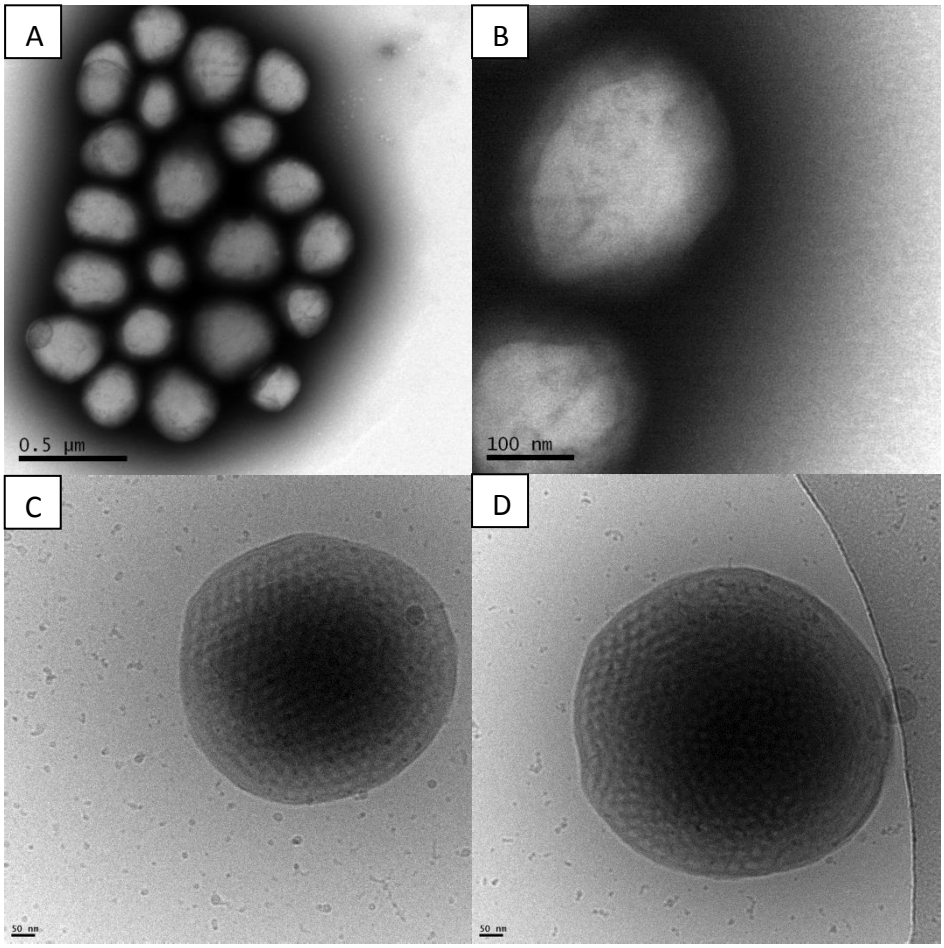

Figure 2.8: **A-B)** Negative stained TEM images of P3 (0.1 wt %) nanospheres (Stained with 5 % uranyl acetate and 1 % acetic acid). **C-D)** Cryo-TEM images of P3 (0.1 wt %) nanospheres with internal bicontinuous morphology.

The TEM images shown in Figure 2.9 A of P3 (1 wt %) show spherical aggregates over a range of sizes with a possible bicontinuous internal morphology. The cryo-TEM images (Figure 2.9 B) confirm the presence of bicontinuous nanospheres, with the porous internal morphology very evident. However these aggregates are not as spherically uniform, when compared with the 0.1 wt % solution, along with having a larger number of small nanospheres.

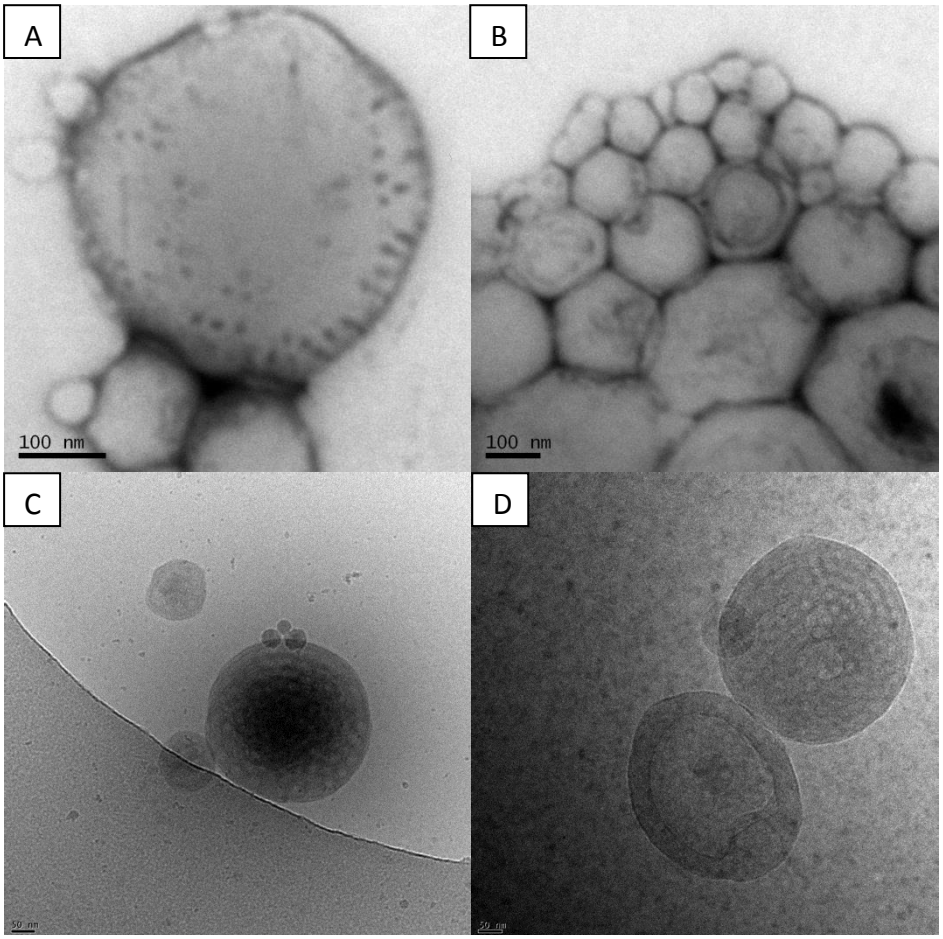

Figure 2.9: **A-B)** Negative stained TEM images of P3(1 wt %) nanospheres (Stained with 5 % uranyl acetate and 1 % acetic acid). **C-D)** Cryo-TEM images of P3 (1 wt %) nanospheres with internal bicontinuous morphology.

The negative stained TEM images in Figure 2.10 A of P3 (4 wt %) show spherical aggregates over a range of sizes with a possible bicontinuous internal morphology. The cryo-TEM images confirm the particles have a bicontinuous internal structure. However the exterior morphology of these aggregates are not as uniformed despite the obvious internal uniform porous structure. In both the 0.1 and 1 wt % solutions the only morphology observed was bicontinuous, in the 4 wt % solution the cryo-

TEM images revealed some aggregates that display both bicontinuous and lamellar internal morphology (Figure 2.10 B). This has been seen previously at PEO 25 wt % but at a concentration of 0.1 and 0.5 wt % in solution[6], only bicontinuous nanospheres were observed for P3 at the same concentration.

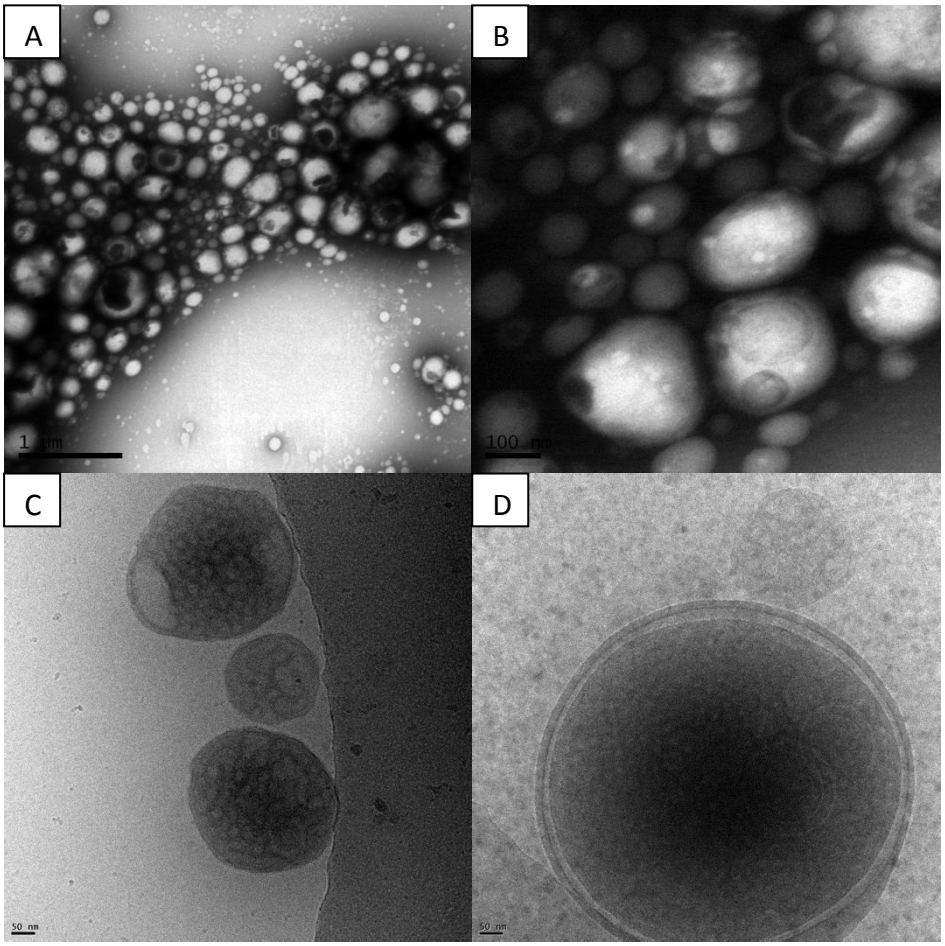

Figure 2.10: A-B) Negative stained TEM images of PEO_{49}-*b*-$PODMA_{21}$ (4 w t%) nanospheres (Stained with 5% uranyl acetate and 1% acetic acid). **C-D)** Cryo-TEM images of PEO_{49}-b-$PODMA_{21}$ (4 wt %) nanospheres with internal bicontinuous morphology.

P7 PEO_{49}-*b*-$PODMA_{16}$ (PEO 30 wt %)

Block copolymer P7 (PEO_{49}-*b*-$PODMA_{16}$) was synthesised with a ratio of PEO:PODMA at 1:16 giving a PEO wt % of 30 %. It was dissolved at varying weight percentages (0.1-5 %) (See Table 2.6) in 4 mL of THF and then self-assembled by the slow addition of 6 mL of deionised water. Each sample was analysed with the DLS at 15 and 35°C, the results are shown in Table 2.9. The number mean values for P7 particles are around 100 nm lower than for P3 indicating that an increase in PEO wt % has an effect on the size of the aggregates. For the weight percentages 0.1-5 % the number mean was higher at 35°C in contrast to P3 aggregates where there was a decreases in particle size. On increase in concentration (wt %) the number mean of the solutions decreased, the same trend seen for P3 particles, this demonstrates the idea that concentration will affect the particle size. As seen in P3 the 1 % solution at 15°C did not follow the same trend and an increase in number mean was observed. A consistent dispersity index was seen on increase of temperature. The dispersity increased on increase in BCP concentration, this was seen previously with P3. The solutions at lower concentrations have narrower size distributions. The solutions made up from P7 have on average a higher dispersity than those of P3 at the same weight percentages.

Table 2.9: Number mean values for self–assembled block copolymer P7 (PEO_{49}-*b*-$PODMA_{16}$) calculated from the Z-average using Dynamic Light Scattering.

wt %	T (°C)	N_{Ave} (d.nm)	SD (± nm)	Z_{Ave} (d.nm)	SD (± nm)	CONTIN (nm)	Đ
0.10	35	338	95	501	18	144/462	0.44
0.10	15	251	91	584	14	272/1352	0.57
1	35	286	103	598	15	185/933	0.48
1	15	272	59	605	23	473/2040	0.51
5	35	113	26	582	33	101/233/812	0.98
5	15	108	39	540	16	108/284/1080	0.98

As with P3 the number % calculated from the Z-average was plotted as a line graph for each sample of P7 at 15 and 35°C. The distribution plots at 15°C can be seen in Figure 2.11. The particles in all three samples have some aggregation this is evident from the bimodal peaks seen in the distribution plots. The plot shows that the 1 and 5 wt % samples have roughly the same sized particles. The 0.1 wt % sample yielded larger particles, which is consistent with the results seen in Table 2.9. Figure 2.11 shows the overlays of the number mean distribution plots for 0.1-5 wt % solutions measured at 35°C, for P7. All plots are bimodal, however the second peak seems to get smaller as the wt % is increased. The 1 and 5 wt % solutions aggregates are very close in size compared with the 0.1 wt % solution whose aggregates are around 100-200 nm larger.

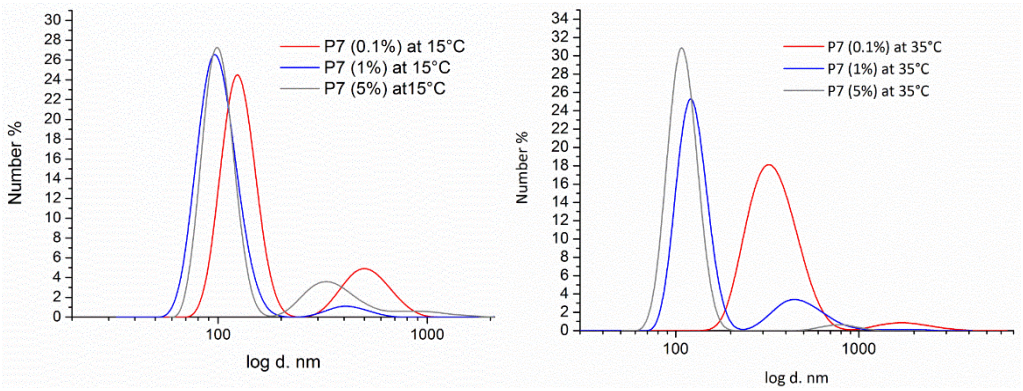

Figure 2.11: DLS distribution plot of P7 (PEO_{49}-*b*-$PODMA_{16}$), wt % 0.1-5 % at 15 °C (A) and 35°C (B).

The N_{ave} and morphologies for P7 at concentrations 0.1-5 wt % are given in Table 2.10**.**

Table 2.10: Size and morphology of PEO-*b*-PODMA aggregates obtained from TEM (calculated from > 40 particles) and cryo-TEM.

Sample	Structure	PEO wt %	wt %	N_{ave} (d.nm)	Morphology
P7	PEO_{49}-*b*-$PODMA_{16}$	30	0.1	60 (Spheres) 95 (Worms)	Cylindrical, micelles, vesicles
P7	PEO_{49}-*b*-$PODMA_{16}$	30	1	209	Micelles, vesicles
P7	PEO_{49}-*b*-$PODMA_{16}$	30	5	80	Micelles, vesicles, bicontinuous nanospheres

The negative stained TEM images in Figure 2.12 A of P7 (0.1 wt %) show spherical and cylindrical aggregates as well as thin films over a range of sizes. The cryo-TEM images (Figure 2.12 B) display the presence of cylindrical micelles (worms), vesicles, multi-lamellar aggregates as well as some aggregates containing bicontinuous morphology. This agrees with the literature[3, 6, 31-32] that the wt % of the hydrophilic block must be below 25 % to fully obtain bicontinuous nanospheres.

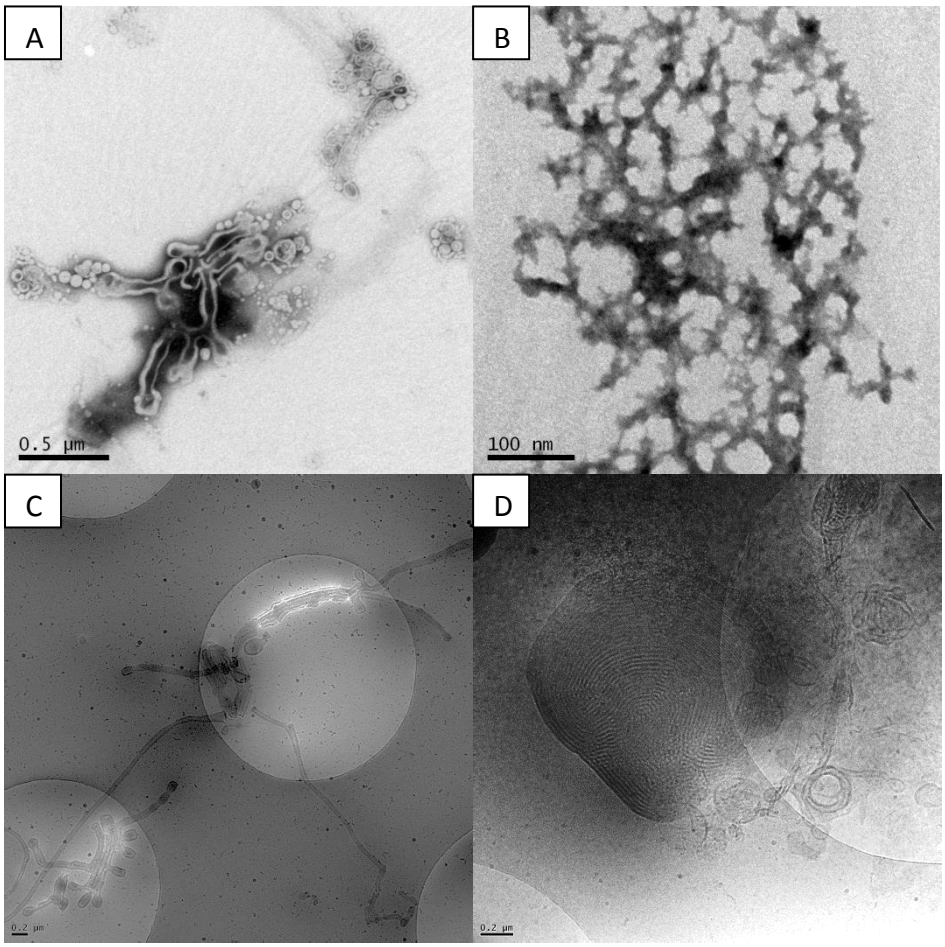

Figure 2.12: A-B) Negative stained TEM images of **P7** (0.1 wt %) nanospheres (Stained with 5 % uranyl acetate and 1 % acetic acid). **C-D)** Cryo-TEM images of **P7** (0.1 wt %) cylindrical micelles and nanospheres with internal bicontinuous morphology as well as multi-lamellar vesicles.

Spherical vesicle sized particles and micelles are evident in the negative stained TEM images of P7 1 wt % solution, shown in Figure 2.13 A with an average particle size of 209 nm (calculated from 40 particles). Vesicles are evident in the cryo-TEM images in Figure 2.13 B, but more interestingly nanospheres with a bicontinuous internal morphology are also present which is consistent with the 0.1 wt % solution. However this morphology is not isolated as it is when the PEO wt % is decreased to 25 %.

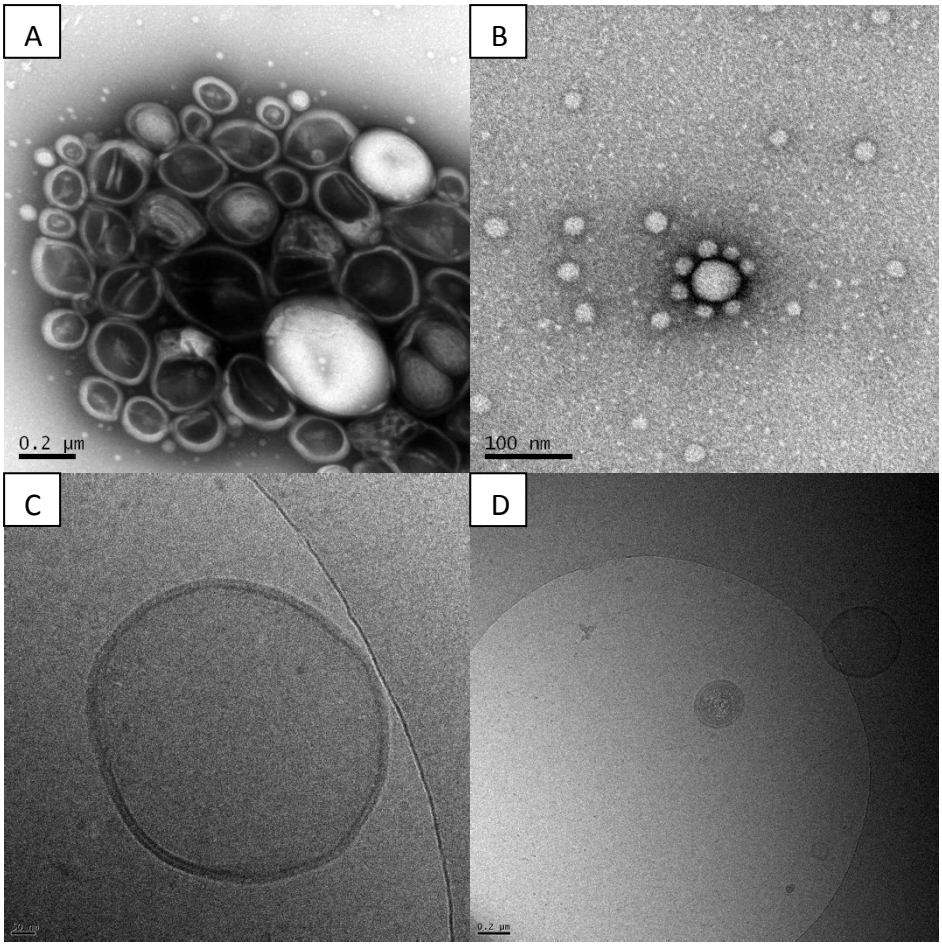

Figure 2.13: A-B) Negative stained TEM images of P7 (1 wt %) nanospheres (Stained with 5 % uranyl acetate and 1 % acetic acid). **C-D**) Cryo-TEM images of P7 (1 wt %) vesicles.

As with the 1 wt % solution, both vesicles and micelles were present in the 5 wt % solution of P7. These morphologies are evident in the negatively stained TEM images in Figure 2.14. The cryo-TEM images show vesicles but also particles with bicontinuous internal morphology, however the exterior morphology is no longer spherical. Multi-lamellar aggregates were also present.

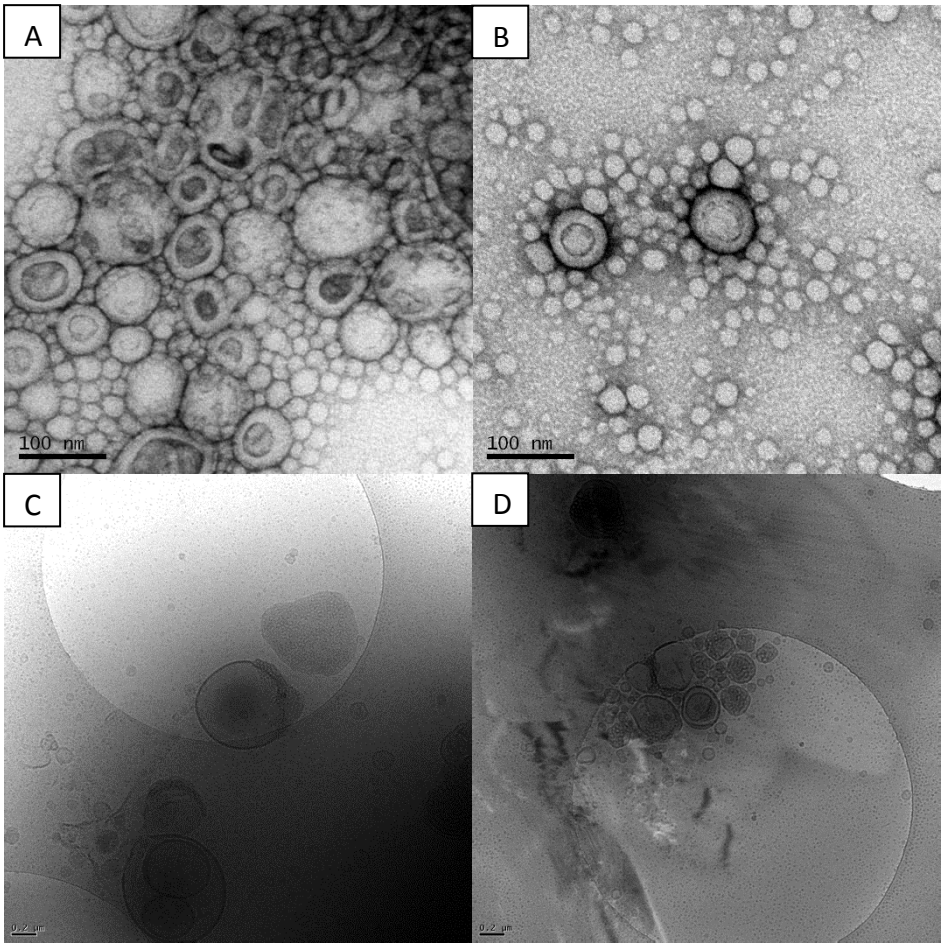

Figure 2.14: A-B) Negative stained TEM images of **P7** (5 wt %) nanospheres (Stained with 5 % uranyl acetate and 1% acetic acid). **C-D)** Cryo-TEM images of **P7** (5 wt %) vesicles and nanospheres with internal bicontinuous morphology as well as lamellar vesicles.

From analysing the DLS and TEM results for both P3 and P7 aggregates it is clear that when PEO-*b*-PODMA has a PEO weight fraction above 25 % the bicontinuous morphology is lost and various other morphologies are seen such a multi-lamellar and cylindrical micelles. The formation of cylindrical micelles was unsurprising when Discher and Eisenberg's guidelines are taken into account which, mentioned previously, outlines that cylindrical morphologies would be seen below 50 wt % hydrophilic block. More interesting is that when looking at the cryo TEM images of P3, spherical aggregates are observed for concentrations 0.1, 1 and 5 wt % in solution. As the concentration is increased the internal bicontinuous morphology is maintained with an increase in disorder. This section has shown that a PEO wt % of 25 % is required to produce spherical particles with a bicontinuous internal morphology and that increasing the PEO wt % results in a change of shape in some

particle to cylindrical, along with a change in internal morphology to multi-lamellar. At 25 PEO wt % (P3) bicontinuous nanospheres were observed with the morphology consistent with an increase in concentration showing that concentration does not affect the resultant morphology.

The number average particle sizes were plotted against the PEO weight fraction for PEO-*b*-PODMA from PEO 15 wt % up to 60 % (Figure 2.15). Both the 40 and 60 % BCPs exhibit sizes consistent with the formation of micelles (<65nm) with the 40 % not following the guidelines set out by Discher and Eisenberg.[27] The largest particles are seen for 25 % with a decrease in particle size as the PEO wt % is increased and decreased by 5 %. The 15 % BCP produced larger particles than for the 20 %.

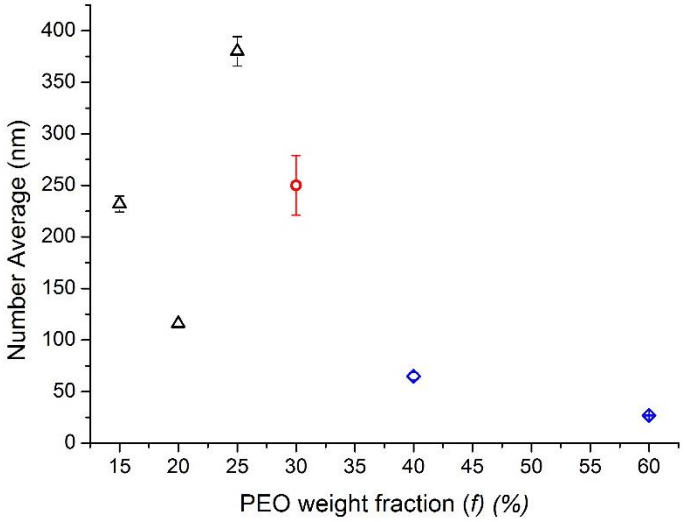

Figure 2.15: Comparison of N_{ave}, calculated from DLS, with PEO weight fraction for polymers P1, P2, P3, P7, P8, and P9. Error bars calculated from 10 runs of same sample. **Δ** represents bicontinuous nanospheres, ○ represents a mixture of morphologies of cylindrical micelles, multi-lamellar and bicontinuous nanospheres, ◊ represents spherical micelles.

Discher and Eisenberg's guidelines would indicate that both P3 (PEO 25 wt %) and P7 (PEO 30 wt %) particles would be vesicles. Comparing the DLS data of both P3 and P7 particle solutions it is evident that as the weight % of the hydrophilic block is increased the particle size decreases. The guidelines given by Discher and Eisenberg do not take into account more complex internal morphologies that may have an effect on particle size. Another factor to take into account is that DLS measurements are calculated with the assumption that the particles are completely spherical, therefore if cylindrical micelles were formed analysis with DLS would not give an

accurate particle size. The particle sizes for both P3 and P7 are similar and are consistent with vesicle size. Further analysis with TEM and cryo-TEM is therefore needed to accurately ascertain the morphology of the particles formed.

2.4.4.2 Preparation of Bicontinuous Nanospheres

In all previous literature of the self-assembly of PEO-*b*-PODMA into bicontinuous nanospheres, [3, 6, 31-33] the same self-assembly method (A) has been used where the BCP was dissolved in a volume of THF, water was then added dropwise followed by the removal of the THF via dialysis for 24 hours. The reason this method was used instead of the direct dissolution method was because the PODMA block is not water soluble and therefore a common solvent was needed to dissolve the BCP. (See method A) The effect of varying the volume of the initial THF/water solution, on the resultant nanospheres diameter, has been investigated by McKenzie *et al.* They found that increasing the THF wt % content results in a decrease in the particle diameter each time. They were able to obtain particle sizes ranging from 70 ±30 nm to 460 ±100 nm while still maintaining the bicontinuous internal morphology. A phase diagram was constructed that correlated the aggregate morphologies with their molecular weight and PEO wt %. This diagram showed that the bicontinuous polymeric nanospheres form consistently at low M_w (<17 kDa) with a PEO wt% of 25 %. This has been confirmed previously in this chapter with PEO-*b*-PODMA (PEO 30 wt %) producing multi-lamellar aggregates consistent with the phase diagram, but cylindrical micelles were also observed which have not been seen before at PEO 30 wt %. This further confirms that it is not just the hydrophilic blocks wt % that affects the morphology, but also the molecular weight.[3] Other research has been undertaken into understanding the affect the self-assembly method has on the morphology. The BCP was dissolved as usual in THF (4 mL), water was then added and the solution analysed with cryo-TEM at set weight fractions of water from 5-63 wt % (0.2 mL – 6 mL). At 10 wt % water multi and unilamellar vesicular structures were observed. As the water content was increased the aggregates transitioned to just unilamellar then tubular and finally large dense fields of polymer at 63 wt % water. During the dialysis stage the polymers start at as large polymer sheets with some phase separation, as the dialysis progressed the sheets became more rounded

aggregates which were still flattened and had phase separation. After the THF has been removed by dialysis the aggregate solution was steadily cooled and bicontinuous nanospheres were observed as the major morphology below 10°C. This process was reversible with an increase in temperature.[34]

This section will investigate further the effect the self-assembly preparation has on the particle size and morphological properties of the nanospheres using PEO-*b*-PODMA with a PEO wt % of 25 % and a M_w of 9.5 kDa. A number of different preparations have been investigated which do not require the dialysis step, this significantly decreases the nanospheres formation time from around 24 hours to a 2-3 hours. Procedure B and C still require the use of THF with fast evaporation to remove, whereas D uses only water, eliminating the risk of THF remaining in solution after removal attempts.

For all procedures PEO-*b*-PODMA (25 wt % PEO) aggregate solutions were prepared at 0.1 wt % in solution. The resultant aggregate solutions were analysed using DLS to determine the particle sizes and dispersity (Đ) at 15 and 35 °C. Procedure A (dialysis) has already been extensively investigated in the self-assembly of PEO-*b*-PODMA bicontinuous nanospheres where the PEO content was 25 wt %. The THF:water ratio used for this procedure was 2:3 producing the largest nanospheres, of all methods, with a number average of 476 nm. Procedure B and C remove the THF *via* rotary evaporation; however slow addition of water is used for procedure C in contrast to the fast addition of water in procedure B. Procedure C produced the second largest nanospheres with a number average of 186 nm and a lower dispersity than procedure A. Procedure B produced the smallest particles with a number average of 78 nm, the smallest aggregates compared to the other procedures. This indicates that the size of the nanospheres can be tailored by simply modifying the procedure for the addition of water to the BCP/THF solution. Procedure D produced aggregates of around 130 nm with use of an emulsifier. There was some loss of polymer during this method as a portion of the polymer was left on the emulsifier probe so the concentration of particles is less than for the other methods.

Table 2.11: Number average, Z-average and dispersity values for self–assembled block copolymer P5 (A, B, C and D) (PEO 25 wt %) calculated using Dynamic Light Scattering.

Method	T (°C)	N_{Ave} (d.nm)	SD (± nm)	Z_{Ave} (d.nm)	SD (± nm)	Đ
A	15	476	132	1119	79	0.67
A	35	284	54	617	27	0.44
B	15	78	13	158	1	0.21
B	35	89	19	166	1	0.22
C	15	186	43	364	8	0.44
C	35	188	56	384	8	0.46
D	15	131	26	273	10	0.39
D	35	154	20	268	7	0.39

The N_{ave} distribution plots for all four methods measured at 15°C are displayed in Figure Number A. The distribution plots for A and B are monomodal with A (dialysis) having the largest average particle size of around 400-500 nm this is consistent with the N_{ave} given in Table 2.11. Procedure B has the smallest average particle size of around 70 nm which is again consistent with the value given in Table 2.11. Both procedure C and D exhibit bimodal distributions which explains why their dispersity is higher than that observed for procedure B. They both have particles sized roughly between 100 and 200 nm. The distributions plots for procedures B-D at 35°C are not significantly different form the plot measured at 15°C. The plot for procedure A shows that the N_{ave} has decreased to around 200 nm, this is consistent with the results observed in Table 2.11.

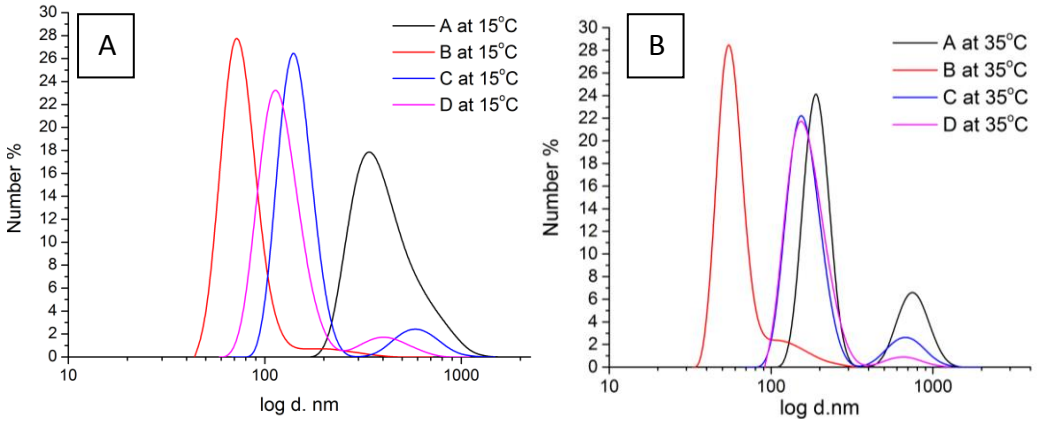

Figure 2.16: DLS distributions plots for the 0.1 wt % aggregate solutions of PEO-*b*-PODMA (PEO 25 wt %) prepared by procedures A-D analysed at **A)** 15°C and **B)** 35°C.

The aggregates produced from all four methods were analysed with TEM to assess their size and morphology. All methods produced spherical aggregates (Figure 2.17) with procedure A producing aggregates of similar sizes with an average of 309 nm. Procedure B and C produced large spherical aggregates and micelles with average sizes of 183 and 92 nm which is inconsistent with the DLS results. TEM images of the aggregates produced using procedure D could not be obtained due to a low concentration of aggregate within the sample. Cryo-TEM images of the aggregate produced from procedures B, C and D could not be obtained due to the low concentration. As previously reported in this chapter procedure A produces bicontinuous nanospheres.

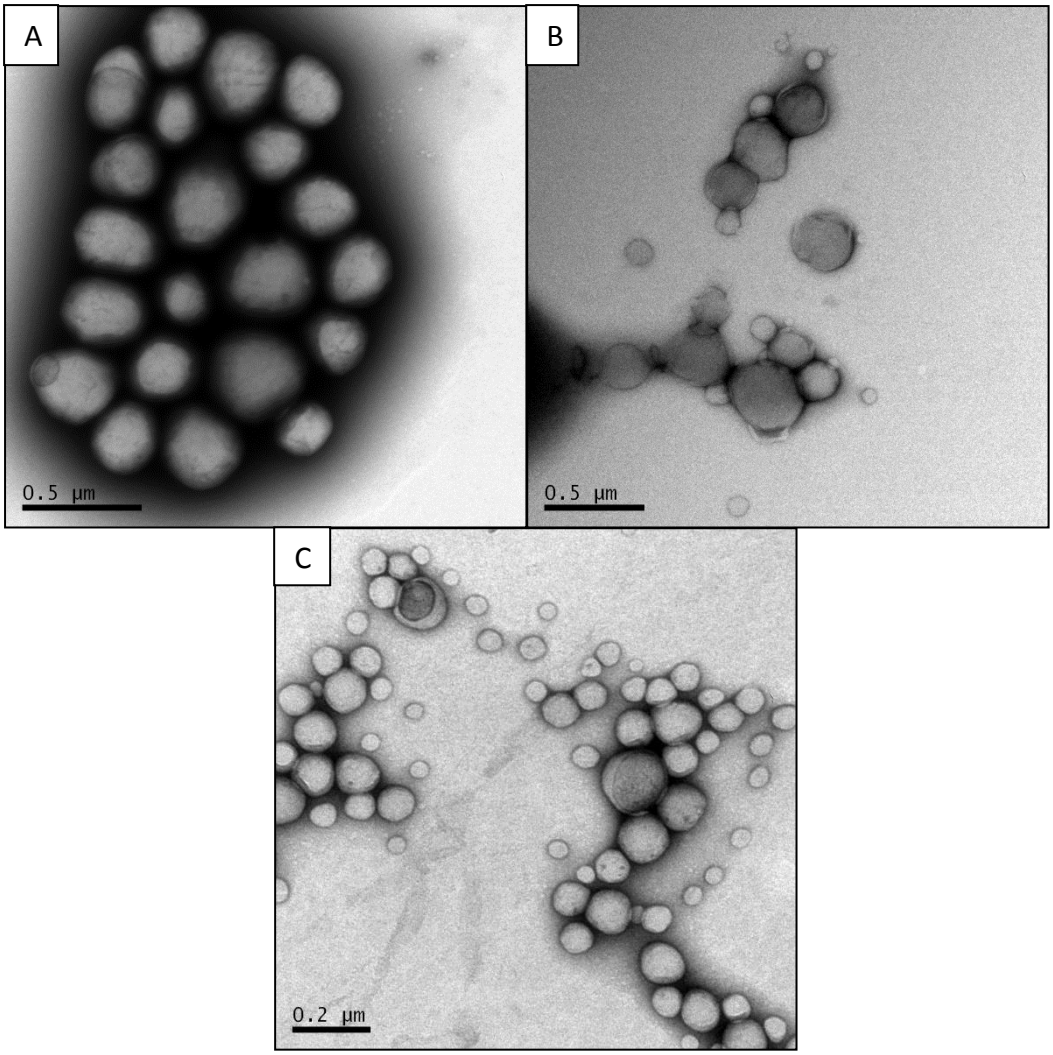

Figure 2.17: Negative stained TEM images of P5 (methods A, B and C)(0.1 wt%) nanospheres (Stained with 5% uranyl acetate and 1% acetic acid).

2.5 Conclusion

PEGME was successfully modified via a condensation reaction with BIBB to produce a number of PEO macroinitiators with various DPs with an active bromide end group. The PEO macroinitiators were then employed as macroinitiators for the synthesis of PEO-*b*-PODMA via ATRP. A number of BCPs of PEO-*b*-PODMA were successfully synthesised with various PEO macroinitiators and across the PEO weight fraction range of 15-60 %. All BCPs had the predicted DP and a dispersity of <1.3 indicating a controlled reaction and that the chain lengths have a narrow dispersity. GPC, ^{1}H-NMR and ^{13}C-NMR confirmed the absence of unreacted PEO macroinitiator, the structure of the BCPs and that the polymers were free of impurities.

It had previously been established that PEO-*b*-PODMA will form bicontinuous nanospheres using procedure A when the PEO weight fraction was at 25 %.[6] This was confirmed in this chapter with the self-assembly of P3 to form bicontinuous nanospheres with N_{ave} sizes by DLS of 400 nm, and by TEM of 300 nm. A PEO weight fraction of 30 % has not previously been studied and the results revealed that a bicontinuous internal morphology can still be achieved at this weight fraction, however a number of other morphologies were also produced such as cylindrical micelles, vesicles and multi-lamellar vesicles. The presence of cylindrical micelles have not been seen previously for this polymer system and requires further investigation to see where this morphology lies on the phase diagram produced by McKenzie *et al.*[3]

The effect a change in polymer concentration had on the particle sizes and morphology was assessed. PEO_{49}-*b*-$PODMA_{21}$ (PEO: 25 wt %) and PEO_{49}-*b*-$PODMA_{16}$ (PEO: 30 wt %) were self-assembled following the dialysis method at concentrations of 0.1, 1, 4 and 5 wt% in solution. The PEO_{49}-*b*-$PODMA_{21}$ (PEO: 25 wt %) solutions demonstrated that as the concentration was increased the internal bicontinuous morphology was maintained although with the 0.1 wt % solutions internal morphology the most ordered. The external spherical morphology was present at 0.1 and 1 wt % in solution while the 4% exhibited non-spherical aggregates. The PEO 30 wt % 0.1 wt % solution exhibited cylindrical micelles amongst other morphologies. This morphology was not present as the concentration was increased.

The aim of these bicontinuous nanospheres is for use in a thermo-responsive drug delivery system. Therefore thermal analysis was carried out on both the bulk and 5 wt% solution for PEO_{44}-*b*-$PODMA_{21}$ (PEO 25 wt %) to determine the T_m and assess the difference in crystallinity between the bulk and aggregate solutions. The results showed that there was a slight increase in T_m from the bulk to aggregate solution, however a possible decrease in crystallinity evident from the decrease in enthalpy change. This difference however could be put down to the fact that the aggregate solution is being measured in water and therefore a transition peak cannot be as accurately obtained. The accuracy of the DSC measurements of aggregate solutions will be further discussed in chapter 3.

The BCP PEO-*b*-PODMA (PEO: 25 wt %) was used as synthesised, and self-assembled following four different procedures in order to determine the procedure that maintained the bicontinuous nanosphere morphology while reducing the preparation time. The resultant aggregate solutions were analysed with DLS, TEM and cryo-TEM. Procedure A, slow water addition followed by dialysis to remove THF, has been used before to successfully self-assemble bicontinuous nanospheres when the PEO weight fraction is at 25 %.[6] DLS revealed that procedure A produced the largest particles, while procedure B, fast addition of water and evaporation of the THF, produced the smallest particles. TEM revealed a different result with the N_{ave} for procedure B being larger than seen in the DLS results. The internal morphology of the aggregates could not be determined by cryo-TEM due to too low concentrations. To be able to establish if bicontinuous nanospheres can indeed be prepared using the different methods a higher concentration of polymer should be used for all methods so that a there is a higher chance of the aggregates being observed with cryo-TEM. Further research is needed into all of the methods with the emulsifier method (procedure D) being the most promising in reducing the amount of time and resources needed to produce bicontinuous nanospheres. A number of different parameters can be modified for the emulsifier method such as the rpm, the temperature of the polymer solution and the time the solution is left emulsifying. It would be interesting to see the effect these parameters have on the resultant morphology.

2.6 References

1. Alexandridis, P.; Lindman, B., Amphiphilic Block Copolymers: Self-Assembly and Applications. *Elsevier Science*: 2000.

2. Coessens, V.; Pintauer, T.; Matyjaszewski, K., Functional polymers by atom transfer radical polymerization. *Progress in Polymer Science* **2001,** 26 (3), 337-377.

3. McKenzie, B. E.; Friedrich, H.; Wirix, M. J. M.; de Visser, J. F.; Monaghan, O. R.; Bomans, P. H. H.; Nudelman, F.; Holder, S. J.; Sommerdijk, N. A. J. M., Controlling Internal Pore Sizes in Bicontinuous Polymeric Nanospheres. *Angewandte Chemie International Edition* **2015,** 54 (8), 2457-2461.

4. Hales, K.; Chen, Z.; Wooley, K. L.; Pochan, D. J., Nanoparticles with Tunable Internal Structure from Triblock Copolymers of PAA-b-PMA-b-PS. *Nano Letters* **2008,** 8 (7), 2023-2026.

5. Yu, K.; Zhang, L.; Eisenberg, A., Novel Morphologies of "Crew-Cut" Aggregates of Amphiphilic Diblock Copolymers in Dilute Solution. *Langmuir* **1996,** 12 (25), 5980-5984.

6. McKenzie, B. E.; Nudelman, F.; Bomans, P. H. H.; Holder, S. J.; Sommerdijk, N., Temperature-Responsive Nanospheres with Bicontinuous Internal Structures from a Semicrystalline Amphiphilic Block Copolymer. *Journal of the American Chemical Society* **2010,** 132 (30), 10256-10259.

7. Grubisic, Z.; Rempp, P.; Benoit, H., A universal calibration for gel permeation chromatography. *Journal of Polymer Science Part B: Polymer Letters* **1967,** 5 (9), 753-759.

8. Grubisic, Z.; Rempp, P.; Benoit, H., A universal calibration for gel permeation chromatography. *Journal of Polymer Science Part B: Polymer Physics* **1996,** 34 (10), 1707-1713.

9. Gaborieau, M.; Castignolles, P., Size-exclusion chromatography (SEC) of branched polymers and polysaccharides. *Analytical and Bioanalytical Chemistry* **2011,** 399 (4), 1413-1423.

10. Rudin, A.; Hoegy, H. L. W., Universal calibration in GPC. *Journal of Polymer Science Part A-1: Polymer Chemistry* **1972,** 10 (1), 217-235.

11. Rehberg, C. E.; Fisher, C. H., Properties of monomeric and polymeric alkyl acrylates and methacrylates. *Industrial and Engineering Chemistry Research* **1948,** 40, 1429-33.

12. Kaufman, H. S.; Sacher, A.; Alfrey, T.; Fankuchen, I., Side-chain crystallization in alkyl polyacrylates. *Journal of the American Chemical Society* **1948,** 70, 3147.

13. Greenberg, S. A.; Alfrey, T., Side-chain crystallization of n-alkyl polymethacrylates and polyacrylates. *Journal of the American Chemican Society* **1954,** 76, 6280-5.

14. Jordan, E. F., Jr.; Feldeisen, D. W.; Wrigley, A. N., Side-chain crystallinity. I. Heats of fusion and melting transitions on selected homopolymers having long side chains. *Journal of Polymer Science, Part A-1: Polymer Chemistry* **1971,** 9 (7), 1835-52.

15. Jordan, E. F.; Artymyshyn, B.; Speca, A.; Wrigley, A. N., Side-chain crystallinity. II. Heats of fusion and melting transitions on selected copolymers incorporating n-octadecyl acrylate or vinyl stearate. *Journal of Polymer Science Part A-1: Polymer Chemistry* **1971,** 9 (11), 3349-3365.

16. Prasad, S.; Jiang, Z.; Sinha, S. K.; Dhinojwala, A., Partial Crystallinity in Alkyl Side Chain Polymers Dictates Surface Freezing. *Physical Review Letters* **2008,** 101 (6), 065505.

17. Hsieh, H. W. S.; Post, B.; Morawetz, H., A crystallographic study of polymers exhibiting side-chain crystallization. *Journal of Polymer Science: Polymer Physics Edition* **1976,** 14 (7), 1241-1255.

18. Platé, N. A.; Shibaev, V. P.; Petrukhin, B. S.; Zubov, Y. A.; Kargin, V. A., Structure of crystalline polymers with unbranched long side chains. *Journal of Polymer Science Part A-1: Polymer Chemistry* **1971,** 9 (8), 2291-2298.

19. Jordan, E. F.; Riser, G. R.; Artymyshyn, B.; Pensabene, J. W.; Wrigley, A. N., Side-chain crystallinity. IV. Mechanical properties and transition temperatures of

copolymers of methyl methacrylate with higher n-alkyl acrylates and N-n-alkylacrylamides. *Journal of Polymer Science Part A-2: Polymer Physics* **1972,** 10 (9), 1657-1679.

20. Hempel, E.; Budde, H.; Höring, S.; Beiner, M., On the crystallization behavior of frustrated alkyl groups in poly(n-octadecyl methacrylate). *Journal of Non-Crystalline Solids* **2006,** 352 (42–49), 5013-5020.

21. Bisht, H. S.; Pande, P. P.; Chatterjee, A. K., Docosyl acrylate modified polyacrylic acid: synthesis and crystallinity. *European Polymer Journal* **2002,** 38 (12), 2355-2358.

22. Yokota, K.; Kougo, T.; Hirabayashi, T., Synthesis, Structure, and Thermal Properties of Widely-Spaced Comb-Like Polymers. *Polymer Journal* **1983,** 15 (12), 891-898.

23. Mogri, Z.; Paul, D. R., Gas sorption and transport in poly(alkyl (meth)acrylate)s. I. Permeation properties. *Polymer* **2001,** 42 (18), 7765-7780.

24. Hirabayashi, T.; Kikuta, T.; Kasabou, K.; Yokota, K., Main-Chain Flexibility and Side-Chain Crystallization of Widely Spaced Comb-Like Polymers. *Polymer Journal* **1988,** 20 (8), 693-698.

25. Karažija, T.; Vidović, E.; Jukić, A., Thermal properties and side chain crystallinity of styrene and n-alkyl methacrylate terpolymers. *Polymer Engineering & Science* **2013,** 53 (11), 2299-2307.

26. Kunisada, H.; Yuki, Y.; Kondo, S.; Goto, K.-i.; Oda, S., Synthesis and Side-Chain Crystallization of Comb-Like Polymers from Isopropenyltriazines Containing Several Long Alkyl Groups. *Polymer Journal* **1992,** 24 (3), 239-246.

27. Discher, D. E.; Eisenberg, A., Polymer vesicles. *Science* **2002,** 297 (5583), 967-973.

28. Antonietti, M.; Foerster, S., Vesicles and liposomes: A self-assembly principle beyond lipids. *Advanced Materials (Weinheim, Germany)* **2003,** 15 (16), 1323-1333.

29. Matsen, M. W.; Bates, F. S., Origins of complex self-assembly in block copolymers. *Macromolecules* **1996,** 29 (23), 7641-7644.

30. Israelachvili, J. N.; Mitchell, D. J.; Ninham, B. W., Theory of self-assembly of hydrocarbon amphiphiles into micelles and bilayers. *Journal of the Chemical Society, Faraday Transactions 2: Molecular and Chemical Physics* **1976,** 72 (0), 1525-1568.

31. Holder, S. J.; Woodward, G.; McKenzie, B.; Sommerdijk, N. A. J. M., Semi-crystalline block copolymer bicontinuous nanospheres for thermoresponsive controlled release. *RSC Advances* **2014,** 4 (50), 26354-26358.

32. McKenzie, B. E.; Holder, S. J.; Sommerdijk, N., Assessing internal structure of polymer assemblies from 2D to 3D CryoTEM: Bicontinuous micelles. *Current Opinion in Colloid & Interface Science* **2012,** 17 (6), 343-349.

33. McKenzie, B. E.; de Visser, J. F.; Friedrich, H.; Wirix, M. J. M.; Bomans, P. H. H.; de With, G.; Holder, S. J.; Sommerdijk, N. A. J. M., Bicontinuous Nanospheres from Simple Amorphous Amphiphilic Diblock Copolymers. *Macromolecules* **2013,** 46 (24), 9845-9848.

34. McKenzie, B. E.; de Visser, J. F.; Portale, G.; Hermida-Merino, D.; Friedrich, H.; Bomans, P. H. H.; Bras, W.; Monaghan, O. R.; Holder, S. J.; Sommerdijk, N. A. J. M., The evolution of bicontinuous polymeric nanospheres in aqueous solution. *Soft Matter* **2016,** *12* (18), 4113-4122.

Chapter 3. Synthesis of Poly (ethylene oxide)-*block*-Poly (docosyl methacrylate) and Poly (ethylene oxide)-*block*-(Poly (octadecyl methacrylate)-*co*-Poly (docosyl methacrylate))

3.1 Abstract

It was established in chapter 2 that PEO-*b*-PODMA exhibits a T_m attributed to the semi-crystalline PODMA block. To gain control over the T_m and therefore the thermos-responsive nature of the bicontinuous nanospheres the PODMA block was copolymerised with verying wt % of docosyl methacrylate, which has a higher melting point than ODMA.

The self-assembly of these block copolymers (PEO wt % 25 %) resulted mainly in bicontinuous nanospheres with some aggregate solutions exhibiting a mixed morphology of both bicontinuous nanospheres and multi-lamellar. The T_m of the bulk block copolymers and aggregate solutions (5 wt % polymer in solution) were analysed with DSC which revealed a T_m range of 21-41°C for the bulk and 23-41°C for the aggregate solutions.

3.2 Introduction

Thermo-responsive polymers, where a change in temperature results in a change in the physical properties of the polymer, have been widely studied for use in a number of applications including the controlled release of pharmaceuticals from polymeric aggregates, such as spherical micelles,[1-2] vesicles[3] or other complex morphologies.[4] Most thermo-responsive polymer aggregates exhibit a lower critical solution temperature (LCST). The LCST is the critical temperature below which the polymer and solvent are miscible and above which they are immiscible causing the polymer to precipitate.[5] One of the most studied thermo-responsive polymers is poly(N-isopropylacrylamide) (PNIPAAm), its use in temperature-responsive drug release has also been widely studied[6]. PNIPAAm exhibits a LCST of around 33°C in aqueous solution[7]. Another well studied LCST responsive polymer is poly(ethylene oxide) (PEO)[8-9], whose LCST in ionic liquids can be fine-tuned by modification of the polymers molecular weight and the concentration of polymer solution. Our approach is to utilise the melting temperature of the hydrophobic block within our amphiphilic block copolymer PEO-*b*-PODMA to self-assemble a thermo-responsive bicontinuous nanosphere for use in controlled drug-release. Use of a semi-crystalline polymer gives the polymer a melting transition. Use of a melting transition (T_m) of a

hydrophobic polymer for thermo-responsive drug release, has been seen previously for poly(trimethylene carbonate)[10] a linear polymer, where heating above the T_m (34°C) resulted in increased membrane permeability in vesicles. The thermo-responsive block was the relatively linear polymer poly(trimethylene carbonate), the use of a linear backbone as the crystalline portion of the polymer does not allow fine tuning of the melting transition as an increase in chain length will not result in a drastic difference in T_m.[11] We are instead using a comb-like hydrophobic polymer (PODMA) as our thermo-responsive block whose melting temperature can be easily manipulated due to the thermo-responsive crystalline segment being a component of the side-chain as opposed to the polymer backbone.[12] It has been well established that the alkyl side chains in comb-like polymers such as poly acrylates and poly methacrylates will crystallise, with the side chains hexagonally packing together independent of the polymer backbone.[13-16]

In chapter 2 we demonstrated that P3 a BCP (block copolymer) with the structure PEO_{49}-*b*-$PODMA_{21}$, and therefore a PEO wt % of 25 %, was successfully self-assembled to form bicontinuous nanospheres across the concentration range 0.1-5 wt %. A T_m for both the bulk (21.5 °C) and 4 wt % aggregate solution (23.4°C) was established using DSC which was attributed to the octadecyl side chains melting.

This ability for the alkyl side chains to crystallise gives rise to a melting transition, this is what gives the PEO-*b*-PODMA comb-like block copolymers their thermo-responsive nature, making them ideal for controlled thermo-responsive drug delivery. The length of the alkyl side chain has a significant effect on the measured T_m. This has been studied extensively in the literature[14-15, 17-18] for poly acrylates and poly methacrylates, with the same trend seen throughout; upon an increase in side chain length an increase in the T_m of the polymer was observed (Table 3.1).

Table 3.1: Differential thermal analysis of a series of poly(methacrylates) and poly(acrylates).[19]

Side chain length (n)	T_m n-methacrylates (°C)	T_m n-acrylates (°C)
16	22	38
18	40	50
22	61	70

Even when the long alkyl side-chains in octadecyl methacrylate were spaced out along the polymer backbone every 6 main carbon atoms by butadiene[13], spaced out every 4 main carbon atoms by the use of other monomers such as styrene and methylstyrene[15] or 18 carbon-side chains randomly interspersed with amorphous side chains of various lengths[20], crystallisation still occurred although the extent of crystallisation was dependent on the flexibility of the polymer backbone[21]. In the case of copolymers of octadecyl acrylate and short side-chains acrylates the Tm increased with an increase in mol % of octadecyl acrylate, as expected.[20] In order to establish control over the thermo-responsive properties of the bicontinuous nanospheres, for use in drug delivery systems, docosyl methacrylate (DSMA) was incorporated into the hydrophobic block of PEO-*b*-PODMA via copolymerisation. PDSMA has a side chain of C_{22} and an increased T_m of around 40°C (DSC), and therefore it was thought that incorporating DSMA into the BCP would allow fine control over the T_m. The copolymerisation of ODMA and DSMA at various wt % ratios was carried out via ATRP using a PEO macroinitiator along with the synthesis of a homopolymer of DSMA using a PEO macroinitiator. The results of these polymerisations are presented in this chapter.

The thermal properties of these copolymers, along with the homopolymers PEO_{49}-*b*-$PODMA_{21}$ and PEO_{44}-*b*-$PDSMA_{12}$, were investigated with the use of DSC to determine the effect an increase in DSMA wt % has on the T_m. The DSC results were compared to DSC measurements of a 50:50 blend of PEO-*b*-PODMA (P3) and PEO-*b*-PDSMA (D3), this was to establish if the synthesis of a copolymer is a necessary step to gain this control.

It has already been established in chapter 2 and previously[22-23] that PEO-*b*-PODMA self-assembles to form bicontinuous nanospheres when the PEO wt % is 15-25 %. Other factors that have an effect on self-assembly of BCPs to form bicontinuous nanospheres have also been investigated previously. McKenzie *et al.*[24] demonstrated that a semi-crystalline hydrophobic block such as PODMA is not necessary to form a bicontinuous morphology, in fact they discovered that the block proportions (mainly the hydrophilic block wt %) and the non-selective cosolvent have a large influence on the resultant morphology, with THF being established as the ideal solvent. Further work by McKenzie *et al.*[23] established that not only does THF aid the self-assembly to bicontinuous nanospheres, but that the volume of THF used affects the number average particle size, with a decrease in THF volume resulting in an increase in particle size.

As it is clear that changing the hydrophobic block should not have significant effect on the BCPs ability to form bicontinuous nanospheres, upon self-assembly, the self-assembly of these copolymers (with PEO 25 wt %) was carried following the dialysis method outlined in chapter 2 (THF solvent) at 0.1, 1 and 5 wt % in solution for comparison with P3. The resultant aggregate solutions were then analysed, as before, with DLS, TEM and cryo-TEM.

3.3 Experimental

3.3.1 Materials and Apparatus for ATRP of Poly(ethylene oxide)-*block*-Poly(docosyl methacrylate) and Poly(ethylene oxide)-*block*-(Poly(octadecyl methacrylate)-*co*-Poly(docosyl methacrylate))

Copper (I) bromide (98 %) and N,N,N',N'',N''-pentamethyldiethylenetriamine (PMDETA) (99 %) and octadecyl methacrylate (ODMA) were used as received from Sigma-Aldrich. Aluminium oxide (activated, neutral, for column chromatography 50-200μm) was purchased from Acros Organics. Tetrahydrofuran (analytical reagent grade), isopropyl alcohol, methanol (analytical grade) and ethanol (analytical grade) were purchased from Fisher Scientific. Xylene was purchased from BDH Lab Supplies. Docosyl methacrylate was supplied by BASF SE and used as supplied. Poly (ethylene oxide) macroinitiator was used as synthesised (chapter 2). The deuterated solvent used in ^{1}H-NMR was used as purchased from Cambridge Isotope Laboratories Incorporated.

All reactions were performed under inert atmospheres (N_2(g)) using a Schlenk line. The infra-red spectra were recorded using a Shimadzu FT-IR spectrometer. ^{1}H-NMR and ^{13}C-NMR spectra were obtained from samples in deuterated chloroform ($CDCl_3$) and recorded on a JEOL ECS-400 spectrometer (400 MHz) at 25°C. Molecular weight averages and dispersity indices were calculated using size exclusion chromatography on a Polymer Laboratories PL-GPC 50 plus gel permeation chromatography system (GPC) using two 5μm mixed C PLgel columns at 40°C. The GPC was calibrated using poly(methyl methacrylate) standards (PMMA). The samples were detected by a refractive index detector (cell volume-6 μl, wavelength-890 nm) with THF eluent.

3.3.2 Materials and Apparatus for the Self-Assembly of Poly(ethylene oxide)-*block*-Poly(docosyl methacrylate) and Poly(ethylene oxide)-*block*-(Poly(octadecyl methacrylate)-*co*-Poly(docosyl methacrylate))

The BCPs were used as synthesised. Distilled water was used as obtained from the tap. *A* syringe pump (220 Voltz, 0.1 Amps, 50Hz) was used from Semat technical Limited at 0.085 mL per minute. A 5 mL dialysis cassette with dialysis membrane (MWCO-12-14000 Daltons) from MEDICELL international Ltd or a dialysis membrane (MWCO-12-14000 Daltons) from MEDICELL international Ltd with dialysis clips were used.

Dynamic Light Scattering

Dynamic light scattering (DLS) measurements were obtained on a Malvern high performance particle sizer (Nano Zetasizer HPPS HPP5001) with a laser at a wavelength of 633nm. The measurements were taken using a clean quartz cuvette containing a 1 mL sample. Measurements were taken at both 15 and 45°C, the temperature was set and the machine was left to settle at this temperature for 10 minutes, after this 10 measurements were taken and an average was obtained.

Transmission Electron Microscopy

Transmission Electron Microscopy (TEM) was carried out on all the self-assembled samples using a JEOL JEM (200-FX) TEM machine (120kV). 5 µl of the sample was pipetted onto a carbon-coated copper grid (200 mesh) and left for 5 minutes and then removed using suction. Using 5 µl of 5 % uranyl acetate the grid was then stained and the solution removed via suction.

Cryo-Transmission Electron Microscopy

Cryo-Transmission Electron Microscopy (cryo-TEM) was performed on a FEI Cryo-Titan with a field emission gun operating at 300 kV. The sample vitrification process was as follows; 3 µl of the self-assembled solution was pipetted onto a surface plasma treated (Cresington Carbon Coater 208) Quantifoil holey (Cu 200 mesh) grid inside a FEI Vitrobot chamber (set to 100 % humidity at room temperature to prevent sample evaporation). The sample was then blotted and plunged into liquid ethane cooled by liquid nitrogen.

3.3.3 Materials and Apparatus for Differential Scanning Calorimetry

Differential scanning calorimetry (DSC) was carried out on the bulk samples D3, C1, C2, C3 and C4, along with the 5 wt % aggregate solutions using a Netzsch DSC 200 Phox with a heating range of -150-600°C. Thermal analysis was carried out across the range -20°C to 80°C for bulk and 5 to 80°C for the 5 wt % solutions. The samples were heated at a rate of 10°C/min. The samples were heated and cooled three times with the first heating run not taken into account to allow for any artifacts present. The enthalpy of fusion and the phase transition temperatures were taken from the second heating run. The bulk samples were measured against an empty aluminium pan as the reference and an aluminium pan filled with water was used as the reference for the 5 wt % solutions to reduce any transitions due to the water.

3.3.4 ATRP of Poly(ethylene oxide)-*block*-Poly(docosyl methacrylate)

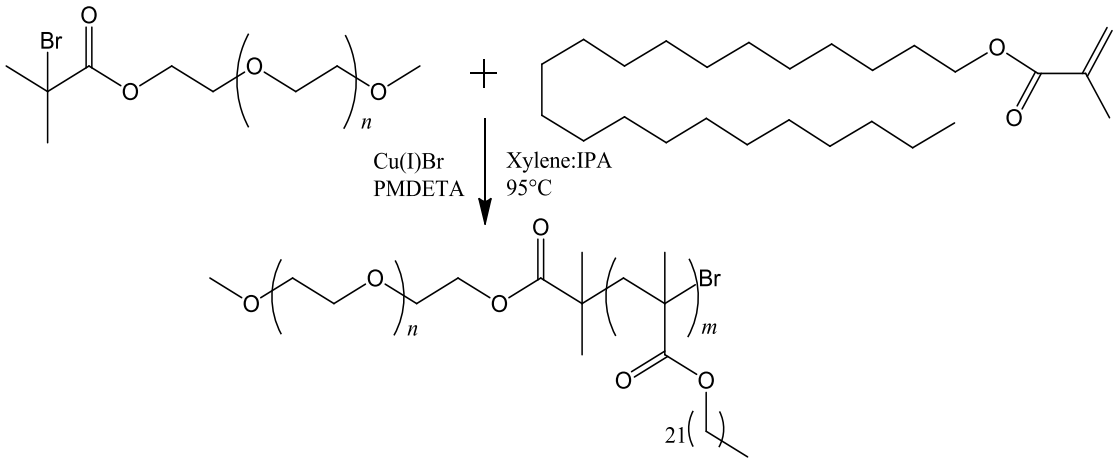

Scheme 3.1: Polymerisation of block copolymer PEO-*b*-PDSMA

The procedure followed for the synthesis of PEO-*b*-PODMA in chapter 2 was used for the synthesis of PEO-*b*-PDSMA as follows; Cu(I)Br (33 mg, 0.23 mmoles) was placed in a 25 mL Schlenk tube with a magnetic stirrer. The PEO Macroinitiator *(OMI02)* (1.00 g, 0.46 mmoles) was dissolved in a xylene:IPA mixture (9:1) (4 mL) and then added to the Schlenk tube along with PMDETA (80 mg, 0.46 mmoles) and docosyl methacrylate (DSMA) (2.19 g, 5.55 mmoles). The Schlenk tube was sealed and the mixture was degassed (N_2) at 95°C for 1 hour. The mixture was then stirred at 95°C for 24 hours under nitrogen. After 24 hours the reaction was stopped by exposure to air and diluting with THF. The mixture was run through an alumina column to remove the catalyst and ligand and half the solvent was evaporated off (rotary evaporator). The polymer was precipitated out into ethanol drop wise at 0°C. The block copolymer was characterised using ^{1}H-NMR and GPC.

(D3) ^{1}H NMR (400 MHz, $CDCl_3$, ppm) δ: 0.88 (triplet, 3H, -$(CH_2)_{21}$-C**H_3**), 1.02 (broad peak, 3H, -CH_2-C-C**H_3**), 1.28 (broad peak, 38H, -(C**H_2**)$_{19}$-), 1.60 (broad peak, 2H, -C**H_2**-$(CH_2)_{19}$-), 3.38 (singlet, 3H, C**H_3**O-), 3.65 (broad triplet, 4H, -O-C**H_2**C**H_2**-O-), 3.92 (broad peak, 2H, -COO-C**H_2**). **(D3) ^{13}C NMR ($CDCl_3$, ppm) δ:** 14.2 (-CH_2CH_2**C**H_3), 18.5 (-C(**C**H_3)$_2$-) 22.7 (-CH_2**C**H_2CH_3), 26.2 (-COO-CH_2CH_2**C**H_2-), 28.2 (Br-C(**C**H_3)-), 28.3 (-COO-CH_2**C**H_2CH_2-), 29.4 (-$CH_2(CH_2)_{15}$**C**H_2-), 29.4 (-**C**$H_2(CH_2)_{15}CH_2$-), 29.8 (-CH_2(**C**H_2)$_{15}CH_2$-), 32.0 (-**C**$H_2CH_2CH_3$), 44.7 (Br-**C**-), 59.1 (**C**H_3O-), 61.7 (Br-C(CH_3)-CH_2-), 65.1(-COO-**C**$H_2CH_2CH_2$-), 70.5 (-O-**C**H_2**C**H_2O-), 175.8 (-**C**OO-$(CH_2)_{21}CH_3$), 176.8 (-**C**OO-CH_2CH_2-).

(D3) FTIR (cm^{-1}): 2916 C-H stretch, 2848 C-H stretch, 1728 C=O stretch, 1467 C-H bend, 1244 C-C stretch, 1145 C-O stretch, 719 C-H rock.

Table 3.2: Reaction conditions for polymers D1-D4 synthesised *via* the above method.

Code	Structure	DSMA (g)	PEO (g)	PMDETA (mg)	Cu(I)Br (mg)	Temperature (°C)	Reaction time (hour)
D1	PEO_{45}-*b*-$PDSMA_{35}$	5.73	I3-1.00	79	33	95	24
D2	PEO_{44}-*b*-$PDSMA_{18}$	2.92	I2- 1.00	80	33	95	24
D3	PEO_{44}-*b*-$PDSMA_{16}$	2.92	I2- 1.00	80	33	95	24
D4	PEO_{44}-*b*-$PDSMA_{12}$	2.19	I2- 1.00	80	33	95	24

3.3.5 ATRP of Copolymer of Poly(ethylene oxide)-*block*-(Poly(octadecyl methacrylate)-*co*-Poly(docosyl methacrylate)

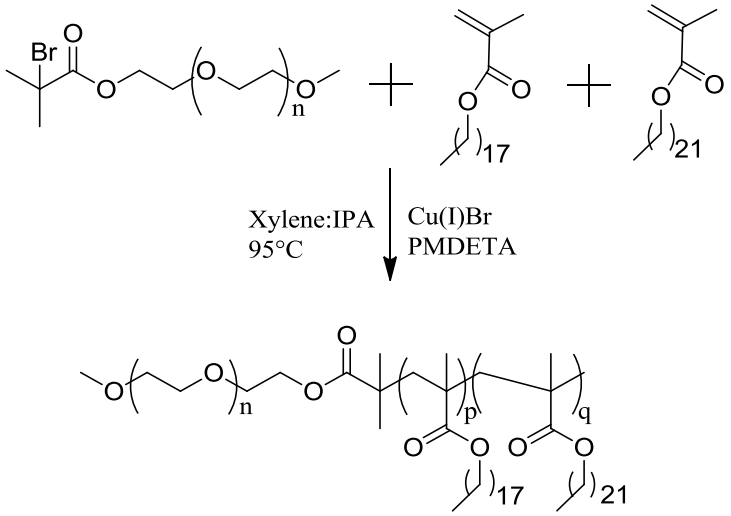

Scheme 3.2: Synthesis of PEO-*b*-(PODMA-*co*-PDOMA)

The procedure used for the synthesis of PEO-*b*-PODMA in chapter 2 was used successfully for the synthesis of PEO-b-PDSMA and therefore the same procedure was used for the synthesis of all PEO-*b*-(PODMA-*co*-PDSMA) BCPs, the only modification was the use of methanol instead of ethanol as the non-solvent for precipitation. Cu(I)Br (32 mg, 0.2268 mmoles) was placed in a 50 mL Schlenk tube with a magnetic stirrer. The PEO macroinitiator (I3-PEO_{45}) (1.00 g, 0.45 mmoles) was dissolved in xylene:IPA mixture (9:1) (4 mL) and then added to the Schlenk tube along with PMDETA (78 mg, 0.45 mmoles) and DSMA (dissolved in xylene:IPA) (1.61 g, 4.08 mmoles). ODMA (1.38 g, 4.08 mmoles) was run through an alumina column to remove the stabiliser and then added to the Schlenk tube. The Schlenk tube was sealed and the mixture was degassed (N_2) for 1 hour. The mixture was then stirred at 95°C for 24 hours under nitrogen. After 24 hours the reaction was stopped by exposure to air and diluting with THF. The mixture was run through an alumina column to remove the catalyst and ligand and the solvent was evaporated off (rotary evaporator). The polymer was precipitated out into methanol drop wise at 0°C. The block copolymer was characterised using ^{1}H-NMR, ^{13}C-NMR and GPC. This method was used to produce the following % ratios of PODMA:PDOMA : 50:50, 25:75, 75:25 and 40:60.

(C2) ^{1}H NMR (400 MHz, $CDCl_3$, ppm) δ: 0.88 (triplet, 3H, -$(CH_2)_{21}$-C**H₃**, -$(CH_2)_{17}$-C**H₃**), 1.02 (broad peak, 3H, -CH_2-C-C**H₃**), 1.28 (broad peak, 38H, -(C**H₂**)$_{19}$-, -(C**H₂**)$_{15}$-), 1.60 (broad peak, 2H, -C**H₂**-$(CH_2)_{19}$-), 3.38 (singlet, 3H, C**H₃**O-), 3.65 (broad triplet, 4H, -O-C**H₂**C**H₂**-O-), 3.92 (broad peak, 2H, -COO-C**H₂**-). **(C2) ^{13}C NMR ($CDCl_3$, ppm) δ:** 14.2 (-CH_2CH_2**C**H_3), 18.5 (-C(**C**$H_3)_2$-) 22.7 (-CH_2**C**H_2CH_3), 26.2 (-COO-CH_2CH_2**C**H_2-), 28.2 (Br-C(**C**H_3)-), 28.3 (-COO-CH_2**C**H_2CH_2-), 29.5 (-$CH_2(CH_2)_{15}$**C**H_2-), 29.5 (-$CH_2(CH_2)_{11}$**C**H_2-), 29.5 (-**C**$H_2(CH_2)_{15}CH_2$-), 29.5 (-**C**$H_2(CH_2)_{11}CH_2$-), 29.8 (-CH_2(**C**$H_2)_{15}CH_2$-), 29.8 (-CH_2(**C**$H_2)_{11}CH_2$-), 32.0 (-**C**$H_2(CH_2)CH_3$), 54.4 (Br-**C**-), 59.1 (Br-C(CH_3)-**C**H_2-), 61.6 (**C**H_3O-), 65.0 (-COO-**C**$H_2CH_2CH_2$-), 70.5 (-O-**C**H_2**C**H_2O-), 177.6 (-**C**OO-$(CH_2)_{21}CH_3$), 176.7 (-**C**OO-CH_2CH_2-). **(C2) FTIR (cm^{-1}):** 2916 C-H stretch, 2848 C-H stretch, 1728 C=O stretch, 1465 C-H bend, 1242 C-C stretch, 1145 C-O stretch, 719 C-H rock.

Table 3.3: Reaction conditions for polymers C1-C4 synthesised *via* the above method.

Code	ODMA (g)	DSMA (g)	PEO (g)	PMDETA (mg)	Cu(I)Br (mg)	Temperature (˚C)	Reaction time (hour)
C1	2.25	0.75	I3-1.00	79	33	95	24
C2	1.38	1.61	I3- 1.00	79	33	95	24
C3	1.07	2.92	I3- 1.00	79	33	95	24
C4	0.75	2.25	I3- 1.00	79	33	95	24

3.3.6 Self-Assembly of PEO-*b*-PDSMA BCPs D3 and D4 and PEO-*b*-(PODMA-*co*-PDSMA) BCPs C1-C4

The BCP was dissolved in THF and left stirring in an oil bath set to 45°C. Deionised water was then added drop-wise (at 5.15 mL/hr) to the solution via a syringe pump to make the total volume up to 10 mL. After the addition of the water the solution was either transferred to a dialysis chamber and sealed with a dialysis membrane or sealed in dialysis tubing with clips, then left spinning in 3L of deionised water pre-heated to 45°C for 24 hours, over the 24 hours the water was changed twice. The self-assembled polymer was then analysed using dynamic light scattering (DLS) and transmission electron microscopy (TEM) to determine the size and dispersity of the aggregates. The masses of the BCPs and the volumes of THF and water used for the relevant wt % in solution are displayed in Table 3.4. 6 mL of THF was used for the 5 wt % concentration instead of 4 mL as precipitation occurred upon the slow addition of water when 4 mL was used, this did not occur when 6 ml was used.

Table 3.4: Weight percentage and masses used for the self-assembly of all PEO-*b*-PDSMA block copolymers.

PEO-*b*-PDSMA wt %	Mass (PEO-*b*-PDSMA) (g)	THF volume (mL)	Water volume (mL)	Total volume (mL)
0.1	0.01	4	6	10
1	0.1	4	6	10
5	0.5	6	4	10

3.4 Results and Discussion

3.4.1 Characterisation of PEO-*b*-PDSMA

The block copolymer PEO-*b*-PDSMA was synthesised by ATRP, using PEO macroinitiator I2 and I3 (Chapter 2). As with the PEO-*b*-PODMA block copolymers, the PEO-*b*-PDSMA BCPs were characterised with GPC and ^{1}H-NMR. The parameters obtained were important for the self-assembly step to better understand the effect these they have on the resultant aggregate morphology and size.

The degree of polymerisation and the molecular weight parameters for D1-D4 were determined by the polymer:initiator ratio for each reaction calculated using ^{1}H-NMR. Table 3.5 displays the results of these measurements along with the GPC results and the values for the PEO macroinitiators used. The BCPs all exhibited a dispersity, Đ, below 1.2, indicating a narrow dispersity in molecular weight. The degree of polymerisation of the PDSMA block was controlled by the initiator:monomer ratio and as ATRP is a controlled reaction the DP was as expected. The PEO wt % for all BCPs were obtained using the PEO and PEO-*b*-PDSMA M_n values calculated from ^{1}H-NMR. This value will come into importance when analysing the self-assembly of these BCPs.

Table 3.5: Parameters for block copolymers PEO-b-PDSMA obtained using ^{1}H-NMR and GPC.

Code	Structure	M_n[a] (Da)	M_w[a] (Da)	Đ[a]	DP[b]	M_n[b] (Da)	PEO wt %
I2	PEO_{44}	3600	3900	1.07	*44*	2160	-
I3	PEO_{45}	3300	3600	1.09	45	2200	-
D1	PEO_{45}-*b*-$PDSMA_{35}$	14500	16900	1.17	35	16020	14
D2	PEO_{44}-*b*-$PDSMA_{18}$	12400	14900	1.19	18	9260	23
D3	PEO_{44}-b-$PDSMA_{16}$	12100	14000	1.15	16	8470	25
D4	PEO_{44}-*b*-$PDSMA_{12}$	11100	12300	1.11	12	6900	31

[a] Calculations from GPC in THF (PMMA Standards)

[b] Calculations from 1H-NMR in CDCl3 by comparing the integrals of peak **a** to peak **f**

To confirm the absence of unreacted macroinitiator (I2) in the precipitated polymer the GPC trace of D3 was analysed, overlaid with that of the macroinitiator I2 (Figure 3.1). There is a monomodal distribution for D3 and ≤ 10 % overlap between the macroinitiator peak and the BCP peak, this suggest that either all the macroinitiator has reacted or been removed in the precipitation process. BCPs D1, D2 and D4 also had monomodal distributions with ≤10 % overlap between the BCP peak and the PEO macroinitiator peak.

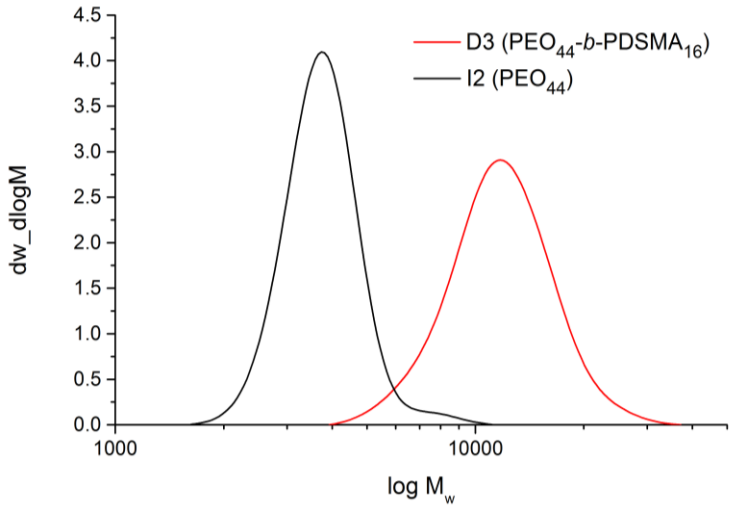

Figure 3.1: GPC traces of PEO_{44}-*b*-$PDSMA_{16}$ (D3) after one precipitation into ethanol, overlaid against macroinitiator PEO_{44} (I2).

The ^{1}H-NMR spectrum of D3 (PEO_{44}-*b*-$PODMA_{16}$) overlaid with macroinitiator I2 was analysed to further determine the purity of the BCP, i.e. that all of the left over monomer and possible unreacted PEO macroinitiator had been removed in the precipitation process. In the spectrum of D3 (Figure 3.2) the methacrylate peaks (vinyl protons) from the monomer at 5.5 ppm and 6.1 ppm are not present, the macroinitiator peak at 4.3 ppm is also not present on the BCP spectrum (red box), this peak was chosen to compare with as once the macroinitiator has reacted this peak should shift to the right to 3.6 ppm. The change in chemical shift for this CH_2 group was because the electronegative bromine attached to the beta carbon caused de-shielding of the hydrogen nucleus giving a higher chemical shift. The polymerisation of the PEO macroinitiator gave the nucleus more shielding and therefore a higher electron density surrounded it due to the loss of the nearby electronegative bromine.

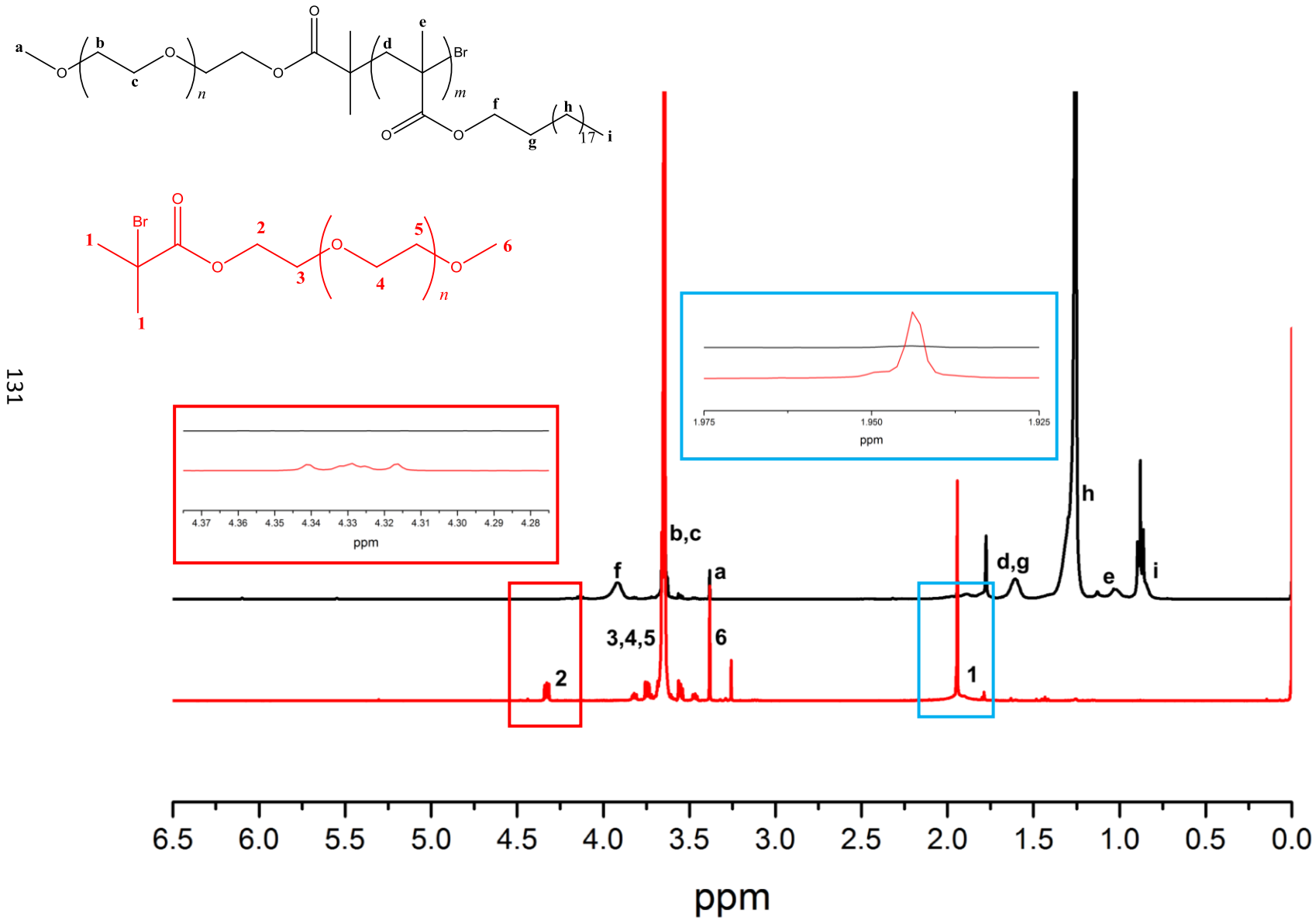

Figure 3.2: ^{1}H-NMR spectra of PEO_{44}-*b*-$PDSMA_{12}$ (D3) (top) overlaid with macroinitiator PEO_{44} (I2) (bottom)

3.4.2 Characterisation of Poly(ethylene oxide)-*block*-(Poly(octadecyl methacrylate)-*co*-Poly(docosyl methacrylate)) Block Copolymers C1-C4

PEO-*b*-PODMA and PEO-*b*-PDSMA were successfully synthesised and their T_m measured to be 21.5 and 41.3˚C respectively, this showed that the T_m of the BCPs can be controlled by the hydrophobic block as the T_m for both was close to that of their relevant monomers (ODMA: 18˚C and DSMA: 33˚C). This led to the idea of polymerising a block copolymer where the hydrophobic block was a random copolymer of both PODMA and PDSMA, synthesised via ATRP. This would show how far the thermo-responsive nature of these BCPs in bulk and as aggregates could be controlled. The random copolymers were synthesised at the following PODMA:PDSMA weight fractions; 0.75:0.25, 0.5:0.5, 0.25:0.75. It was predicted from observing the T_m results of these BCPs that a 40:60 PODMA:PDSMA copolymer should yield aggregates with a T_m around body temperature (35-39°C). The DSC results will be further discussed later on in this chapter.

The copolymers were synthesised at varying ratios of PODMA:PDSMA with PEO macroinitiator I3 (synthesis-chapter 2). The resultant copolymers were analysed using GPC to determine their dispersity and molecular weight parameters. ^{1}H-NMR was used to confirm the structure of the polymer, the purity and to determine the degree of polymerisation which as then used to calculate M_n. The DP was determined by comparing the integrals of a CH_3 group present in the macroinitiator (3.66 ppm, peak a) to a CH_2 group (3.92 ppm, peak f)) that is seen in both PODMA and PDSMA. The results of these measurements are displayed in Table 3.6.

The use of ATRP for these reactions means that the polymer growth can be more controlled than conventional radical poylmerisaiton, this is why all the copolymers have a dispersity index of below 1.13, this signifies a very narrow molecular weight distribution. The M_n and M_w, also calculated using GPC, can be seen in the table. The DP for each block copolymer was calculated from ^{1}H-NMR as mentioned above. The PEO wt % of these polymers was established by dividing the M_n of the PEO macroinitiator by the total copolymer M_n. The aim was to have all the copolymers to have a PEO wt % of 25 %, as seen in the table, this was achieved. The GPC calculated

M_n differs from the ^{1}H-NMR calculated M_n, therefore the ^{1}H-NMR results were used for all calculations concerning M_n. The reason for this difference, as previously discussed in chapter 2, is due to the BCPs having a different hydrodynamic volume to the PMMA calibrants used in the GPC, giving rise to different retention times.

Table 3.6: Parameters for block copolymers PEO-*b*-(PODMA-*co*-PDOMA) obtained using ^{1}H-NMR and GPC.

Code	Structure	M_n[a] (Da)	M_w[a] (Da)	Đ[a]	DP[b]	M_n[b] (Da)	PEO wt %	PODMA:PDOMA Ratio[c]
OMI11	*PEO_{45}*	*3300*	*3600*	*1.09*	*45*	*2204*	-	-
C1	PEO_{45}-*b*-($PODMA_{15}$-*co*-$PDOMA_4$)	11100	12500	1.13	19	8850	25	75:25
C2	PEO_{45}-*b*-($PODMA_9$-*co*-$PDOMA_9$)	11100	12500	1.12	18	8792	25	50:50
C3	PEO_{45}-*b*-($PODMA_7$-*co*-$PDOMA_{11}$)	12100	13600	1.13	18	8915	25	40:60
C4	PEO_{45}-*b*-($PODMA_5$-*co*-$PDOMA_{13}$)	10800	12100	1.12	19	9016	25	25:75

[a] Calculations from GPC in THF (PMMA Standards)
[b] Calculations from ^{1}H-NMR in $CDCl_3$ by comparing the integrals of peak **a** to peak **f**
[c] Calculated from feed ratio

The GPC traces were analysed to ensure all the PEO macroinitiator was reacted during the reaction, or removed during the precipitation process. As seen in Figure 3.3 the GPC traces for the random block copolymers show monomodal distributions with no shoulder peaks, and ≤ 10 % overlap between the macroinitiator and the BCP.

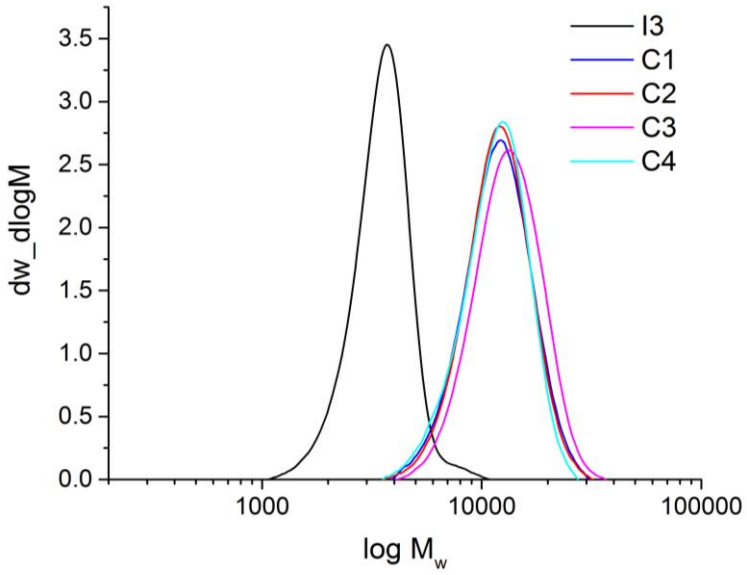

Figure 3.3: GPC traces of PEO (I3) macroinitiator against C1, C2, C3 and C4 block copolymers (PEO-*b*-(PODMA-*co*-PDSMA))

The ^{1}H-NMR spectrum for C2 (PEO-*b*-(PODMA$_9$-*co*-PDOMA$_9$)) against macroinitiator I3 (PEO$_{45}$) can be viewed in Figure 3.4 and representative of all the copolymers synthesised (C1-C4). It confirmed the structure of the BCP giving a DP of 18. The absence of a number of peaks in the BCP spectrum confirms the success of the polymerisation. The peak at 4.3ppm on the macroinitiator spectrum has shifted to 3.6ppm on the BCP spectrum, this confirms there is no unreacted macroinitiator present in the sample. Also there is an absence of a peak at 5.5ppm and 6.1ppm (the vinyl monomer peaks) meaning there is no monomer present in the sample.

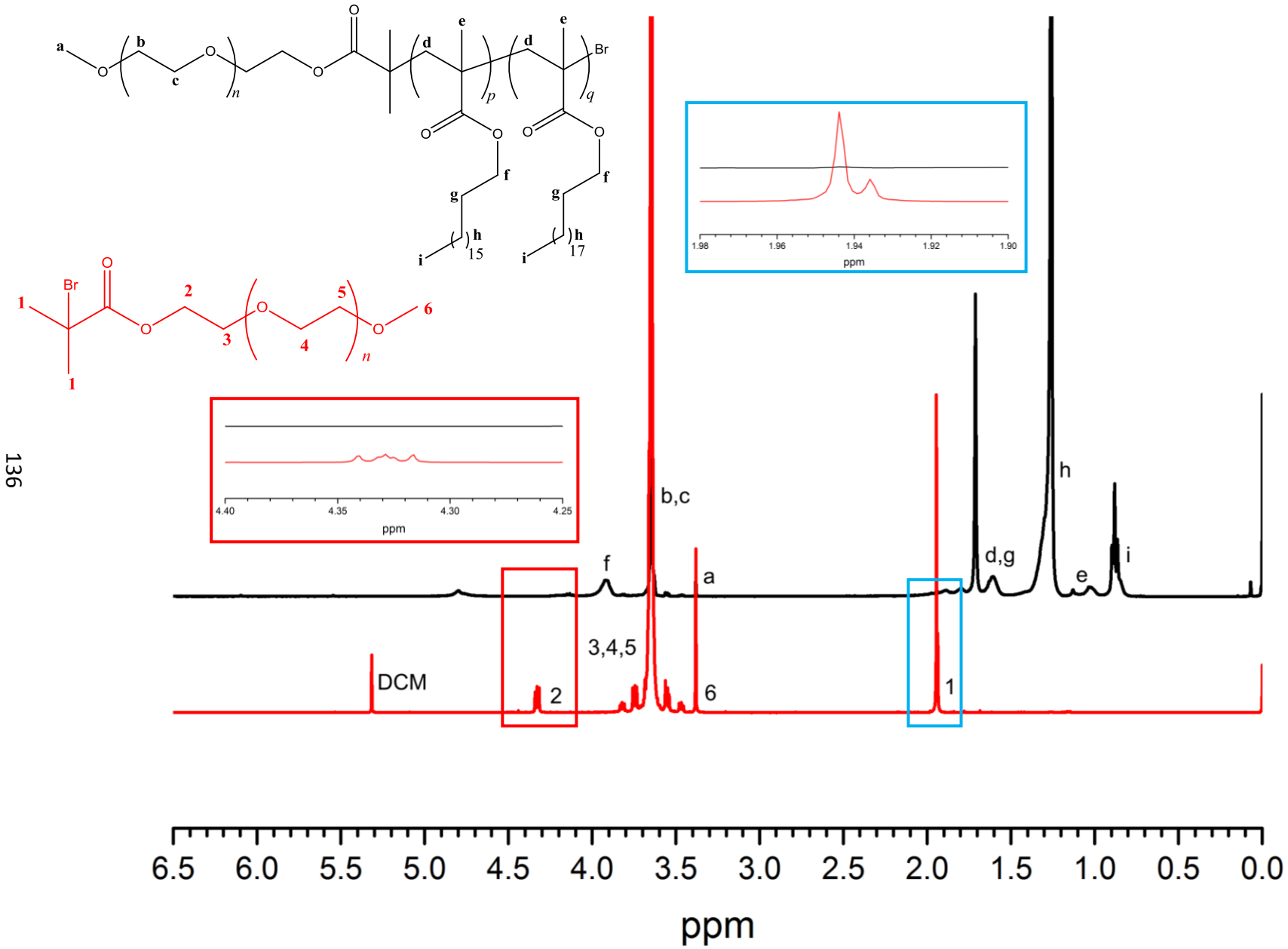

Figure 3.4: H-NMR spectra of PEO_{44}-*b*-($PODMA_9$-*co*-$PDSMA_9$) (ORM69) (top) overlaid with macroinitiator PEO_{45} (OMI11) (bottom)

3.4.3 Self-Assembly of Poly(ethylene oxide)-*block*-Poly(docosyl methacrylate) using Procedure A

PEO-*b*-PDSMA was dissolved in THF followed by the slow addition of deionised water (5.15 mL/hr). The solution was dialysed against deionised water to remove the THF. The self-assembled polymer was then analysed using Dynamic Light Scattering (above and below the calculated T_m (41°C) and Scanning Electron Microscopy to determine the size and dispersity of the aggregates.

Varying masses of each polymer were dissolved in THF and water was then added to these solutions to produce polymer concentrations of 0.1 to 5 wt %. The effect of polymer concentration upon the self-assembly was studied. The mass of block copolymer used to make each corresponding weight percentage are seen in Table 3.7. As previously mentioned 6 mL of THF was used for the 5 wt % concentration due to precipitation occurring when 4 mL of THF was used.

Table 3.7: Weight percentage and masses used for the self-assembly of all PEO-*b*-PDSMA block copolymers.

PEO-*b*-PDSMA wt %	Mass (PEO-*b*-PDSMA) (g)	THF volume (mL)	Water volume (mL)	Total volume (mL)
0.1	0.01	4	6	10
1	0.1	4	6	10
5	0.5	6	4	10

3.4.3.1 D3 (PEO_{44}-b-$PDSMA_{16}$) (PEO 25 wt %)

Block copolymer D3 (25 wt % PEO) was synthesised with a 1:16 ratio of PEO:PDSMA. D3 was self-assembled to produce a variety of polymer weight percentages in solution (0.1-5 wt %) (Table 3.7). Each sample was then analysed with DLS at 15 and 45°C and the results are shown in Table 3.8.

The reason for the samples being measured, using DLS, at 15 and 45˚C was to observe the affect heating the aggregates above their calculated DSC T_m would have on their size and dispersity. The DSC results will be discussed later in this chapter.

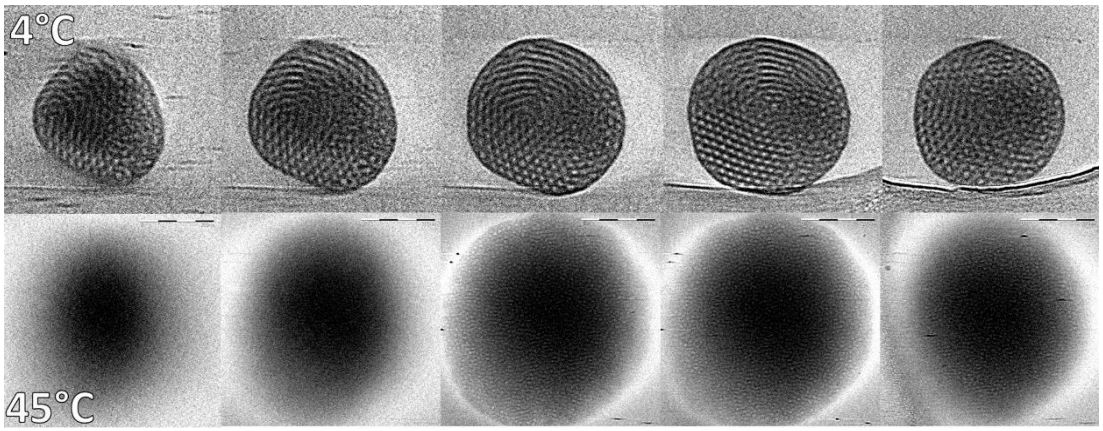

Figure 3.5: Cryo-TEM images of self-assembled bicontinuous nanospheres formed from semi crystalline block copolymer poly(ethylene oxide)-block-poly(octadecyl methacrylate) (PEO_{39}-*b*-$PODMA_{17}$) in aqueous dispersion. First vitrified at 4˚C where there is an ordered bicontinuous internal structure and then vitrified at 45˚C where the internal structure has become a disordered microphase separated state. This image was reproduced from ref[22].

For all the self-assembled polymers the number mean (N_{ave}) and z-average (Z_{ave}) diameters were larger at 45°C than at 15˚C. This has been previously observed for PEO-*b*-PODMA by McKenzie *et al*.[22] where a sample of PEO_{39}-*b*-$PODMA_{17}$ was self-assembled at 0.1 wt % following the dialysis method, the resultant solution was vitrified at both 4 and 45˚C. Figure 3.5 shows that when the sample was vitrified below the T_m (24.2˚C) the aggregates have an ordered bicontinuous internal microphase-separated structure, however when vitrification was carried out above the T_m the sample exhibited a disordered micro-phase separated structure, with a loss of the bicontinuity.

Both the 0.1 wt % and 5 wt % solutions had a low Đ at both temperatures which indicates a narrower size distribution, with an increased Đ for the 1 wt % solution. Upon an increase in concentration from 0.1- 1 wt % an increase in particle size was observed, this was also seen for PEO-*b*-PODMA at 25 wt % PEO (chapter 2). A large increase in Đ is also seen for the 1 wt% indicating a larger size distribution which explains the larger N_{ave}. There is a decrease in particle size for the 5 wt % concentration from the 0.1 and 1 wt %. This is most likely due to the increased volume of THF used to initially dissolve the BCP, 4 mL of THF was used in the self-assembly process for the 0.1 and 1 wt% solutions, however 6 mL of THF was used for the 5 wt % solution to ensure no polymer precipitation occurred. We have recently reported (McKenzie *et al.*[23]) that the size of PEO-*b*-PODMA (PEO: 25 wt %) nanospheres can be tailored by fine-tuning the PODMA-solvent interfacial energy, this was done by modifying the volume ratio of THF:water used. It was shown that as the wt % of THF was increased the particle diameter decreased from approximately 300 nm, when 4 mL of THF was used, to approximately 165 nm when 6 mL of THF was used. These results explain the decrease in particle size for the 5 wt % solution of PEO_{44}-*b*-$PDSMA_{16}$ (D3) observed here. The particles sizes observed here for PEO-*b*-PDSMA (PEO 25 wt %) are consistent with those observed for PEO-*b*-PODMA (PEO 25 wt %) in chapter 2, with the exception of the 5 wt % concentration, which as discussed is due to an increase in the wt % of THF used.

Table 3.8: Number mean values for self–assembled block copolymer D3 (PEO_{49}-*b*-$PODMA_{16}$) (25 wt % PEO) calculated from the Z-average using Dynamic Light Scattering.

wt %	T (°C)	N_{Ave} (d.nm)	SD (± nm)	Z_{Ave} (d.nm)	SD (± nm)	CONTIN	Đ
0.1	15	340	23	404	4	607/210	0.19
0.1	45	365	12	455	5	557/234	0.18
1	15	431	84	709	31	446/197	0.45
1	45	431	47	752	27	365	0.46
5	15	145	48	200	2	203	0.15
5	45	170	17	204	1	226	0.14

Figure 3.6 A shows the distribution plots for D3 at 15°C. The 0.1 wt % solution is monomodal suggesting a narrow size distribution as seen in Table 3.8. The distribution plots for the 1 and 5 wt % solutions exhibit bimodal distributions. Table 3.8 showed that the 5 wt % solution had a smaller number mean than the 1 wt % and this is evident from the size distribution plots. The plots show that the majority of the 1 wt % solutions particles have roughly the same number average particle size as the 0.1 wt % solution, the higher number average observed in Table 3.8 is most likely due to the small number % of particles with a N_{ave} of around 1000 nm.

The aggregate solutions were then analysed at 45°C using DLS (Figure 3.6 B). The 0.1 and 5 wt % solutions exhibited a low Đ as seen in Table 3.8, this is supported by the distribution plots in Figure 3.6 B which are monomodal with a shoulder peak, indicating a narrow size distribution. The shoulder peak is most likely due to aggregation of the particles as they melt when heating above their T_m. The 1 wt % solution has a bimodal distribution which explains the larger Đ, than the 0.1 and 5 wt % solutions, as there are either two average particle sizes or the particles have aggregated together.

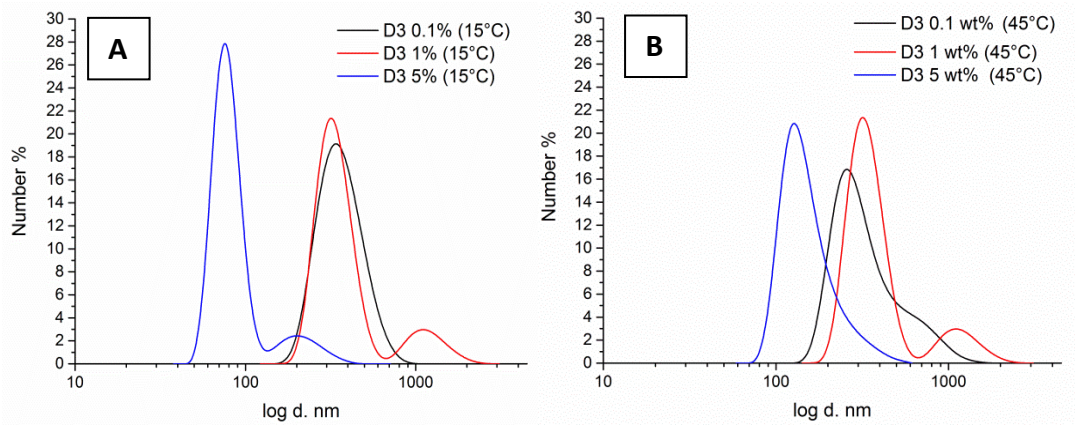

Figure 3.6: DLS distribution plot of D3 (PEO_{44}-*b*-$PDSMA_{16}$) wt % 0.1-5 % at 15 °C **(A)** and 45˚C **(B)**.

The TEM images of D3 at 0.1 wt % in solution can be seen in Figure 3.7 (A-B). They show spherical aggregates with a number average particle size of 280 ± 111 nm (calculated from 40 particles) and a porous surface, which indicates bicontinuous morphology. This particle size is slightly smaller than that observed with DLS, this is most likely due to the fact that DLS is measuring the solvated particle, whereas with

TEM the sample has been dried onto a grid losing any internal water, therefore the particle size will shrink.[25] The DLS size distribution plot for 0.1 wt % showed a size range of 200-1000 nm and this range is confirmed in the TEM image in Figure 3.7 B. The cryo-TEM images were analysed (Figure 3.7 B) and revealed that all the particles exhibit an internal bicontinuous morphology with some bicontinuous nanospheres having small regions of multi-lamellar (Figure 3.7 C). This has been seen previously with PEO-*b*-PODMA nanospheres.[22] The internal pore diameter has been estimated to be 25 ± 4 nm by measuring the pores of the nanosphere in Figure 3.7 C. We have previously reported that the internal pore size of PEO-*b*-PODMA bicontinuous nanospheres can be controlled by varying the hydrophilic block weight percent.[23] A decrease in the wt % of the hydrophilic block (PEO) results in a decrease in the internal pore diameter of the nanospheres with the DP of the hydrophilic block having an insignificant effect. Bicontinuous PEO-*b*-PODMA nanospheres with the same PEO wt % of 25 % (0.1 wt %) exhibited pore sizes of 19 ± 3 nm, this shows that changing the hydrophobic block to PDSMA results in an increase in internal the average pore diameter.

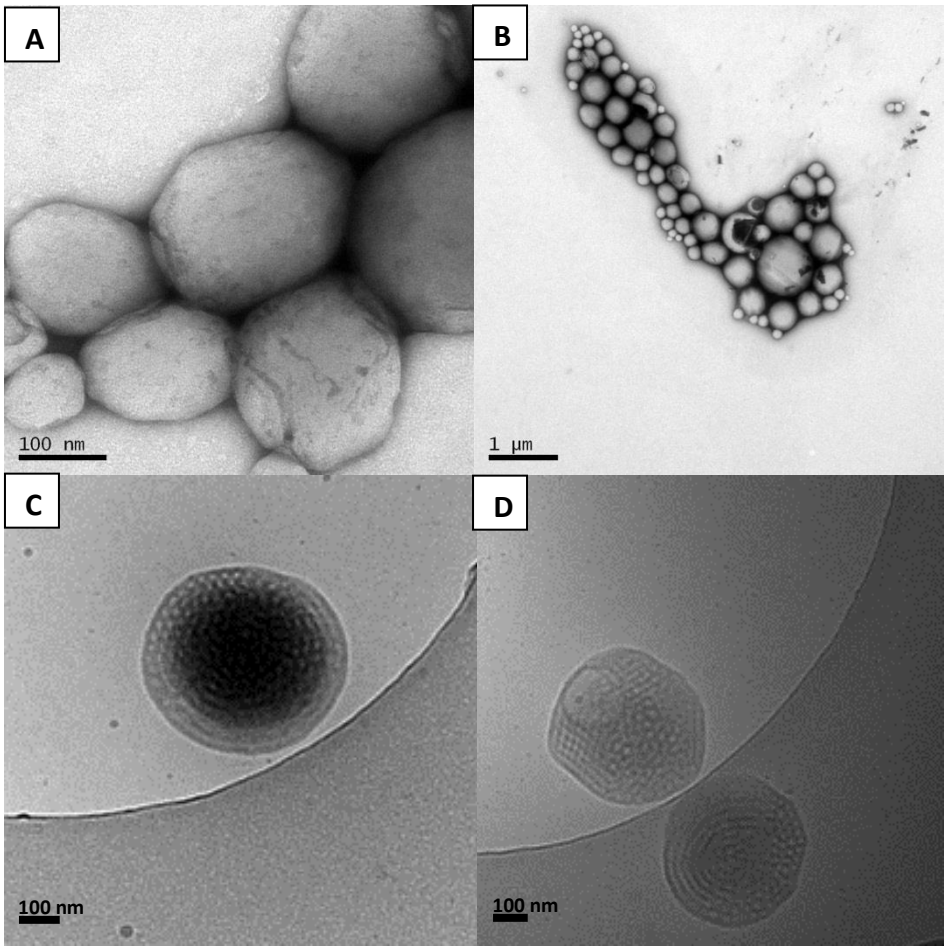

Figure 3.7: A-B) Negative stained TEM images of D3 (PEO_{44}-*b*-$PDSMA_{16}$)(0.1 wt %) nanospheres (Stained with 5% uranyl acetate and 1% acetic acid) **C-D)** Cryo-TEM images of D3 (PEO_{44}-*b*-$PDSMA_{16}$) (0.1 wt%) nanospheres with internal bicontinuous morphology with some multi-

Figure 3.8 (A-B) displays the TEM images of D3 at 1 wt% in solution. The images show spherical aggregates with possible internal morphologies of bicontinuous (Figure 3.8A) and multi-lamellar (Figure 3.8 B). The number average particle size was measured to be 125 ± 70 nm by TEM (calculated from 60 particles) which is much smaller than the N_{ave} obtained from DLS, this could be due to only a small section of the entire sample being viewed with TEM. The cryo-TEM images (Figure 3.8 C-D) revealed the spherical aggregates have a bicontinuous internal morphology with the particle sizes ranging from 200 nm (E) to 1145 nm (D) with some particles exhibiting multi-lamellar regions within the bicontinuous nanosphere (shown by red arrow in Figure 3.8 D and zoomed in image in Figure 3.8 F). The large size range confirms the bimodal distributions. An estimated average pore size was determined to be 25 ± 3 nm, this was established from analysing the nanosphere in Figure 3.8 C. This pore

size is the same as that observed for D3 0.1 wt % solution. It confirms that modifying the BCP to include PDSMA as the hydrophobic block instead of PODMA results in a larger pore size within the bicontinuous nanospheres.

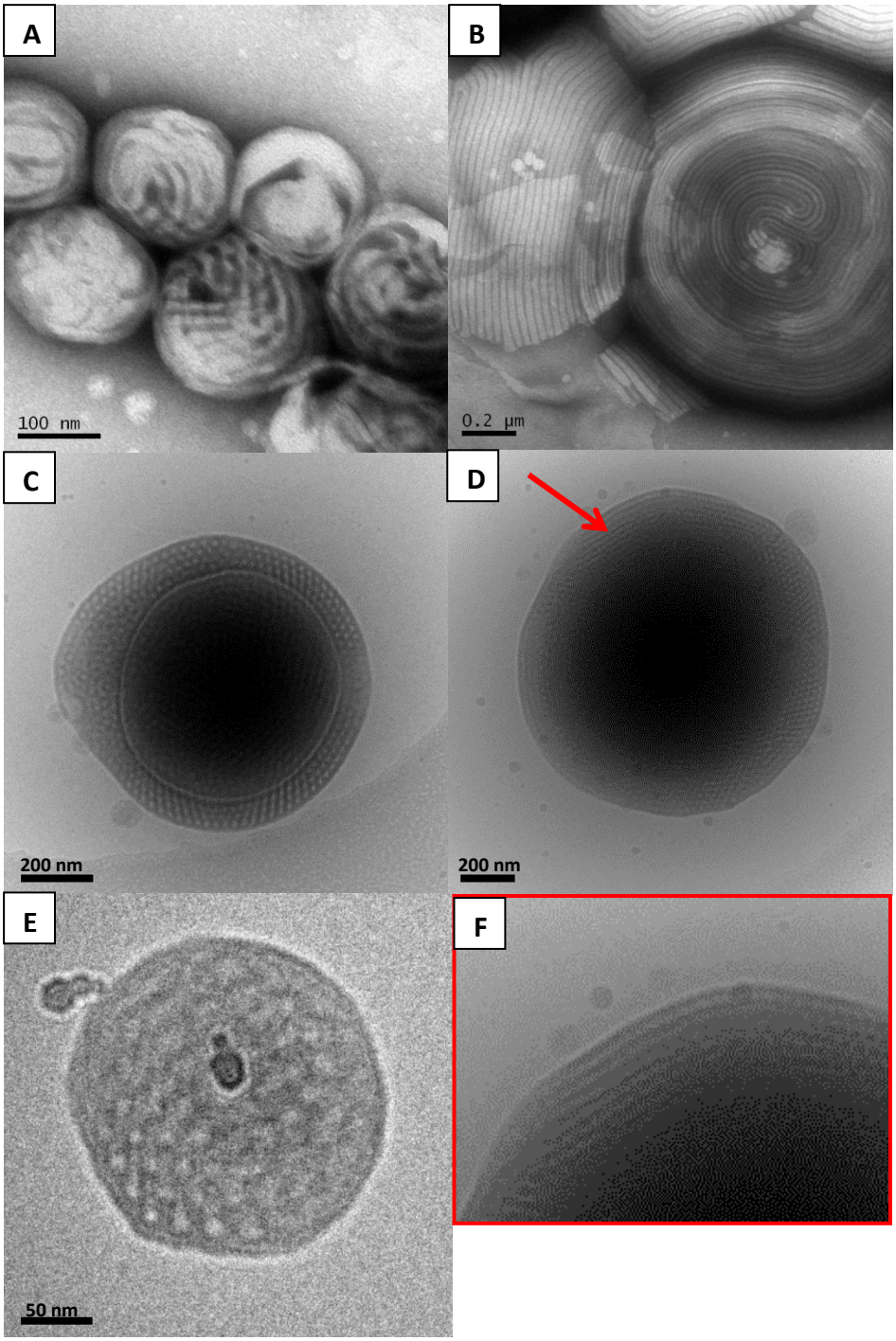

Figure 3.8: ***A-B)*** Negative stained TEM images of D3 (PEO_{44}-*b*-$PDSMA_{16}$)(1 wt %) nanospheres (Stained with 5 % uranyl acetate and 1 % acetic acid) **C-E)** Cryo-TEM images of D3 (PEO_{44}-*b*-$PDSMA_{16}$) (1 wt %) nanospheres with internal bicontinuous morphology. Red arrow highlights multi-lamellar regions within bicontinuous nanospheres. **F)** A zoomed in image of the lamellar region highlighted by the red arrow in D.

The aggregates of D3 at 5 wt % obtained by negative staining TEM are displayed in Figure 3.9. As with the 0.1 and 1 wt % solutions, the spherical aggregates are evident with some displaying a porous surface. The N_{ave} calculated from TEM was 120 nm (calculated from 40 particles). CONTIN analysis by DLS gave one average particle size of 200 ± 46 nm, however the number average distribution plots for the 5 wt % solution shows two distributions, one with a N_{ave} of 80 nm, and a smaller number % of particles at 200 nm. This distribution in particle sizes is observed in the TEM images, with a large proportion of particles around 50-100 nm. Unfortunately we were not able to obtain cryo-TEM images for this sample.

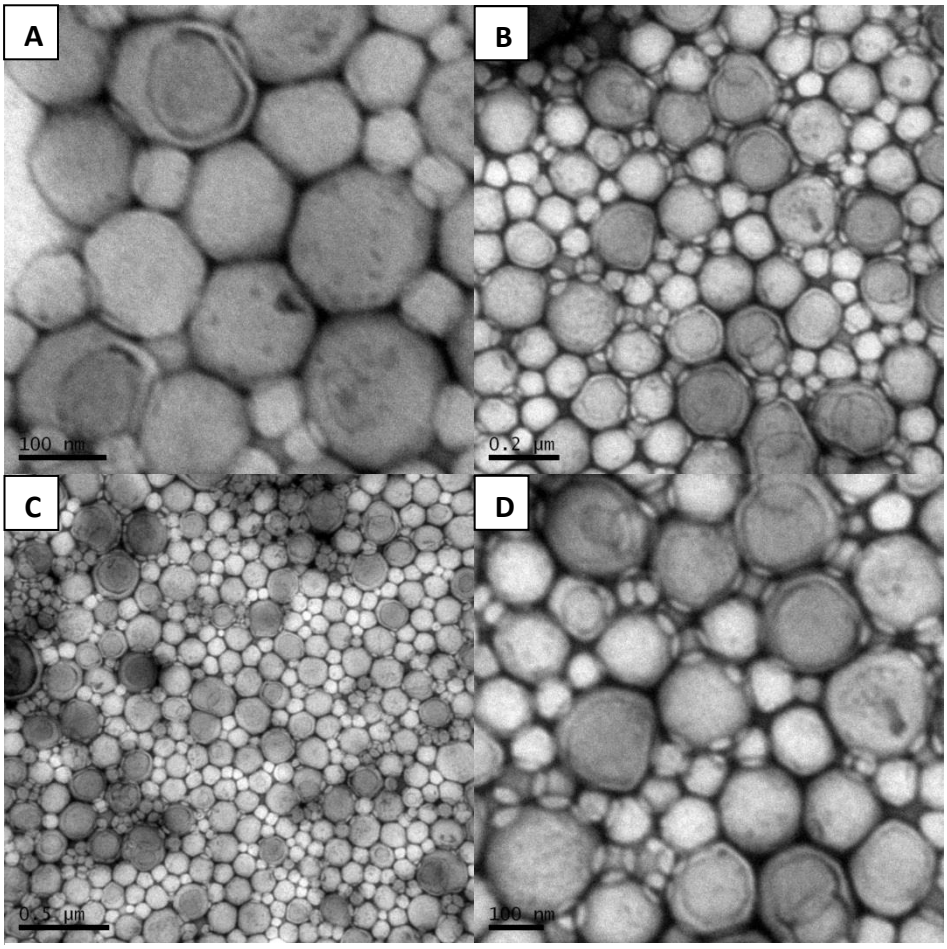

Figure 3.9: **A-D)** Negative stained TEM images of D3 (PEO_{44}-*b*-$PDSMA_{16}$) (5 wt %) nanospheres (Stained with 5 % uranyl acetate and 1 % acetic acid).

3.4.3.2 D4 (PEO_{44}-b-$PDSMA_{12}$) (PEO 30 wt %)

The BCP D4 (PEO_{44}-*b*-$PDSMA_{12}$) was synthesised with a ratio of PEO:PDSMA at 1:12 giving a PEO wt % of 30 %. It was dissolved at varying weight percentages (0.1-5 %) in 4mL of THF for the 0.1 and 1 wt % solutions and 6 mL THF for the 5 wt % solution, and then self-assembled by the slow addition of deionised water to make the total volume up to 10 m. Each sample was then analysed using DLS at 15 and 45°C, above and below the calculated T_m for PEO-*b*-PDSMA, the results are shown in Table 3.9.

The table shows a small increase in particle size from the 0.1 wt % solution to the 1 wt% solution, this trend has already been observed for D3. There is then a large decrease in particle size for the 5 wt % solution, again as discussed with D3 this is most likely due to an increase in the THF wt% used initially[23]. For the 0.1 and 1 wt % solutions the aggregate sizes are consistent, between 486-502 nm. The N_{ave} particle size of the 5 wt % solution is below 200 nm. The size distribution of the aggregates formed also changes with a change in wt %. This is represented on the table by the Đ results where by as the wt % in solution increases, the Đ (size distribution) decreases. This means at higher polymer concentrations the aggregates have a narrower size distribution. This differs slightly from the results for the self-assembly of D3 where the 0.1 wt % and 5 wt % solutions had a low dispersity compared to the 1 wt % solution. It should be noted however that all solution of D3 has lower dispersities than those observed for D4.

Table 3.9: Number mean values for self–assembled block copolymer D4 (PEO_{44}-*b*-$PDSMA_{12}$) calculated from the Z-average using Dynamic Light Scattering.

wt %	T (°C)	N_{Ave} (d.nm)	SD (± nm)	Z_{Ave} (d.nm)	SD (± nm)	CONTIN	Đ
0.1	15	486	125	1338	184	322	0.68
0.1	45	487	143	1322	78	314	0.73
1	15	502	113	994	62	577/163	0.49
1	45	491	115	1054	48	511/158/ 75	0.47
5	15	193	36	346	11	504/153	0.40
5	45	198	27	366	8	585/177	0.38

Figure 3.10 A illustrates the size distribution of the aggregates formed for all concentrations in solution at 15°C. All plots are bimodal with the second peak (larger N_{ave}) decreasing in number % as the concentration is increased. This explains the trend in Đ with the 5 wt % solution having the narrowest size distribution of particles. The distributions confirm that the 0.1 and 1 wt % solutions have very similar N_{ave} values of around 300 nm for the main peak, and 1300 nm for the second smaller peak. The CONTIN data does not match the distributions observed except for the 5 wt % solution with two distributions at 150 nm and 500 nm, this is because the CONTIN analysis is calculated directly from the correlation function as is the z-average. The N_{ave} is calculated from the z-average and it a better representative of bimodal distributions due to the z-averages bias towards larger particles. The size distribution for all D4 aggregate solutions at 45°C can be seen in Figure 3.10 B. The 0.1 and 1 wt % solutions both have a bimodal distribution with relatively similar particle sizes, consistent with the results seen in Table 3.9. The 5 wt % solution has a bimodal distribution with a smaller N_{ave} than the 0.1 and 1 wt % solutions.

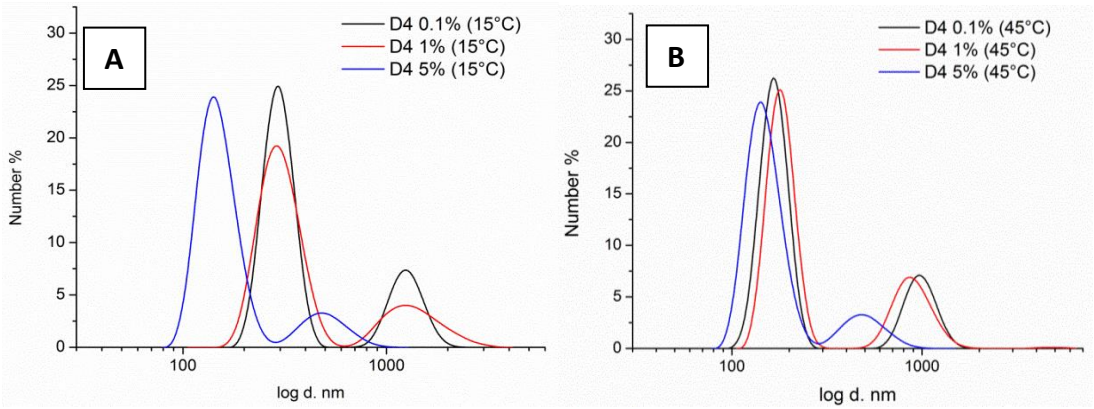

Figure 3.10*:* DLS distribution plot of D4 (PEO_{44}-*b*-$PDSMA_{12}$), wt. % 0.1, 1% and 5% in solution at 15°C **(A)** and 45˚C **(B)**.

It should be noted that DLS measurements rely on the aggregates being perfectly spherical, if another morphology other than spherical aggregates is present, such a cylindrical micelles, then the results obtained via DLS will not be accurate.

The aggregate solutions of D4 (PEO: 30 wt %) at 0.1-5 wt % were analysed using TEM and the 0.1 and 1 wt % solutions were further analysed with cryo-TEM, to confirm the effect a change in the hydrophilic blocks weight fraction has on the resultant

morphology and to compare these results to that of P7 (PEO_{49}-*b*-$PODMA_{16}$, PEO 30 wt %) seen in chapter 2. Interestingly, changing the PEO wt % from 25 to 30 wt % resulted in a number of different morphologies, this change was previously observed between P3 (PEO_{49}-*b*-$PODMA_{21}$ - PEO 25 wt %) and P7 (PEO_{49}-*b*-$PODMA_{16}$ - PEO 30 wt %). The TEM images of the 0.1 wt % solution can be seen in Figure 3.11 (A-B). They exhibit cylindrical micelles, also known as "worms" (B) and multi-lamellar regions surrounded by worms (A). Further analysis using cryo-TEM (Figure 3.11 B-C) demonstrated a spherical aggregate with an internal morphology of multi-lamellar, with a bicontinuous core, and further evidence of the worms attached to a multi-lamellar aggregate. The two morphologies present explains the two N_{ave} distributions observed with DLS. Cylindrical micelles and multi-lamellar spherical aggregates were also observed for P7 (PEO-*b*-PODMA, PEO 30 wt %) in chapter 2 at the same concentration (0.1 wt %).

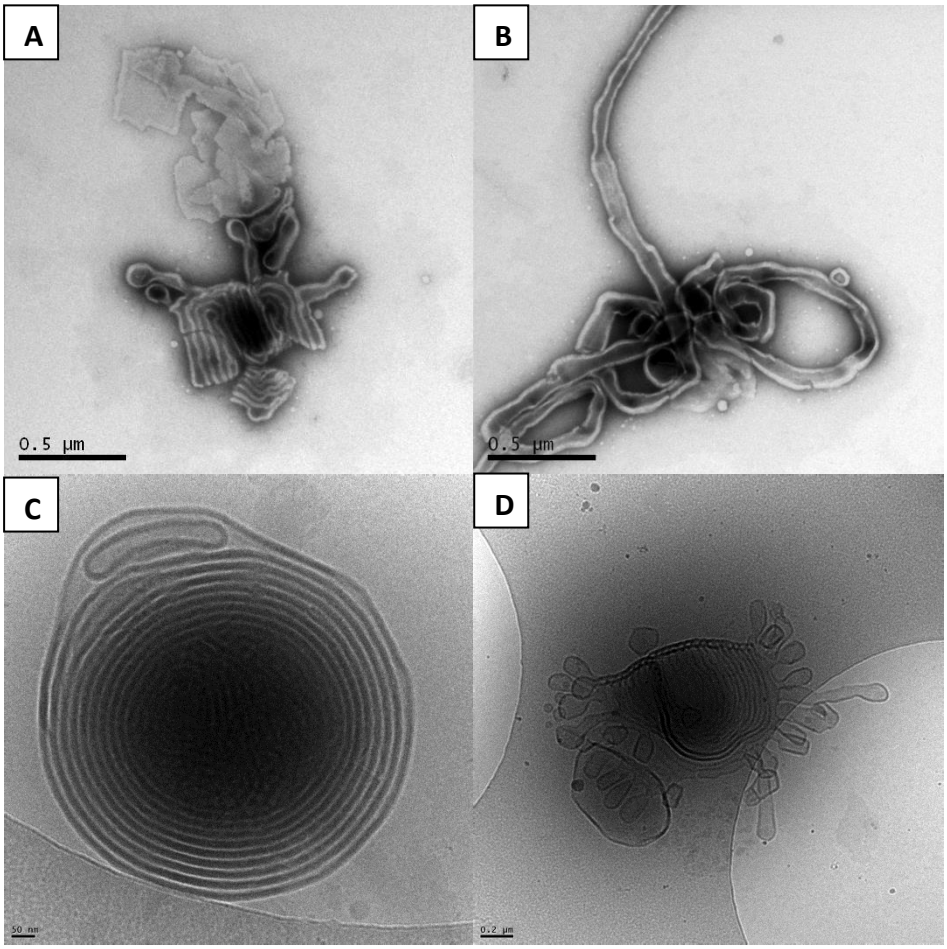

Figure *3.11*: A-B) Negative stained TEM images of D4 (PEO_{44}-*b*-$PDSMA_{12}$) (0.1 wt %) nanospheres (Stained with 5 % uranyl acetate and 1 % acetic acid). **C-D)** Cryo-TEM images of D4 (PEO_{49}-*b*-$PDSMA_{12}$) (0.1 wt %) nanospheres with internal multi-lamellar/bicontinuous morphology.

The cylindrical morphology is a result of the molecular curvature of the block copolymer which influences the packing of the polymer chains. As discussed in chapter 1 the cylindrical morphology can be predicted from the packing parameter ($p=v/a_o l_o$), which should be $1/3 \leq p \leq 1/2$ for cylindrical micelles to form[26]. The rules for predicating morphology based on hydrophilic weight fraction outlined by Discher and Eisenberg (2002)[27] and observed by others in the literature[28] suggest cylindrical micelles will form when the hydrophilic block wt % is just less than 50 % (35-45 % roughly) in the case of P7 our hydrophilic block the wt % is 30 % but cylindrical micelles are still present. The phase diagram proposed by McKenzie at al. (2015)[23] for PEO-*b*-PODMA BCPs indicates that PEO-*b*-PODMA with PEO weight fraction of 30 % and a M_w of around 18 kDa, will from large compound vesicles upon the addition of water. Cylindrical micelles have not been observed for this polymer system. However McKenzie *et al.* also explains that the molecular weight of the BCP also affects the resultant morphology, with the M_w of D4 being significantly smaller (11 kDa) than the BCP that produced large compound vesicles, this might be the reason for the variation in morphology of a BCP with the same hydrophilic weight fraction. It should also be noted that cylindrical micelles will only form within a narrow range of compositions[29] and conditions which is most likely why this morphology was not observed upon an increase in D4 concentration (from 0.1-5 wt %). These cylindrical micelles form along-side multi-lamellar vesicles. These vesicles were expected from viewing the phase diagram (Figure 3.12) where they are present at 35 wt % PEO and roughly 6 kDa. It would be interesting to further investigate the formation of these observed cylindrical micelles of PEO-*b*-PODMA and PEO-*b*-PDSMA by looking at the self-assembled morphologies at PEO wt % slightly above and below 30 % while maintaining the M_w range.

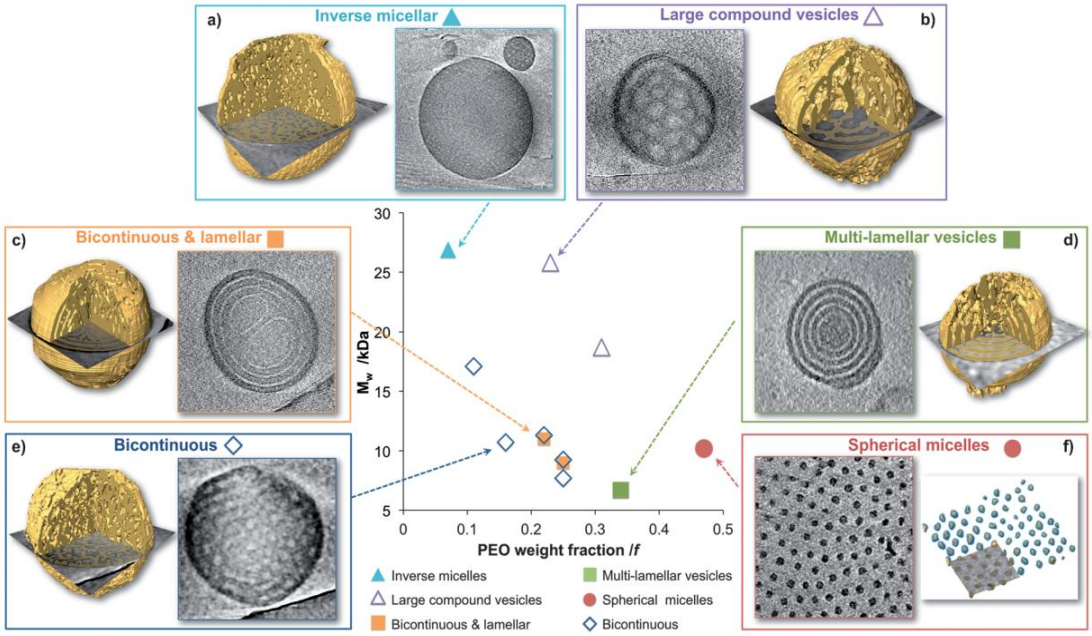

Figure 3.12: Partial phase diagram of the self-assembly behaviour of PEO-*b*-PODMA block copolymers with corresponding slices through the 3D reconstructions, and computer-aided visualizations from the reconstructed tomograms (segmentations in yellow) that show the different morphologies. The computer-aided visualizations were conducted by combining the use of a mathematical filter to reduce noise and an adaptive threshold to segment the hydrophobic PODMA phase (shown in yellow). Reproduced from ref.[23]

The TEM images (Figure 3.13 A-B) of the 1 wt % solution shows spherical aggregates, across the size range 40-200 nm, they indicate a possible internal morphology of multi-lamellar/bicontinuous (Figure 3.13 B). The cryo-TEM images show spherical vesicles (Figure 3.13 C) and spherical aggregates whose morphology exhibits a mix of multi-lamellar and bicontinuous (Figure 3.13 D). The cryo-TEM images revealed a particle size range of 120-725 nm which explains the bimodal distribution plot seen from DLS. Vesicles and multi-lamellar aggregates with bicontinuous cores were also observed for P7 (PEO-*b*-PODMA, PEO 30 wt %).

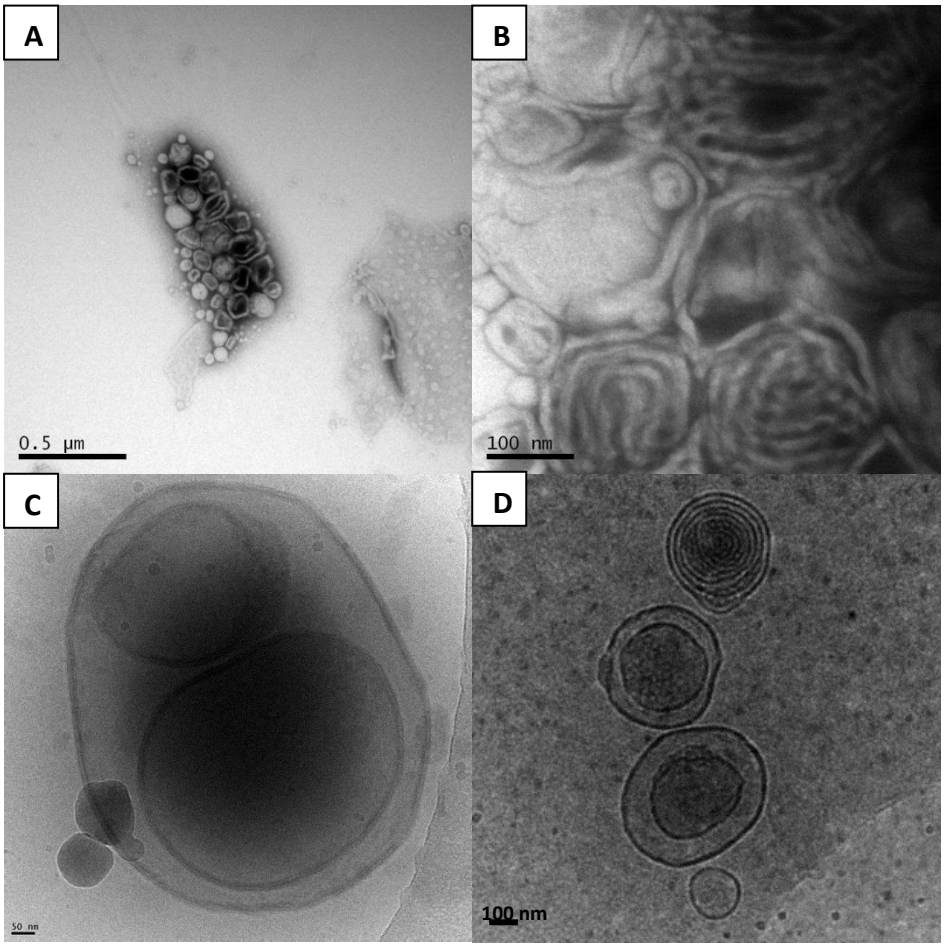

Figure 3.13: **A-B)** Negative stained TEM images of D4 (PEO_{44}-*b*-$PDSMA_{12}$) (1 wt %) nanospheres (Stained with 5 % uranyl acetate and 1 % acetic acid). **C-D)** Cryo-TEM images of D4 (PEO_{49}-*b*-$PDSMA_{12}$) (1 wt%) nanospheres with internal multi-lamellar/bicontinuous morphology.

The TEM images of D4 at 5 wt % in solution (Figure 3.14) shows spherical aggregates, some with a porous surface indicating possible internal bicontinuous morphology (shown by red arrow in Figure 3.14 B) and possible multi-lamellar morphology (shown by green arrow in Figure 3.14 A). The size range for these particles calculated from TEM is 40-400 nm and this explains the smaller N_{ave} observed from DLS. The mix of aggregate sizes also explains the bimodal distribution plot for D4 5 wt %. Unfortunately cryo-TEM images were not taken for this sample.

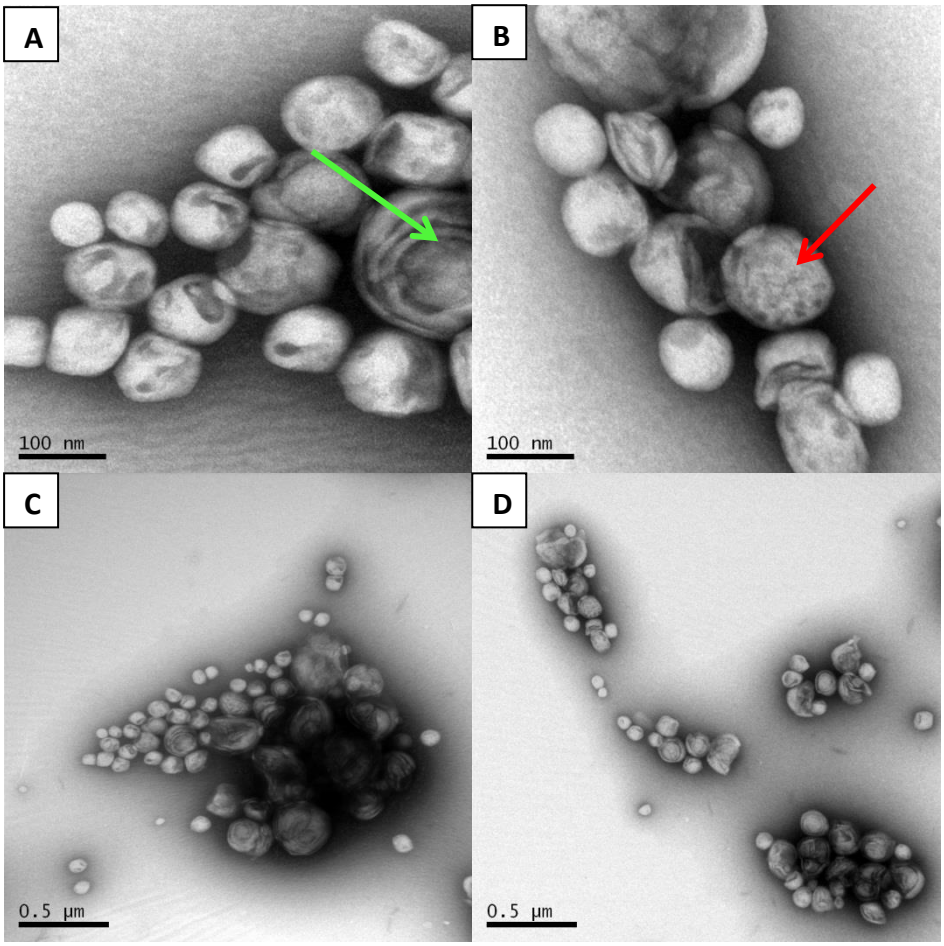

Figure 3.14: A-D) Negative stained TEM images of D4 (PEO_{44}-*b*-$PDSMA_{12}$) (5 wt %) nanospheres (Stained with 5% uranyl acetate and 1% acetic acid). Green arrow indicates the multi-lamellar regions. Red arrow indicates bicontinuous regions.

Upon increase in PEO wt % (hydrophilic block) the bicontinuous morphology was mainly lost, instead multi-lamellar aggregates were observed across the three concentrations with some portions of the multi-lamellar aggregates retaining their bicontinuity. Cylindrical micelles are seen for the 0.1 wt % solution only. These results are consistent with those observed for P7 (PEO_{49}-*b*-$PODMA_{16}$ – 30 wt % PEO) (PEO_{49}-*b*-$PODMA_{16}$ – 30 wt% PEO) indicating that a change of the hydrophobic block from PODMA to PDSMA has no significant effect on the resultant morphologies.

3.4.4 Self-Assembly of PEO-*b*-(PODMA-*co*-PDSMA) BCPs C1-C4

A blend of P4 (PEO-*b*-PODMA, PEO 25 wt%) and D3 (PEO_{44}-*b*-$PDSMA_{16}$, PEO 25 wt%) was prepared at a wt% ratio of 50:50. Self-assembly was then carried out on this BCP blend using the dialysis method. Precipitation occurred upon the slow addition of water. This was surprising as the two BCPs didn't even aggregate individually, indicating that their inability to crystallise with each other also affected their ability to aggregate individually. The bulk blended sample was analysed with DSC, the results of which will be discussed later in this chapter.

Having established that the polymer blend would not yield bicontinuous nanospheres due to their inability to crystallise with each other, a series of BCPs were synthesised with a copolymer hydrophobic block of PODMA:PDSMA at varying wt% ratios. The copolymers were synthesised with a PEO wt% of 25 wt% as it has been shown in this chapter and chapter 2 that this is the optimum wt% of the hydrophilic block for BCPs to form bicontinuous nanospheres in aqueous media. The copolymers synthesised in 3.3.5 were self-assembled following the dialysis method previously used for both PEO-*b*-PODMA and PEO-*b*-PDSMA. Each copolymer was self-assembled at 0.1, 1 and 5 wt% in solution, this was to establish whether having the copolymer as the hydrophobic block had an effect on the self-assembly nature of the BCP, i.e. can it still produce bicontinuous nanospheres across a range of concentrations as seen previously with PEO-*b*-PODMA and PEO-*b*-PDSMA. Post self-assembly the aggregate solutions were analysed using DLS, TEM and cryo-TEM to establish the average particle size, morphology and pore size. The masses of BCP and volumes of THF used for each wt% in solution can be seen in Table 3.10. As with PEO-*b*-PDSMA, 6 mL of THF was used to dissolve the BCPs C1-C4 for the 5 wt % solutions as a volume less than 6 mL caused precipitation upon addition of water.

Table 3.10: Weight percentage and masses used for the self-assembly of all PEO-*b*-PDSMA block copolymers.

BCP wt %	Mass BCP (g)	THF volume (mL)	Water volume (mL)	Total volume (mL)
0.1	0.01	4	6	10
1	0.1	4	6	10
5	0.5	6	4	10

3.4.4.1 C1 (PEO_{45}-b-$PODMA_{15}$-co-$PDSMA_4$) (PODMA:PDSMA 75:25)

Block copolymer C1 (25 wt% PEO) was synthesised with a ratio of 1:19 PEO:PODMA/PDSMA giving a PEO wt.% of 25% and a wt% ratio of PODMA:PDMSA of 75:25. The BCP was dissolved at varying concentrations in THF and then self-assembled by the slow addition of deionised water to produce 0.1, 1 and 5 wt% with a total volume of 10 mL. Each sample was then analysed with DLS at 15 and 45°C (above and below predicted T_m calculated with DSC). (Table 3.11)

Upon increase in the measurement temperature, from 15°C to 45°C, a slight increase in N_{ave} was observed for the 0.1 and 1 wt% solutions. This is most likely due to particle aggregation and as the PDSMA side chains are heated above their T_m (DSC) the PDSMA side chains melt becoming disordered. Again this loss of order has been previously observed for PEO-*b*-PDSMA (D3) and reported by McKenzie *et al*.[22]

An increase is seen in number average particle size, from the 15°C measurements, when the 0.1 and 1 wt% solutions are measured at 45˚C from 15°C, above the expected transition temperature the aggregates are aggregating together and the polymer chains, having melted, are losing their bicontinuous structure and dispersing. The 5 wt% sees a slight decrease in number average particle size when measured at 45°C. The dispersity, Đ, for all the aggregate solutions is below 0.2 this indicates a narrow particle size distribution in all solutions. The average particle size is largest for the 0.1 wt% in solution, this was observed previously with both P3 and D3.

Table 3.11: Particle sizes for self–assembled block copolymer C1 (PEO_{44}-b-(PODMA-*co*-$PDSMA_{12}$) calculated using dynamic light scattering.

wt %	T (°C)	N_{Ave} (d.nm)	SD (± nm)	Z_{Ave} (d.nm)	SD (± nm)	CONTIN	Đ
0.1%	15	268	26	337	3	409/168	0.14
0.1%	45	312	33	347	2	391/148	0.11
1%	15	180	15	229	1	215/514/4390	0.20
1%	45	187	14	228	2	222/501/2052	0.18
5%	15	194	37	236	3	254/90/819	0.16
5%	45	186	30	241	2	265/550/107	0.15

The number average size distribution plots for C1 0.1, 1 and 5 wt % solutions measured at 15°C are illustrated in Figure 3.15 A. The 0.1 wt % solution is monomodal with a shoulder peak with an N_{ave} of approximately 450 nm and the main peak having a N_{ave} of approximately 200 nm. This is consistent with the CONTIN data seen in Table 3.11. The 1 wt% solution is monomodal with a shoulder peak, the main peak (largest number %) has a number average of around 150 nm with the shoulder peak being around 200 nm. This explains the slightly higher Đ value. The 5 wt% solution is monomodal with a narrow size distribution, explaining the small Đ value, it shows a number average particle size of approximately 200 nm, consistent with the results seen in Table 3.11.

The number average distribution plots for C1 0.1, 1 and 5 wt % solutions measured at 45˚C are plotted in Figure 3.15 B. All concentrations are monomodal, this explains the decrease in Đ when compared to the measurements taken at 15˚C. The 0.1 wt % solution has a number average particle size of approximately 300 nm, the number average particle size for the 1 and 5 wt % solution from the distribution plot are approximately 200 nm. These results are consistent with those seen in Table 3.11.

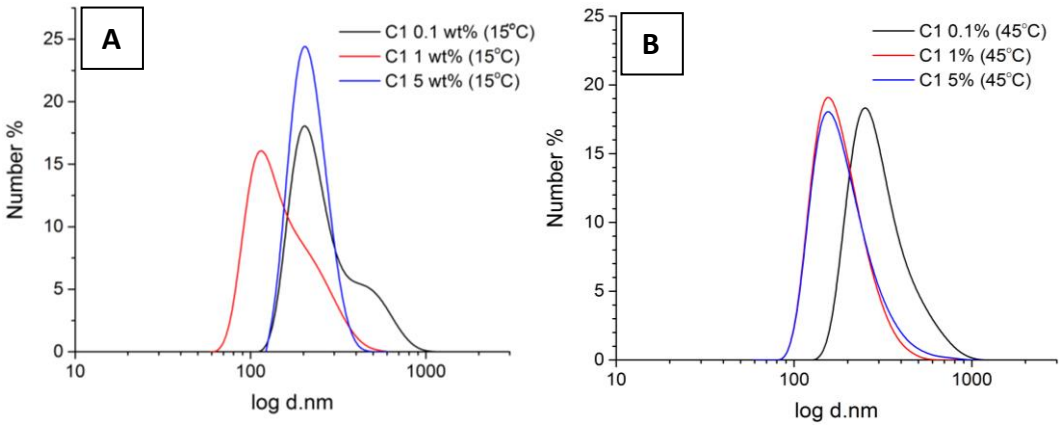

Figure 3.15: DLS number average distribution plots of C1 (PEO_{45}-*b*-($PODMA_{15}$-*co*-$PDSMA_4$), at 0.1, 1 and 5 wt % in solution at 15°C **(A)** and 45°C **(B)**.

This decrease in N_{ave} upon increase in concentration was not expected. Generally it has been reported in the literature,[30] that upon an increase in polymer concentration an increase in particle size is observed. This was seen for surfactants in general by Nagy *et al.* where an increase in surfactant concentration resulted in an increase in micelle particle size. Wang *et al.*[25] investigated the effect of concentration on the self-assembly of poly(methyl methacrylate)-block-poly(methacrylic acid) (PMMA-co-PMAA). They found that not only does an increase in concentration cause an increase in particle size, but that the morphology of the particles changes upon a change in polymer concentration. This phenomenon, a morphological change upon a polymer concentration change, has been observed many times in the literature.[30-31]

The aggregate solutions of C1 were further analysed with TEM and cryo-TEM to establish their particle shape, size and internal morphology. The TEM images of C1 (Figure 3.16) 0.1 wt % solution display spherical aggregates with a number average particle size of 272 nm (calculated from 30 particles) which is close to the N_{ave} calculated via DLS. A porous structure is evident in Figure 3.16 A indicating a bicontinuous internal morphology, possible multi-lamellar regions mixed in with bicontinuous regions are also indicated in Figure 3.16 B (shown by red arrows). Analysis of the cryo-TEM images revealed the spherical particles have well defined internal bicontinuous morphology with the particle sizes all being roughly 450 nm with some bicontinuous nanospheres displaying small lamellar regions (shown by arrow in Figure 3.16 D). These results are consistent with those observed for both P3 (PEO-*b*-PODMA, PEO 25 wt %) and D3 (PEO-*b*-PDSMA, PEO 25 wt %) at the same

concentration. The average pore size was estimated to be 29 ± 6 nm, by measuring the pore sizes of the nanosphere in Figure 3.16 C. This value is 10 nm bigger than the pore sizes observed for a PEO-*b*-PODMA (PEO 25 wt%) nanosphere by Mckenzie *et al.*[23] C1 at 0.1 wt% exhibits a larger pore size also, than PEO-*b*-PDSMA (D3-24 nm) at the same concentration.

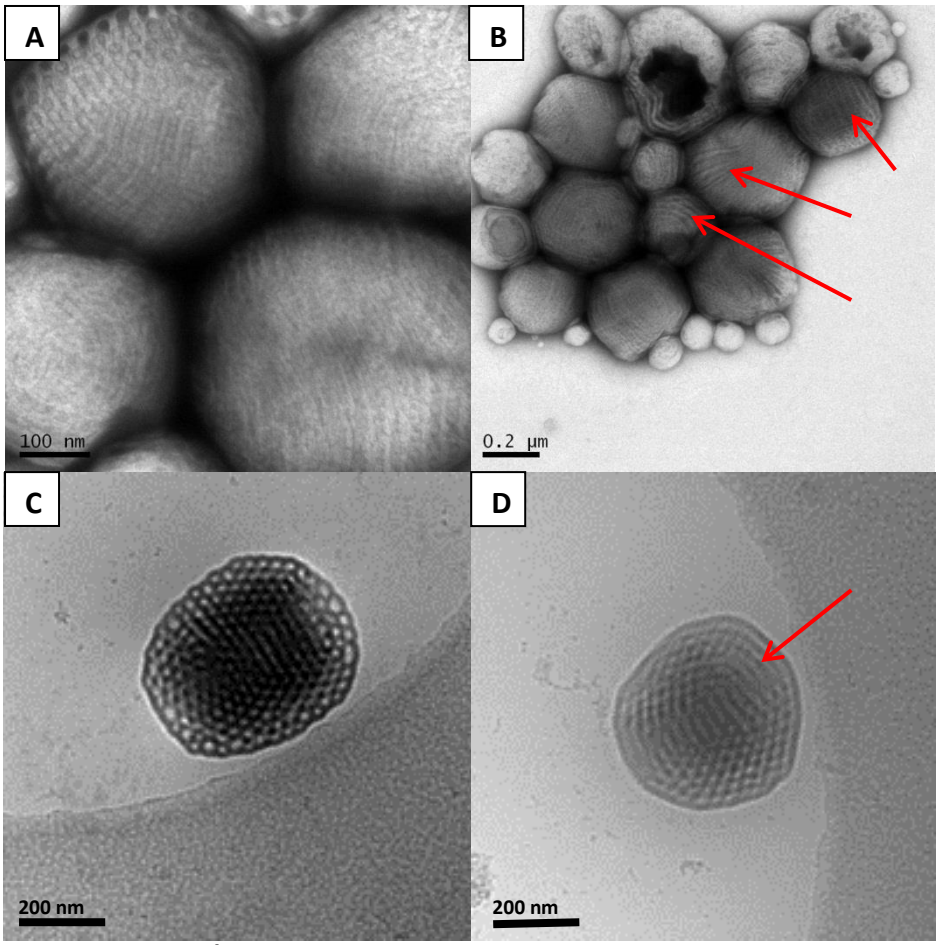

Figure 3.16: A-B) Negative stained TEM images of C1 (PEO_{45}-*b*-($PODMA_{15}$-*co*-$PDSMA_5$)) (0.1 wt %) nanospheres (Stained with 5 % uranyl acetate and 1 % acetic acid). **C-D)** Cryo-TEM images of C1 (PEO_{45}-*b*-($PODMA_{15}$-*co*-$PDSMA_5$)) (0.1 wt %) nanospheres with internal bicontinuous morphology. The red arrow indicates lamellar region within the bicontinuous nanospheres.

The TEM images of C1 1 wt % solution (Figure 3.17) revealed spherical aggregates with a possible bicontinuous morphology seen in Figure 3.17 A and multi-lamellar regions seen in Figure 3.17 B (shown by red arrow). The number average particle size established from TEM was 212 nm (calculated from 35 particles). The cryo-TEM images confirm the spherical aggregates have internal bicontinuous morphology (Figure 3.17 E+F) with a small proportion having multi-lamellar internal morphology

(shown by red arrow in Figure 3.17 D arrowed) and the external shape is not as ordered as seen with P3 and D3. The bicontinuous estimated average pore size is 29 ± 4 nm measured from the nanosphere squared in Figure 3.17 F. This is the same pore size as that observed for C1 at 0.1 wt %. Again it is larger than both the pore sizes observed for D3 at the same concentration and PEO-*b*-PODMA (PEO 25 wt%) observed by McKenzie *et al.* [23]

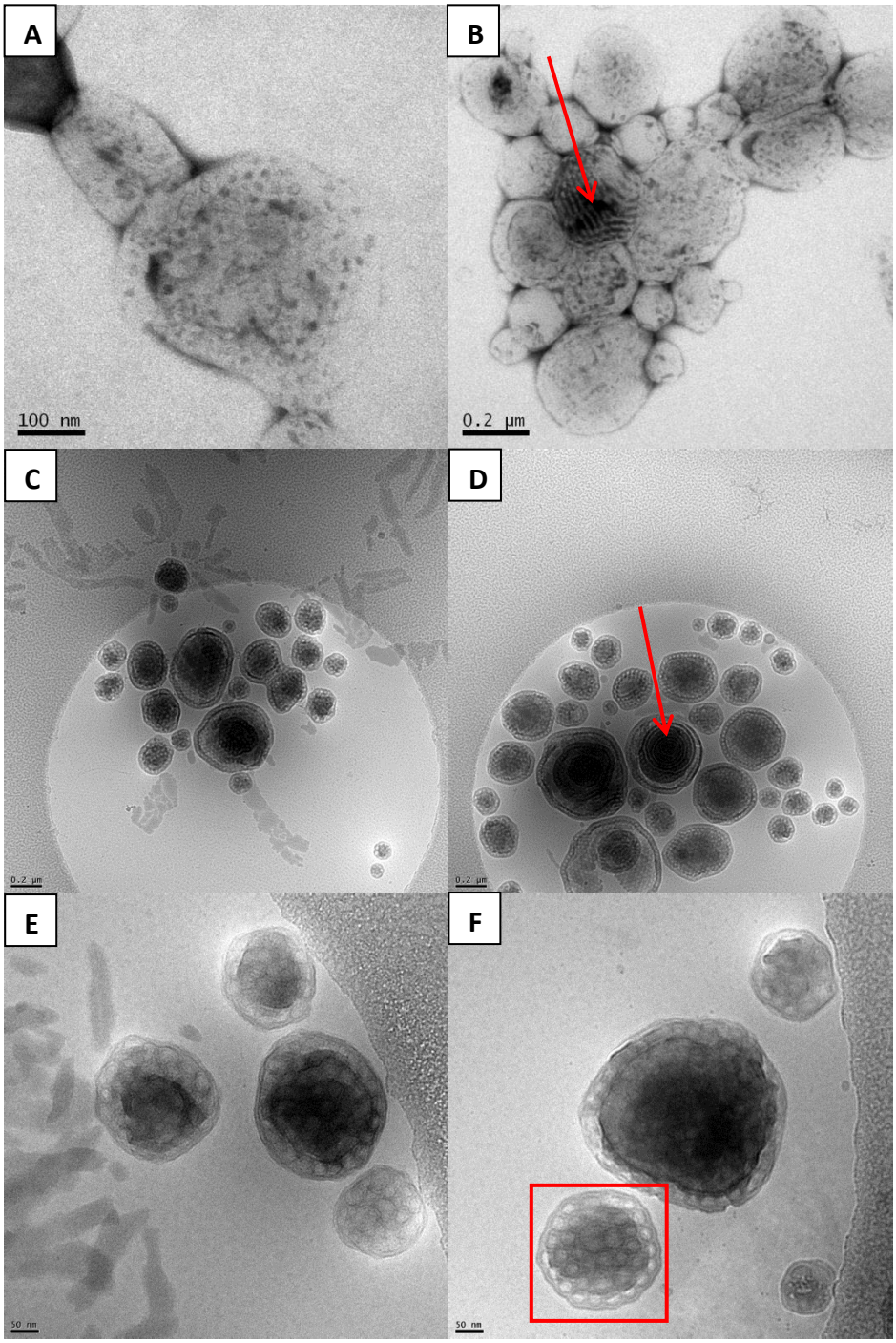

Figure 3.17: A-B) Negative stained TEM images of C1 (PEO_{45}-*b*-($PODMA_{15}$-*co*-$PDSMA_5$)) (1 wt %) nanospheres (Stained with 5 % uranyl acetate and 1 % acetic acid). The red arrow indicates multi-lamellar regions **C-F)** Cryo-TEM images of C1 (PEO_{45}-*b*-($PODMA_{15}$-*co*-$PDSMA_5$)) (1 wt %) nanospheres with internal bicontinuous and multi-lamellar morphology. The red arrow indicates multi-lamellar regions. The red box highlights the nanosphere used to establish the average pore diameters in these bicontinuous nanospheres.

The C1 5 wt% solution followed the same trend observed for the lower concentrations; the TEM images (Figure 3.18) show spherical aggregates with possible bicontinuous morphology. An increase in aggregate formation is evident from the TEM images, this confirms that an increase in polymer concentration does result in an increase in number of aggregates formed. The number average particle size established from TEM was 159 nm (calculated from 30 particles), this is slightly smaller than the N_{ave} observed with DLS (194 nm) but is most likely due to particle dehydration in TEM. These results show that as the concentration of polymer is increased the particle size decreases, this was also observed from DLS measurements. The internal bicontinuous morphology was confirmed with cryo-TEM. The average pore size was estimated to be 28 ± 5 nm, by measuring the nanosphere highlighted in Figure 3.18 D. This average pore size is consistent with those observed for C1 bicontinuous nanospheres at both 0.1 and 1 wt %.

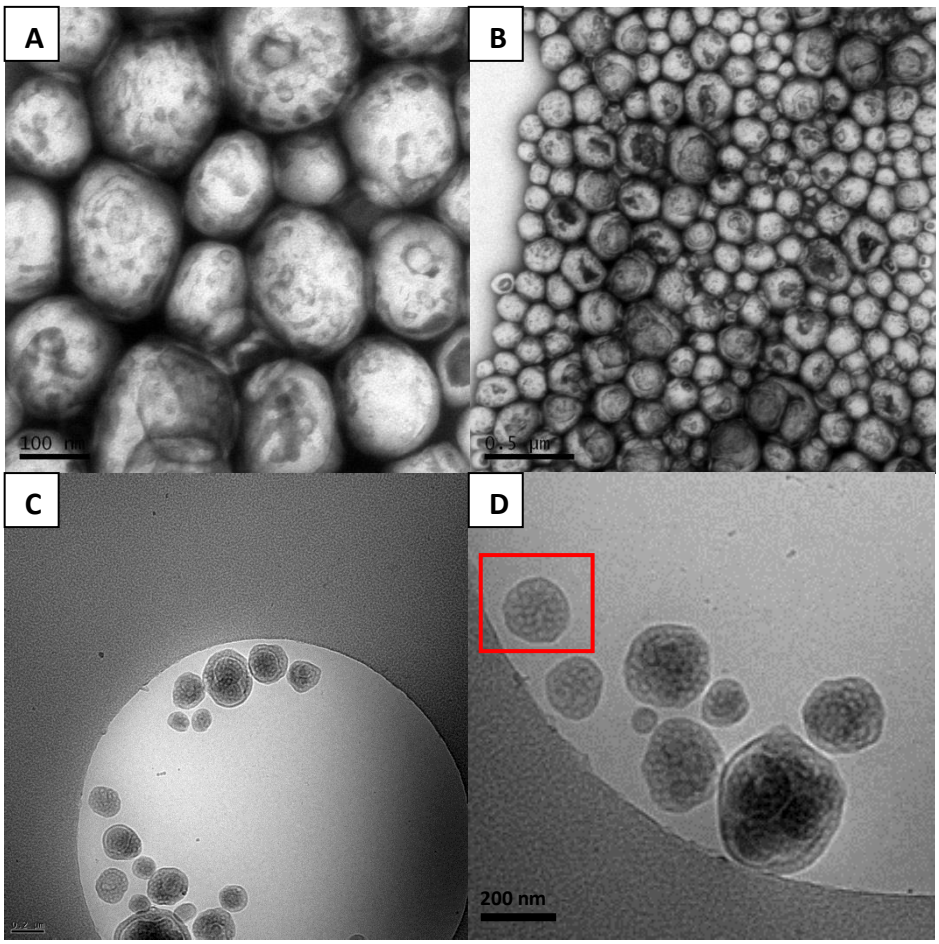

Figure 3.18: A-B) Negative stained TEM images of C1 (PEO_{45}-*b*-($PODMA_{15}$-*co*-$PDSMA_5$)) (5 wt %) nanospheres (Stained with 5 % uranyl acetate and 1 % acetic acid). **C-D)** Cryo-TEM images of C1 (PEO_{45}-*b*-($PODMA_{15}$-*co*-$PDSMA_5$)) (5 wt %) nanospheres with internal bicontinuous morphology. The red box indicates the nanospheres used to obtain the average pore diameter from these bicontinuous

3.4.4.2 C2 (PEO_{45}-b-$PODMA_9$-co-$PDSMA_9$) (PODMA:PDSMA 50:50)

Block copolymer C2 (25 wt % PEO) was synthesised with a PODMA:PDSMA wt % ratio of 50:50. C2 was self-assembled at 0.1, 1 and 5 wt% in solution. Each sample was then analysed by DLS at 15 and 45°C (above and below predicted T_m calculated using DSC).

For all concentrations there is not a significant difference in the number average particle size with an increase in DLS measurement temperature from 15 to 45°C. As mentioned previously this most likely due to a loss of the internal bicontinuity but not in the external spherical shape. As seen previously for P3 (PEO_{49}-*b*-$PODMA_{21}$)

there is an increase in dispersity upon an increase in polymer concentration. The number average particle sizes (N_{ave}) decrease with an increase in concentration. The decrease in N_{ave} for the 5 wt % solution was expected, again due to an increase in THF volume used in the initial self-assembly stage. The decrease in particle size from 0.1-1 wt % was not expected and does not follow the literature, where generally an increase in polymer concentration results in an increase in particle size.[25, 31]

Table 3.12: Number average and Z-average particle sizes for self–assembled block copolymer C2 (PEO_{45}-*b*-($PODMA_9$-*co*-$PDSMA_9$) calculated using Dynamic Light Scattering.

wt %	T (°C)	N_{Ave} (d.nm)	SD (± nm)	Z_{Ave} (d.nm)	SD (± nm)	CONTIN	Đ
0.1	15	382	50	611	10	207/835	0.27
0.1	45	415	23	622	8	206/787	0.26
1	15	196	25	316	6	170/584	0.30
1	45	183	14	256	2	187/523	0.26
5	15	178	32	327	6	166/424/3288	0.44
5	45	174	21	299	4	180/784/3440	0.42

The number average distribution plots of C2 0.1, 1 and 5 wt % solutions at 15˚C are all bimodal (Figure 3.19 A). The 0.1 wt % solution has two distinct peaks. The particle size at the highest number % is approximately 200 nm with a lower number % at approximately 700 nm, this is consistent with the CONTIN analysis for 0.1 wt % (15°C) displayed in Table 3.12. The 1 wt % solution shows a peak at approximately 200 nm with a large number %, the smaller peak is at approximately 700 nm the same result seen for the 0.1 wt % solution. The 5 wt% particle size distribution has a large peak at approximately 100 nm, this is the size of the majority of the aggregates in solution, and the smaller peak indicates that some particles are a lot larger with a number average particle size of approximately 400-500 nm.

The number average distribution plots of C2 0.1, 1 and 5 wt % solutions (Figure 3.19 B) measured at 45°C show that the 0.1 and 5 wt% solutions have bimodal distributions, and the 1 wt % solution has one peak with a shoulder. The 0.1 wt % solution as two peaks with large number % as seen when measured at 15°C. For the

5 wt % solution an increase in the N_{ave} for the main peak from 100 nm to 200 nm is observed upon increase in measurement temperature. The second peak (450 nm) has decreased in number % compared to when measured at 15°C.

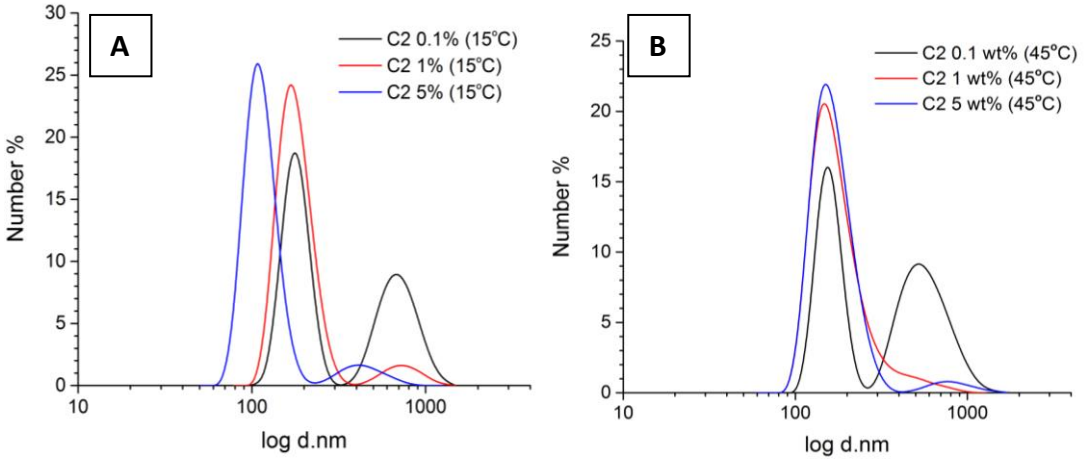

Figure 3.19: DLS number average distribution plots of C2 (PEO_{45}-*b*-($PODMA_9$-*co*-$PDSMA_9$) at 0.1, 1 and 5 wt % in solution at 15°C **(A)** and 45˚C **(B)**.

The negatively stained TEM images of C2 0.1 wt % revealed spherical aggregates with a number average particle size of 374 nm (calculated from 30 particles). The images also indicate possible bicontinuous internal morphology (shown by red arrows in Figure 3.20 A) along with multi-lamellar (shown by green arrows in Figure 3.20 A). Further investigation of the nanospheres internal morphology was carried out by cryo-TEM (Figure 3.20 B). These images revealed spherical particles across the size range 150-950 nm, this explains the two peaks displayed in the distribution plots for this sample, the CONTIN analysis also indicates two different distributions around 200 and 800 nm. Nanospheres with bicontinuous internal morphologies (highlighted in red in Figure 3.20 C) and some particles exhibiting mixed morphologies of both bicontinuous and multi-lamellar.

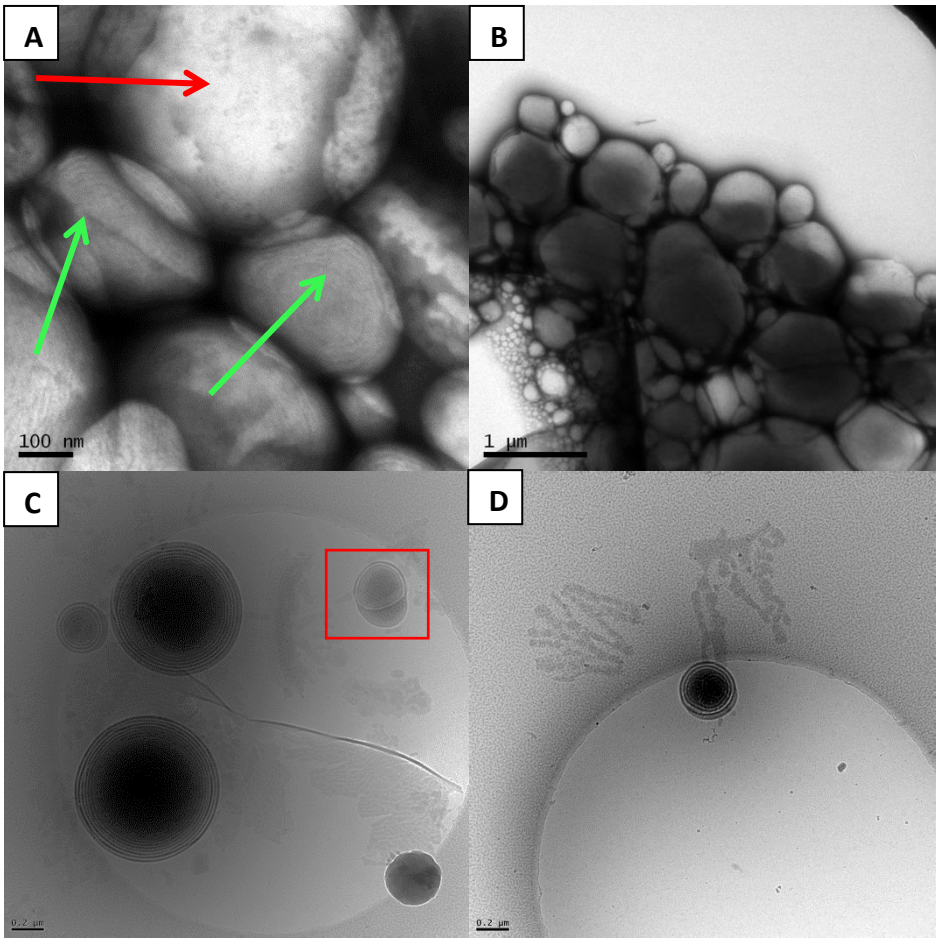

Figure 3.20: A-B) Negative stained TEM images of C2 (PEO_{45}-*b*-($PODMA_9$-*co*-$PDSMA_9$)) (0.1 wt %) nanospheres (Stained with 5 % uranyl acetate and 1 % acetic acid). The red arrow highlights possible bicontinuous morpholgoy and the green arrows highlight possible multi-lamellar morphology. **C-D)** Cryo-TEM images of C2 (PEO_{45}-*b*-($PODMA_9$-*co*-$PDSMA_9$)) (0.1 wt %) nanospheres with internal bicontinuous morphology. The red box highlights the nanospheres used to calculate the pore diameter in these bicontinuous nanospheres.

C2 at 1 wt % in solution produced spherical aggregates with a number average particle size of 132 ± 62 nm (calculated from 40 particles) as revealed from the TEM images (Figure 3.21), this particle size is slightly smaller than that observed for the highest number % of particles via DLS (200 nm), 1000 nm sized aggregates were not observed with TEM or cryo-TEM but were indicated from the DLS distribution plot for this sample, it could be that the higher sized peak on DLS was due to contamination of dust in the sample. Cryo-TEM revealed the internal morphology of the spherical aggregates to be bicontinuous, showing that an increase in concentration does not affect the resultant morphology. The estimated average pore

diameter was calculated to be 25 ± 2 nm, calculated from the aggregate in Figure 3.21 E (shown by red arrow). The same pore size was observed for D3 (PEO-*b*-PDMSA) at the same concentration. A slight decrease in pore size was observed from 29 nm for C1 (PODMA:PDSMA 75:25) at the same concentration.

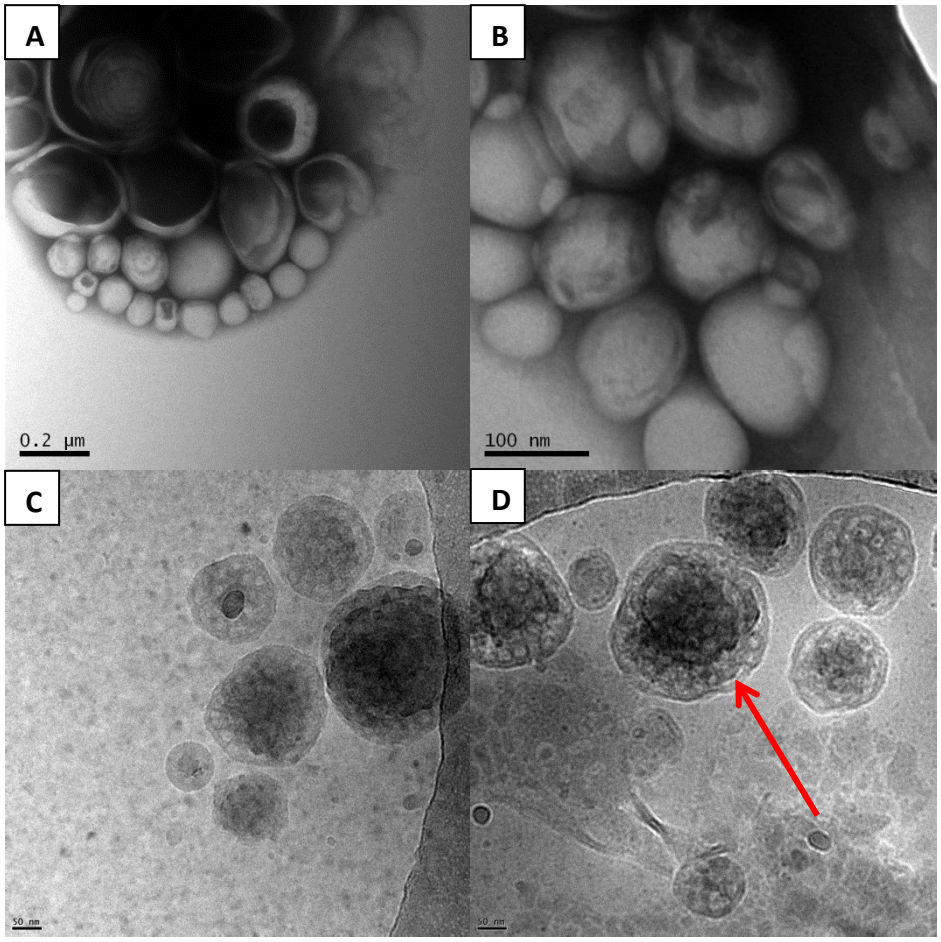

Figure 3.21: A-B) Negative stained TEM images of C2 (PEO_{45}-*b*-($PODMA_9$-*co*-$PDSMA_9$)) (1 wt %) nanospheres (Stained with 5 % uranyl acetate and 1 % acetic acid). **C-D)** Cryo-TEM images of C2 (PEO_{45}-*b*-($PODMA_9$-*co*-$PDSMA_9$)) (1 wt %) nanospheres with internal bicontinuous morphology. The red arrow indicates the nanospheres used to estimate the average pore diameter of these bicontinuous nanospheres.

Spherical aggregates with evident surface pores can be seen in Figure 3.22 (A-B) for C2 5 wt % with a number average particle size of 150 ± 37 nm (calculated from 40 particles), this is consistent with the main N_{ave} observed from DLS. The cryo-TEM images revealed particles around 400-600 nm with multi-lamellar exterior internal morphology with a bicontinuous core (shown by red arrows in Figure 3.22 C-D). We know this to be a smaller proportion of the sample, by viewing the DLS distribution

plot which shows a smaller number % of particles with an N_{ave} of around 450 nm. There are also a larger number of particles that are solely bicontinuous (shown by the green box in Figure 3.22 C), these particles are evident in Figure 3.22 C and a magnified image of this section is present in Figure 3.22 E. These particles are much smaller within the size range 60-175 nm which is consistent with the main peak observed in the distribution plot for this sample obtained via DLS.

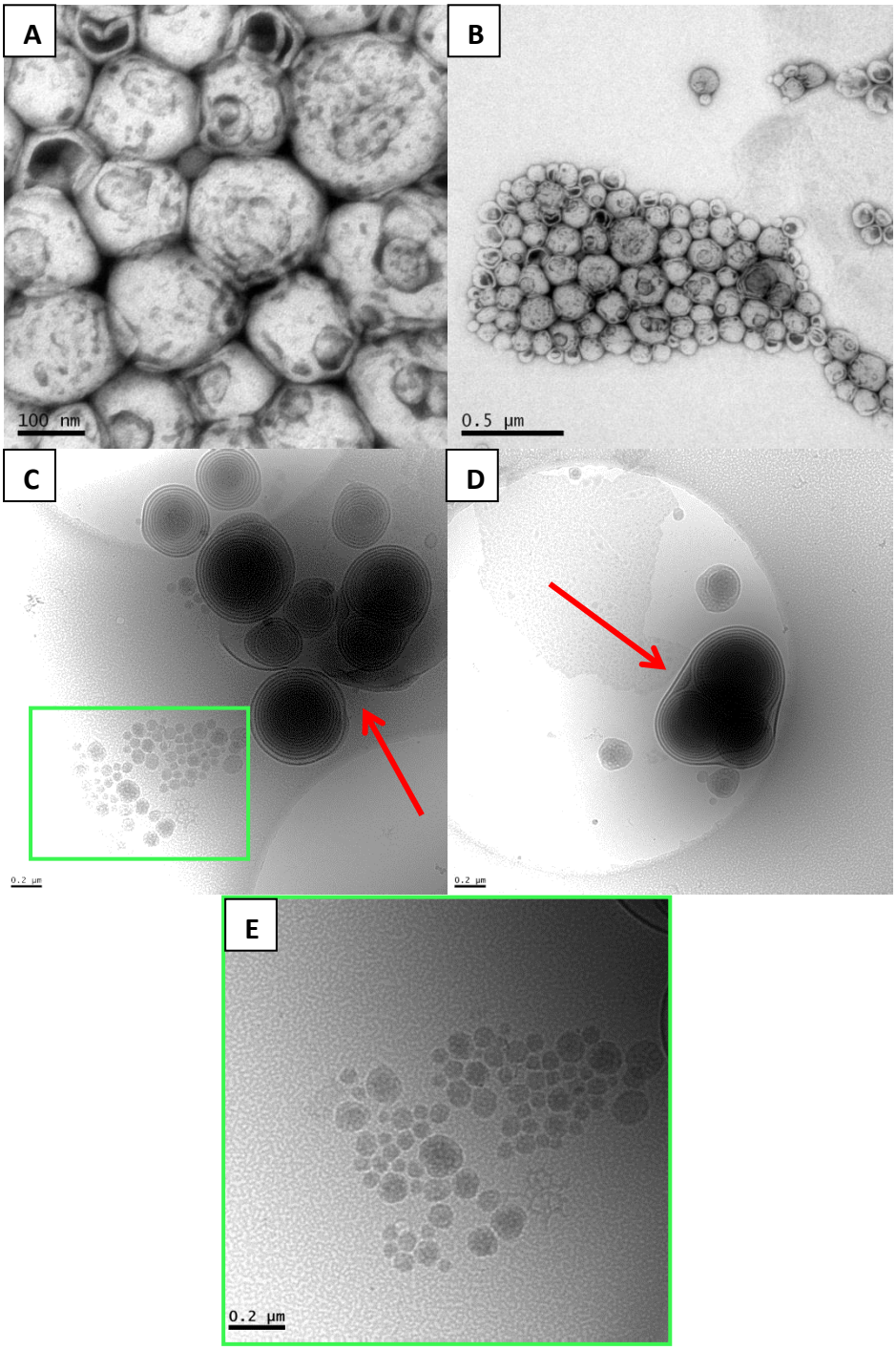

Figure 3.22: A-B) Negative stained TEM images of C2 (PEO_{45}-*b*-($PODMA_9$-*co*-$PDSMA_9$)) (5 wt %) nanospheres (Stained with 5 % uranyl acetate and 1 % acetic acid). **C-D)** Cryo-TEM images of C2 (PEO_{45}-*b*-($PODMA_9$-*co*-$PDSMA_9$)) (5 wt %) nanospheres with internal bicontinuous morphology. Red arrows indicated multi-lamellar regions. **E)** Zoomed in image of the bicontinuous nanospheres highlighted in the green box in C.

3.4.4.3C3 (PEO_{44}-b-$PODMA_7$-co-$PDSMA_{11}$) (PODMA:PDSMA 40:60)

C3 was self –assembled at 0.1-5 wt % in solution and analysed with DLS at 15 and 45°C (above and below the T_m calculated with DSC). The DLS results (Table 3.13) show a decrease in number average particle size on increase in polymer concentration, as previously stated for C1 and C2 this trend was not expected for the increase from 0.1 to 1 wt% solutions as it does not agree with the literature [25, 30]. The decrease in N_{ave} for the 5 wt % was expected due to the increased volume of THF used in the initial dialysis stage.[23] An increase in concentration also sees a decrease in the particle dispersity, indicating that an increase in concentration gives a lower distribution in particle size. This was unexpected as the opposite trend was observed with P3 and C2. When the DLS measurement temperature is increased from 15-45°C an insignificant change in the N_{ave} was observed.

Table 3.13: Number mean values for self–assembled block copolymer C1 (PEO_{44}-*b*-(PODMA-*co*-$PDSMA_{12}$) calculated from the Z-average using Dynamic Light Scattering.

wt %	T (°C)	N_{Ave} (d.nm)	SD (± nm)	Z_{Ave} (d.nm)	SD (± nm)	CONTIN	Đ
0.1	15	288	78	598	42	202/2856/719	0.50
0.1	45	351	57	681	73	256/977	0.52
1	15	201	26	290	11	218/1257	0.37
1	45	199	11	266	2	192/584	0.26
5	15	143	42	207	3	244/5335	0.17
5	45	169	24	212	1	243/5030	0.17

The number average distribution plot, measured at 15°C, (Figure 3.23 A) of C3 0.1 wt % is bimodal, the 1 wt % has a shoulder peak and the 5 wt % is monomodal. The main peak for the 1 wt % solution has a smaller N_{ave} then the 5 wt % solution despite the N_{aves} calculated (Table 3.13) showing the 5 wt % has a smaller particle size. This would be due to the shoulder peak on the 1 wt % plot contributing to the N_{ave}. The N_{ave} calculated for the 0.1 wt % coincides with the main peak seen in the distribution, the CONTIN analysis indicates more than one distribution which is confirmed from the distribution plot.

The number average distribution plots of C3 measured at 45°C show the 0.1 wt % has a bimodal distribution with the 1 and 5 wt % solutions having monomodal distributions with a shoulder peak. The CONTIN data for 0.1 wt % at 45°C suggest two number average particle sizes of 250 and 1000 nm which is consistent with the distribution plots displayed in Figure 3.23B. The presence of the shoulder peaks in the 1 wt % (increased from measurements taken at 15°C) and 5 wt % distribution plots indicates the melting of the long alkyl chains on the methacrylate backbone have cause aggregation between particles.

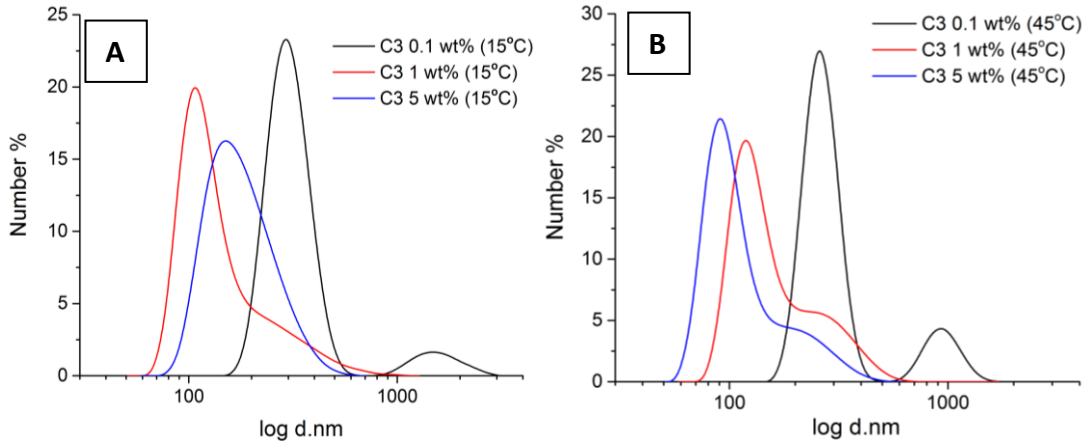

Figure 3.23: DLS number average distribution plots of C3 (PEO_{45}-*b*-($PODMA_7$-*co*-$PDSMA_{11}$), at 0.1, 1 and 5 wt % in solution at 15°C **(A)** and 45°C **(B)**.

The analysis of C3 0.1 wt % solution, using negatively stained TEM (Figure 3.24 A) proved difficult to achieve a high quality image, however the results did reveal spherical aggregates with particles sizes across the range 250-1000 nm, which is consistent with the two peaks observed on the distribution plot of the 0.1 wt % sample from DLS. Unfortunately cryo-TEM images were not obtained for this sample so the internal morphology could not be determined.

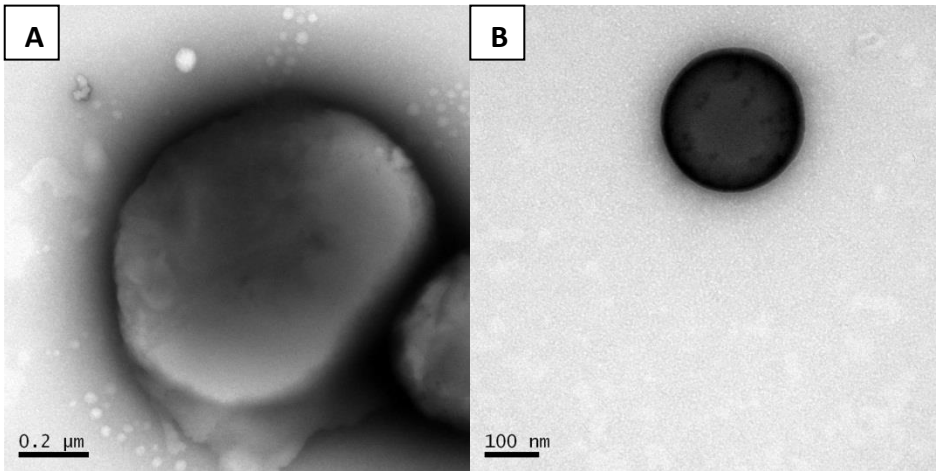

Figure 3.24: A-B) Negative stained TEM images of C3 (PEO_{45}-*b*-($PODMA_7$-*co*-$PDSMA_{11}$)) (0.1 wt %) nanospheres (Stained with 5 % uranyl acetate and 1 % acetic acid).

The TEM images of C3 1 wt % aggregate solution (Figure 3.25 A) shows spherical aggregates with a number average particle size of 125 ± 57 nm (calculated from 55 particles) across the size range 55-350 nm, the main peak observed from the distribution plot of this sample obtained from DLS was around 125 nm. From analysis with cryo-TEM (Figure 3.25 B) the internal morphology of these spherical aggregates was confirmed to be bicontinuous, with some exhibiting a porous membrane separated from the bicontinuous core (shown by the red arrow in Figure 3.25 D). Some spherical aggregates were present with internal multi-lamellar morphology (shown by the blue arrow in Figure 3.25 C) and vesicles were also observed (shown by the green arrow in Figure 3.25 D).

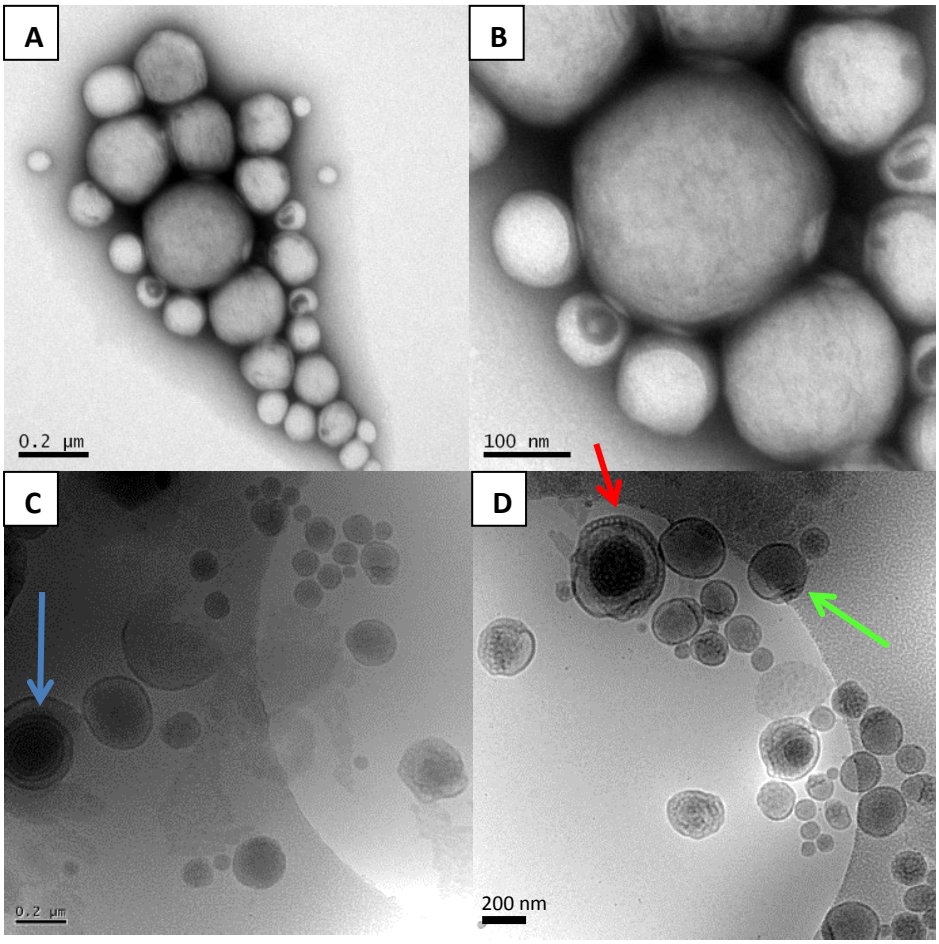

Figure 3.25: A-B) Negative stained TEM images of C3 (PEO_{45}-*b*-($PODMA_{7}$-*co*-$PDSMA_{11}$)) (1 wt %) nanospheres (Stained with 5 % uranyl acetate and 1 % acetic acid). **C-D)** Cryo-TEM images of C3 (PEO_{45}-*b*-($PODMA_{7}$-*co*-$PDSMA_{11}$)) (1 wt %) nanospheres with internal bicontinuous morphology and vesicles. The red arrow indicates bicontinuous nanospheres, the blue arrow indicates multi-lamellar aggregates and the green arrow indicates vesicles.

C3 5 wt % solution was analysed with TEM by the negative staining of the sample. The TEM images (Figure 3.26 A-B) show spherical aggregates at a high concentration with some particles indicating bicontinuous morphology due to the surface pores evident. The number average particle size was calculated to be 100 ± 42 nm (calculated from 35 particles), slightly lower than that calculated from DLS (143 nm). Analysis with cryo-TEM revealed a small proportion of large aggregates (300-700 nm) with internal multi-lamellar morphology (shown by the green arrow in Figure 3.26 C). A larger proportion of bicontinuous nanospheres are present as seen in Figure 3.26 C (shown by the red arrows) and Figure 3.26 D with a size range of 45-170 nm, the DLS results gave an N_{ave} of 143 nm which is within the range of the bicontinuous

nanospheres. The presence of these mixed morphology was also seen for C1 and C2 at the same concentration, however a higher proportion of multi-lamellar nanospheres seems to be present.

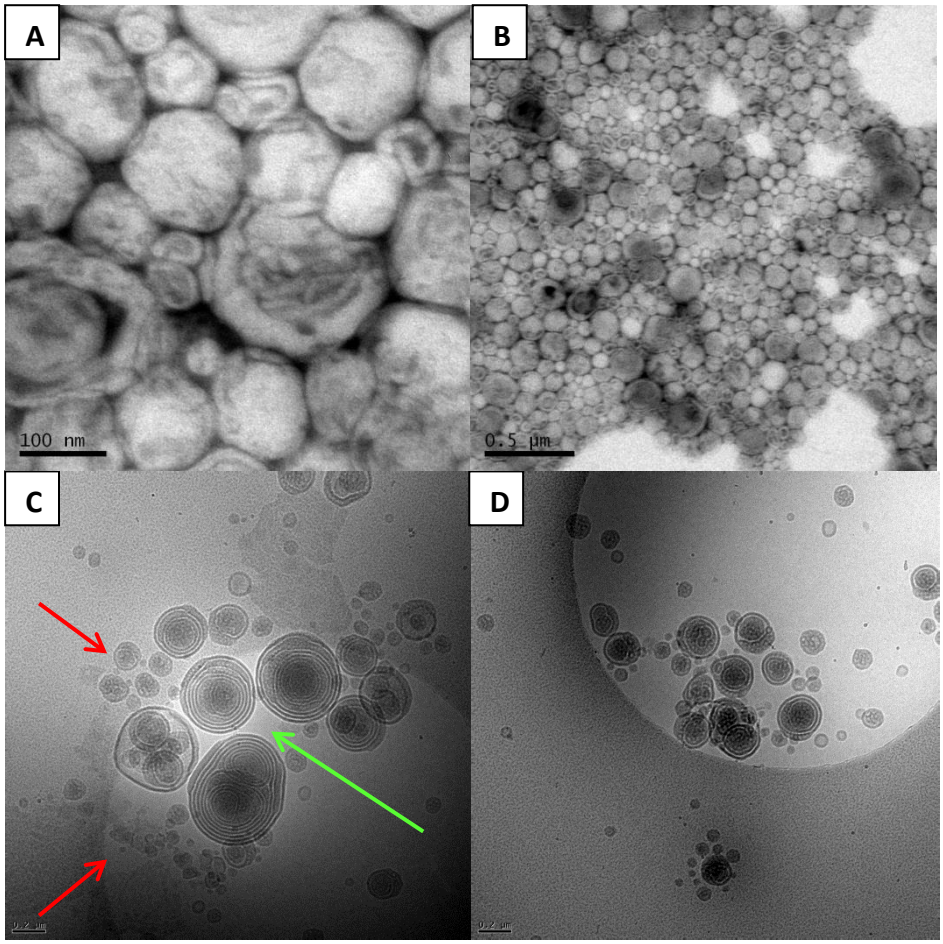

Figure 3.26: A-B) Negative stained TEM images of C3 (PEO_{45}-*b*-($PODMA_{7}$-*co*-$PDSMA_{11}$)) (5 wt %) nanospheres (Stained with 5 % uranyl acetate and 1 % acetic acid). **C-D)** Cryo-TEM images of C3 (PEO_{45}-*b*-($PODMA_{7}$-*co*-$PDSMA_{11}$)) (5 wt %) nanospheres with internal bicontinuous morphology and multi-lamellar internal morphology. The red arrows indicate bicontinuous nanospheres, the green arrow indicates multi-lamellar.

3.4.4.4C4 (PEO_{44}-b-$PODMA_5$-co-$PDSMA_{13}$) (PODMA:PDSMA 25:75)

The DLS results for the self-assembly of C4 (PEO- 25 wt %) at 0.1-5 wt % (Table 3.14) show that upon increase in concentration from 0.1 wt % to 1 wt % there is a slight increase in N_{ave}, this result was unusual when compared to the results seen for C1-C3 where an increase in concentration resulted in a decrease in N_{ave}. The result is however consistent with those observed in the literature discussed previously.[25, 30-31] As seen for samples C1-C3 there is a decrease in N_{ave} upon an increase in concentration to 5 wt %, this is most likely due to an increase in the initial THF volume used in the dialysis method, the effects of which have been discussed previously in this chapter. The dispersity in particle size, Đ, is relatively low for 0.1 and 5 wt % concentrations, there is an increase in dispersity for the 1 wt % solution which is explained by the presence of a bimodal distribution in particle size seen in the plots in Figure 3.27. A slight increase in N_{ave} was generally observed when the DLS measurement temperature was increased from 15 to 45°C. As previously discussed this is down to the polymer particles aggregating together as the alkyl side-chains melt when heated above their T_m.

Table 3.14: Number mean values for self–assembled block copolymer C4 (PEO_{44}-b-(PODMA-*co*-$PDSMA_{12}$) calculated from the Z-average using Dynamic Light Scattering.

wt %	T (°C)	N_{Ave} (d.nm)	SD (± nm)	Z_{Ave} (d.nm)	SD (± nm)	CONTIN	Đ
0.1	15	302	30	824	357	271/504	0.17
0.1	45	344	22	391	7	376/168	0.24
1	15	353	31	530	10	291/800	0.42
1	45	350	11	501	12	300/825	0.38
5	15	116	19	174	2	171/299	0.21
5	45	159	5	199	2	183/1500	0.24

The distribution plots for C4 0.1-5 wt % solutions, obtained from DLS at 15°C, are displayed in Figure 3.27 A. The plots for 0.1 and 5 wt% solutions are monomodal with the 0.1 wt % solution exhibiting an N_{ave} of around 300 nm which is consistent with the N_{ave} seen in Table 3.14. The distribution plot for 5 wt% indicates an N_{ave} of around 100 nm which is consistent with the value in Table 3.14. The 1 wt % distribution is

bimodal with the main peak having an N_{ave} of around 200 nm and the smaller peak being around 650 nm. This explains the increased dispersity in particle size given in Table 3.14.

The distribution plot for C4 0.1 wt % obtained from DLS at 45°C (Figure 3.27 B) shows a monomodal distribution, the peak has broadened compared the same sample measured at 15°C (Figure 3.27 A), this is most likely due to aggregation of the particles above the hydrophobic blocks T_m. The distribution plot for 1 wt % is monomodal with a shoulder peak, the larger N_{ave} peak observed for 15°C (65 nm) seems to have decreased in particle size indicating that upon melting the polymers making up the larger particles have dispersed. The distribution plot for the 5 wt % solution is still monomodal although the N_{ave} seems to have increased with an increase in measurement temperature, from 100 nm to 175 nm. Again this is most likely due to particle aggregation. This would also explain the increase in dispersity (Table 3.14) upon an increase in measurement temperature.

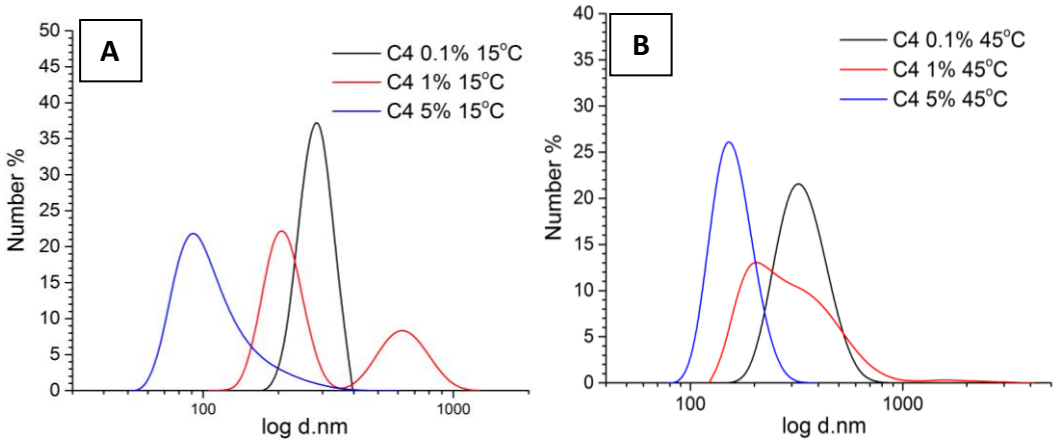

Figure 3.27: DLS number average distribution plots of C4 (PEO_{45}-*b*-($PODMA_5$-*co*-$PDSMA_{13}$) at 0.1, 1 and 5 wt % in solution at 15°C **(A)** and 45°C **(B)**.

C4 at 0.1 wt % was analysed using negatively stained TEM (Figure 3.28 A-B), due to the low concentration it was difficult to get high quality images for this sample, however the images obtained show spherical aggregates across the size range 190-440 nm. The DLS distribution plot for the same sample shows a size range of 200-400 nm, therefore the TEM results are consistent with the DLS results. The images also suggest a bicontinuous morphology, indicated by the porous surface present.

Unfortunately cryo-TEM images of this sample were not obtained so the possible bicontinuous morphology could not be confirmed.

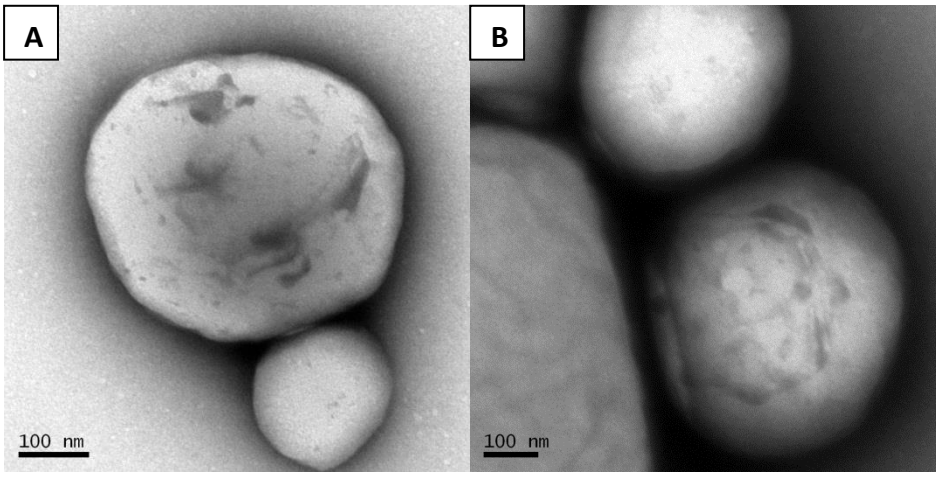

Figure 3.28: A-B) Negative stained TEM images of C4 (PEO_{45}-*b*-($PODMA_5$-*co*-$PDSMA_{13}$)) (0.1 wt %) nanospheres (Stained with 5 % uranyl acetate and 1 % acetic acid).

Analysis of C4 at 1 wt % with negatively stained TEM revealed spherical aggregates with an N_{ave} by TEM of 250 ± 65 nm (calculated from 30 particles). This average is consistent with the main peak present in the DLS distributions plots. Cryo-TEM images of the particles were not obtained so the internal morphology could not be determined, however when C4 was self-assembled at 1 wt % in the presence of ibuprofen, bicontinuous nanospheres were observed. These results will be discussed in chapter 4.

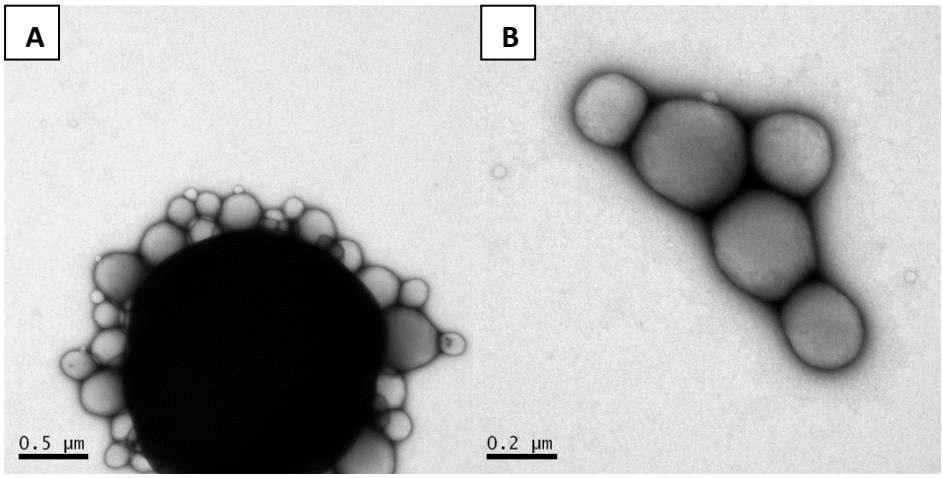

Figure 3.29: A-B) Negative stained TEM images of C4 (PEO_{45}-*b*-($PODMA_5$-*co*-$PDSMA_{13}$)) (1 wt %) nanospheres (Stained with 5 % uranyl acetate and 1 % acetic acid).

The analysis of C4 5 wt % with negatively stained TEM (Figure 3.30 A-B) shows spherical aggregates with a N_{ave} size of 130 ± 48 nm (calculated from 30 particles) which is consistent with the value obtained from DLS. It also suggests bicontinuous morphology, indicated by the porous surface evident in the images. The cryo-TEM images (Figure 3.30 C-D) confirm this internal bicontinuous morphology, with some aggregates exhibiting bicontinuous internal morphology with regions of multi-lamellar (shown by the red arrow in Figure 3.30 C). The cryo-Tem images reveal aggregates within the size range 120-360 nm these larger aggregates are not seen in the distribution plot for this sample but the CONTIN analysis does indicate particles around 300 nm.

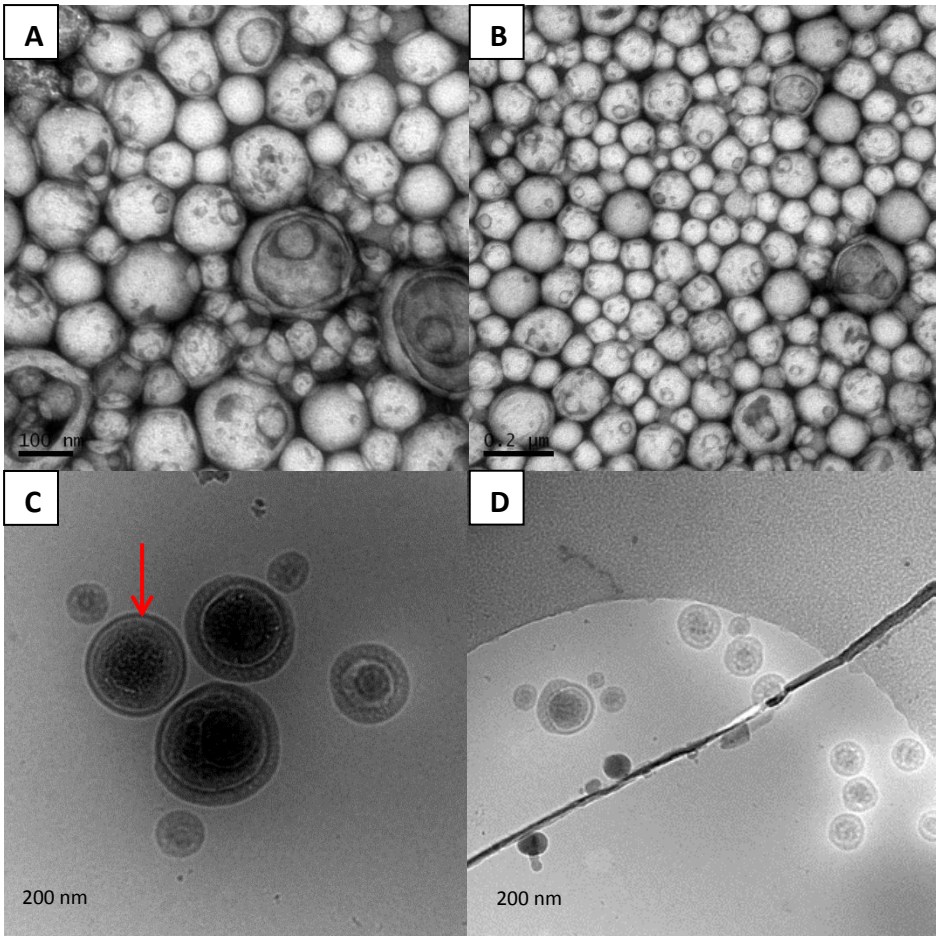

Figure 3.30: A) Negative stained TEM images of C4 (PEO_{45}-*b*-($PODMA_5$-*co*-$PDSMA_{13}$)) (5 wt %) nanospheres (Stained with 5 % uranyl acetate and 1 % acetic acid). **B)** Cryo-TEM images of C4 (PEO_{45}-*b*-($PODMA_5$-*co*-$PDSMA_{13}$)) (5 wt %) nanospheres with internal bicontinuous morphology. The red arrow indicates multi-lamellar regions within bicontinuous nanospheres.

3.4.5 Effect of Docosyl Methacrylate wt % on Aggregate Size and Morphology

The effect an increase in DSMA wt % has on the overall trend in particle size and morphology for a 25 wt % PEO polymer system for all concentrations will be reviewed in the section. The DLS N_{ave} sizes for P3, C1-C4 and D3 0.1 wt % are plotted against DSMA wt% in Figure 3.31. The plot shows that at 0 wt % DSMA (P3-PEO_{44}-*b*-$PODMA_{21}$) the largest N_{ave} was observed. After which an increase in DSMA wt % results in an increase in N_{ave}, with an anomaly at 50 wt % DSMA. This trend was expected as the average side-chain length is increased, so if the N_{agg} stays the same then an increased particle size will be observed.

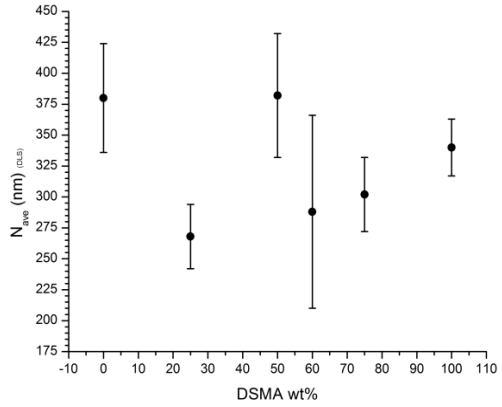

Figure 3.31: Plot of N_{ave} (from DLS) of P3(PEO_{49}-*b*-$PODMA_{21}$), C1-C4 (PEO-*b*-(PODMA-*co*-PDSMA) and D3 (PEO_{44}-*b*-$PDSMA_{12}$) bicontinuous nanospheres at 0.1 wt % against the DSMA wt %.

The plot of N_{ave} against DSMA wt % for the 1 wt % solutions shows a similar trend as the 0.1 wt % plot. The largest N_{ave} was observed for 0 wt % DSMA (P3), and then an increase in N_{ave} as DSMA wt % was increased.

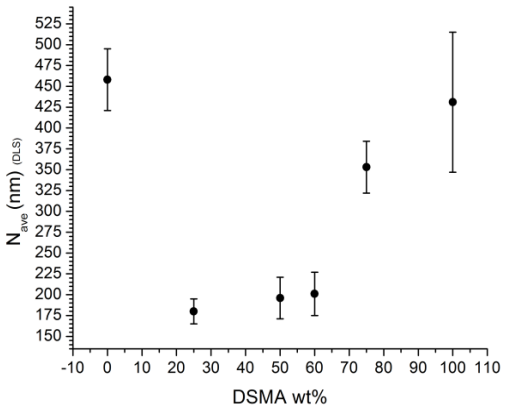

Figure 3.32 Plot of N_{ave} (from DLS) of P3(PEO_{49}-*b*-$PODMA_{21}$), C1-C4 (PEO-*b*-(PODMA-*co*-PDSMA) and D3 (PEO_{44}-*b*-$PDSMA_{12}$) bicontinuous nanospheres at 1 wt % against the DSMA wt %.

The 5 wt% solutions did not follow the same trend when the N_{ave} was plotted against the DSMA wt %. As with the 0.1 and 1 wt % solutions when PSDMA was at 0 wt % the largest N_{ave} was observed. However instead of seeing an increase in N_{ave} with an increase in DSMA wt % the opposite effect was observed. This may well be due to a difference in the self-assembly procedure where a larger volume of THF was used in the initial dissolution stage.[23]

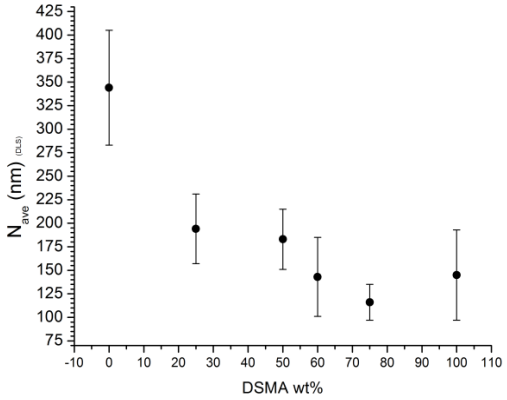

Figure 3.33: Plot of N_{ave} (from DLS) of P3(PEO_{49}-*b*-$PODMA_{21}$), C1-C4 (PEO-*b*-(PODMA-*co*-PDSMA) and D3 (PEO_{44}-*b*-$PDSMA_{12}$) bicontinuous nanospheres at 1 wt % against the DSMA wt %.

When analysing the cryo-TEM images (Figure 3.34) of the aggregates at 0.1 wt %, it is clear that an increase in DSMA wt % does not have a significant effect on the aggregate morphology. The bicontinuous internal morphology was maintained throughout, with small region of lamellar observed for the 100 wt % DSMA sample (Figure 3.34F)

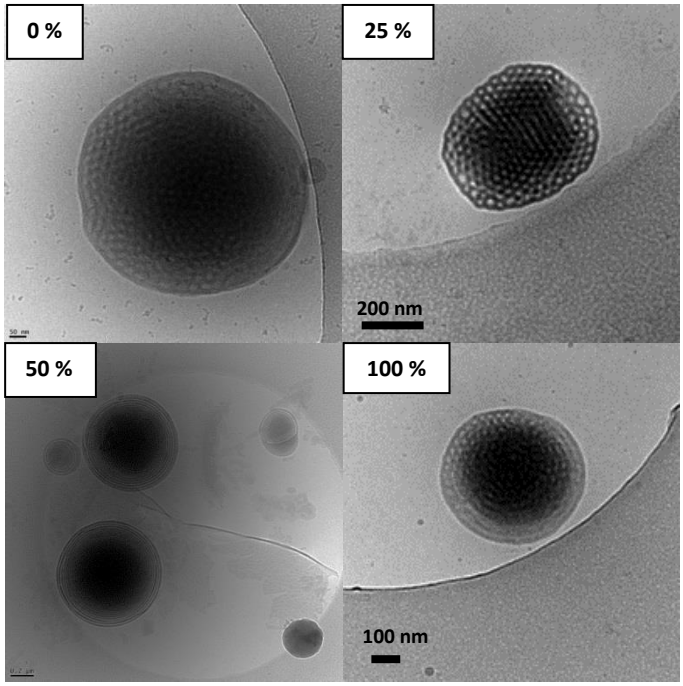

Figure 3.34: Cryo-TEM images of P3 0.1 wt % (top left), C1 0.1 wt % (top right), C2 0.1 wt % (bottom left) and D3 0.1 wt % (bottom right).

At 1 wt % an increase in DSMA wt % resulted in aggregates with bicontinuous and lamellar regions. (Figure 3.35)

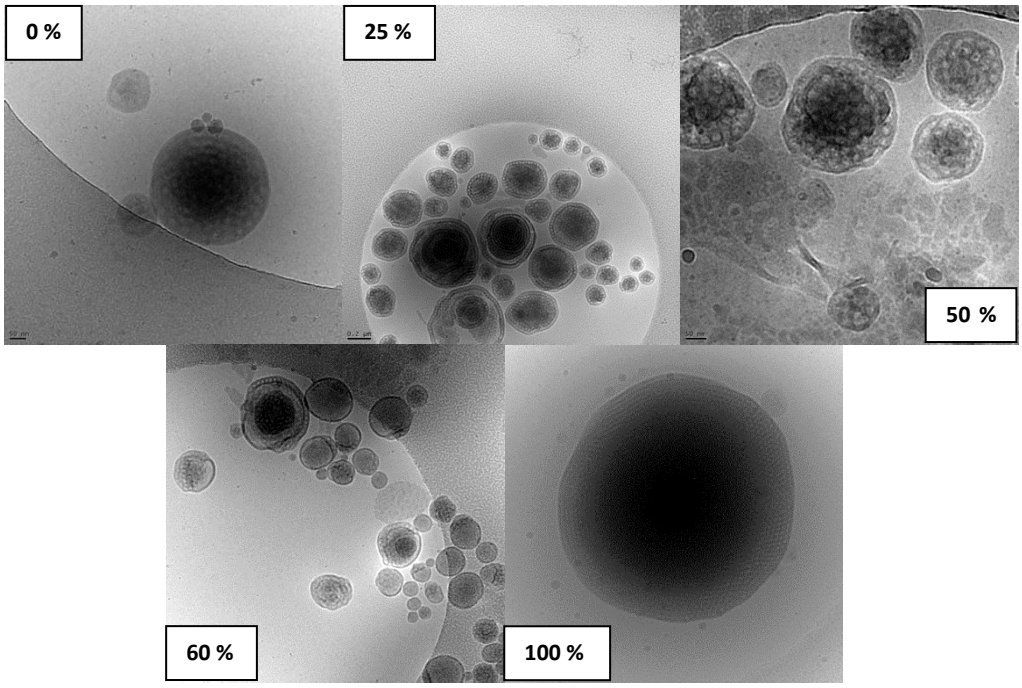

Figure 3.35: Cryo-TEM images of P3 1 wt % (top left), C1 1 wt % (top middle), C2 1 wt % (top right), C3 1 wt % (bottom left), D3 1 wt % (bottom left).

The 5 wt % aggregates also saw an increase in the number of multi-lamellar regions within the nanospheres with some exhibiting multi-lamellar aggregates and bicontinuous nanospheres at different sizes, as already discussed in this chapter (Figure 3.36).

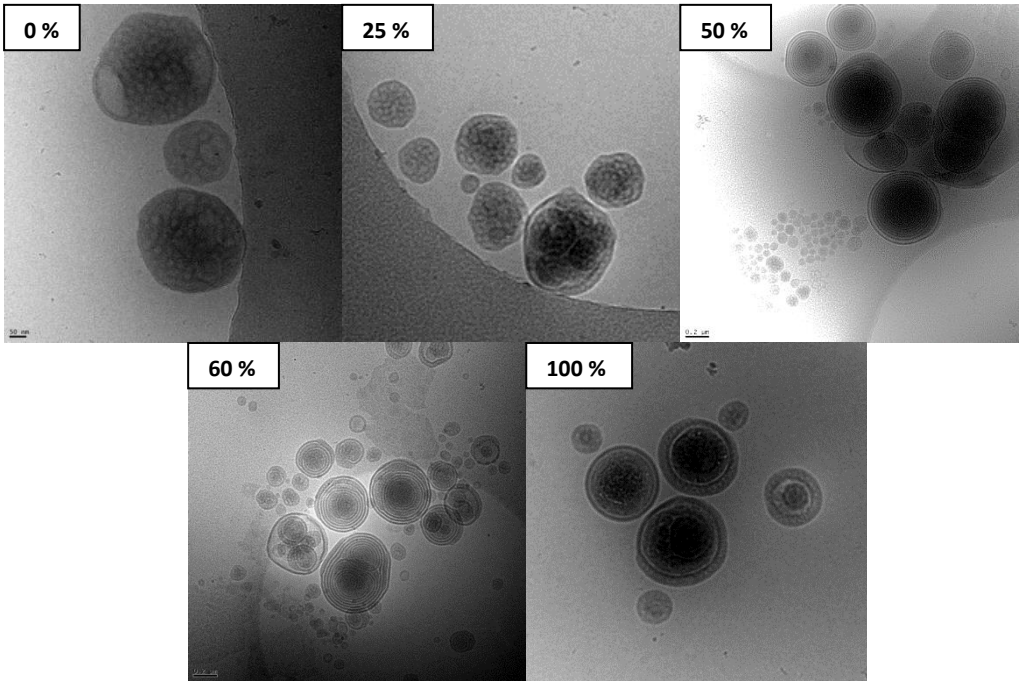

Figure 3.36: Cryo-TEM images of P3 5 wt % (top left), C1 5 wt % (top middle), C2 5 wt % (top right), C3 5 wt % (bottom left) and D3 5 wt % (bottom right).

The effect concentration can have on the size of the polymer aggregates formed has already been discussed. It is evident from the cryo-TEM images that as the polymer concentration is increased the aggregates lose some of their ordered exterior spherical morphology and a higher proportion of multi-lamellar morphologies were observed for the 5 wt % solutions (Figure 3.36). This change in morphology upon a polymer concentration increase has been seen previously in the literature.[31] Wang *et al.* investigated the self-assembly of PMAA-*co*-PMMA and found that upon an increase in copolymer concentration the morphology of the aggregates changed from hollow spheres to worm-like aggregates, then filled spheres and finally vesicles.[25] This has also been observed by Eisenberg *et al.* where PS-b-PAA was self-assembled in DMF/water and with increasing polymer concentration a morphological change was observed for the aggregates from spherical micelles to larger connected spindle-like micelles.[30]

The choice of cosolvent can also have an effect on the aggregate morphology when following the dialysis self-assembly method. This was observed by McKenzie *et al.* (2013)[24] for a PEO-*b*-PBMA BCP. Two different cosolvent systems were used, THF/water and dioxane/water. With the use of THF bicontinuous nanospheres were observed, however with the use of dioxane multi-lamellar aggregates were present. This was due to the relative affinities of the two blocks to the solvents. Upon looking at their solubility parameters, which indicted that PBMA is better solubilised by THF than dioxane, giving the block fluidity to be able to form these ordered assemblies.[23] The PEO is better solubilised by the dioxane, explaining the multi-lamellar morphology, as the PEO is more swollen therefore increasing the volume within the PEO hydrophilic head group during self-assembly. An increase in hydrophilic block volume deters the inverse curvature of the polymer allowing a lamellar morphology to prevail. This could explain the increase in multi-lamellar morphologies observed upon an increase in DSMA wt % within the copolymers at 5 wt %. As DSMA wt % is increased the average side-chain length also increases, it is possible due to this increase the hydrophobic block is less solubilised by the THF and therefore PEO being more solubilised by the THF as a larger volume in comparison to the hydrophobic block.

3.4.6 Differential Scanning Calorimetry

The DSC results for the analysis of P3 were looked at in chapter 2 and revealed the T_m to be 21.3°C for the bulk and 23.4°C for the 4 wt % aggregate solution. As discussed previously, the T_m observed via DSC is due to the octadecyl side chains crystallinity. DSMA has a higher T_m than ODMA due having an additional four CH_2 groups on the side chain, therefore it was first thought that a series of blends of PEO-*b*-PODMA and PEO-*b*-PDSMA would result in a systematic increase in T_m upon increase in PEO-*b*-PDSMA.

The self-assembly of a 50:50 blend of P3 (PEO_{49}-*b*-$PODMA_{21}$) and D3 (PEO_{44}-*b*-$PDSMA_{16}$) was attempted but yielded precipitation on addition of the water. This is most likely due to their inability to co-crystallise as Paul *et al.* [33] established. The two blend components will crystallise independently, but not with each other, the presence of another polymer will also inhibit the crystallisation. Paul *et al.* found that

the length of the alkyl chain needs to be close to each other for co-crystallisation to occur and that when a 50:50 blend of two polyacrylates, one with an alkyl side chain of C_{18} and the other C_{22}, was prepared by solution casting films the results showed they were inhomogeneous. A DSC thermogram of the melting transition of the 50:50 blend of P4 and D3 in bulk is shown in Figure 3.37 clearly showing two melting transitions. The first peak is due to the melting of the octadecyl side chains in P4 (22.8°C) and the transition at 41.3°C is due to the melting of the docosyl side chains in D3. These results show that the polymerisation of a copolymer of PODMA and PDSMA as the hydrophobic block would allow better crystallisation of the alkyl side chains.

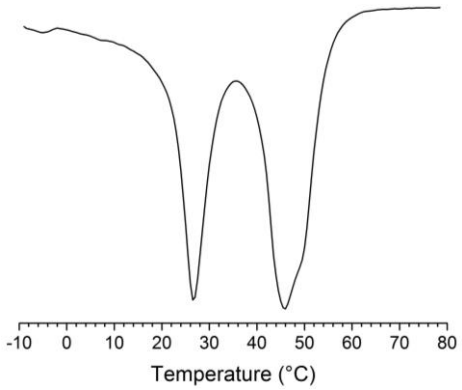

Figure 3.37: DSC thermogram of a 50:50 blend of bulk P4 (PEO_{44}-*b*-$PODMA_{19}$) and D3 (PEO_{44}-*b*-$PDSMA_{16}$) both with a PEO wt % of 25 %.

BCPs with PEO as the hydrophilic block and a PODMA:PDMSA copolymer as the hydrophobic block were successfully synthesised, at varying ratios of PODMA:PDSMA, with well-defined molecular weights and low dispersity. The incorporation of DSMA into the hydrophobic block at increasing wt% should allow control over the T_m and produce aggregates with melting points across a wide temperature range. As seen in this chapter the integration of DSMA, *via* polymerisation, into the thermo-responsive hydrophobic block still allows the BCP to self-assemble forming bicontinuous nanospheres at concentrations 0.1-5 wt % in solution, as seen previously with P3.

The bulk samples of P3, C1-C4 and D3 were analysed using DSC to determine their melting transition temperatures (T_m). The values are given in Table 3.15 and the thermograms are plotted in Figure 3.38. It is clear from the thermograms that as the wt % of PDSMA was increased, and therefore the average side-chain length, the T_m

increases. This demonstrates that the thermal properties of the bulk BCPs can be easily tailored by the modification of the hydrophobic block (the thermo-responsive block). This trend is also evident in the plot of T_m against DSMA wt % (Figure 3.39).A similar trend was observed by Paul *et al*.[34], where they measured the T_m of a series of copolymers with varying mole ratios of two different alkyl acrylate monomers with different side-chain lengths. As the average side chain length increased the T_m also increased. This has also been observed by Greenberg and Alfrey (1954)[35] where they measured the T_m of a number of monomers including acrylates and methacrylates with varying lengths of alkyl side chains, the trend was the same regardless of the backbone. The other observation when viewing the melting transition thermograms of the bulk BCPs is that as the chain length is increased within the copolymers (C1-C4), the transition is observed across a larger range (broader peaks see Table 3.15) this has been observed many times in the literature for copolymers.[13, 35] However the opposite effect has also been observed with melting peaks becoming broader as the concentration of a shorter side-chain length co-monomer increases by Paul *et al.*[34], this is said to be due to an increase in smaller crystals caused by the decrease in crystallinity. It should be noted however that the side chain length of the commoner was 6 CH_2 units which is below the minimum number of carbons needed (8-10 CH_2)[12, 35-36] for crystallisation to occur. The possible reason for the melting peak broadening upon increase in DSMA wt % could be down to the synthesis. If the ODMA and DSMA monomer have different rates of activation then the result could be that one region of PODMA and one of PDSMA was present within the hydrophobic block rather than being a truly random copolymer. This separation means two crystallisable domains will be present with some cross over. However it is unlikely the addition of four CH_2 upon the alkyl aide-chain would greatly affect the reactivity of the double bond within the methacrylate.

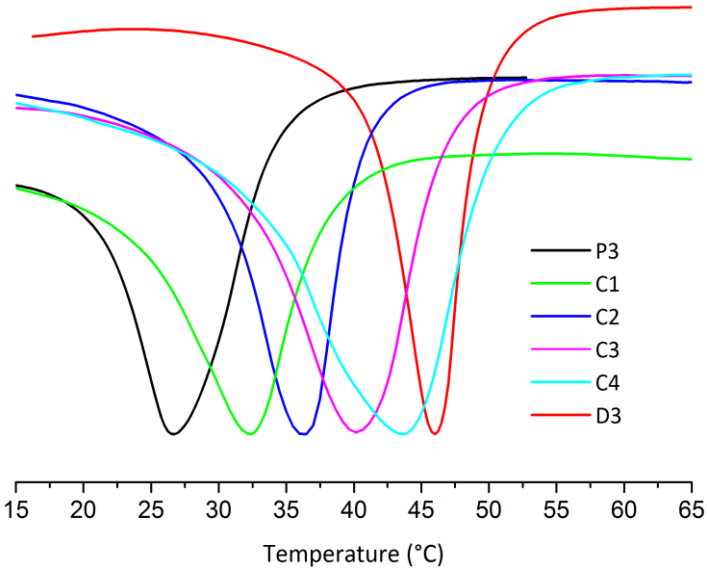

Figure 3.38: DSC thermograms of P3 (PEO_{49}-*b*-$PODMA_{21}$), D3 (PEO_{44}-*b*-$PDSMA_{12}$) and C1-C4 (PEO-*b*-(PODMA-*co*-PDSMA) measured using an empty aluminium pan as a reference. The transition plots y axis are normalised to the plot of D3.

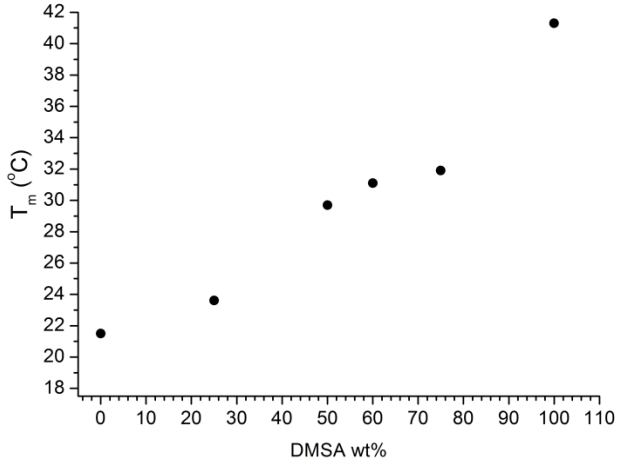

Figure 3.39: A plot of T_m against DSMA wt % for the bulk BCPs.

Table 3.15 shows the T_m, ΔH_f (enthalpy change of fusion) and D_c (degree of crystallinity) for BCPs P3, C1-C4 and D3. The enthalpy of fusion, ΔH_f (KJ/mol), was calculated from the area (J/g) of the melting transitions using Equation 3.1. Where A is the area (J/g), MW is the average molecular weight of the side-chain repeat unit ((MW C18 x mol %) + (MW C22 x mol %)) and as the hydrophobic block represents 75 wt % of the BCP this was taken into account by multiplying by 1.25.

Equation 3.1: Calculation of enthalpy change of fusion

$$\Delta H_f = A\left(\frac{1}{1000}\right) \text{MW x } 1.25$$

The degree of crystallinity (D_c) indicates the amount of polymer in a crystalline state. The D_c of the hydrophobic block was calculated using Equation 3.2 where ΔH_f is the enthalpy change of fusion for the hydrophobic block and $q_{m,CH2}$ is the heat of melting per CH_2 unit in the alkyl side chain calculated to be 3.4 KJ/mol from DSC measurements of octadecane by Beiner *et al.*[37] and other literature on alkanes.[11, 38]

Equation 3.2: Calculation of degree of crystallinity (D_c) of the hydrophobic block

$$Dc = \frac{\Delta H_f}{q_{m,CH_2}} \; x \; 100$$

The calculated ΔH_f and D_c for the hydrophobic block of P3, C1-C4 and D3 bulk samples are given in Table 3.15. P3's ODMA (DP-21) side chains have a D_c value of 16 %, a homopolymer of PODMA with a similar chain length (DP-27) gave a D_c of 31 % when measured using DSC by Beiner *et al.*.[11] This indicates that the presence of the PEO within the BCP has an effect on the octadecyl side chains ability to pack and form a crystalline state, which may be due to it contributing to the backbone rigidity which hinders the side chains reaching a crystalline order. [11, 13-15, 35]

Upon increasing the wt % of PDSMA within the copolymers (C1-C4) (increase in alkyl side chain length) an increase in Dc was observed, this is expected as more CH_2 units can now contribute to the side chain crystallinity. A slight decrease in Dc was seen for the homopolymer of the hydrophobic block, PDSMA, which is most likely due to a large decrease in the DP of the hydrophobic block from 19 for the copolymers to 16 for the PDSMA polymer. This trend can be observed in Figure 3.40.

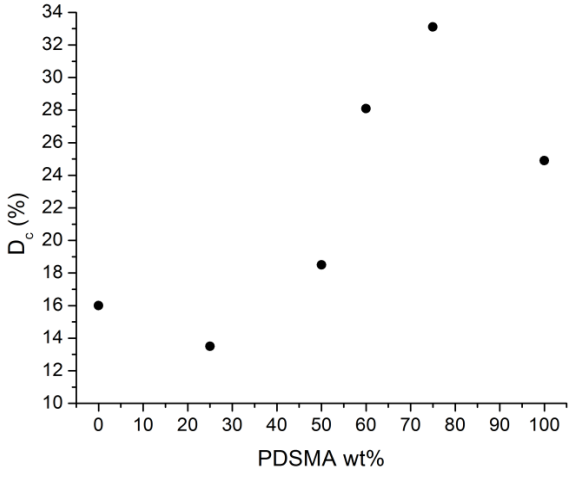

Figure 3.40: Plot of PDSMA wt % v degree of crystallinity (D_c calculated using DSC).

Table 3.15: DSC melting transition values for PEO-*b*-PODMA, PEO-*b*-PDSMA and all PEO-*b*-(PODMA-*co*-PDSMA) copolymers. All values are taken from the second heating run.

Code	Structure	Average side-chain length	Peak (°C) *Start* (°C)	Peak (°C) *End* (°C)	Peak (˚C)	T_m Onset (°C)	ΔH (KJ/mol)	D_c (%)	Repeat unit M_w (g/mol)	PODMA: PDSMA Ratio
P3	PEO_{49}-*b*-$PODMA_{21}$	18	*13.6*	*33.9*	*26.6*	*21.5*	9.78	16.0	253	100:0
C1	PEO_{45}-*b*-($PODMA_{15}$-*co*-$PDSMA_4$)	18.8	6.61	37.8	32.4	23.6	8.64	13.5	264	75:25
C2	PEO_{45}-*b*-($PODMA_9$-*co*-$PDSMA_9$)	20	7.6	40.4	36.2	29.7	12.55	18.5	281	50:50
C3	PEO_{45}-*b*-($PODMA_7$-*co*-$PDSMA_{11}$)	20.44	6.1	46.1	39.5	31.1	19.53	28.1	287	40:60
C4	PEO_{45}-*b*-($PODMA_5$-*co*-$PDSMA_{13}$)	20.88	9.2	52.7	42.5	31.9	23.48	33.1	293	25:75
D3	PEO_{44}-*b*-$PDSMA_{16}$	22	27.1	49.3	46.0	41.3	18.64	24.9	309	0:100

The values for the melting transitions of P3, C1-C4 and D3 aggregate solutions calculated from DSC are displayed in Table 3.16. DSC measurements of the BCP aggregate solutions were measured against a water filled aluminium pan to try and eliminate the transition from the water within the aggregate sample. The full DSC thermograms for P3, C1-C4 and D3 are displayed in Figure 3.41, showing the water transition at the start of the plot and the small melting transitions seen for each aggregate solution. The peaks were enlarged to establish the melting transition seen in the DSC thermograms of P3, C1-C4 and D3 aggregate solutions (Figure 3.42), these thermograms show the same trend as seen with the bulk samples, upon an increase in PDSMA wt % the T_m also increase. The trend is further highlighted in the plot of Tm against DSMA wt % in Figure 3.43. There is not as distinct a difference between C2 (50:50 PODMA:PDSMA) and C3 (40:60 PODMA:PDSMA) as there was with the bulk. The T_m onset for both C2 and C3 is 35°C with C3 having a narrower transition than C2.

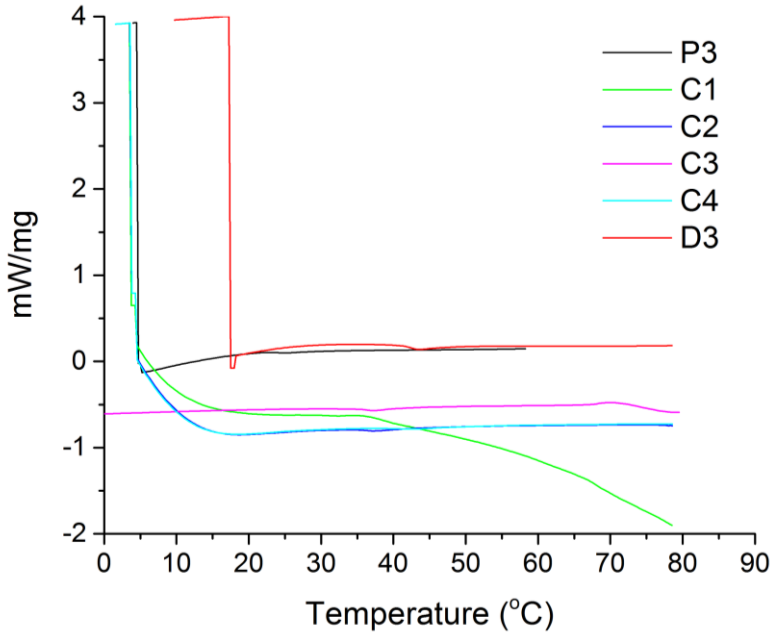

Figure 3.41: Full DSC heating thermograms of P3 (PEO_{49}-*b*-$PODMA_{21}$) 4 wt % aggregate solution, D3 (PEO_{44}-*b*-$PDSMA_{16}$) 5 wt % aggregate solution and C1-C4 (PEO-*b*-(PODMA-*co*-PDSMA) 5 wt % aggregate solutions measured using an aluminium pan containing 50 mg of water as a reference.

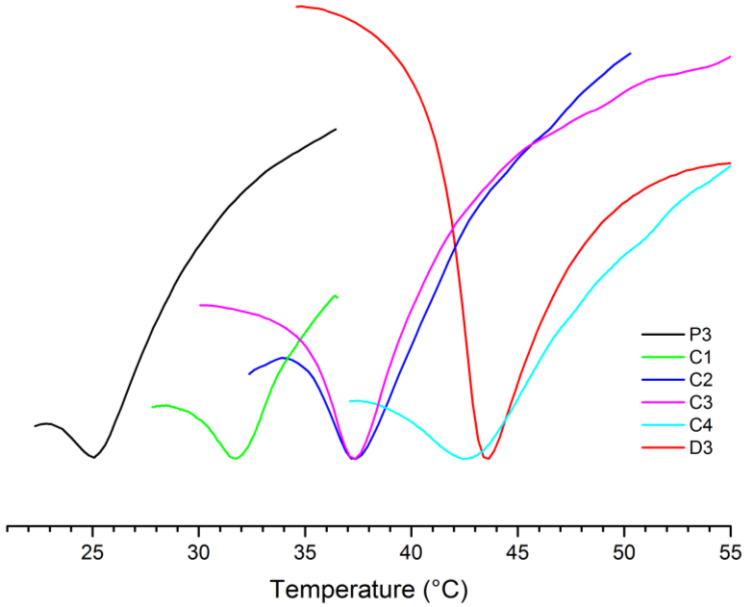

Figure 3.42: DSC thermograms of P3 (PEO_{49}-*b*-$PODMA_{21}$) 4 wt % aggregate solution, D3 (PEO_{44}-*b*-$PDSMA_{16}$) 5 wt % aggregate solution and C1-C4 (PEO-*b*-(PODMA-*co*-PDSMA) 5 wt % aggregate solutions measured using an aluminium pan containing 50 mg of water as a reference. The transition plots y axis is normalised.

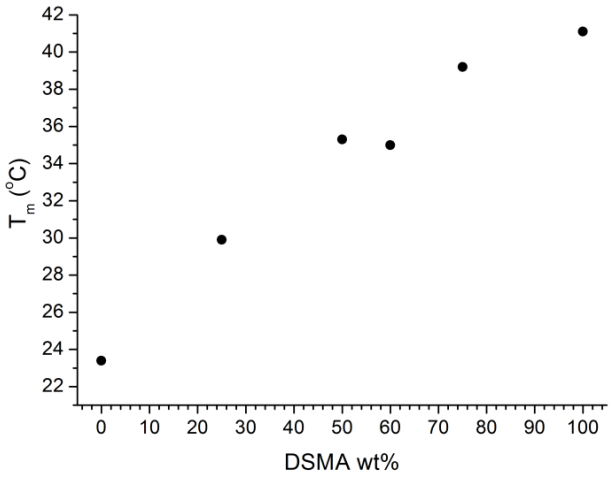

Figure 3.43: A plot of T_m against DSMA wt % for the 5 wt % BCP aggregate solutions.

The ΔH_f for the hydrophobic block of the BCPs P3, C1-C4 and D3, at 4 and 5 wt % in solution, were calculated as before using Equation 3.1. However, as the polymer only represents 4 wt % for the P3 aggregate solution and 5 wt % for the others, the area (J/g) was multiplied by 25 and 20 respectively so that the area of the transition is for weight of the hydrophobic polymer block only. Equation 3.1 was then followed as before with the newly calculated areas. The results can be seen in Table 3.16 where

the D_c for all BCPs are significantly lower than for the bulk samples. This may not indicate a decrease in crystallinity but could be due to a large amount of error in DSC measurement of the transition. Due to the low concentration of polymer within the aggregate solution, small transitions were observed for all aggregate samples when compared to the corresponding bulk samples transitions. This made calculating the area of the peak difficult as it there was a large uncertainty in the start and end of the melting transition, an example of how the area was calculated for each aggregate solution is displayed in Figure 3.44 where the start and end of the peak for P3 5 wt % have been defined. These results for the Tm and enthalpies, and therefore the D_c are best described as estimates. However they give good guidance for the relative behaviour of the aggregates. Perhaps the use of microcalorimetric measurements would allow more accurate measurements of the heat flow and therefore the D_c and could be utilised in the future for determining the thermal properties of these aggregates in solution.

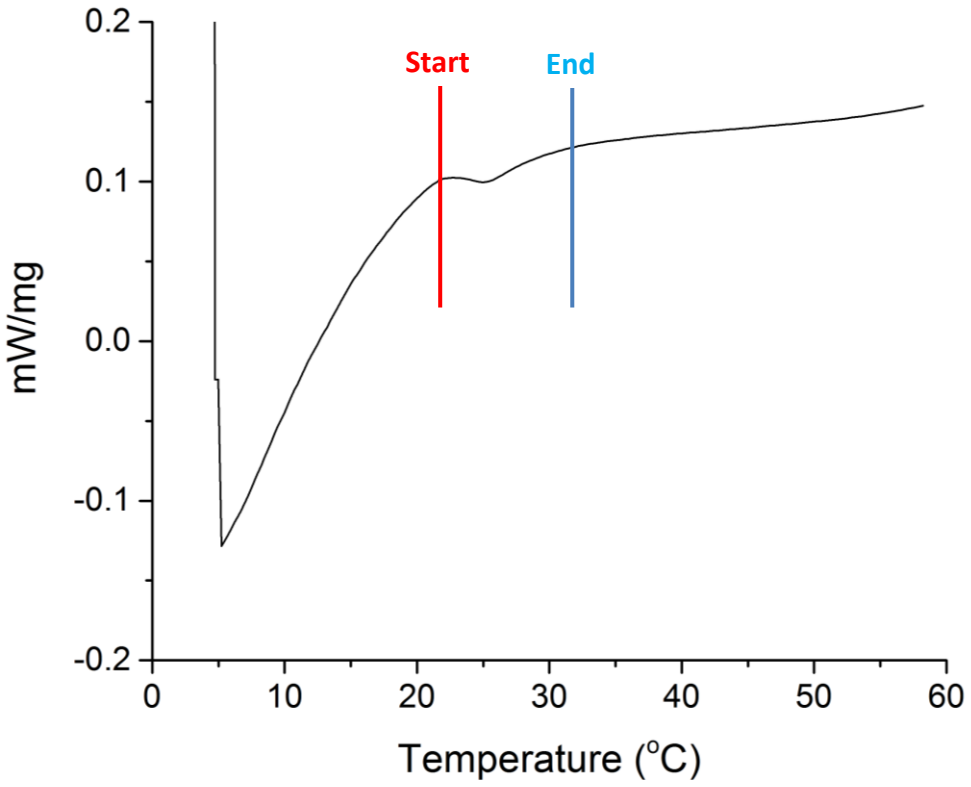

Figure 3.44: DSC thermogram of P3 (PEO_{49}-*b*-$PODMA_{21}$) at 4 wt % in solution with clearly defined start and end points for the melting transition.

As the PDSMA wt % within the BCP is increased the D_c increases with an initial decrease from 0-25 % (P3-C1). This trend, the increase in D_c, was expected because

as the chain length increases the number of CH_2 groups that can contribute to the crystallinity increases. A large increase in D_c was observed from P3 to D3 the two homopolymers of PEO-*b*-PODMA and PEO-*b*-PDSMA. This could be due to D3 having more room for the docosyl side chains to crystallise. The pore wall thickness of a bicontinuous nanosphere of D3 was estimated to be 14.5 ± 1 nm (from TEM), this is larger than the pore wall thickness observed for PEO-*b*-PODMA bicontinuous nanospheres (9.5 ± 2 – 11.5 ± 3 nm) by McKenzie *et al.*[23]. It should be noted that this significantly larger difference in D_c could also be due to the D3 aggregate solution having a more defined transition (Figure 3.42 red). As stated before this allowed greater accuracy in the measurement of the peak area which was then used to calculate D_c (Equation 3.2).

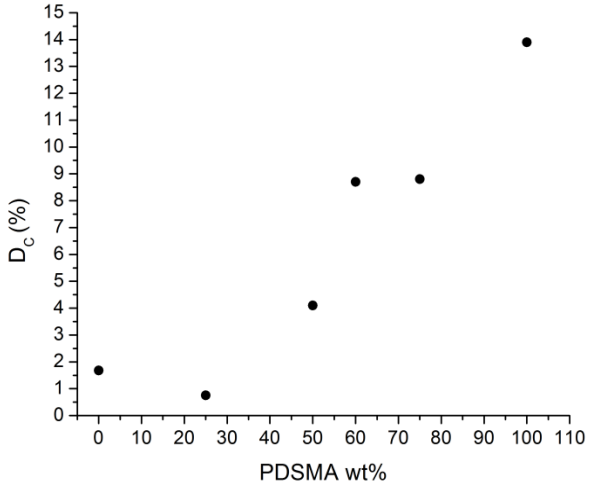

Figure 3.45: Plot of PDSMA wt % v D_c (degree of crystallinity calculated from DSC results).

Table 3.16: DSC melting transition values for PEO-*b*-PODMA, PEO-*b*-PDSMA and all PEO-*b*-(PODMA-*co*-PDSMA) copolymer aggregates at 4 and 5 wt % in solution. All values are taken from the second heating run.

Code	Structure	Peak (°C)		Peak (˚C)	T_m Onset (°C)	ΔH (KJ/mol)	D_c (%)	PODMA:PDOMA Ratio
		Start (°C)	*End (°C)*					
P3	PEO_{49}-*b*-$PODMA_{21}$ (4 wt %)	22.6	30.0	24.9	23.4	1.03	1.7	100:0
C1	PEO_{45}-*b*-($PODMA_{15}$-*co*-$PDSMA_4$) (5 wt %)	28.3	35.5	31.8	29.9	0.48	0.75	75:25
C2	PEO_{45}-*b*-($PODMA_9$-*co*-$PDSMA_9$) 5 wt %)	34.1	44.3	37.3	35.3	2.78	4.1	50:50
C3	PEO_{45}-*b*-($PODMA_7$-*co*-$PDSMA_{11}$) (5 wt %)	29.6	45.9	37.3	35.0	6.05	8.7	39:61
C4	PEO_{45}-*b*-($PODMA_5$-*co*-$PDSMA_{13}$) (5 wt %)	37.3	50.8	42.4	39.2	6.24	8.8	25:75
D3	PEO_{44}-*b*-$PDSMA_{16}$ (5 wt %)	35.5	48.2	43.5	41.1	10.36	13.9	0:100

3.5 Conclusion

A series of PEO-*b*-PDSMA BCPs were successfully synthesised with PEO wt % within the range 15-30 %, using a PEO macroinitiator whose synthesis and characterisation is outlined in chapter 2. BCPs D1-D4 were synthesised with well-defined DP and PEO wt % and a dispersity of ≤1.19 indicating that the reactions were controlled and that they all have a narrow molecular weight distribution. From analysis with GPC and ^{1}H-NMR it can be stated that the resultant BCP bulk samples were free from impurities and the macroinitiators initiation step was successful. The procedure for the synthesis of PEO-*b*-PODMA was followed for the synthesis of PEO-*b*-(PODMA-*co*-PDSMA) with great success. From analysis with ^{1}H-NMR the DP of the PODMA-*co*-PDSMA block was determined to be as predicted. The reactions were controlled resulting in pure bulk samples with dispersity's of ≤1.13 indicating a narrow molecular weight and chain length distribution.

The self-assembly dialysis method (chapter 2-procedure A) was used for the self-assembly of PEO-*b*-PDSMA (PEO wt % 25 and 30) at 0.1, 1 and 5 wt % concentrations in solution. This was to assess the effect of PDSMA, as the hydrophobic block, upon the size and morphology of the aggregates and for comparison with PEO-*b*-PODMA aggregates at the same concentrations. D4 (PEO-*b*-PDSMA, 30 wt % PEO) resulted in cylindrical micelles, multi-lamellar internal morphology and vesicles. The morphologies were also observed for P7 (PEO-*b*-PODMA), which has the same PEO wt % (30 %). The self-assembly of D3 (PEO-*b*-PDSMA, 25 wt % PEO) produced bicontinuous nanospheres at all concentrations, these results are consistent with those observed for P3 (PEO-*b*-PODMA, 25 wt % PEO). It has clearly been demonstrated that a longer alkyl side-chain length upon the methacrylate backbone has no effect on the self-assembled polymer morphologies.

The copolymers PEO-*b*-(PODMA-*co*-PDSMA) were self-assembled following the previously successful dialysis method also at 0.1, 1 and 5 wt % concentrations in solution to investigate the copolymers effect on polymer aggregate morphology and size. All copolymers produced bicontinuous nanospheres across at all concentrations however when the concentration was increased to 5 wt % some of the nanospheres

had regions of multi-lamellar morphology. The regions seemed to increase in size and number as the wt % of PDSMA was increase, so from C1-C4.

The successfully synthesised BCPs D3 (PEO_{44}-*b*-$PDSMA_{16}$) and C1-C4 (PEO-*b*-(PODMA-*co*-PDSMA) with increasing PDSMA wt %) were analysed with DSC to determine their T_m and analyse their crystallinity properties compared with P3 (PEO_{49}-*b*-$PODMA_{21}$). The results showed that incorporating DSMA into the hydrophobic block allows control over the T_m. As the wt % of PDSMA increased the T_m also increased. The degree of crystallinity (D_c) also showed this trend for the copolymers C1-C4 with an increase in D_c as the wt % of PDSMA was increased.

One of the intended uses for these thermo-responsive bicontinuous nanospheres are for controlled drug delivery. The control over the thermo-responsive properties means that the drug delivery that would be controlled due to the porous structure of the nanospheres could be further controlled by modification of the T_m. Therefore the 4 wt % aggregate solution of P3 and the 5 wt % aggregate solutions of C1-C4 and D3 were analysed using DSC. A smaller enthalpy was observed for the melting transition of all BCP aggregate solutions compared to the bulk samples. This was due to the polymer only being 5 wt % of the total volume held by the crucible. Therefore the enthalpies were recalculated to take into account the low polymer volume. The same trend in T_m was observed for the aggregate solutions as for the bulk polymer samples. There was no difference in T_m between C2 (PODMA:PDSMA 50:50) and C3 (PODMA:PDSMA 40:60) which was not the case for the bulk samples. However these results were very promising and clearly show the control achieved over the T_m of the bicontinuous nanospheres.

3.6 References

1. Hu, Y.; Darcos, V.; Monge, S.; Li, S., Thermo-responsive drug release from self-assembled micelles of brush-like PLA/PEG analogues block copolymers. *International Journal of Pharmaceutics* **2015,** *491* (1–2), 152-161.

2. Liu, N.; Li, B.; Gong, C.; Liu, Y.; Wang, Y.; Wu, G., A pH- and thermo-responsive poly(amino acid)-based drug delivery system. *Colloids and Surfaces B: Biointerfaces* **2015,** *136*, 562-569.

3. Du, J.; O'Reilly, R. K., Advances and challenges in smart and functional polymer vesicles. *Soft Matter* **2009,** *5* (19), 3544-3561.

4. Holder, S. J.; Woodward, G.; McKenzie, B.; Sommerdijk, N. A. J. M., Semi-crystalline block copolymer bicontinuous nanospheres for thermoresponsive controlled release. *RSC Advances* **2014,** *4* (50), 26354-26358.

5. Ward, M. A.; Georgiou, T. K., Thermoresponsive Polymers for Biomedical Applications. *Polymers* **2011**.

6. Li, Z.-X.; Lu, M.-G.; Wu, K.; Zhang, Y.-F.; Miao, L.; Li, Y.-W.; Guo, H.-L.; Zheng, J., Temperature-responsiveness and sustained delivery properties of macroporous PEG-co-PNIPAAm-co-PCL hydrogels. *Polymer Engineering & Science* **2015,** *55* (1), 223-230.

7. Hocine, S.; Li, M.-H., Thermoresponsive self-assembled polymer colloids in water. *Soft Matter* **2013,** *9* (25), 5839-5861.

8. Choi, E.; Yethiraj, A., Entropic Mechanism for the Lower Critical Solution Temperature of Poly(ethylene oxide) in a Room Temperature Ionic Liquid. *ACS Macro Letters* **2015,** *4* (7), 799-803.

9. Lee, H.-N.; Newell, N.; Bai, Z.; Lodge, T. P., Unusual Lower Critical Solution Temperature Phase Behavior of Poly(ethylene oxide) in Ionic Liquids. *Macromolecules* **2012,** *45* (8), 3627-3633.

10. Sanson, C.; Diou, O.; Thevenot, J.; Ibarboure, E.; Soum, A.; Brulet, A.; Miraux, S.; Thiaudiere, E.; Tan, S.; Brisson, A.; Dupuis, V.; Sandre, O.; Lecommandoux, S., Doxorubicin Loaded Magnetic Polymersomes: Theranostic Nanocarriers for MR Imaging and Magneto-Chemotherapy. *ACS Nano* **2011,** *5* (2), 1122-1140.

11. Hempel, E.; Budde, H.; Höring, S.; Beiner, M., On the crystallization behavior of frustrated alkyl groups in poly(n-octadecyl methacrylate). *Journal of Non-Crystalline Solids* **2006,** *352* (42–49), 5013-5020.

12. Kaufman, H. S.; Sacher, A.; Alfrey, T.; Fankuchen, I., Side-chain crystallization in alkyl polyacrylates. *Journal of the American Chemical Society* **1948,** *70*, 3147.

13. Yokota, K.; Kougo, T.; Hirabayashi, T., Synthesis, Structure, and Thermal Properties of Widely-Spaced Comb-Like Polymers. *Polymer Journal* **1983,** *15* (12), 891-898.

14. Mogri, Z.; Paul, D. R., Gas sorption and transport in poly(alkyl (meth)acrylate)s. I. Permeation properties. *Polymer* **2001,** *42* (18), 7765-7780.

15. Hirabayashi, T.; Kikuta, T.; Kasabou, K.; Yokota, K., Main-Chain Flexibility and Side-Chain Crystallization of Widely Spaced Comb-Like Polymers. *Polymer Journal* **1988,** *20* (8), 693-698.

16. Jordan, E. F., Jr.; Feldeisen, D. W.; Wrigley, A. N., Side-chain crystallinity. I. Heats of fusion and melting transitions on selected homopolymers having long side chains. *Journal of Polymer Science, Part A-1: Polymer Chemistry* **1971,** *9* (7), 1835-52.

17. O'Leary, K. A.; Paul, D. R., Physical properties of poly(n-alkyl acrylate) copolymers. Part 1. Crystalline/crystalline combinations. *Polymer* **2006,** *47* (4), 1226-1244.

18. Bisht, H. S.; Pande, P. P.; Chatterjee, A. K., Docosyl acrylate modified polyacrylic acid: synthesis and crystallinity. *European Polymer Journal* **2002,** *38* (12), 2355-2358.

19. Platé, N. A.; Shibaev, V. P., Comb-like polymers. Structure and properties. *Journal of Polymer Science: Macromolecular Reviews* **1974,** *8* (1), 117-253.

20. Jordan, E. F.; Artymyshyn, B.; Speca, A.; Wrigley, A. N., Side-chain crystallinity. II. Heats of fusion and melting transitions on selected copolymers incorporating n-octadecyl acrylate or vinyl stearate. *Journal of Polymer Science Part A-1: Polymer Chemistry* **1971,** *9* (11), 3349-3365.

21. Platé, N. A.; Shibaev, V. P.; Petrukhin, B. S.; Zubov, Y. A.; Kargin, V. A., Structure of crystalline polymers with unbranched long side chains. *Journal of Polymer Science Part A-1: Polymer Chemistry* **1971,** *9* (8), 2291-2298.

22. McKenzie, B. E.; Nudelman, F.; Bomans, P. H. H.; Holder, S. J.; Sommerdijk, N., Temperature-Responsive Nanospheres with Bicontinuous Internal Structures from a Semicrystalline Amphiphilic Block Copolymer. *Journal of the American Chemical Society* **2010,** *132* (30), 10256-10259.

23. McKenzie, B. E.; Friedrich, H.; Wirix, M. J. M.; de Visser, J. F.; Monaghan, O. R.; Bomans, P. H. H.; Nudelman, F.; Holder, S. J.; Sommerdijk, N. A. J. M., Controlling Internal Pore Sizes in Bicontinuous Polymeric Nanospheres. *Angewandte Chemie International Edition* **2015,** *54* (8), 2457-2461.

24. McKenzie, B. E.; de Visser, J. F.; Friedrich, H.; Wirix, M. J. M.; Bomans, P. H. H.; de With, G.; Holder, S. J.; Sommerdijk, N. A. J. M., Bicontinuous Nanospheres from Simple Amorphous Amphiphilic Diblock Copolymers. *Macromolecules* **2013,** *46* (24), 9845-9848.

25. Wang, B.; Ni, X.; Yu, M.; Cao, Y., Polymeric micelle as the pseudostationary phase in electrokinetic chromatography. *Journal of Chromatography A* **2012,** *1245*, 190-198.

26. Blanazs, A.; Armes, S. P.; Ryan, A. J., Self-Assembled Block Copolymer Aggregates: From Micelles to Vesicles and their Biological Applications. *Macromolecular Rapid Communications* **2009,** *30* (4-5), 267-277.

27. Discher, D. E.; Eisenberg, A., Polymer vesicles. *Science* **2002,** *297* (5583), 967-973.

28. Cai, S.; Vijayan, K.; Cheng, D.; Lima, E.; Discher, D., Micelles of Different Morphologies—Advantages of Worm-like Filomicelles of PEO-PCL in Paclitaxel Delivery. *Pharmaceutical Research* **2007,** *24* (11), 2099-2109.

29. Wang, X.; Guerin, G.; Wang, H.; Wang, Y.; Manners, I.; Winnik, M. A., Cylindrical Block Copolymer Micelles and Co-Micelles of Controlled Length and Architecture. *Science* **2007,** *317* (5838), 644-647.

30. Zhang, L.; Eisenberg, A., Thermodynamic vs Kinetic Aspects in the Formation and Morphological Transitions of Crew-Cut Aggregates Produced by Self-Assembly of Polystyrene-b-poly(acrylic acid) Block Copolymers in Dilute Solution. *Macromolecules* **1999,** *32* (7), 2239-2249.

31. Feng, C.; Lu, G.; Li, Y.; Huang, X., Self-Assembly of Amphiphilic Homopolymers Bearing Ferrocene and Carboxyl Functionalities: Effect of Polymer Concentration, β-Cyclodextrin, and Length of Alkyl Linker. *Langmuir* **2013,** *29* (34), 10922-10931.

32. Yu, Y.; Eisenberg, A., Control of Morphology through Polymer-Solvent Interactions in Crew-Cut Aggregates of Amphiphilic Block Copolymers. *Journal of the American Chemical Society* **1997,** *119* (35), 8383-8384.

33. Kirkland, B. S.; Paul, D. R., Gas transport in poly(n-alkyl acrylate)/poly(m-alkyl acrylate) blends. *Polymer* **2008,** *49* (2), 507-524.

34. O'Leary, K. A.; Paul, D. R., Physical properties of poly(n-alkyl acrylate) copolymers. Part 2. Crystalline/non-crystalline combinations. *Polymer* **2006,** *47* (4), 1245-1258.

35. Greenberg, S. A.; Alfrey, T., Side-chain crystallization of n-alkyl polymethacrylates and polyacrylates. *Journal of the American Chemical Society* **1954,** *76*, 6280-5.

36. Rehberg, C. E.; Fisher, C. H., Properties of monomeric and polymeric alkyl acrylates and methacrylates. *Industrial and Engineering Chemistry* **1948,** *40*, 1429-33.

37. Hempel, E.; Budde, H.; Höring, S.; Beiner, M., Side chain crystallization in microphase-separated poly(styrene-block-octadecylmethacrylate) copolymers. *Thermochimica Acta* **2005,** *432* (2), 254-261.

38. Höhne, G. W. H., Another approach to the Gibbs–Thomson equation and the melting point of polymers and oligomers. *Polymer* **2002,** *43* (17), 4689-4698.

Chapter 4. Encapsulation and Thermo-Responsive Controlled release of Ibuprofen from Semi-Crystalline Block Copolymer Bicontinuous Nanospheres.

4.1 Abstract

The thermo-responsive nature of BCPs PEO-*b*-PODMA, PEO-*b*-PDSMA and PEO-*b*-(PODMA-*co*-PDSMA) bicontinuous nanospheres (BN) was demonstrated in chapters 2 and 3, this chapter looks at the effect the T_m has upon the rate of release of an encapsulate from these BNs. The chosen hydrophobic encapsulate was ibuprofen and the effect upon the self-assembly of BNs was investigated. It was found that a PEO wt % of 25 % resulted in particles of micellar size (60 nm). When the PEO wt % was decreased to 15 wt % BNs were formed. The rate of release of ibuprofen was then measured using HPLC and it was found that upon and increase in DSMA wt % within the BCP, a decrease in release rate of ibuprofen was observed.

4.2 Introduction

The use of BCP micelles, cylindrical micelles and vesicles as encapsulates for the controlled delivery of pharmaceuticals in biomedical applications has been widely studied.[1-2] There is high interest in using BCP aggregates as carriers for hydrophobic drugs. The BCP aggregates, in particular micelles and vesicles, have a hydrophobic core that a hydrophobic drug can be encapsulated within[3], this allows hydrophobic drugs such as ibuprofen, that have low water solubility,[4] to be encapsulated within the hydrophobic core, greatly increasing their solubility allowing higher drug concentrations to be transported.[5] The BCP aggregate also provides protection for the drug from external biological conditions that may cause hydrolysis or enzymatic degradation,[6] this is achieved by using a corona forming hydrophilic drug such as PEO that resist protein adsorption and cellular adhesion.[5] Targeted delivery can be achieved with the use of a polymer nanocarrier that can be modified to include certain functional molecules or groups.[1, 7-8] One of the advantages of using BCP aggregates as drug carriers is that the physical and chemical properties of the polymer can be modified[9] to allow control over the size, morphology and stimuli-responsive nature of the resultant aggregates.

In chapters 2 and 3 it has been demonstrated that bicontinuous nanospheres can be self-assembled from PEO-*b*-PODMA, PEO-*b*-PDSMA and a copolymer of PEO-*b*-(PODMA-*co*-PDSMA). As discussed already micelles and vesicles can be used for the encapsulation of hydrophilic and lipophilic drugs within their hydrophobic core.

Bicontinuous nanospheres are composed of hydrophilic interconnected channels that are solvated by aqueous media, contained within a continuous network of the hydrophobic core.[10] This gives them a unique potential as a dual pharmaceutical carrier, as a lipophilic and a hydrophilic drug could be encapsulated within the nanosphere owing to the coexistence of both the hydrophilic and hydrophobic internal regions.[11]

PEO is one of the most commonly used hydrophilic blocks for the formation of BCP drug carriers.[9] The use of PEO in BCP aggregates is due to a number of reasons, PEO is highly soluble in aqueous solution and other solvents so is ideal for many self-assembly methods, it is also non-toxic and doesn't interact with biological components.[2] This makes PEO ideal as the hydrophilic block within our bicontinuous nanospheres.

Hydrophobic drugs can be encapsulated using a number of different polymer self-assembly methods. The first is direct dissolution of the polymer and drug in aqueous solution.[6] Low loading amounts have been observed with this method[6] due to reliance on the solubility partition coefficient[9], which is the ability of the drug to solubilise in the aqueous phase and also the hydrophobic core. The dialysis method is commonly employed when all or part of the BCP is insoluble in water alongside an insoluble hydrophobic drug.[12] The BCP and drug are dissolved in a common organic solvent that is miscible with water, then dialysed against water to remove the solvent and form the polymer aggregates.[13] It has been found that the loading capacity increases when the dialysis method has been employed.[5]

There is great interest in improving the uptake of anti-inflammatory drugs such as ibuprofen as they are an alternative to opioids for use in pain treatment, opioids can have adverse side-affects[14]. One of the drawbacks of ibuprofen is its lipophilic nature, low water solubility, which makes it unsuitable for injection[14], even if cosolvents such as ethanol are used there is a risk of drug precipitation once the formulation entered the body,[15] not to mention the possible side-effects associated with the chosen cosolvent. Ibuprofen also has a short half-life calculated to be 1 to 3 hours by T.G. Kanter (1979)[16]. Polymer nanocarriers therefore can be employed to solve both these

problems, by keeping the ibuprofen dissolved when it enters the body and by controlling and sustaining its release.

The use of a stimuli-response for the release of pharmaceuticals from BCP aggregates has long been studied. With modification of the BCP a number of different stimuli-responses can be achieved. These include pH [17], temperature [1817-19], glucose[20], light, electric field and ultrasound[21]. The most commonly used temperature responsive nature of BCPs is their LCST. As previously discussed in chapter 3 polymers which exhibit an LCST have a cloud point which is the critical temperature below which the polymer is soluble and above which the polymer is insoluble and will precipitate out.[22] The thermo-responsive release of ibuprofen from BCP aggregates has been studied many times in the literature.[23-25] The use of a crystallisable side chain upon the polymer backbone, to give the self-assembled polymer its thermo-responsive nature, is a relatively new idea.

In this chapter the encapsulation and controlled release of hydrophobic drug ibuprofen, within the BCP bicontinuous nanospheres will be examined. The encapsulation of ibuprofen was carried out using the dialysis method, due to the low solubility of both the PODMA block and ibuprofen in water. The encapsulation and thermo-responsive controlled release of pyrene from PEO_{45}-*b*-$PODMA_{20}$ (PEO 25 wt %) has previously been investigated by Holder *et al*.[11] They found that below the PODMA melting transition (20-25˚C) the release profiles of pyrene, detected using fluorescence, were very similar. Upon heating above the T_m (30-40˚C) there was an increase in rate of release of pyrene. This clearly demonstrates that the melting of the hydrophobic PODMA block has a significant effect on the rate of release of pyrene. Following on from this work we have now manipulated the melting transition of the hydrophobic block by incorporating DSMA at increasing wt %, and the effect of these increasing melting transitions upon the rate of release of ibuprofen will be demonstrated in this chapter.

4.3 Experimental

4.3.1 Materials and Apparatus for the Self-Assembly of PEO-*b*-PODMA, PEO-*b*-PDSMA and PEO-*b*-(PODMA-*co*-PDSMA) block copolymers with ibuprofen

The BCP P1 and P4 were used as synthesised in chapter 2. D1 and D3 were used as synthesised in chapter 3. C1 and C4 were used as synthesised in chapter 3. 4-Isobutyl-alpha-methylphenylacetic acid, 99 % (Ibuprofen) was purchased from Alfa Aesar. Distilled water was used as obtained. *A* syringe pump (220 Voltz, 0.1 Amps, 50Hz) was used from Semat technical Limited at 0.085 mL per minute. A dialysis membrane (MWCO-12-14000 Daltons) from MEDICELL international Ltd with dialysis clips was used.

Dynamic Light Scattering

Dynamic light scattering (DLS) measurements were obtained on a Malvern High Performance Particle Sizer (Nano Zetasizer HPPS HPP5001) with a laser at a wavelength of 633nm. The measurements were taken using a clean quartz cuvette containing a 1 mL sample. Measurements were taken at 10°C, the temperature was set and the machine was left to settle at this temperature for 10 minutes, after this 10 measurements were taken and an average was obtained.

Transmission Electron Microscopy

Transmission electron microscopy (TEM) was carried out on all the self-assembled samples using a JEOL JEM (200-FX) TEM machine (120kV). 5 µl of the sample was pipetted onto a carbon-coated copper grid (200 mesh) and left for 5 minutes and then removed using suction. Using 5 µl of 5 % uranyl acetate the grid was then stained, and removed via suction.

Cryo-Transmission Electron Microscopy

Cryo-Transmission Electron Microscopy (cryo-TEM) was performed on a FEI Cryo-Titan with a field emission gun operating at 300 kV. The sample vitrification process was as follows; 3 µl of the self-assembled solution was pipetted onto a surface plasma treated (Cresington Carbon Coater 208) Quantifoil holey (Cu 200 mesh) grid inside a FEI Vitrobot chamber (set to 100 % humidity at room temperature to prevent sample evaporation). The sample was then blotted and plunged into liquid ethane cooled by liquid nitrogen.

4.3.2 Self-assembly of PEO-*b*-PODMA, PEO-*b*-PDSMA and PEO-*b*-(PODMA-*co*-PDSMA) block copolymers with ibuprofen

The BCP (0.1 g) and Ibuprofen (0.02 g) were dissolved in 6 mL of THF and left stirring at 10°C. 4 mL of Deionised water was then added drop-wise to the solution via a syringe pump to make the total volume up to 10 mL. After the addition of the water the solution was sealed in dialysis tubing with clips and then dialysed against distilled water at 10°C for 3 days. Over the 3 days the water was changed twice. The self-assembled polymer was then analysed using Dynamic Light Scattering (DLS) and Transmission Electron Microscopy (TEM) to determine the size and dispersity of the aggregates.

4.3.3 Materials an Apparatus for the controlled release of Ibuprofen from PEO-*b*-PODMA, PEO-*b*-PDSMA and PEO-*b*-(PODMA-*co*-PDSMA) block copolymer bicontinuous nanospheres

Distilled water was used as obtained. A dialysis membrane (MWCO-12-14000 Daltons) from MEDICELL international Ltd was used with a 1 mL QuixSep micro dialyser purchased from Scienova. Acetonitrile (HPLC grade) was purchased from Fisher Scientific, triethylamine (99 %) was purchased from Acros Organics and orthophosphoric acid (85 %) was purchased from BDH laboratory supplies.

High performance Liquid Chromatography

HPLC was carried out on a Dionex UltiMate 3000 UHPLC with a UV detector set to 222, 219, 264 and 190 nm. A modified literature method was used as follows[26]; A Nucleosil C18 5 micron column was used (150 mm x 4.6 mm) as the stationary phase with an isocratic mobile phase of triethylamine and orthophosphoric acid buffer (1:1.5) and acetonitrile in the ratio of 40:60 buffer:acetonitrile. The method was carried out at with a flow rate of 1 mL/min and the column temperature kept at 25°C. The total run time for each chromatogram was 10 minutes with a blank in between each run.

4.3.4 Construction of Ibuprofen Calibration Curve

Ibuprofen was dissolved in distilled water (1 L) and left stirring for 24 hours to ensure complete dissolution. A serial dilution was carried out on this solution (25 mL) by 50 % each time until a series of 10 solutions were obtained with a concentration range of 1.00 X 10^{-5} mol dm^{-3} to 1.96 x 10^{-7} mol dm^{-3}. The solutions were then analysed using HPLC, following the method above, to construct a calibration curve.

4.3.5 Controlled release of Ibuprofen from PEO-*b*-PODMA, PEO-*b*-PDSMA and PEO-*b*-(PODMA-*co*-PDSMA) block copolymer bicontinuous nanospheres

The self-assembled BCP and ibuprofen solution (1 mL) was transferred to a 1 mL QuixSep dialyser and dialysed against 750 mL of distilled water for 6 hours with 5 mL of the dialysing water collected at time intervals throughout the 6 hour period. These 5 mL aliquots were then analysed using HPLC to determine the ibuprofen concentration with use of the calibration curve.

4.4 Results and Discussion

4.4.1 Calibration of Ibuprofen with HPLC

Three batches of ibuprofen calibrants in water, across the concentration range 1.96 x 10^{-7} – 1.00 x 10^{-5} mol dm^{-3}, were prepared via a serial dilution. One of these batches was then then analysed using a UV-Vis spectrometer to determine the UV absorbance wavelength. It was determined from the UV spectrum of Ibuprofen that the λmaxima of the absorbance bands were at 264 and 222 nm, which was consistent with the literature.[24] The calibrants were then analysed with HPLC equipped with a four channel UV detector, as the UV-Vis was not sensitive enough for the low concentrations. A full UV-Vis spectrum was carried out on the HPLC to confirm the absorbance band for ibuprofen, which revealed two more possible wavelengths as well as 222 and 264 nm. The four channels were set to 222, 264, 190 and 219 nm to determine the most accurate wavelength to use, so that even low concentrations could be detected. The 222 nm wavelength proved to be the most reliable as at 264 nm low concentrations of ibuprofen could not be detected and at 190 nm the absorbance of ibuprofen was obscured by the absorbance of water. A calibration curve was then plotted of the area of the HPLC peak against concentration, an average area was taken of all thee calibrants at each concentration. The data was fitted linearly with a R^2 value of 0.999 and an equation for the slope being x=y+0.0011/72.771.

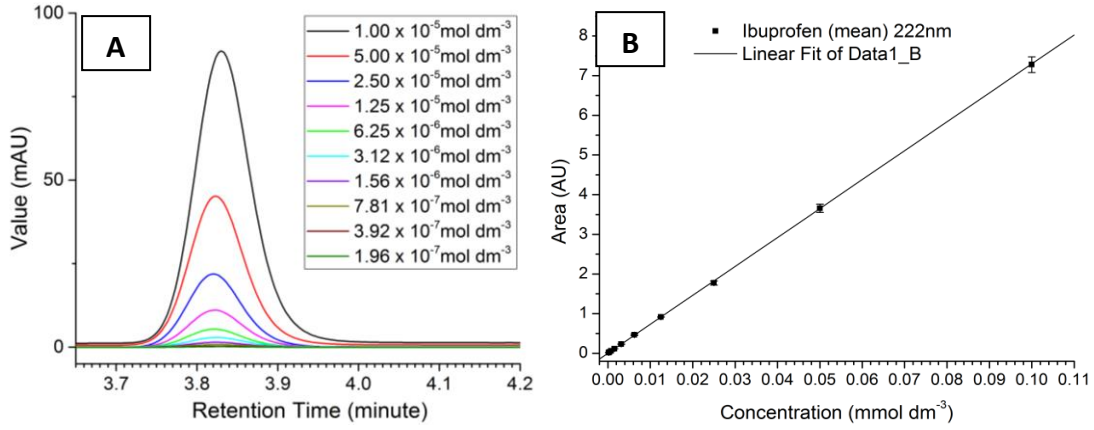

Figure 4.1: A) HPLC chromatograms of the ibuprofen calibrants with decreasing concentration by 50 % each time. **B)** Calibration curve of ibuprofen in water, obtained using UHPLC.

4.4.2 Encapsulation of Ibuprofen within PEO-*b*-PODMA Bicontinuous Nanospheres

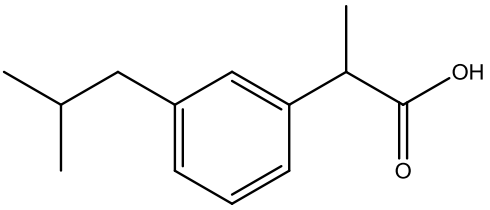

Figure 4.2: Structure of Ibuprofen

As previously established in the literature[27] and chapter 2, bicontinuous nanospheres can be obtained by the self-assembly of PEO-*b*-PODMA when the PEO block is at 25 wt %. With this knowledge, the encapsulation of ibuprofen within PEO-*b*-PODMA was carried out with P4 (PEO_{44}-*b*-$PODMA_{19}$ – PEO 25 wt %) with a polymer concentration of 1 wt % (P4-Ib). Analysis of P4-Ib with DLS was performed at 10°C, and revealed aggregates with an N_{ave} of around 60 nm, which indicates a micellar structure.[28] These results were compared to those obtained for the self-assembly of P4 not in the presence of ibuprofen. The DLS distribution plots (Figure 4.3) show a significant decrease in particle size with the presence of ibuprofen. As previously discussed in chapter 2, Eisenberg *et al.*[29] established a rule for the aggregation of block copolymers in solution, for micelles to form the hydrophilic wt % should be > 45 %. In the case of P4, the hydrophilic wt % is 25 % this indicates that the ibuprofen may be contributing to the hydrophilic wt % by acting as a surfactant. This was not surprising as ibuprofen has been seen to aggregate in solution by itself[30-31] but also contributes to the micellisation of other surfactants[32] and interacts with polymers during self-assembly in order to solubilise in water.[31] Ibuprofen has also been found to induce micellisation of polymer dextran-graft-poly (N-isopropylacrylamide) caused by the hydrogen bonding of the amide groups of poly (N-isopropylacrylamide) and the carboxyl groups of ibuprofen.[33]

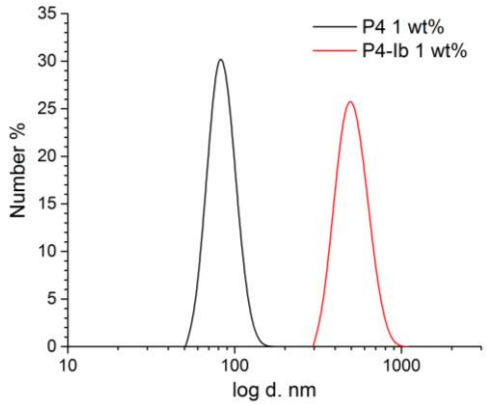

Figure 4.3: DLS N_{ave} distribution plots of P4 1 wt % (PEO_{44}-*b*-$PODMA_{19}$) and P4-Ib 1 wt % (PEO_{44}-*b*-$PODMA_{19}$) at 1 wt % in solution with 0.2 wt % ibuprofen) measured at 10˚C.

To counter the interference of ibuprofen with the self-assembly of bicontinuous nanospheres, a polymer was synthesised with a PEO wt % of 15 % (P1), this polymers characterisation was assessed in chapter 2. P1 was self-assembled at 1 wt % with ibuprofen and then analysed with DLS. The DLS results for P1-Ib are given in Table 4.1 with those of P4-Ib. Upon a decrease in PEO wt % from 25 to 15 % a significant increase in N_{ave} was observed from 60 nm to 226 nm, for the encapsulated ibuprofen aggregates. This demonstrates that a decrease in PEO wt % discourages micellisation and causes vesicular sized aggregates to form. The difference between the N_{ave} of P4-Ib and P1-Ib particles is also evident in from the DLS distribution plots (Figure 4.4A).

Table 4.1: DLS parameters of P4 (PEO_{44}-*b*-$PODMA_{19}$) and P4-Ib (PEO_{44}-*b*-$PODMA_{19}$ with ibuprofen) and P1 (PEO_{45}-*b*-$PODMA_{36}$) AND P1-Ib (PEO_{45}-*b*-$PODMA_{36}$ with ibuprofen) calculated at 10°C.

Sample	PEO wt %	N_{Ave} (d.nm)	SD (± nm)	Z_{Ave} (d.nm)	SD (± nm)	Đ
P4	25	453	77	845	28	0.55
P4-Ib	25	60	13	395	103	0.95
P1	15	332	17	396	8	0.19
P1-Ib	15	226	24	245	2	0.10

The distribution plot comparing the number average distribution in particle size of P1 1 wt % with P1-Ib 1 wt % (Figure 4.4 B) shows that the presence of ibuprofen during the self-assembly process does not significantly decrease the N_{ave}, with the P1

1 wt % sample having an N_{ave} of around 350 nm compared with 250 nm when ibuprofen was present.

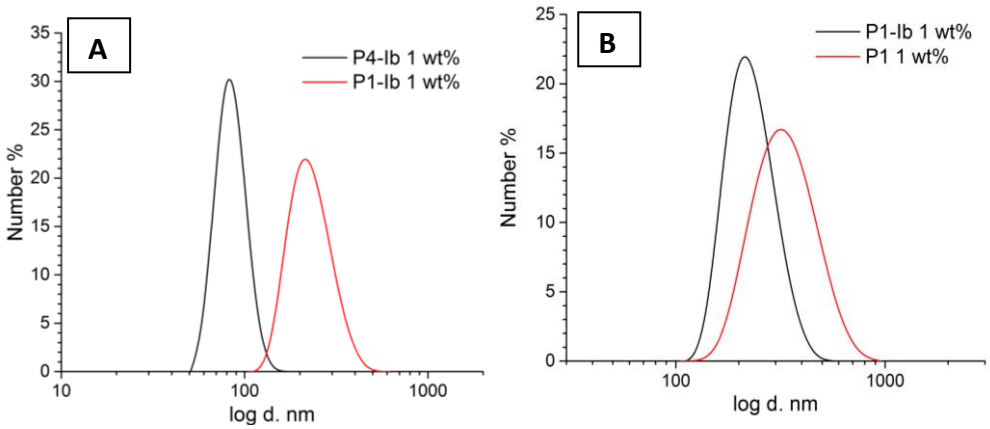

Figure 4.4: DLS N_{ave} distribution plots of **A)** P4-Ib 1 wt % (PEO_{44}-*b*-$PODMA_{19}$ with ibuprofen) against P1-Ib 1 wt % (PEO_{45}-*b*-$PODMA_{36}$ with ibuprofen). **B)** P1-Ib 1 wt % (PEO_{45}-*b*-$PODMA_{36}$ with ibuprofen) plotted against P1 1 wt % (PEO_{45}-*b*-$PODMA_{36}$).

It was established, from DLS analysis, that decreasing the PEO wt % from 25 to 15 % resulted in particles with an increased N_{ave} within the size range of bicontinuous nanospheres (70-460 nm)[34]. The P1-Ib particles, alongside P1 1 wt % for comparison, were analysed with cryo-TEM. The cryo-TEM images of P1 1 wt % (Figure 4.5 A) show spherical aggregates with an internal bicontinuous morphology. Bicontinuous nanospheres of PEO-*b*-PODMA (PEO 15 wt %) have been observed previously by McKenzie *et al.*[34] with an M_n was around 10 KDa, we have observed them for an increased M_n of 15 KDa. The P1-Ib sample also shows bicontinuous nanospheres, within the size range of 100-450 nm (Figure 4.5 B). The dark regions and small dark flecks are a result of poor vitrification of the sample, most likely due to either the solidification of the liquid ethane, or that the liquid nitrogen used to cool the ethane contributed to the vitrification process, when liquid nitrogen vitrifies the samples a N_2 (g) layer forms on the surface causing the sample to cool slower resulting in ice crystals. These images confirm that the self-assembly of bicontinuous nanospheres can be obtained with a decrease in hydrophilic wt % of the BCP. The controlled release of ibuprofen from these nanospheres will be investigated later in this chapter.

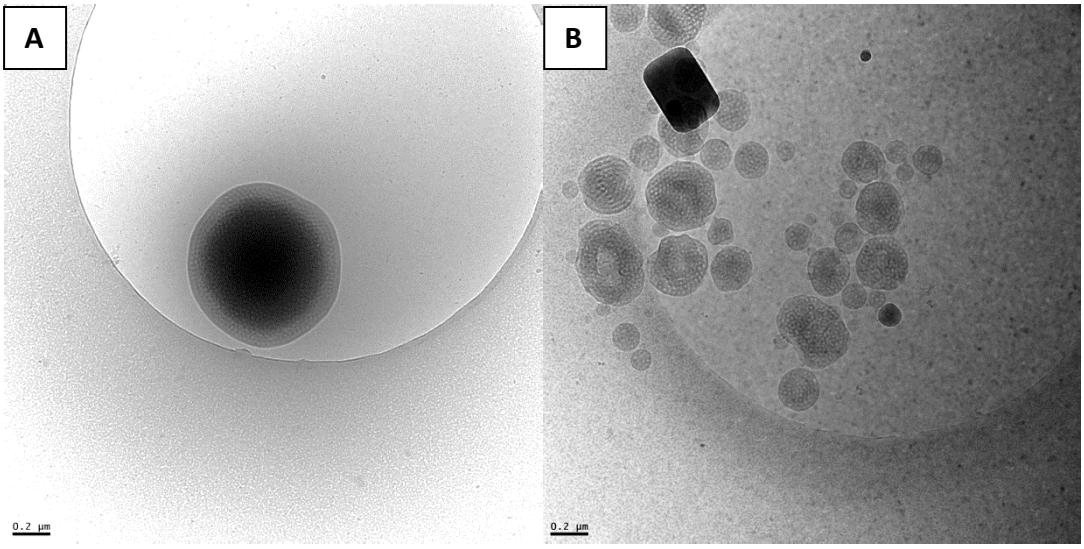

Figure 4.5: Cryo-TEM images of **A)** P1 (PEO_{44}-*b*-$PODMA_{19}$) (1 wt %) nanospheres with internal bicontinuous morphology. **B)** P1-Ib (PEO_{44}-*b*-$PODMA_{19}$) (1 wt %) nanospheres with internal bicontinuous morphology, the dark sections in the image are a result of ice forming.

4.4.3 Encapsulation of Ibuprofen within PEO-*b*-(PODMA-*co*-PDSMA) Bicontinuous Nanospheres at varying PDSMA wt %

The self-assembly of PEO-*b*-PODMA in the presence of ibuprofen produced micelles with an N_{ave} of around 60 nm when the PEO wt % was at 25 %, when the wt % was reduced to 15 wt % larger particles of around 225 nm were observed, and the bicontinuous internal structure was confirmed by cryo-TEM. As it was thought that the ibuprofen was contributing to the hydrophilic wt % by acting as a surfactant, it was presumed the same effect would be observed for the copolymers PEO-*b*-(PODMA-*co*-PDSMA). PEO-*b*-(PODMA-*co*-PDSMA) BCPs were prepared with a range of DSMA wt % at 15 wt % PEO. The BCPs were self-assembled in the presence of ibuprofen and on addition of water precipitation occurred. Although, once these samples were filtered (1.2 µm filter), DLS confirmed the presence of particles, a successful self-assembly is one without this precipitation due to lose of polymer and ibuprofen. The BCPs C1-C4 with a PEO wt % of 25 % were then self-assembled in the presence of ibuprofen. C2 (PEO_{45}-*b*-($PODMA_9$-*co*-$PDOMA_9$)) and C3 (PEO_{45}-*b*-($PODMA_7$-*co*-$PDOMA_{11}$)) formed cloudy solutions upon the addition of water,

however the suspensions were not stable and when left overnight separation of the polymer and water occurred.

4.4.3.1 C1 (PEO_{44}-b-($PODMA_{15}$-co-$PDSMA_4$)) (PODMA:PDSMA 75:25)

The self-assembly of C1 at 1 wt % in solution with 0.2 wt % ibuprofen formed a cloudy solution that was stable post dialysis (C1-Ib). Analysis of the particle size and distribution was carried out with DLS at 10°C and compared to the self-assembled C1 1 wt % with no ibuprofen (Table 4.2). There is a small decrease in N_{ave} from 180 nm for the C1 1 wt % samples to 140 nm with the presence of ibuprofen.

Table 4.2: DLS parameters of C1 (PEO_{44}-*b*-($PODMA_{15}$-*co*-$PDSMA_4$) and C1-Ib (PEO_{44}-*b*-($PODMA_{15}$-*co*-$PDSMA_4$) with ibuprofen) calculated at 10°C.

Sample	PEO wt %	N_{Ave} (d.nm)	SD (± nm)	Z_{Ave} (d.nm)	SD (± nm)	Đ
C1	25	180	15	230	1	0.20
C1-Ib	25	140	50	327	6	0.47

The DLS distribution plots (Figure 4.6) of C1 1 wt % and C1-Ib 1 wt % show that there is an insignificant difference in N_{ave} between the two samples. In fact in the presence of ibuprofen it appears that the distribution in particle size decreases. The reason for the higher Đ given in Table 4.2 is most likely due the small second peak seen in the distribution plot of C1-Ib which has a higher N_{ave} of around 600 nm.

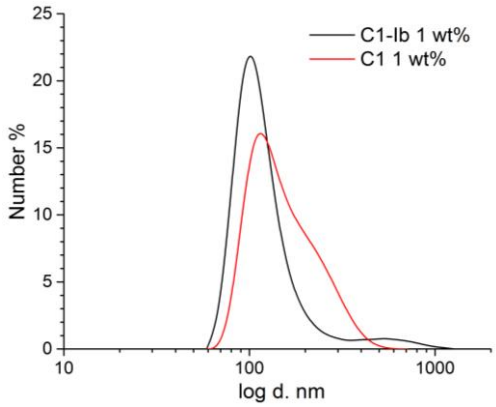

Figure 4.6: DLS N_{ave} distribution plots of C1 1 wt % (PEO_{44}-*b*-($PODMA_{15}$-*co*-$PDSMA_4$) and C1-Ib 1 wt % (PEO_{44}-*b*-($PODMA_{15}$-*co*-$PDSMA_4$) at 1 wt % in solution with 0.2 wt % ibuprofen) measured at 10°C.

As previously reported in chapter 3, C1 at 1 wt % in solution produces spherical aggregates with internal bicontinuous morphology, with some particles exhibiting

multi-lamellar internal morphology (Figure 4.7 A). The cryo-TEM images of C1-IB 1 wt % in solution produced particles with the same morphologies, the majority of which have bicontinuous morphology with some exhibiting multi-lamellar internal morphology, as seen with C1 1 wt % where ibuprofen was not present. The bicontinuous nanospheres were present across the size range 100-425 nm, the C1 1 wt % sample with no ibuprofen produced bicontinuous nanospheres across similar range of 100-550 nm. This clearly shows that the inclusion of ibuprofen has not significantly affected the particle size and the formation of bicontinuous nanospheres.

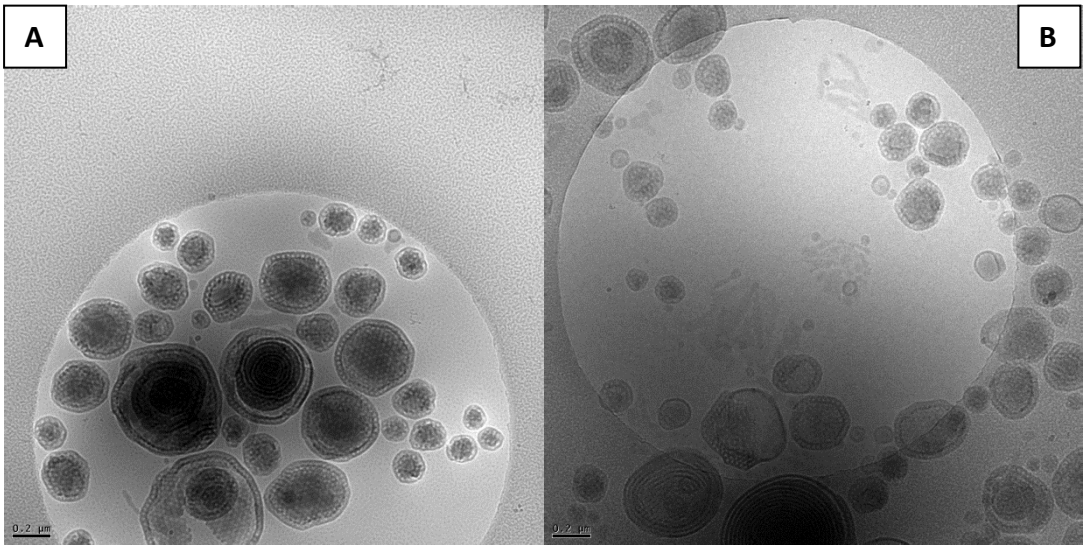

Figure 4.7: Cryo-TEM images of **A)** C1 (PEO_{44}-*b*-$PODMA_{19}$) (1 wt %) nanospheres with internal bicontinuous morphology and some regions of multi-lamellar. **B)** C1-Ib (PEO_{44}-*b*-$PODMA_{19}$) (1 wt %) nanospheres with internal bicontinuous morphology and some regions of multi-lamellar.

4.4.3.2 C4 (PEO_{44}-b-($PODMA_5$-co-$PDSMA_{13}$)) (PODMA:PDSMA 25:75)

The self-assembly of C4 at 1 wt % in solution with 0.2 wt % ibuprofen formed a cloudy solution that was stable post dialysis (C4-Ib). Analysis of the particle size and distribution was carried out with DLS at 10°C and compared to the self-assembled C4 1 wt % with no ibuprofen (Table 4.3). The table shows a small increase in N_{ave} in the presence of ibuprofen, although the dispersity in particle size also increases with the presence of ibuprofen.

Table 4.3: DLS parameters of C4 (PEO_{44}-*b*-($PODMA_{5}$-*co*-$PDSMA_{13}$) and C4-Ib (PEO_{44}-*b*-($PODMA_{5}$-*co*-$PDSMA_{13}$) with ibuprofen) calculated at 10°C.

Sample	PEO wt %	N_{Ave} (d.nm)	SD (± nm)	Z_{Ave} (d.nm)	SD (± nm)	Đ
C4	25	354	33	529	10	0.42
C4-Ib	25	408	96	888	37	0.68

The DLS distribution plots are bimodal for both samples (Figure 4.8). The second peak for both samples having an N_{ave} of around 600 nm. The first peak for C4-Ib 1 wt % has a lower N_{ave} (150 nm) than for C4 1 wt % (200 nm) showing that in the presence of ibuprofen a decrease in N_{ave} was observed in contrast to the values given in Table 4.3. CONTIN analysis indicated that some particles were present in the solution at around 4000 nm for C4-Ib which could be why there was an increasing the N_{ave} observed in Table 4.3 in comparison the distribution plots.

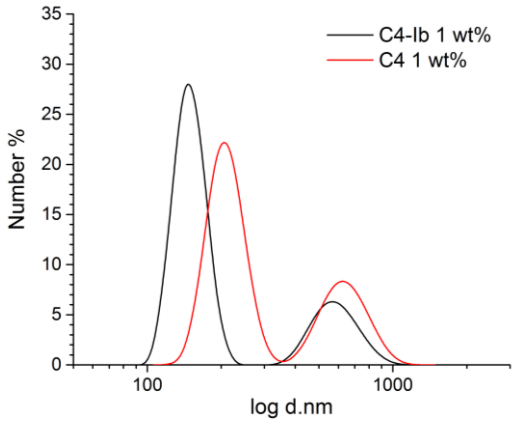

Figure 4.8: DLS N_{ave} distribution plots of C4 1 wt % (PEO_{44}-*b*-($PODMA_{5}$-*co*-$PDSMA_{13}$) and C4-Ib 1 wt % (PEO_{44}-*b*-($PODMA_{5}$-*co*-$PDSMA_{13}$) at 1 wt % in solution with 0.2 wt % ibuprofen) measured at 10°C.

The aggregate solution of C4 at 1 wt % was analysed previously in chapter 3 and the negatively stained TEM images revealed spherical aggregates with possible complex internal morphology (Figure 4.11A). Analysis of the C4-Ib 1 wt % solution with cryo-TEM was attempted, however high quality images could not be achieved. The negatively stained TEM images of D3-Ib 1 wt % show spherical aggregates with some exhibiting multi-lamellar internal morphology (Figure 4.9 D) and some showing a well-defined bicontinuous morphology (Figure 4.9 C). The spherical aggregates of C4-Ib were present across the size range 200-400 nm. The aggregates of C4 1 wt % were observed across a wider size range of 200-900 nm.

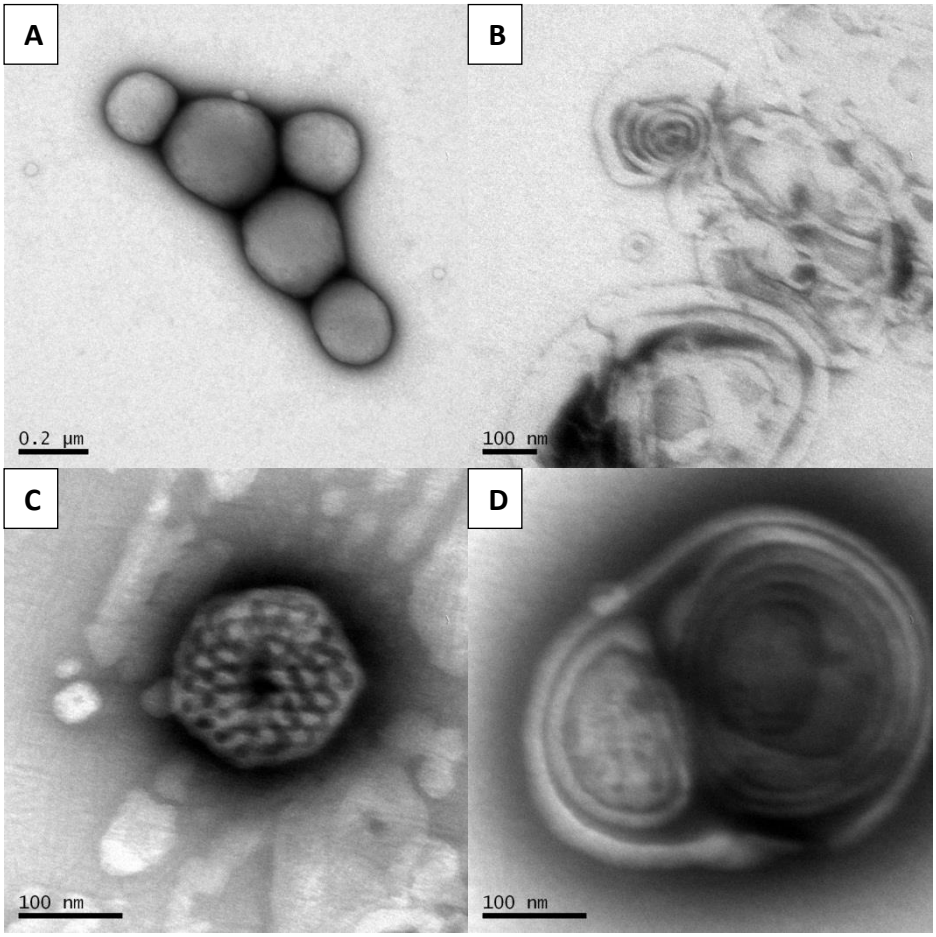

Figure 4.9: Negatively stained TEM images of **A-B)** C4 (PEO_{44}-*b*-($PODMA_5$-*co*-$PDSMA_{13}$)) (1 wt %) nanospheres. **C-D)** TEM images of D3-Ib (PEO_{44}-*b*-($PODMA_5$-*co*-$PDSMA_{13}$)) (1 wt %) nanospheres with possible internal bicontinuous morphology and some regions of multi-lamellar.

4.4.4 Encapsulation of Ibuprofen within PEO-*b*-PDSMA Bicontinuous Nanospheres

As with the PEO-*b*-(PODMA-*co*-PDSMA) copolymer samples, the self-assembly of PEO-*b*-PDSMA with ibuprofen was attempted with a PEO-*b*-PDSMA BCP with a 15 wt % PEO content. Upon addition of water to the polymer, ibuprofen THF solution precipitation of the polymer and ibuprofen occurred. When D3 (PEO_{44}-*b*-$PDSMA_{16}$, 25 wt % PEO) was self-assembled at 1 wt % in solution with ibuprofen a cloudy solution was produced with no precipitation. The D3-Ib 1 wt % solution was analysed with DLS at 10°C and the results were compared to that of D3 1 wt % with no ibuprofen. The N_{ave} of D3 and D3-Ib are roughly the same, this indicates that the incorporation of ibuprofen does not greatly affect the aggregate size.

Table 4.4: DLS parameters of D3 (PEO_{44}-*b*-$PDSMA_{16}$) at 1 wt % and D3-Ib (PEO_{44}-*b*-$PDSMA_{16}$ with ibuprofen) at 1 wt % calculated at 10°C.

Sample	PEO wt %	N_{Ave} (d.nm)	SD (± nm)	Z_{Ave} (d.nm)	SD (± nm)	Đ
D3	25	431	84	709	31	0.45
D3-Ib	25	420	91	819	79	0.67

The DLS number average distribution plots (Figure 4.10) for D3 1 wt % and D3-Ib 1 wt % show that the main N_{ave} for D3-Ib 1 wt % is slightly larger than that of D3 1 wt %, with both samples exhibiting a bimodal distribution which explains the high dispersities in size given in Table 4.4.

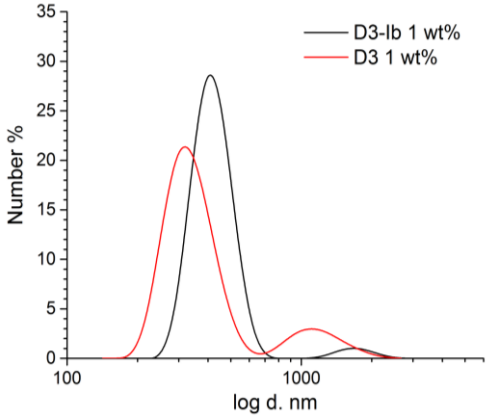

Figure 4.10: DLS N_{ave} distribution plots of D3 1 wt % (PEO_{44}-*b*-$PDSMA_{16}$) and D3-Ib 1 wt % (PEO_{44}-*b*-$PDSMA_{16}$ at 1 wt % in solution with 0.2 wt % ibuprofen) measured at 10°C.

The aggregate solution of D3 at 1 wt % was analysed previously in chapter 3 and the cryo-TEM images revealed spherical aggregates with an internal bicontinuous morphology (Figure 4.11 A). Analysis of the D3-Ib 1 wt % solution with cryo-TEM was attempted, however high quality images could not be achieved. The negatively stained TEM images of D3-Ib 1 wt % reveal spherical aggregates with some exhibiting multi-lamellar internal morphology (Figure 4.11 B) and some indicating bicontinuous morphology (Figure 4.11 C). The spherical aggregates of D3-Ib were present across the size range 250-600 nm. The aggregates of D3 1 wt % were observed across a wider size range of 150-850 nm. The larger size range was evident from the DLS distribution plots for D3 1 wt % where two size distributions were present (Figure 4.10). This clearly shows that the inclusion of ibuprofen has not significantly affected

the particle size and the formation of bicontinuous nanospheres, although some multi-lamellar aggregates are present which were not observed for D3 1 wt %.

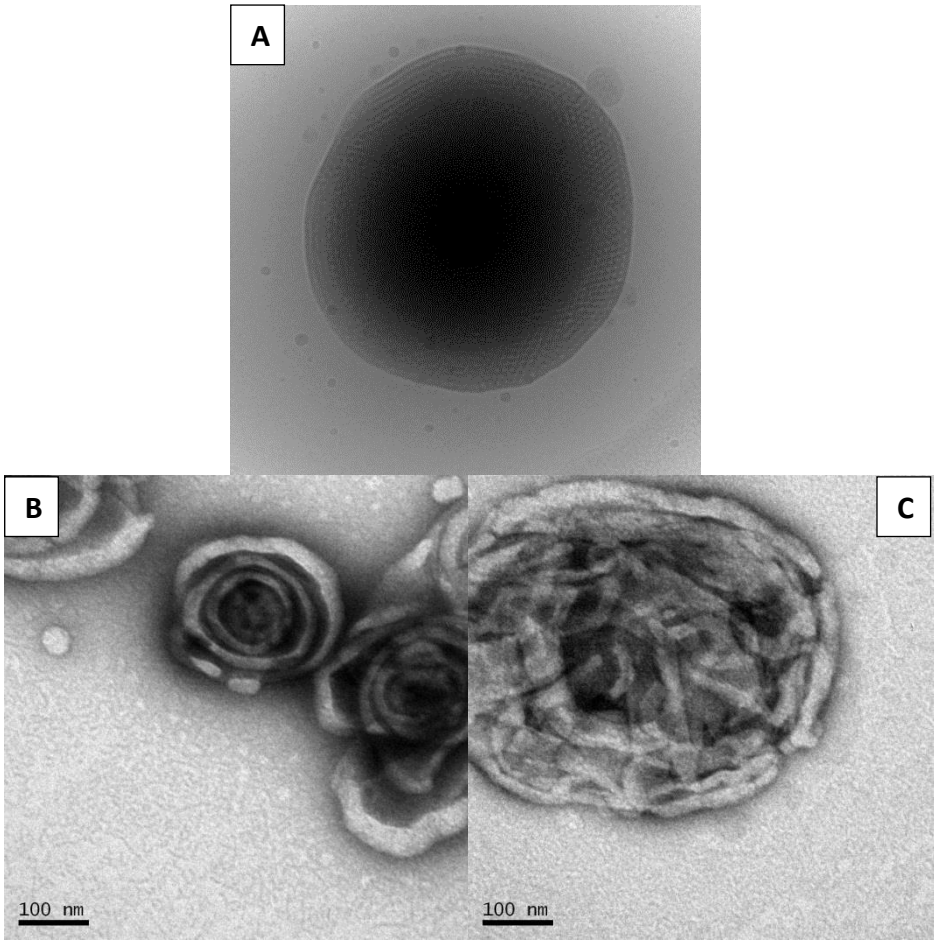

Figure 4.11: A) Cryo-TEM images of D3 (PEO_{44}-*b*-$PDSMA_{16}$) (1 wt %) nanospheres with internal bicontinuous morphology. **B-C)** TEM images of D3-Ib (PEO_{44}-*b*-$PDSMA_{16}$) (1 wt %) nanospheres with possible internal bicontinuous morphology and some regions of multi-lamellar.

4.4.5 Controlled release of Ibuprofen from PEO-*b*-PODMA Bicontinuous Nanospheres

As discussed in the introduction the controlled release of hydrophobic pyrene from PEO-*b*-PODMA bicontinuous nanospheres has been previously demonstrated by Holder *et al.*[11] with a faster rate of release observed above PODMA's T_m. As with the release of pyrene, the thermo-responsive nature of release was investigated for ibuprofen. The PEO-*b*-PODMA bicontinuous nanospheres were prepared in the presence of ibuprofen, the results of which have been discussed previously. Samples of P1-Ib dispersions (1 cm^3) were isolated from water (0.75 dm^3) in a Quixsep dialyser sealed with a dialysis membrane, this was the method used to measure the release

of pyrene.[11] The water was kept at a set temperature (25, 35 and 40°C) to study the temperature effects on rate of release, and samples were taken of the dialysis water at given times over the course of 6 hours. The concentration of ibuprofen in these samples was determined by analysis with HPLC to determine the peak area and then using the calibration curve to determine the concentration.

UV-Vis spectrometry was used to analysis the polymer-ibuprofen samples pre and post-release to determine the percentage of ibuprofen left within the PBNs. The spectrum gave an absorbance >3 which means that the change in absorbance of the ibuprofen peak (222 nm) could not accurately be measured due to the Beer-lambert relationship becoming non-linear above an absorbance of 1 due to high concentration.

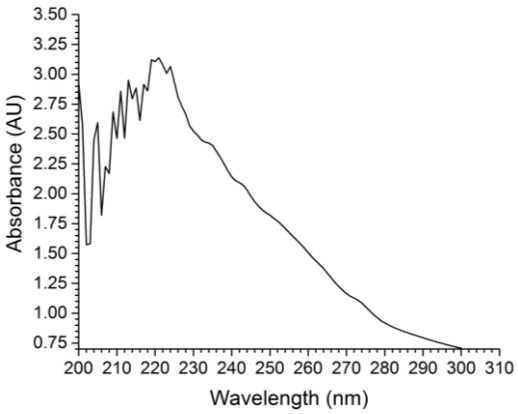

Figure 4.12: Uv spectrum of P1-Ib.

The release efficiencies at each temperature were estimated by extrapolation of the 40°C curve seen in Figure 4.14A to a constant value, i.e. the maximum possible release of ibuprofen. Therefore the % of ibuprofen left within the bicontinuous nanospheres for each temperature is given in Table 4.5 with a decrease in % upon an increase in measurement temperature. The release efficiencies of ibuprofen at 25 and 35 °C (40 and 60 %) match those observed by Holder *et a.l*[11] for pyrene, the 40°C release efficiency is much larger (83 %) than that observed for pyrene (72 %), this is most likely due to ibuprofen having a higher water solubility (0.101 mmol dm^{-3})[35] than pyrene (6.67 x 10^{-4} mmol dm^{-3})[36-38]. Based on the release efficiencies and mass of ibuprofen within the BPNs at the start, the loading capacity was calculated to be 0.3µg of ibuprofen in 100 mg of polymer giving a loading capacity percentage of 0.3 % of the mass of the polymer. The final concentration in the dialysis solution after 6

hours decreases with an increase in measurement temperature confirming the rate of release is temperature dependent. The moles and masses of ibuprofen within the BPNs were calculated using the final concentration in solution and the release efficiency percentages. The values show that at each temperature the BPNs contained roughly the same amounts of ibuprofen with a small decrease at 35°C.

Table 4.5: Data used to estimate release efficiencies of ibuprofen from BPNs at various temperatures.

T (˚C)	% Ib in solution	% Ib in BPN	Conc. in solution (mol m^{-3})	Moles in solution	Moles in BPN start	Moles in BPN end	Mass in BPN start (g$x10^{-4}$)
0	0	100	-	-	-	-	-
25	40	60	8.63×10^{-7}	6.47×10^{-7}	1.62×10^{-6}	9.72×10^{-7}	3.3
35	60	40	9.47×10^{-7}	7.10×10^{-7}	1.18×10^{-6}	4.72×10^{-7}	2.4
40	83	17	1.72×10^{-6}	1.33×10^{-6}	1.60×10^{-6}	2.72×10^{-7}	3.3

The fractional release values were calculated using the extrapolation of the 40°C curve as was the release efficiencies (Figure 4.14A), the fractional release values were plotted against time (Figure 4.14B). This demonstrates that the melting of the PODMA block effects the rate of release of ibuprofen as seen previously with the release of pyrene.[11] The solubility of Ibuprofen may also contribute to the increased rate of release. Garzón and Martínez (2004)[39] established that the solubility of ibuprofen is temperature dependent. They investigated the solubility of ibuprofen in an aqueous solution kept at 7.4 pH and 0.15 mol l^{-1} ionic strength to emulate the conditions of blood in the body. They found that the solubility of ibuprofen increased with an increase in temperature as demonstrated in Figure 4.12. The low solubility of hydrophobic drugs limits the drugs dissolution rate,[40] with this in mind it is possible that due to an increase in ibuprofen solubility with an increase in temperature, the dissolution rate would also be seen to increase and therefore it is not just the melting of the PODMA block that contributes to the increase in dissolution rate of the ibuprofen from the PEO-*b*-PODMA nanospheres. It can also be estimated that it is not solely the increased solubility of ibuprofen upon an increase in temperature that affected the rate of dissolution. The concentration of ibuprofen released at 300

minutes at 25, 35 and 40°C was plotted (Figure 4.13B) and shows a non-linear plot compared to the linear plot of solubility against temperature (Figure 4.13A)

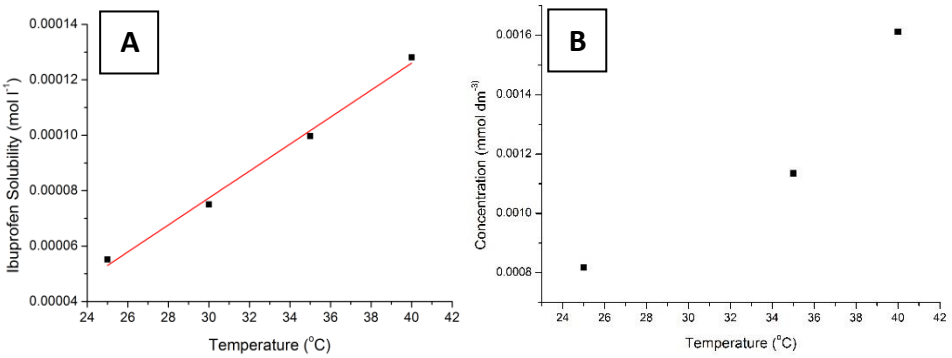

Figure 4.13: A) Plot of Ibuprofen solubility against temperature. Reproduced from data in reference.[39] **B)** Plot of concentration of ibuprofen released from P1 at 300 minutes against temperature.

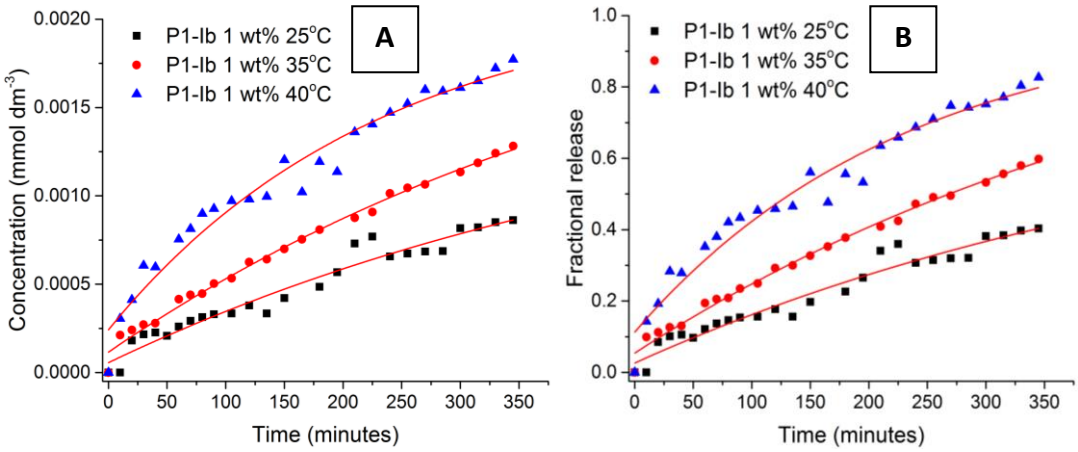

Figure 4.14: A) Release profiles of ibuprofen from bicontinuous nanospheres formed from PEO_{45}-*b*-$PODMA_{36}$ at various temperatures. **B)** Fractional release profiles of ibuprofen from bicontinuous nanospheres formed from PEO_{45}-*b*-$PODMA_{36}$ at various temperatures

The fractional release rate of ibuprofen at each temperature was calculated from the linear fit of the fractional release profiles above 0.1. They were calculated to be 1.68 x 10^{-5} s^{-1} at 25˚C, 2.41 x 10^{-5} s^{-1} at 35˚C, 2.70 x 10^{-5} s^{-1} at 40°C. The release rates of pyrene from PEO-*b*-PODMA BNs were calculated by Holder *et al*. to be 5.0 x 10^{-5} s^{-1} (25°C), 8.5 x 10^{-5} s^{-1} (30°C) and 1.67 x 10^{-4} s^{-1} (40°C). These results show that the release rate constants of ibuprofen are lower than that of pyrene from the same polymer system. The trend for the release rate constants of ibuprofen is the same as

that of pyrene, showing that the thermoresponsive nature of the hydrophobic block still effects the rate of release.

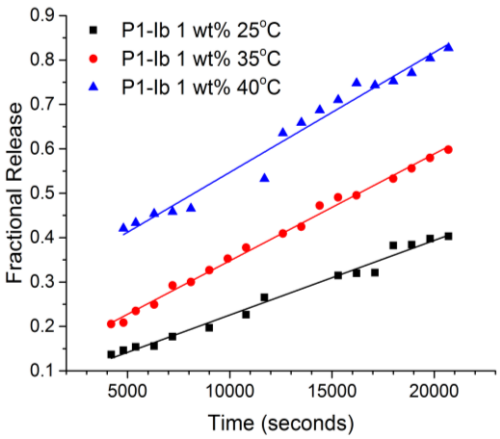

Figure 4.15: Linear Fit of the fractional release of ibuprofen from P3 nanospheres, the slope of the line was used to calculate the release rate constants at each temperature.

The release patterns of drugs vary, with some releasing at a constant slow zero or first order and those that release an initial rapid dose followed by a slow or first order rate of release.[41] In order for drug concentration to be maintained at the desired site or within the blood a rapid dose followed by controlled slow release is desired in order to attain the effective therapeutic concentration.[42-43] The use of kinetic modelling in relation to drug release profiles, gives an indication to a number of physical parameters related to the drug release. A number of model dependent methods were employed to determine the dissolution profile of ibuprofen at each given temperature. The functions applied, via fitting of the release profiles, were Korsmeyer–Peppas, Weibull and zero-order (Figure 4.15)[43-44]. Once the most suitable function was determined, i.e. the function that fitted the release profile the best, then the dissolution profile could be determined.

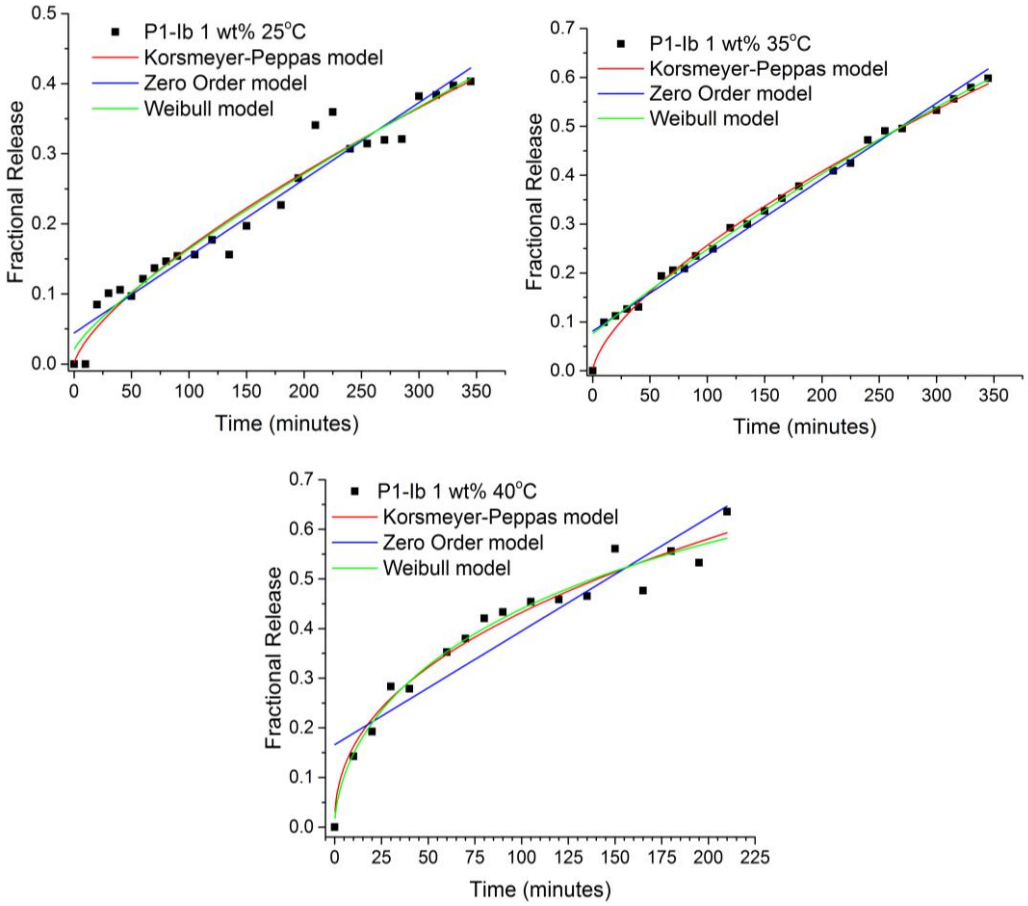

Figure 4.16: Results of curve fitting for matching release models to release of ibuprofen from PEO_{45}-*b*-$PODMA_{36}$ bicontinuous nanospheres at 25, 35 and 40°C.

From viewing the fits (Figure 4.15) it was determined that the Korsmeyer-Peppas model matched the release profiles the closest. Korsmeyer *et al*. developed a simple model to describe drug release from a polymeric system that relates the drug release to time (Equation 4.1).[44-45]

Equation 4.1: Korsmeyer-Peppas model

$$\frac{M_t}{M_\infty} = at^n$$

Where M_t/M_∞ is the fraction of drug released at time t, a is a constant incorporating structural and geometrical characteristics of the drug dosage form and n is the release exponent. This n value can be used to determine different release mechanisms with n = 0.43 indicating Fickian diffusion, n= 0.43-0.85 indicates Non-Fickian transport, 0.85 is Case II transport and > 0.85 indicates Super case II transport for a spherical sample.[46] These n values were determined using the portion of the release curve where M_t/M_∞ is <0.60. The values are present in Table 4.6 along with

the relevant drug transport mechanism and the rate of release as a function of time. Generally glassy polymers will exhibit non-Fickian like behaviour and rubbery polymers will follow Fickian diffusion, this is because rubbery polymers[47] have a relaxation time that is almost immediate whereas the relaxation time of glassy polymers is longer. The relaxation time is the time taken by one portion of the polymer entanglement network to react to a change in another portion.[48] Alfrey *et al* (1966)[49] gave the following classification for the drug release mechanisms from polymers with regard to the diffusion rate and relaxation times; for Fickian diffusion the rate of diffusion is much slower than the relaxation time, for non-Fickian transport the diffusion and relaxation times are comparable, for case II transport the diffusion is rapid in comparisons to the relaxation process meaning the relaxation is the determining factor. For P1-Ib both the 25 and 35°C ibuprofen release profiles follow non-Fickian transport, where encapsulate release is determined by polymer relaxation rates. At 40°C the profile follows Fickian diffusion where the determining factor is the rate of diffusion, this could be due to the polymer being heated above its melting temperature.

Table 4.6: Interpretation of diffusional release mechanisms from polymeric films. The a and n values were calculated form the Korsmeyer-Peppas model equation, where n is the release exponent and a is the structural and geometrical component.

T (°C)	a	n	Drug transport mechanism	Rate as a function of time
25	1.3×10^{-5}	0.72	Non-Fickian/ anomalous transport	t^{n-1}
35	2.5×10^{-6}	0.67	Non-Fickian/ anomalous transport	t^{n-1}
40	9.5×10^{-5}	0.43	Fickian diffusion	$t^{-0.43}$

4.4.6 Controlled Release of Ibuprofen from PEO-*b*-(PODMA-*co*-PDSMA) Bicontinuous Nanospheres

4.4.6.1 C1 (PEO_{44}-b-($PODMA_{15}$-co-$PDSMA_4$)) (PODMA:PDSMA 75:25)

In the presence of ibuprofen C1 can self-assemble to form bicontinuous nanospheres (BN) at 1 wt % in solution. The presence of bicontinuous nanospheres was confirmed with cryo-TEM. To determine the release profiles of ibuprofen from C1-Ib BNs samples of the aggregate solution (1 mL) were sealed in a QuixSep dialyser with dialysis membrane. The samples were then dialysed against distilled water (0.75 dm^3) kept at a set temperature (25, 35 and 45°C) and samples of the dialysis water (5 mL) were collected at time intervals across a 6 hour period. The samples were then analysed with HPLC to determine the concentration of ibuprofen released over time. The concentrations calculated using the calibration curve were then plotted against time to assess the release profiles at each temperature. The release profiles are shown in Figure 4.17, and show that the results are hard to fit due to a large number of anomalies, this meant that the data could not be extrapolated as the maximum concentration calculated was less than that observed at 360 minutes (6 hours) therefore the release efficiencies and fractional release could not be calculated. This experiment will need to be repeated to see if a clearer release profile can be obtained.

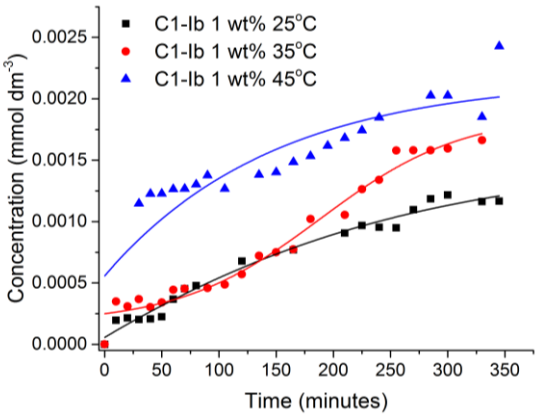

Figure 4.17: Release profiles of ibuprofen from bicontinuous nanospheres formed from PEO_{44}-*b*-($PODMA_{15}$-*co*-$PDSMA_4$) at various temperatures.

4.4.6.2 C4 (PEO_{44}-b-($PODMA_5$-co-$PDSMA_{13}$)) (PODMA:PDSMA 25:75)

It has already been established that in the presence of ibuprofen C4 forms bicontinuous nanospheres at 1 wt % in solution. Aliquots of C4-Ib dispersions (1 cm^3) were isolated from water (0.75 dm^3) in a QuixSep dialyser sealed with a dialysis membrane, as with P1-Ib. To study the temperature effects on rate of release the dialysis water was kept at set temperatures (25, 35 and 45°C), this time measuring at a higher temperature than with P1-Ib due to C4's higher T_m, which was observed using DSC (chapter 3). Aliquots (5 mL) were taken at intervals across a 6 hour period and then analysed with HPLC to determine the concentration of ibuprofen that had been released at set time intervals.

The release efficiencies (% Ib in solution) were calculated in the same way as for P1-Ib with the extrapolation of the 45°C release rate plot (Figure 4.18A) to get a maximum release concentration. The % of ibuprofen remaining within the nanospheres as then calculated using the release efficiencies. These values show (Table 4.7) that as the measurement temperature is increased above the hydrophobic blocks T_m (39.2°C), the release of ibuprofen also increases across the same time period. The moles in the BPNs at the start are very similar for the 25 and 35°C aggregate solutions, with a slight increase for the 45°C. This is also reflected in the mass of ibuprofen within the BPNs at the start. Using the release efficiencies and the mass of ibuprofen in the BPNs at the start, a loading capacity of 0.85 % of the total mass of polymer was calculated. This is higher than the loading capacity of P1-Ib, and could be due to a longer side-chain length within the hydrophobic block, trapping the ibuprofen within the nanospheres.

Table 4.7: Data used to estimate release efficiencies of ibuprofen from BPNs at various temperatures.

T (°C)	% Ib in solution	% Ib in BPN	Conc. in solution (mol m^{-3})	Moles in solution	Moles in BPN start	Moles in BPN end	Mass in BPN at start (g x 10^{-4})
0	0	100	-	-	-	-	-
25	20	80	1.02×10^{-6}	7.65×10^{-7}	3.83×10^{-6}	3.06×10^{-6}	7.9
35	37	63	1.9×10^{-6}	1.43×10^{-6}	3.86×10^{-6}	2.43×10^{-6}	8.0
45	60	40	3.05×10^{-6}	2.79×10^{-6}	4.65×10^{-6}	1.86×10^{-6}	9.6

The fractional release values were calculated as with P3-Ib from the extrapolation of the 45°C fit from the graph in Figure 4.18A. The values were then plotted against time to give the fractional release profiles (Figure 4.18B). The fractional release increases with an increase in temperature over the same time scale. This was the same trend observed for the release of ibuprofen from P3-Ib 1 wt % and demonstrates the effect temperature has on the rate of release.

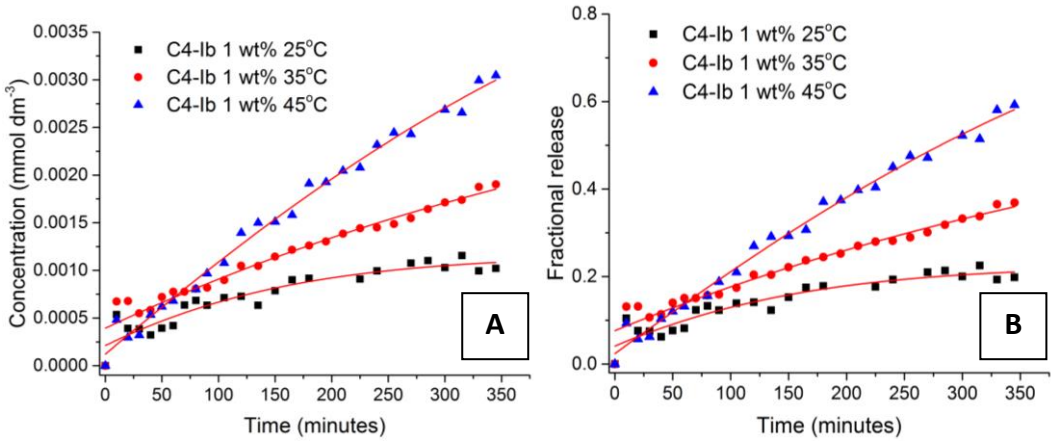

Figure 4.18: A) Release profiles of ibuprofen from bicontinuous nanospheres formed from PEO_{44}-*b*-($PODMA_5$-co-$PDSMA_{13}$) at various temperatures. **B)** Fractional release profiles of ibuprofen from bicontinuous nanospheres formed from PEO_{44}-*b*-($PODMA_5$-*co*-$PDSMA_{13}$) at various temperatures.

Just as with P1-Ib the fractional release rate of ibuprofen from C4 BNs was calculated from the linear fit of the fractional release profiles above 0.1 at each temperature. They were calculated to be 5.43 x 10^{-6} s^{-1} at 25˚C, 1.26 x 10^{-5} s^{-1} at 35˚C, 2.39 x 10^{-5} s^{-1} at 45°C. These rate constants are smaller than the rate constants observed for P1-IB at the corresponding temperatures. This suggests that the inclusion of DMSA within the hydrophobic block may have an effect on the rate of release. This effect will be looked at in more detail later in this chapter.

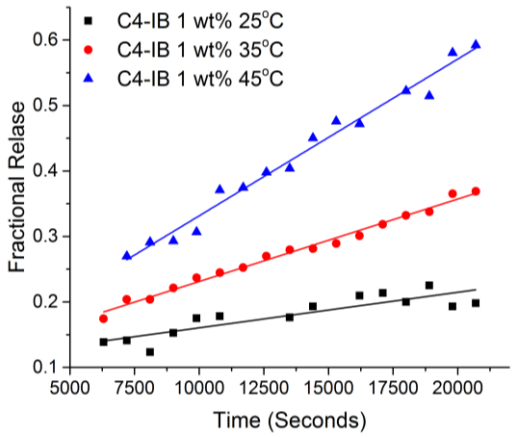

Figure 4.19: Linear Fit of the fractional release of ibuprofen from C4 nanospheres, the slope of the line was used to calculate the release rate constants at each temperature.

The same functions applied to the fractional release of ibuprofen from P1-Ib were used for C4-Ib to determine the dissolution profile of ibuprofen at each give temperature. The most suitable fit was determined to be the Korsmeyer-Peppas model. The value of n (release exponent) at each temperature was determined from the fractional release profiles with the fraction at <0.6. These values are given in Table 4.8 along with the relevant drug release transport mechanism. The release profile of ibuprofen at 25°C has and n value out of range for determining the transport mechanism. Both the 35 and 45°C release profiles follow non-Fickian transport. The non-Fickian diffusion was expected due to the glassy polymers generally exhibiting non-Fickian type transport.[48]

Table 4.8: Interpretation of diffusional release mechanisms from polymeric spheres. The a and n values were calculated form the Korsmeyer-Peppas model equation, where n is the release exponent and a is the structural and geometrical component.

T (°C)	a	n	Drug transport mechanism	Rate as a function of time
25	0.02093	0.40	-	-
35	0.02035	0.48	Non-Fickian/ anomalous transport	t^{n-1}
45	0.0051	0.81	Non-Fickian/ anomalous transport	t^{n-1}

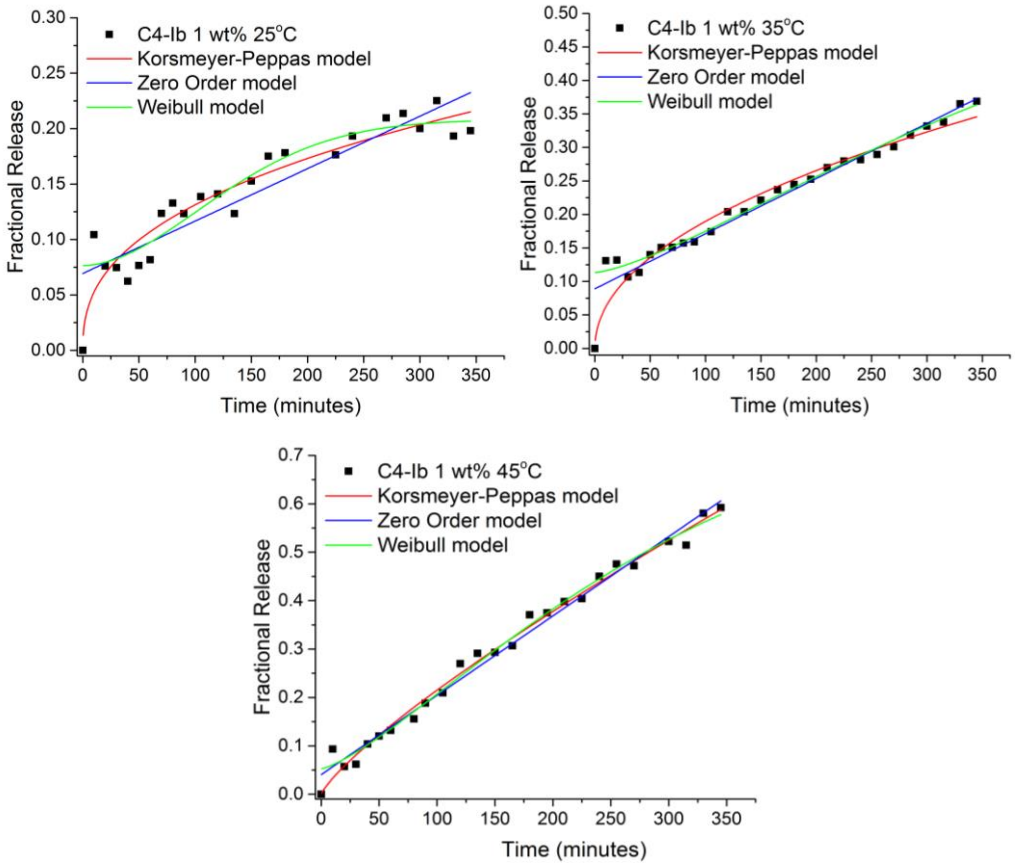

Figure 4.20: Results of curve fitting for matching release models to release of ibuprofen from PEO_{44}-*b*-($PODMA_5$-co-$PDSMA_{13}$) bicontinuous nanospheres at 25, 35 and 45°C.

4.4.7 Controlled Release of Ibuprofen from PEO-*b*-PDSMA Bicontinuous Nanospheres

The self-assembly of D3 1 wt % (PEO_{44}-*b*-$PDSMA_{16}$) in the presence of ibuprofen produced bicontinuous nanospheres. The controlled release of ibuprofen from these nanospheres was then assessed. Aliquots of D3-Ib 1 wt % aggregate solution (1 mL) were sealed in a QuixSep dialyser with dialysis membrane, the sample was then dialysed against distilled water (0.75 dm^3) and samples of the water were collected at certain time intervals across a 6 hour period.

The release efficiencies (% Ib in solution Table 4.9) were calculated by extrapolation of the 45°C concentration release profile to obtain the maximum concentration of ibuprofen that could potentially be released. The % of ibuprofen remaining within the BPNs was then calculated using the release efficiencies. The same trend in release efficiencies observed for P3-Ib and C4-Ib was seen for D3-Ib, an increase in release % upon an increase in temperature, this was expected as the BCP was heated above its

T_m (41.1°C). The moles and mass of ibuprofen in the BPNs at the start are very similar for all temperatures. An average mass was then calculated and use to determine that D3-IB 1 wt % had a loading capacity of 1.13 %, the highest loading capacity of all the polymer systems tested.

Table 4.9: Data used to estimate release efficiencies of ibuprofen from BPNs at various temperatures.

T (°C)	% Ib in solution	% Ib in BPN	Conc. in solution (mol m^{-3})	Moles in solution	Moles in BPN start	Moles in BPN end	Mass in BPN at start (g x 10^{-3})
0	0	100	-	-	-	-	-
25	16	84	1.44 x 10^{-6}	1.08 x 10^{-6}	6.75 x 10^{-6}	5.67 x 10^{-6}	1.27
35	22	78	2.01 x 10^{-6}	1.51 x 10^{-6}	6.86 x 10^{-6}	5.35 x 10^{-6}	1.10
45	30	70	2.81 x 10^{-6}	2.11 x 10^{-6}	7.03 x 10^{-6}	4.92 x 10^{-6}	1.02

The fractional release of ibuprofen from D3 BNs was calculated by extrapolation of the 45°C concentration release profile (Figure 4.21) to determine the maximum release concentration. The concentrations released at each temperature were then divided by this maximum concentration to get the fractional release values. The fractional release was plotted against time to give the fractional release profiles (Figure 4.21B). Upon an increase in experimental temperature the fractional release increases across the same time scale of 6 hours. This trend was also observed for the fractional release of ibuprofen from P3-IB 1 wt % and C4-Ib 1 wt %.

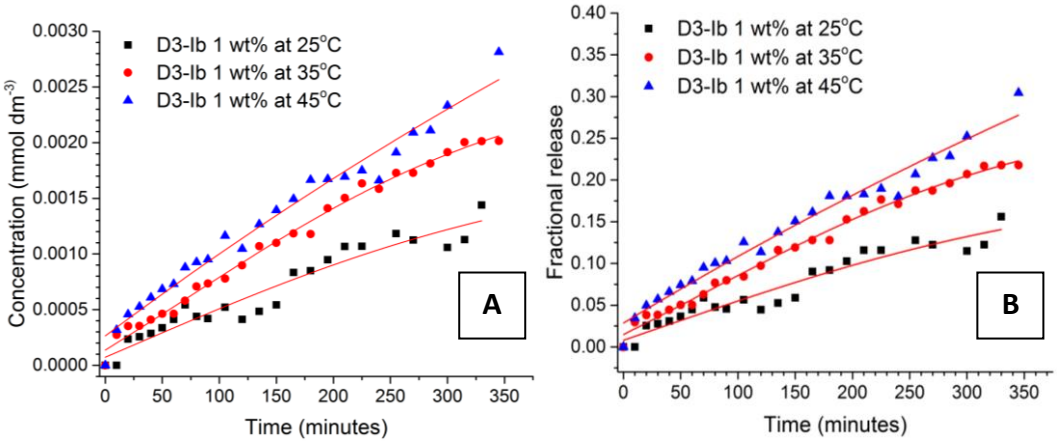

Figure 4.21: A) Release profiles of ibuprofen from bicontinuous nanospheres formed from PEO_{44}-*b*-$PDSMA_{16}$ at various temperatures. **B)** Fractional release profiles of

ibuprofen from bicontinuous nanospheres formed from PEO_{44}-*b*-$PDSMA_{16}$ at various temperatures.

The fractional release rate constants for ibuprofen from D3-IB 1 wt % BNs was calculated using a linear fit of the fractional release against time where fractional release was 0.1-0.6 (Figure 4.22). The release rate constants were taken from the slope of the linear fit. They were calculated to be 5.86 x 10^{-6} s^{-1} at 25°C, 8.95 x 10^{-6} s^{-1} at 35°C, 1.15 x 10^{-5} s^{-1} at 45°C. The rate constants are smaller than those of C4-Ib 1 wt % again indicating that a higher DSMA wt % within the hydrophobic block results in a slower rate of release of ibuprofen.

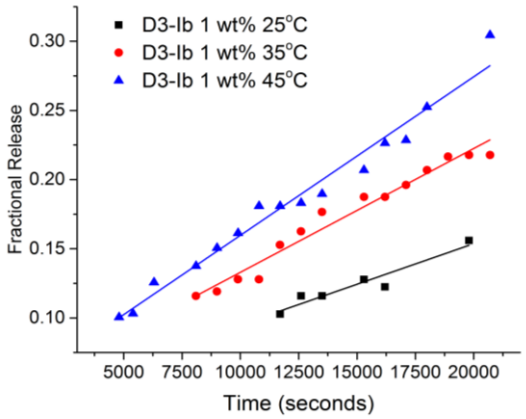

Figure 4.22: Linear Fit of the fractional release of ibuprofen from D3-Ib 1 wt % nanospheres, the slope of the line was used to calculate the release rate constants at each temperature.

The fractional release profiles of D3-Ib at 25, 35 and 45°C were fitted with dissolution models to determine the dissolution profiles. The functions that were fitted to the profiles were Korsmeyer-Peppas model, zero-order model and Weibull model. The Korsmeyer-Peppas model was the closest fit to the release profiles (Figure 4.23). The release exponent n, was determined for the release profiles at all three experimental temperatures, these were calculated from the Korsmeyer-Peppas equation. The values of n given in Table 4.10 indicates that at all three temperatures the release mechanism follows non-Fickian transport, which was as expected due to glassy polymers generally exhibiting non-Fickian transport.[48]

Table 4.10: Interpretation of diffusional release mechanisms from polymeric spheres. The a and n values were calculated form the Korsmeyer-Peppas model equation, where n is the release exponent and a is the structural and geometrical component.

T (°C)	a	n	Drug transport mechanism	Rate as a function of time
25	0.00165	0.77	Non-Fickian/ anomalous transport	t^{n-1}
35	0.00268	0.76	Non-Fickian/ anomalous transport	t^{n-1}
45	0.00472	0.69	Non-Fickian/ anomalous transport	t^{n-1}

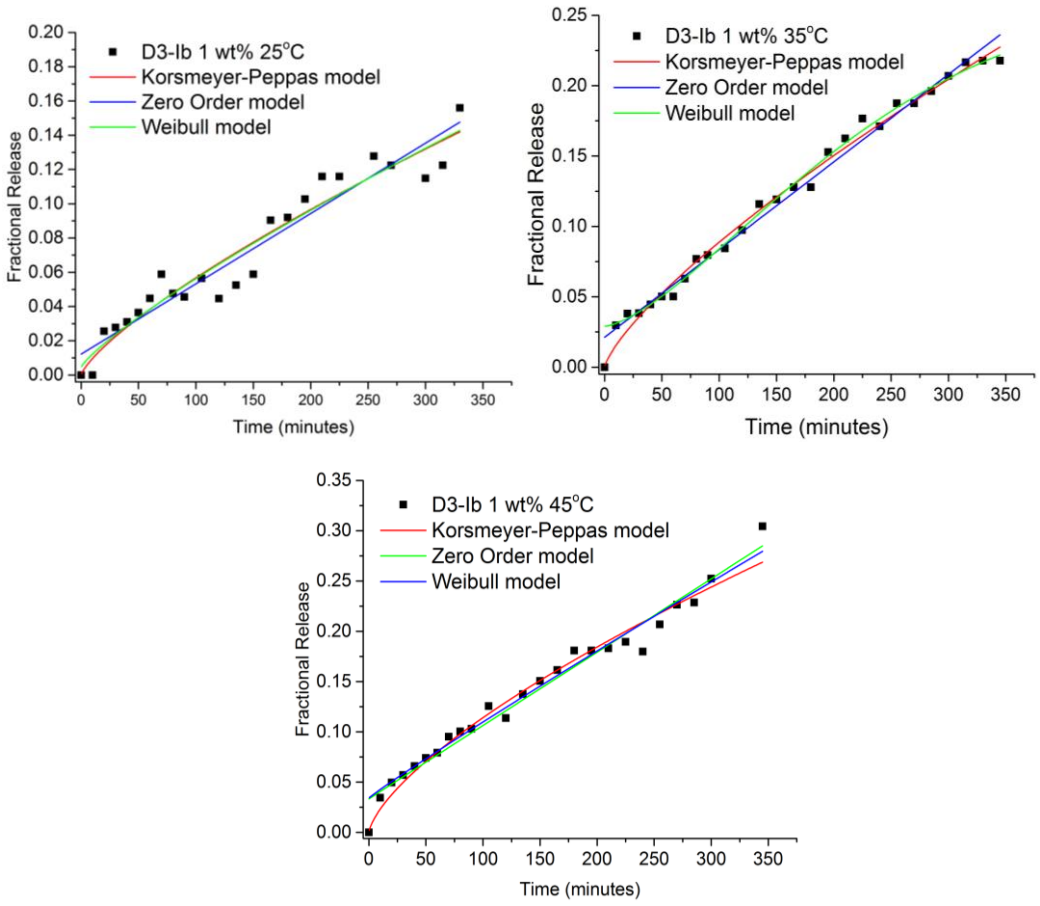

Figure 4.23: Results of curve fitting for matching release models to release of ibuprofen from PEO_{44}-*b*-$PDSMA_{16}$ bicontinuous nanospheres at 25, 35 and 45°C.

4.4.8 Effect of increasing DSMA wt % on the fractional release rate of ibuprofen

The fractional release of ibuprofen from P1-Ib 1 wt % (0 wt % DSMA), C4-Ib 1 wt % (75 wt % DSMA) and D3-Ib (100 wt % DSMA) were plotted against time at 25, 35 and 45°C with a fractional release of >0.1 and fitted linearly (Figure 4.24). It is evident from the release profiles that as the DMSA wt % within the hydrophobic block is increased the rate of release of ibuprofen decreases. This is evident from the slope of the linear fit but also by viewing the fractional release amounts across the same time scale.

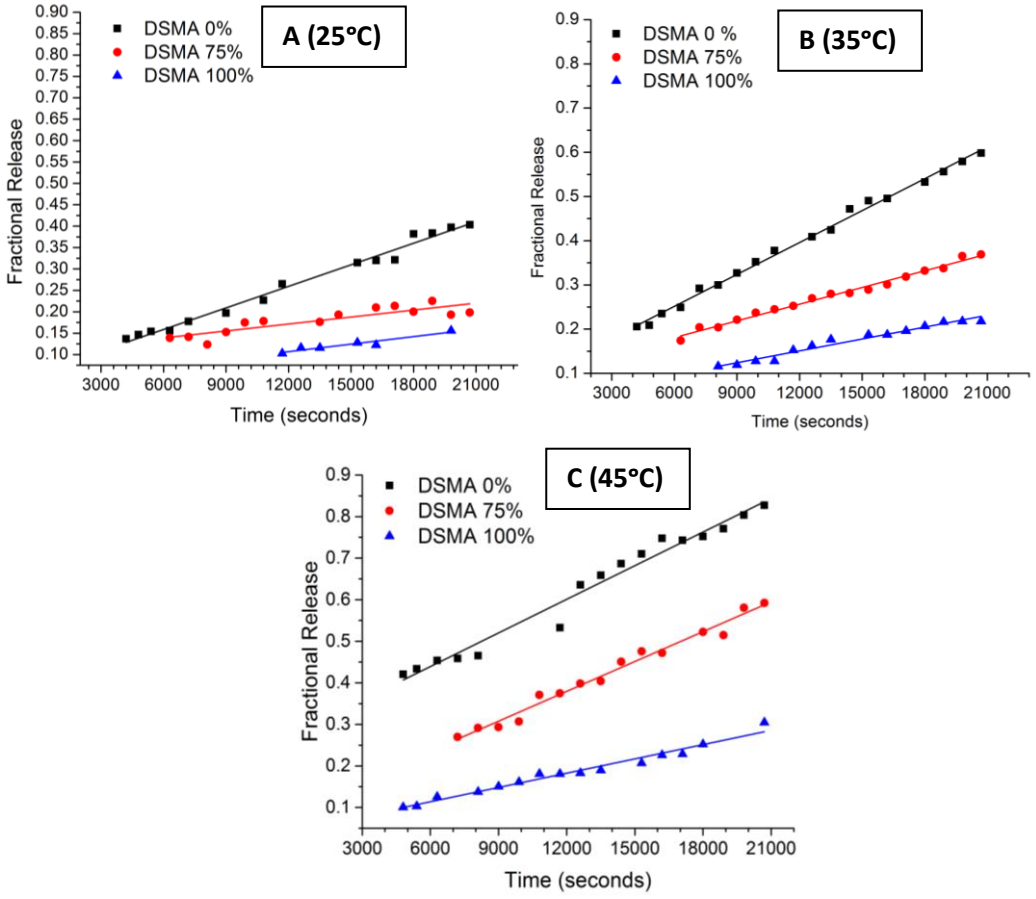

Figure 4.24: Linear Fit of the fractional release of ibuprofen from bicontinuous nanospheres with 0 % DSMA (P1-Ib), 75 % DSMA (C4-Ib) and 100 % DSMA (D3-Ib) at different experimental temperatures (A-25°C, B-35°C and C- 40°C for 0 % DSMA and 45°C for 75 % and 100 % DSMA). The slope of the line was used to calculate the release rate constants at each temperature.

This trend of decreased rate of release with an increase in DSMA wt % is also evident from the fractional rate constants plotted in Figure 4.25.

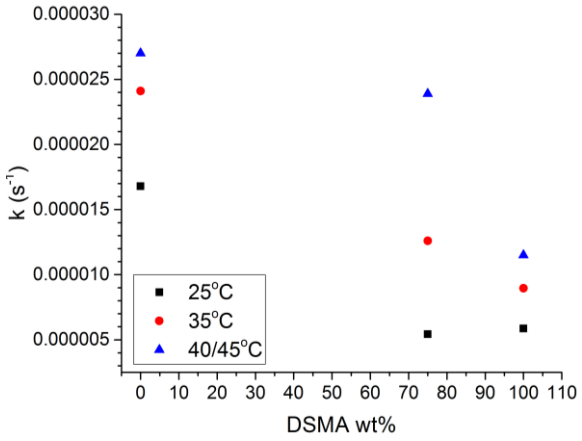

Figure 4.25: Fractional release rate constants at 25°C, 35°C and 40°C (for 0 wt % DSMA)/45°C (for 75 and 100 wt % DSMA) with increasing DSMA wt % within the hydrophobic block.

4.5 Conclusion

The construction of a concentration calibration curve of ibuprofen using UV-Vis spectroscopy was unsuccessful due to its inability to detect low concentrations of ibuprofen. The UV spectrum did however indicate two possible wavelengths to use when analysing the ibuprofen calibrants with HPLC (UV detector). Two additional wavelengths were determined by running a full UV spectrum of ibuprofen with the HPLC. The areas of the calibrants peaks were plotted against the relevant concentration to construct the calibration curve, three series of calibrants were analysed to establish error, which was minimal and the calibration curve gave an R^2 of 0.999.

Encapsulation of ibuprofen (20 mg) within PEO-b-PODMA bicontinuous nanospheres was attempted using a PEO-*b*-PODMA BCP with a PEO wt % of 25 %. This combination produced particles with an N_{ave} of 60 nm indicating micellisation occurred and bicontinuous nanospheres were not formed. It was established that this was most likely due to the interaction of ibuprofen with the the BCP, as ibuprofen can act as a surfactant. Bicontinuous nanospheres were successfully self-assembled in the presence of ibuprofen by lowering the hydrophilic blocks (PEO) wt % within the BCP to 15 %. There was minimal difference in N_{ave} analysed by DLS between the BCP at 1 wt % and the BCP at 1 wt % in the presence of ibuprofen. Cryo-TEM images confirmed that both solutions formed bicontinuous nanospheres.

The encapsulation of ibuprofen within bicontinuous nanospheres of PEO-*b*-(PODMA-*co*-PDSMA) with a PEO wt % of 15 % was attempted, however upon addition of water precipitation occurred although particles were still detected from DLS measurements. The self-assembly of PEO-*b*-(PODMA-*co*-PDSMA) (with varying DMSA wt %) with a PEO wt % of 25 % was carried out and the BCPs C1 (DSMA 25 wt %) and C4 (DSMA 75 wt %) successfully produced bicontinuous nanospheres in the presence of ibuprofen with no precipitation occurring, the N_{ave} of the BCPs with ibuprofen were not significantly different than when the BCPs were self-assembled without ibuprofen, clearly showing that the ibuprofen did not affect the polymers ability to form aggregates. The same results were seen for PEO-*b*-PDSMA (PEO 25 wt %) where

in the presence of ibuprofen PEO-b-PDSMA self-assembled to form bicontinuous nanospheres. C2 (DSMA 50 wt %) and C3 (DSMA 60 wt %) produced cloudy solutions upon addition of water but the suspensions were not stable.

The controlled release of ibuprofen from PEO-*b*-PODMA BNs was carried out at 25, 35 and 40°C. The rate of release and rate constants increased with an increase in measurement temperature as seen before for the release of pyrene from PEO-b-PODMA (PEO 25 wt %) BNs. The fractional release profiles were obtained and revealed that at 25 and 35˚C the drug transport mechanism was Non-Fickian diffusion which means that the release of ibuprofen was primarily determined by polymer relaxation rates as opposed to Fickian diffusion which is determined by diffusion rates. The 45˚C fractional release profile followed Fickian diffusion which was thought to be due to the BCP being heated above its T_m, causing a change in the dissolution profile.

The release profile of Ibuprofen from PEO_{45}-*b*-($PODMA_{15}$-*co*-$PDMSA_3$) (C1-DSMA 25 wt %) had a large number of outliers at all measurement temperatures, meaning the fractional release profiles could not be obtained so the details of the drug transport mechanism could not be obtained. The fractional release profiles of PEO_{45}-*b*-($PODMA_5$-*co*-$PDSMA_{13}$) (C4-DSMA 75 wt %) were obtained at set temperatures of 25, 35 and 45°C. As with PEO-*b*-PODMA the rate of release and rate constants increased with an increase in measurement temperature, this shows that the melting of the hydrophobic block effects the rate of dissolution of ibuprofen, the increased solubility of the ibuprofen upon an increase in temperature also plays a role in the increased rate of dissolution, the increase in rate of release is larger than the increase in ibuprofen solubility with an increase in temperature. This suggests that the melting of the hydrophobic block has a larger role in the increased rate of dissolution. The rate of release and rate constants were smaller than for PEO-*b*-PODMA indicating that an increased side chain length upon the hydrophobic blocks backbone plays a role in the rate of dissolution of ibuprofen. The fractional release profile at 35 and 45°C revealed the drug transport mechanism to be non-Fickian transport.

The fractional release profiles of PEO_{44}-*b*-$PDSMA_{16}$ (PEO 25 wt %) at set temperatures of 25, 35 and 45°C revealed non-Fickian transport mechanism for all temperatures,

this means the rate of dissolution relies more on the polymer relaxation time than the rate of diffusion. The rate of release and release rate constants were also determined from the fractional release profiles, the same trend of an increase in dissolution rate upon an increase in measurement temperature, seen with both PEO-*b*-PODMA and PEO-*b*-(PODMA-*co*-PDSMA) BNs, was seen for PEO-*b*-PDSMA. The rate constants were the smallest when comparing all the polymer systems, again this was further indication that a longer side-chain upon the polymer backbone affects the rate of dissolution of the ibuprofen.

From these results it is evident that the thermo-responsive hydrophobic block affects the rate of drug dissolution from bicontinuous nanospheres, and that an increased side-chain length, and therefore an increased T_m will also slow down the rate of release.

4.6 References

1. Kedar, U.; Phutane, P.; Shidhaye, S.; Kadam, V., Advances in polymeric micelles for drug delivery and tumor targeting. *Nanomedicine: Nanotechnology, Biology and Medicine* **2010,** *6* (6), 714-729.

2. Miyata, K.; Christie, R. J.; Kataoka, K., Polymeric micelles for nano-scale drug delivery. *Reactive and Functional Polymers* **2011,** *71* (3), 227-234.

3. Zhang, Y.; Chen, J.; Zhang, G.; Lu, J.; Yan, H.; Liu, K., Sustained release of ibuprofen from polymeric micelles with a high loading capacity of ibuprofen in media simulating gastrointestinal tract fluids. *Reactive and Functional Polymers* **2012,** *72* (6), 359-364.

4. Mohammed, A. R.; Weston, N.; Coombes, A. G. A.; Fitzgerald, M.; Perrie, Y., Liposome formulation of poorly water soluble drugs: optimisation of drug loading and ESEM analysis of stability. *International Journal of Pharmaceutics* **2004,** *285* (1–2), 23-34.

5. Rösler, A.; Vandermeulen, G. W. M.; Klok, H.-A., Advanced drug delivery devices via self-assembly of amphiphilic block copolymers. *Advanced Drug Delivery Reviews* **2001,** *53* (1), 95-108.

6. Yang, L.; Alexandridis, P., Physicochemical aspects of drug delivery and release from polymer-based colloids. *Current Opinion in Colloid & Interface Science* **2000,** *5* (1–2), 132-143.

7. Liechty, W. B.; Kryscio, D. R.; Slaughter, B. V.; Peppas, N. A., Polymers for Drug Delivery Systems. *Annual review of chemical and biomolecular engineering* **2010,** *1*, 149-173.

8. Chen, W.-H.; Luo, G.-F.; Lei, Q.; Jia, H.-Z.; Hong, S.; Wang, Q.-R.; Zhuo, R.-X.; Zhang, X.-Z., MMP-2 responsive polymeric micelles for cancer-targeted intracellular drug delivery. *Chemical Communications* **2015,** *51* (3), 465-468.

9. Allen, C.; Maysinger, D.; Eisenberg, A., Nano-engineering block copolymer aggregates for drug delivery. *Colloids and Surfaces B: Biointerfaces* **1999,** *16* (1–4), 3-27.

10. McKenzie, B. E.; Holder, S. J.; Sommerdijk, N., Assessing internal structure of polymer assemblies from 2D to 3D CryoTEM: Bicontinuous micelles. *Current Opinion in Colloid & Interface Science* **2012,** *17* (6), 343-349.

11. Holder, S. J.; Woodward, G.; McKenzie, B.; Sommerdijk, N. A. J. M., Semi-crystalline block copolymer bicontinuous nanospheres for thermoresponsive controlled release. *RSC Advances* **2014,** *4* (50), 26354-26358.

12. La, S. B.; Okano, T.; Kataoka, K., Preparation and characterization of the micelle-forming polymeric drug indomethacin-incorporated poly(ethylene oxide)–poly(β-benzyl L-aspartate) block copolymer micelles. *Journal of Pharmaceutical Sciences* **1996,** *85* (1), 85-90.

13. Kim, S. Y.; Shin, I. L. G.; Lee, Y. M.; Cho, C. S.; Sung, Y. K., Methoxy poly(ethylene glycol) and ϵ-caprolactone amphiphilic block copolymeric micelle containing indomethacin.: II. Micelle formation and drug release behaviours. *Journal of Controlled Release* **1998,** *51* (1), 13-22.

14. Lamprecht, A.; Saumet, J.-L.; Roux, J.; Benoit, J.-P., Lipid nanocarriers as drug delivery system for ibuprofen in pain treatment. *International Journal of Pharmaceutics* **2004,** *278* (2), 407-414.

15. J.S. Werry, M. G. A., Practitioner's Guide to Psychoactive Drugs for Children and Adolescents. **2013,** *2*, 27.

16. Kantor, T. G., Ibuprofen. *Annals of Internal Medicine* **1979,** *91* (6), 877-882.

17. Zhao, L.; Zhu, L.; Liu, F.; Liu, C.; Shan, D.; Wang, Q.; Zhang, C.; Li, J.; Liu, J.; Qu, X.; Yang, Z., pH triggered injectable amphiphilic hydrogel containing doxorubicin and paclitaxel. *International Journal of Pharmaceutics* **2011,** *410* (1-2), 83-91.

18. Li, K.; Yu, L.; Liu, X.; Chen, C.; Chen, Q.; Ding, J., A long-acting formulation of a polypeptide drug exenatide in treatment of diabetes using an injectable block copolymer hydrogel. *Biomaterials* **2013,** *34* (11), 2834-2842.

19. Licciardi, M.; Amato, G.; Cappelli, A.; Paolino, M.; Giuliani, G.; Belmonte, B.; Guarnotta, C.; Pitarresi, G.; Giammona, G., Evaluation of thermoresponsive properties and biocompatibility of polybenzofulvene aggregates for leuprolide delivery. *International Journal of Pharmaceutics* **2012,** *438* (1-2), 279-286.

20. Kotsuchibashi, Y.; Agustin, R. V. C.; Lu, J.-Y.; Hall, D. G.; Narain, R., Temperature, pH, and Glucose Responsive Gels via Simple Mixing of Boroxole- and Glyco-Based Polymers. *ACS Macro Letters* **2013,** *2* (3), 260-264.

21. Priya James, H.; John, R.; Alex, A.; Anoop, K. R., Smart polymers for the controlled delivery of drugs – a concise overview. *Acta Pharmaceutica Sinica B* **2014,** *4* (2), 120-127.

22. Ward, M. A.; Georgiou, T. K., Thermoresponsive Polymers for Biomedical Applications. *Polymers* **2011**.

23. Tran, T.; Hernandez, M.; Patel, D.; Burns, E.; Peterman, V.; Wu, J., Controllable and switchable drug delivery of ibuprofen from temperature responsive composite nanofibers. *Nano Convergence* **2015,** *2* (1), 1-7.

24. Zhu, Y.-f.; Shi, J.-l.; Li, Y.-s.; Chen, H.-r.; Shen, W.-h.; Dong, X.-p., Storage and release of ibuprofen drug molecules in hollow mesoporous silica spheres with modified pore surface. *Microporous and Mesoporous Materials* **2005,** *85* (1–2), 75-81.

25. Tran, T.; Hernandez, M.; Patel, D.; Wu, J., Temperature and pH Responsive Microfibers for Controllable and Variable Ibuprofen Delivery. *Advances in Materials Science and Engineering* **2015,** *2015*, 6.

26. S. Pattanaik, S. M., G. Pattnaik and J. Panda, Assay method development and validation of ibuprofen tablets by HPLC. *Der Pharmacia Sinica* **2013,** *4*, 91-96.

27. McKenzie, B. E.; Nudelman, F.; Bomans, P. H. H.; Holder, S. J.; Sommerdijk, N., Temperature-Responsive Nanospheres with Bicontinuous Internal Structures from a Semicrystalline Amphiphilic Block Copolymer. *Journal of the American Chemical Society* **2010,** *132* (30), 10256-10259.

28. R. Lui, M. L. F., G.S. Kwon, *Water-Insoluble Drug Formulation*. 2nd ed.; CRC Press: 2008; Vol. 13.

29. Discher, D. E.; Eisenberg, A., Polymer vesicles. *Science* **2002,** *297* (5583), 967-973.

30. Rub, M. A.; Azum, N.; Kumar, D.; Asiri, A. M.; Marwani, H. M., Micellization and microstructural studies between amphiphilic drug ibuprofen with non-ionic surfactant in aqueous urea solution. *The Journal of Chemical Thermodynamics* **2014,** *74*, 91-102.

31. Ridell, A.; Evertsson, H.; Nilsson, S.; Sundelöf, L.-O., Amphiphilic association of ibuprofen and two nonionic cellulose derivatives in aqueous solution. *Journal of Pharmaceutical Sciences* **1999,** *88* (11), 1175-1181.

32. Rangel-Yagui, C. O.; Hsu, H. W. L.; Pessoa-Jr, A.; Tavares, L. C., Micellar solubilization of ibuprofen : influence of surfactant head groups on the extent of solubilization. *Revista Brasileira de Ciências Farmacêuticas* **2005,** *41*, 237-246.

33. Tan, S. W.; Wang, H. J.; Tu, K. H.; Jiang, H. L.; Wang, L. Q., Ibuprofen induced drug loaded polymeric micelles. *Chinese Chemical Letters* **2011,** *22* (9), 1123-1126.

34. McKenzie, B. E.; Friedrich, H.; Wirix, M. J. M.; de Visser, J. F.; Monaghan, O. R.; Bomans, P. H. H.; Nudelman, F.; Holder, S. J.; Sommerdijk, N. A. J. M., Controlling Internal Pore Sizes in Bicontinuous Polymeric Nanospheres. *Angewandte Chemie International Edition* **2015,** *54* (8), 2457-2461.

35. Yalkowsky SH, D. R., The Aquasol Database of Aqueous Solubility. Tucson, AZ: Univ AZ, College of Pharmacy 1992; Vol. 5.

36. Miller, M. M.; Wasik, S. P.; Huang, G. L.; Shiu, W. Y.; Mackay, D., Relationships between octanol-water partition coefficient and aqueous solubility. *Environmental Science & Technology* **1985,** *19* (6), 522-529.

37. Pearlman, R. S.; Yalkowsky, S. H.; Banerjee, S., Water Solubilities of Polynuclear Aromatic and Heteroaromatic Compounds. *Journal of Physical and Chemical Reference Data* **1984,** *13* (2), 555-562.

38. Schwarz, F. P., Determination of temperature dependence of solubilities of polycyclic aromatic hydrocarbons in aqueous solutions by a fluorescence method. *Journal of Chemical & Engineering Data* **1977,** *22* (3), 273-277.

39. Garzón, L.; Martínez, F., Temperature Dependence of Solubility for Ibuprofen in Some Organic and Aqueous Solvents. *Journal of Solution Chemistry* **2004,** *33* (11), 1379-1395.

40. Khadka, P.; Ro, J.; Kim, H.; Kim, I.; Kim, J. T.; Kim, H.; Cho, J. M.; Yun, G.; Lee, J., Pharmaceutical particle technologies: An approach to improve drug solubility, dissolution and bioavailability. *Asian Journal of Pharmaceutical Sciences* **2014,** *9* (6), 304-316.

41. Fu, Y.; Kao, W. J., Drug Release Kinetics and Transport Mechanisms of Non-degradable and Degradable Polymeric Delivery Systems. *Expert opinion on drug delivery* **2010,** *7* (4), 429-444.

42. X. Ding, A. W. G. A., J.R. Robinson, *Remington: The Science and Practive of Pharamacy* 21st ed.; Lippincott, Williams and Wilkins: 2006; Vol. 47.

43. Dash S., M. P. N., Nath L., Chowdhury P., Kinetic modeling on drug release from controlled drug delivery systems. *Acta poloniae pharmaceutica* **2010,** *67* (3), 217-223.

44. Costa, P.; Sousa Lobo, J. M., Modeling and comparison of dissolution profiles. *European Journal of Pharmaceutical Sciences* **2001,** *13* (2), 123-133.

45. Korsmeyer, R. W.; Gurny, R.; Doelker, E.; Buri, P.; Peppas, N. A., Mechanisms of solute release from porous hydrophilic polymers. *International Journal of Pharmaceutics* **1983,** *15* (1), 25-35.

46. Chime Salome A*, O. G. C. a. O. I. I., Kinetics and Mechanisms of Drug Release from Swellable and Non Swellable Matrices: A Review. *Research Journal of Pharmaceutical, Biological and Chemical Sciences* **2013,** *4* (2), 97.

47. Crank, J., *The mathmatics of diffusion*. 2nd ed.; Clarendon Press: 1979.

48. Edwards, D. A., Non-fickian diffusion in thin polymer films. *Journal of Polymer Science Part B: Polymer Physics* **1996,** *34* (5), 981-997.

49. Alfrey, T.; Gurnee, E. F.; Lloyd, W. G., Diffusion in glassy polymers. *Journal of Polymer Science Part C: Polymer Symposia* **1966,** *12* (1), 249-261.

Chapter 5 : Introducing Acid Block and End Group Functionality into Bicontinuous Nanospheres Pre and Post Self-Assembly

5.1 Abstract

The interterwinned but not interconnected channels within these bicontinuous nanospheres gives them ideal properties for use in inorganic templating. With this in mind acid functionality was incorporated into the bicontinuous nanospheres. PMAA-*b*-PODMA (poly(methacrylic acid)-*block*-poly(octadecyl methacrylate)) was synthesised (via ATRP) with hydrophilic wt % of 20 %. The BCP was then self-assembled and cryo-TEM images revealed the presence of bicontinuous nanospheres alongside a number of other morphologies. An alternative approach to the incorporation of acid functionality within the bicontinuous nanospheres was through the self-assembly of PEO-*b*-PS and PEO-*b*-PODMA to form bicontinuous nanospheres followed by the removal of PEO via alkaline hydrolysis, leaving an acid end group. The sel-assembly of PEO-*b*-PS at various PEO-PS ratios also revealed stomatocytes, with bicontinuous nanospheres only observed under very specific conditions.

5.2 Introduction

In the previous chapters it has been demonstrated that PEO-*b*-(PODMA-*co*-PDSMA) (with varying ratios of PODMA:PDSMA) self-assembles to form nanospheres with a well-defined internal bicontinuous morphology. The dialysis method was used as outlined in the literature[1-4] and it was established that the hydrophilic block (PEO) should have a weight percent of 15-25 % for bicontinuous nanospheres to form. These bicontinuous nanospheres have shown promise for use as a controlled release drug delivery system as shown by Holder *et. al* (2014)[3] with the encapsulation and controlled release of pyrene previously discussed in chapter 4 but also in chapter 4 with the encapsulation and release of ibuprofen. Another proposed application of these complex bicontinuous nanospheres is as inorganic templates. Amphiphilic block copolymers have been used previously as templates for metal and superconductor particle formation when one block interacts with a metal or metal salt, they have also been used as templates for mesoporous silicates.[5] In particular for biomimetic mineralisation. Xu and Colfen *et. al* (2006) define biomimetic mineralisation as mineralisation in aqueous solutions at ambient or near ambient conditions.[6] This makes the bicontinuous nanospheres ideal for this application as

they are self-assembled in aqueous media with the internal structure composed of interconnected aqueous channels, it also keeps its complex structure when at ambient temperatures. The framework of the bicontinuous nanospheres could therefore potentially be used for biomimetics.

The synthesis of functionalised polymers has been widely investigated particularly with the use of ATRP.[7] ATRP is tolerant of a range of functional groups allowing functionality to be incorporated within the polymer chain by use of a funciotnal monomer. A number of initiators can be used to incorporate functionality onto the end groups of polymers, yielding functionalities such as vinyl, hydroxyl, epoxide, and cyano amongst other groups. The end groups can also be modified post polymerisation using nucleophilic substitution[8] or electrophilic addition reactions[9] when the polymerisation has been terminated with an alkyl halide group.

Acrylic acid and methacrylic acid are hard to directly synthesise via ATRP due to the interactions of the acid groups with the catalyst. Carboxylic acids react with the Cu(II) species to form metal carboxylates inhibiting the deactivation step.[10] They also interfere with nitrogen based ligands by protonating the nitrogen, interfering with the ligands ability to coordinate with the metal centre.[7] To overcome this, protecting groups on the acid group can be used during the ATRP reaction, and the acid deprotected post synthesis. The most commonly used protecting group is t-butyl[11, 12], however other acid protecting groups have been used such as trimethylsilyl, tertrahydropyranyl and benzyl[13] amongst others.[14]

This chapter reports the synthesis and self-assembly of an acid functionalised amphiphilic block copolymer that upon self-assembly form bicontinuous nanospheres. PAA can be synthesised with the use of a Cu(I)Br/PMDETA catalyst system and readily acts as a macroinitiator for the synthesis of block copolymers[15] but can also be grown from a polystyrene macroinitiator.[16] PMAA has previously been synthesised as the second block of a BCP from PS[17] and PEO[12] macroinitiators, but to the best of our knowledge it has not been used as a macroinitiator for the synthesis of a long-side chained methacrylate such as PODMA. Poly(methacrylic acid) (protected with a tert-butyl group) was synthesised *via* ATRP and took the place of the PEO block as the hydrophilic region within the copolymer PMAA-*b*-PODMA. This

acid functionality will allow the PMAA-*b*-PODMA bicontinuous nanospheres to be used in biomimetic mineralisation where the acid functional groups can interact with a metal or metal salt. The PMAA block gives the BCP a pH responsive property.[18] This means PMAA-*b*-PODMA could produce bicontinuous nanospheres that can be used as drug carriers with pH responsive properties alongside the thermo-responsive property due to the T_m of PODMA block[1] in contrast to using the LCST of the hydrophobic block.[19]

The use of poly(methacrylic acid) for mineralisation has been reported previously, where poly(methacrylic acid) brushes were synthesised using sodium methacrylate via surface initiated-ATRP with a Cu((I)Br/Cu(II)Br/bipyridine catalyst/ligand system in aqueous media at room temperature. The polymer was then used for the mineralisation of calcium carbonate.[20] Poly(methacrylic acid) has also been used previously as the hydrophilic block in the self-assembly of BCP aggregates such as micelles[12, 21, 22].

Acid functional groups have been widely used for the mineralisation of $CaCO_3$, the most abundant biomineral, which has three main crystalline polymorphs, calcite, aragonite and vaterite.[23] Addadi and Weiner reported the nucleation of calcite upon a poly(aspartic acid) absorbed on sulfonated polystyrene nucleation platform. Their results indicated that ordered arrangements of functional groups, particularly acid groups within a macromolecular template controlled the biomineralisation.[24] This observation, that having organised functional acidic groups upon the template surface leads to controlled crystallisation of $CaCO_3$ has been well documented.[25] The acid groups themselves and their orientation drives the biomineralisation of $CaCO_3$. In nature these mineral crystals form under well-controlled conditions commonly using an initial formation of an organic framework, upon which the crystals grow.[26] The organic matrixes are said to direct and control crystal growth and are characteristically acidic.

A second approach to introducing acid functionality I also reported in this chapter by the synthesis of poly(ethylene oxide)-*block*-poly(styrene) (PEO-*b*-PS) via ATRP with varying wt % of PEO. The ATRP of PS has been widely studied with the use of various initiators such as phenyl ethyl bromide[27], alkyl dithiocarbamate[28] and macroinitiators

such as PEO[29, 30]. The catalytic system tends to be Cu(I)Br/PMDETA with an anisole solvent, although Cu(I)Cl has also been used with success.[31, 32] PEO-*b*-PS was self-assembled following the dialysis method in THF and water with varying volume ratios of THF:water witth the intention off forming bicontinuous nanospheres with the BCP being acid functionalised post synthesis by the cleaving of the PEO block via alkaline hydrolysis. The advantage of using the PS block is it will produce a block copolymer with a high T_g (100˚C) which is in a glassy state and only starts to flow at temperatures above 100˚C. This means the bicontinuous morphology should be able to be preserved under high temperatures, unlike the PEO-*b*-PODMA bicontinuous nanospheres which lose their internal morphology upon increase in temperature above their T_m (23.4°C).

The self-assembly of PEO-*b*-PS to form bicontinuous nanospheres proved difficult, as the self-assembly of PEO-*b*-PODMA into bicontinuous nanospheres has been investigated thoroughly the removal of PEO from PEO-*b*-PODMA nanospheres with KOH was also investigated.

5.3 Experimental

5.3.1 Materials and Apparatus for the Synthesis of Block Copolymers Poly (methacrylic acid)-block-Poly (octadecyl methacrylate) and Poly (ethylene oxide)-block-Poly (styrene)

Poly (ethylene oxide) macroinitiators (I2-M_n 2160g/mol) were synthesised from Poly (ethylene glycol) methyl ether (M_n ca. 2000) (synthesis Chapter 2) and purified as reported in chapter 2. PEO_{44}-*b*-$PODMA_{19}$ (P4) was synthesised and purified following the method given in chapter 2. Ethyl- α-bromoisobutyrate (98 %), tert-butyl methacrylate (98 %), octadecyl methacrylate (ODMA), copper (I) bromide (98 %), copper (II) bromide (98 %), N,N,N',N'',N''-pentamethyldiethylenetriamine (PMDETA) (99 %), styrene (99 %), and potassium hydroxide were all used as received from Sigma-Aldrich. Aluminium oxide (activated, neutral, for column chromatography 50-200 µm) was purchased from Acros Organics. Tetrahydrofuran (analytical reagent grade), propan-2-ol and methanol (analytical grade) were purchased from Fisher Scientific. Xylene was purchased from BDH Lab Supplies. The deuterated solvent chloroform used for ^{1}H-NMR was used as purchased from Cambridge Isotope Laboratories Incorporated. Hydrochloric acid (36 %) was purchased from Fisher Scientific.

All reactions were performed under inert atmosphere using a Schlenk line. The infra-red spectra were recorded using a FT-IR spectrometer. ^{1}H-NMR spectra were obtained by dissolving the sample in deuterated chloroform ($CDCl_3$) and recorded on a JEOL ECS-400 spectrometer (400 MHz) at 25°C. Molecular weight averages and dispersity indices were determined using size exclusion chromatography on a Polymer Laboratories Gel Permeation Chromatographer (GPC) using two 5 µm mixed C PLgel columns at 40°C and an RI detector. The GPC was calibrated using poly (methyl methacrylate) standards (PMMA). The samples were all dissolved in THF and detected by a refractive index detector.

5.3.2 Materials and Apparatus for the Self-Assembly of Poly (methacrylic acid)-block-Poly (octadecyl methacrylate) and Poly (ethylene oxide)-block-Poly (styrene)

The BCP poly (methacrylic acid)-*block*-poly(octadecyl methacrylate) was synthesised following the method outlined in chapter 2 and poly (ethylene oxide)-*block*-poly (styrene) BCPs were synthesised following the method used in chapter 3. Distilled water was used. A syringe pump (220 Voltz, 0.1 Amps, 50 Hz) was used from Semat Technical Limited at 0.085 mL per minute. A 5 mL dialysis cassette was used with dialysis membrane (MWCO-12000-14000 Daltons) from MEDICELL international Ltd. The dialysis method was used as reported previously in chapters 2 and 3 with varying volumes of THF and water.

Dynamic Light Scattering

Dynamic light scattering (DLS) measurements were obtained on a Malvern High Performance Particle Sizer (Nano Zetasizer HPPS HPP5001) with a laser at a wavelength of 633 nm. The measurements were taken using a quartz cuvette containing a 1 mL sample. Measurements were taken at both 15 and 35°C, the temperature was set and the machine was left to settle at this temperature for 10 minutes, after this 10 measurements were taken and an average was obtained.

Transmission Electron Microscopy

Transmission electron microscopy (TEM) was carried out on all the self-assembled samples using a JEOL JEM (200-FX) TEM machine (120kV). 5 µl of the sample was pipetted onto a carbon-coated copper grid (200 mesh) and left for 5 minutes and then removed using suction. The sample was then stained by pipetting 5 µl of 5 % uranyl acetate onto the sample and then removed via suction.

Cryo-Transmission Electron Microscopy

Cryo-transmission electron microscopy (cryo-TEM) was performed on a FEI Cryo-Titan with a field emission gun operating at 300 kV. The sample vitrification process was as follows; 3 µl of the self-assembled solution was pipetted onto a surface plasma treated (Cresington Carbon Coater 208) Quantifoil holey (Cu 200 mesh) grid inside a FEI Vitrobot chamber (set to 100 % humidity at room temperature to prevent sample evaporation). The sample was then blotted and plunged into liquid ethane cooled by liquid nitrogen.

5.3.3 Synthesis of Poly (tert-butyl methacrylate) via ATRP I7-I13

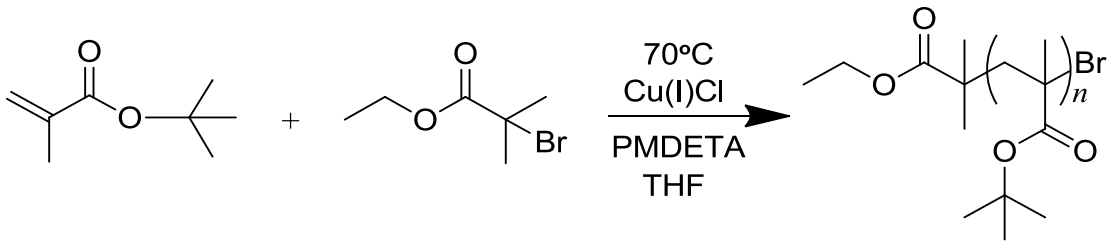

Scheme 5.1: Synthesis of Poly (tert-butyl methacrylate)

A typical procedure was used as follows; A 25 mL Schlenk tube was attached to a Schlenk line. Ethyl-α-bromoisobutyrate (0.61 g, 3.13 mmol) (initiator), Cu(I)Cl (0.62 g, 6.25 mmol), and PMDETA (3.25 g, 18.75 mmol) were added to the Schlenk tube with a magnetic stirrer. THF (27.78 g, 31.25 mL) was deoxygenated, by bubbling nitrogen through the sample for 30 minutes, and added to the tube via a nitrogen purged syringe to make a solution of 0.1 mol/L of ethyl-α-bromoisobutyrate. The monomer tert-butyl methacrylate (tBMA) (20 g, 140.65 mmol) was added to the flask via a nitrogen purged syringe with continued stirring. The solution then underwent three freeze-pump-thaws to remove the oxygen. The solution was sealed under vacuum and heated to 70°C for 4 hours. The reaction was terminated by placing the schlenk tube into liquid nitrogen. The resultant solution was diluted with THF and run through an alumina column to remove the ligand and copper catalyst. The solvent was evaporated off (rotary evaporator) and the polymer precipitated out into a 50:50 methanol/water mix. The resultant solid was then dried under vacuum at room temperature. The polymer was characterised using GPC, ^{1}H-NMR and ^{13}C-NMR then used as a macroinitiator in a block copolymerisation with the protecting group removed post synthesis. Table 5.1 shows the different conditions used to make PtBMA macroinitiator. **(I6) ^{1}H NMR (400 MHz, $CDCl_3$, ppm) δ:** 1.06 (broad, 3H, -CH_2-C-C**H_3**), 1.41 (broad, 9H, -$C(CH_3)_3$)), 1.81 (broad, 2H, -C**H_2**-COO-), 4.10 (multiplet, 2H, CH_3C**H_2**O-). **(I6) ^{13}C NMR ($CDCl_3$, ppm) δ:** 14.1 (**C**H_3CH_2O-), 25.7 ($C(CH_3)_2COO$-), 27.9 ($C(CH_3)_3$), 28.1 (**C**H_3C-), 46.2 (CH_3**C**-), 46.5 (**C**$(CH_3)_2$), 68.1 (**C**H_2C(Br)-), 80.9 (-**C**$(CH_3)_3$), 173.2 (CH_3CH_2O**C**(O)-), 177.0 (-**C**$OOC(CH_3)_3$). **(I6) FTIR (cm^{-1}):** 2978 C-H stretch, 2937 CH- stretch, 1701 C=O stretch, 1475 C-H bend, 1251 C-C stretch, 1138 C-O stretch, 844 C-Br stretch.

Table 5.1: Reaction conditions for macroinitiators I7-I13 synthesised *via* the above method.

Code	EBIB	tBMA	PMDETA	BPy	C(I)Cl	Cu(I)Br	Cu(II)Br	Solvent	Temperature (°C)	Reaction time (hour)
I7	0.151 g	5.00 g	81 mg	-	0.154 g	-	-	THF	90	3.5
I8	0.153 g	5.00 g	-	0.244 g	-	0.224 g	-	THF	90	4
I9	0.781 g	5.00 g	0.271 g	-	-	0.112 g	0.0175 g	THF	90	4
I10	0.781 g	5.00 g	0.271 g	-	-	0.112 g	0.0175 g	Xylene	75	4
I11	0.781 g	5.00 g	0.271 g	-	-	0.112 g	0.0175 g	Xylene	75	4.5
I12	0.781 g	5.00 g	0.271 g	-	-	0.112 g	0.0175 g	Xylene	75	4.5
I13	0.781 g	5.00 g	0.271 g	-	-	0.112 g	0.0175 g	Toluene	75	4

5.3.4 Synthesis of Poly (methacrylic acid)-*block*-Poly (octadecyl methacrylate) via ATRP (A1-A19)

Step 1: Polymerisation of Poly (tert-butyl methacrylate)-*block*-Poly (octadecyl methacrylate)

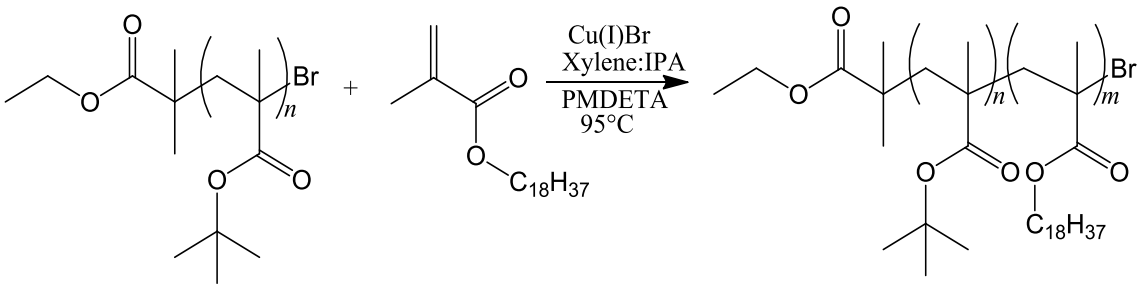

Scheme 5.2: Synthesis of Poly (tert-butyl methacrylate)-block-Poly (octadecyl methacrylate).

The synthesis of PODMA used in chapter 2 was initially followed for the synthesis of PtBMA-*b*-PODMA as follows; Cu (I) Br (0.0435 g, 0.30 mmol) was placed in a 25 mL Schlenk tube with a magnetic stirrer. The P(tBMA) macroinitiator (I6) (1.00 g, 0.15 mmol) was dissolved in xylene:IPA mixture (9:1) (6 mL) and then added to the Schlenk tube along with PMDETA (0.1577 g, 0.9102 mmol) and octadecyl methacrylate (ODMA) (7.1369 g, 21.08 mmol). The Schlenk tube was sealed and the mixture was degassed (N_2) for 1 hour. The mixture was then stirred at 95°C for 24 hours under nitrogen. After 24 hours the reaction was stopped by exposure to air and diluting with THF. The mixture was run through an alumina column to remove the catalyst and ligand and three quarters of the solvent was evaporated off (rotary evaporator). The reaction mix was analysed with GPC which revealed a bimodal distribution. Therefore the polymer was back-precipitated into methanol drop wise at 0°C. The resultant solid was then dried in a vacuum oven at room temperature overnight. The block copolymer was characterised using ^{1}H-NMR and GPC. The synthesis of PtBMA-*b*-PODMA was attempted using macroinitiators I6-I13 under a range of conditions following the above method. Table 5.2 shows the reaction conditions for the synthesis of all PtBMA-*b*-PODMA BCPs.

(A1) ^{1}H NMR (400 MHz, $CDCl_3$, ppm) δ: 0.88 (triplet, 3H, -$(CH_2)_{17}$-C**H_3**) 1.02 (broad peak, 3H, -CH_2-C-C**H_3**), 1.28 (broad peak, 38H, -(C**H_2**)$_{16}$-), 1.54 (singlet, 9H, -C$(CH_3)_3$), 1.60 (broad peak, 2H, -C**H_2**-C-CH_3), 3.92 (broad peak, 2H, -COO-C**H_2**-). **(A1) FTIR (cm$^-$**

[1]): 2916 C-H stretch, 2848 C-H stretch, 1728 C=O stretch, 1465 C-H stretch, 1240 C-C stretch, 1145 C-O stretch, 721 C-H rock.

Table 5.2: Reaction conditions for PtBMA-*b*-PODMA BCPs A2-A19 synthesised *via* the above method at 95°C for 24 hours.

Code	PtBMA	ODMA	PMDETA	BPy	Cu(I)Br	Cu(II)Br	Cu(I)Cl	Cu(II)Cl	Solvent	[I]:[M]:[Cu(I)]:[Cu(II)]:[Ligand]
A1	I6-1.00 g	7.136 g	0.158 g	-	44 mg	-	-	-	Xylene:IPA	1 : 140 : 2 : 0 : 6
A2	I7-1.00 g	2.326 g	51 mg	-	14 mg	-	-	-	Xylene:IPA	1 : 140 : 0.5 : 0 : 1
A3	I6-1.00 g	2.969 g	44 mg	-	-	-	12 mg	-	Xylene:IPA	1 : 34 : 0.5 : 0 : 1
A4	I6-0.50 g	0.873 g	13 mg	-	-	-	7 mg	1 mg	Xylene:IPA	1 : 34 : 1 : 0.1 : 1
A5	I6-0.50 g	0.873 g	-	11 mg	-	-	7 mg	-	Xylene:IPA	1: 34 : 1: 0 : 1
A6	I6-0.50 g	0.873 g	13 mg	-	-	-	7 mg	-	Toluene	1: 34 : 1: 0 : 1
A7	I8-0.50 g	1.742 g	43 mg	-	12 mg	-	-	-	Xylene:IPA	1 : 62 : 1 : 0 : 3
A8	I8-0.50 g	1.236 g	43 mg	-	12 mg	-	-	-	Xylene:IPA	1 : 44 : 1 : 0 : 3
A9	I9-0.50 g	1.428 g	39 mg	-	16 mg	-	-	-	Xylene:IPA	1 : 19 : 0.5 : 0 : 1
A10	I9-0.50 g	1.428 g	39 mg	-	-	-	11 mg	-	Xylene:IPA	1 : 19 : 0.5 : 0 : 1
A11	I10-1.00 g	2.982 g	85 mg	-	35 mg	-	-	-	Xylene:IPA	1 : 19 : 0.5 : 0 : 1
A12	I10-0.25 g	0.456 g	21 mg	-	8 mg	-	-	-	Xylene:IPA	1 : 11 : 0.5 : 0 : 1
A13	I10-0.25 g	0.456 g	21 mg	-	-	-	6 mg	-	Xylene:IPA	1 : 11 : 0.5 : 0 : 1
A14	I10-0.20 g	0.364 g	21 mg	-	-	-	8 mg	-	Xylene:IPA	1 : 11 : 0.75 : 0 : 1
A15	I11-1.00 g	2.092 g	0.107 g	-	-	-	31 mg	-	Xylene:IPA	1 : 10 : 0.5 : 0 : 1
A16	I11-1.00 g	2.092 g	0.107 g	-	-	-	31 mg	-	Toluene	1 : 10 : 0.5 : 0 : 1
A17	I12-0.25 g	0.517 g	29 mg	-	-	-	7 mg	-	Xylene:IPA	1 : 9 : 0.5 : 0 : 1
A18	I13-0.25 g	0.517 g	29 mg	-	-	-	7 mg	-	Toluene	1 : 9 : 0.5 : 0 : 1
A19	I13-0.25 g	0.517 g	26 mg	-	-	-	7 mg	-	Toluene	1 : 9 : 0.5 : 0 : 1

Step 2: Deprotection of poly(tert-butyl methacrylate)-*block*-poly(octadecyl methacrylate) (A1)

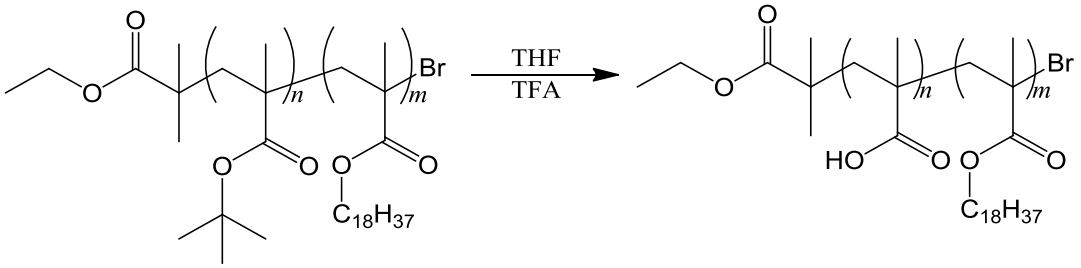

Scheme 5.3: Removal of the protecting group (tert-butyl) via acid addition to yield Poly(methacrylic acid)-block-Poly(octadecyl methacrylate).

The following method was used to remove the tert-butyl protecting group; The BCP was dissolved in THF to make a 5 wt % solution. TFA five times the molar amount of tBMA was added and the solution was stirred for 24 hours at room temperature. The polymer solution was then concentrated by evaporation of the solvent (rotary evaporation) and the product precipitated out into ethanol. The resultant solid was then dried in a vacuum oven at room temperature overnight. The block copolymer was characterised using ^{13}C-NMR, GPC and ^{1}H-NMR.

(A1) ^{1}H NMR (400 MHz, $CDCl_3$, ppm) δ: 0.88 (triplet, 3H, -$(CH_2)_{17}$-C**H**$_3$) 1.02 (broad peak, 3H, -CH_2-C-C**H**$_3$), 1.28 (broad peak, 38H, -(C**H**$_2$)$_{16}$-), 1.54 (singlet, 9H, -C$(CH_3)_3$), 1.60 (broad peak, 2H, -C**H**$_2$-C-CH_3), 3.92 (broad peak, 2H, -COO-C**H**$_2$-). **(A1) FTIR (cm^{-1}):** 3348 O-H stretch, 2920 C-H stretch, 2852 C-H stretch, 1730 C=O stretch, 1458 C-H stretch, 1240 C-C stretch, 1149 C-O stretch, 669 C-H rock.

5.3.5 Synthesis of Poly(ethylene oxide)-block-Poly(styrene) via ATRP for S1-S3

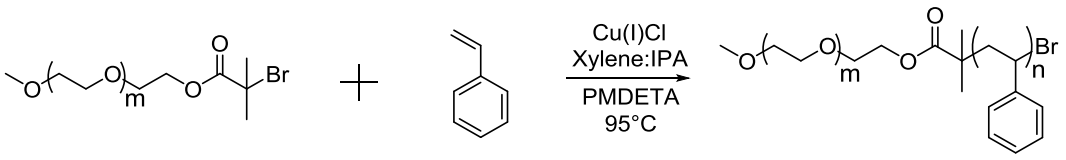

Scheme 5.4: Synthesis of PEO-*b*-PS via ATRP using a PEO macroinitiator

PEO macroinitiator (OMI02, 1.0 g, 0.46 mmol) was dissolved in xylene:IPA (5 mL 9:1) and then placed in a Schlenk tube. Styrene (4.0015 g, 38.42 mmol), PMDETA (0.4814 g, 2.78 mmol) and Cu(I)Cl (0.09166 g, 0.93 mmol) were placed in the Schlenk tube along with a magnetic stirrer bar. The tube was sealed and the reaction mixture degassed for 1 hour. The reaction then left for 66-70 hours at 95°C under continuous stirring. After 66-70 hour the reaction was exposed to air and a sample was taken for both ^{1}H-NMR and GPC. The reaction mix was dissolved in THF and passed down a column filled with aluminium oxide to remove the copper catalyst. The solvent was evaporated off using a rotary evaporator. The product was precipitated out into methanol drop wise at 0°C. The resultant solid was collected via Buchner filtration and dried in a vacuum oven at room temperature. It was then analysed using ^{1}H-NMR and GPC. Variations in reaction conditions are given in Table 5.3

(S1) ^{1}H NMR (400 MHz, $CDCl_3$, ppm) δ: 1.42 (broad peak, 2H, -C**H$_2$**CH(C_6H_5)-), 1.85 (broad peak, 1H, -CH_2C**H**(C_6H_5)-), 3.38 (singlet, 2H, -OC**H$_3$**), 3.64 (broad peak, 4H, -C**H$_2$**C**H$_2$**O-), 6.3-7.2 (broad peaks, 5H, -CH_2CH(C_6**H$_5$**)-). **(S1) ^{13}C NMR ($CDCl_3$, ppm) δ:** 40.5 (-**C**(C_6H_5)-), 44.2 (-**C**H_2-C(C_6H_5)-), 70.6 (-**C**H_2**C**H_2O-), 125.7 (-C_6H_5 para), 127.7 (-C_6H_5 ortho), 128.1 (-C_6H_5 meta), 145.5 (-C-(**C**-(C_5H_5))). **(S1) FTIR (cm^{-1}):** 3024 C-H stretch (aromatics), 2924 C-H stretch (alkanes), 1600 C=O stretch, 1492 C-C stretch (aromatic), 1452 C-H bend (alkane), 1105 C-O stretch, 756 C-H rock (alkanes), 696 C-H "oop" (aromatic), 538 C-Br stretch.

Table 5.3: Reaction conditions for polymers S1-S3 synthesised *via* the above method.

Code	Styrene	PEO macro-initiator	PMDETA	Cu(I)Cl	PEO: Styrene (molar ratio)	Temperature (˚C)	Reaction time (hour)
S1	5.589 g	I2-1.00 g	0.481 g	0.092 g	1:117	95	66
S2	4.008 g	I2- 1.00 g	0.481 g	0.092 g	1:83	95	96
S3	2.750 g	I2- 0.92 g	0.443 g	0.085 g	1:62	95	70

5.3.6 Self-Assembly of Poly(methacrylic acid)-*block*-Poly(octadecyl methacrylate)

The block copolymer A1 was dissolved in 4 mL of THF and stirred at 35°C. 6 mL of deionised water was added drop-wise *via* a syringe pump at a rate of 5.15 mL/hr. The solution was then dialysed against 3 L of deionised water pre-heated to 35°C. The solution was dialysed for 24 hours with the water being changed twice. The solution was then analysed using DLS and TEM to establish the particle size and morphology. This method was used for all weight percent's in solution.

5.3.7 Self-Assembly of Poly(ethylene oxide)-*block*-Poly(styrene)

The block copolymers S1-S3 were dissolved in varying volumes of THF (4-8 mL) and left stirring at 45°C. Deionised water was added drop-wise via a syringe pump at a rate of 5.15 mL/hr to make the solution up to 10 mL. The solution was then dialysed against 3 L of deionised water pre-heated to 45°C. The solution was left dialysing to remove the THF, with the water being changed twice over a 24 hour period. The BCP solution was then analysed using DLS and TEM to determine the particle sizes, dispersity and morphology. This method was used for all self-assembled polymer solutions of S1-S3.

5.3.8 Removal of PEO from PEO_{44}-*b*-PS_{114} bicontinuous nanospheres via alkaline hydrolysis

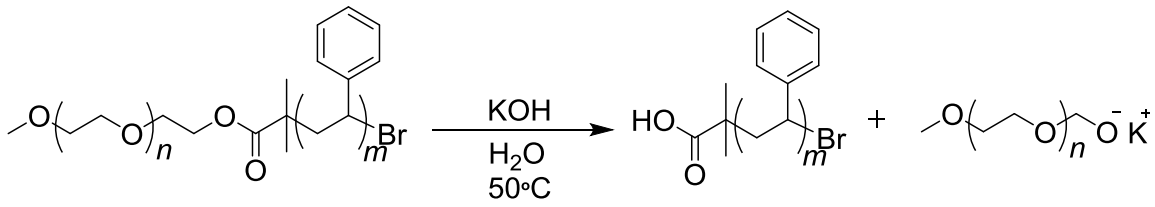

Scheme 5.5: Removal of PEO from PEO_{44}-*b*-PS_{114} bicontinuous nanospheres using KOH.

S1 was self-assembled at 0.1 wt % in solution using 6 mL of THF following the method outlined in section 0. A stir bar and S1 0.1 wt % 6 mL THF (5 ml) were placed in a round bottom flask. Potassium hydroxide (0.41 g, 7.31 mmol) was added to the flask to make the solution up to concentration of 1.46 mol dm^{-3}. The solution was heated to 50°C and left to stir overnight. The solution was then filtered using a 1.2 µm filter and dialysed against distilled water at 35°C overnight. The solution was then analysed using ^{1}H-NMR, DLS and TEM.

5.4 Results and Discussion

5.4.1 Synthesis Characterisation of Poly (tert-butyl methacrylate) Macroinitiators I6-I19

Poly (tert-butyl methacrylate) was synthesised using ATRP, the procedure is outlined in detail in section 5.2.2. Yang *et al.*[11] synthesised PtBMA via ATRP using a PEG macroinitiator, they used Cu(I)Cl/PMDETA as the catalyst/ligand system, THF as the solvent and the reaction takes place at 90°C. Tam *et al.*[12] follows a similar procedure using PEG as the macroinitiator in the synthesis of PtBMA, Cu(I)Cl as the catalyst and the reaction takes place at 95°C however the solvent used was anisole and the ligand was HMTETA. We used a modified version of both procedures initially using THF as the solvent, PMDETA/Cu(I)Cl as the ligand/catalsyst system and EBIB as the initiator.

This synthesis gave a polymer with a low dispersity and with a well-defined molecular weight (See Table 5.4). However not all the polymer chains initialise when used as a macroinitiator in the synthesis of PtBMA-*b*-PODMA resulting in bimodal distribution when analysed using GPC. This could be due to slow-initiation because of the C-Cl active end group. A well-controlled and successful ATRP relies on a good equilibrium between the activation step (K_{act}) of forming radicals, and the deactivation step (K_{deact}) of forming alkyl halides[33-35]. It is now well known that the relationship between K_{act} and K_{deact} needs to be $K_{act} << K_{deact}$, i.e a low radical concentration is needed throughout the reaction to ensure control and discourage termination.[36, 37] Matyjaszewski *et al.*[36] studied the K_{act} for series of ATRP alkyl halide initiators and found that a number of factors had an effect on the activity of the initiator. The position of the halide group within the molecule, i.e. primary secondary or tertiary, had an effect on the initiator activity with K_{act} following the order $1^o < 2^o < 3^o$. The substituent in the α position, in relation to the halide group, effected the K_{act}, with a more radical stabilising substituent the initiator was more active. The halide group itself has an effect on the K_{act} of the initiator, Matyjaszewski *et al.* found that alkyl bromides are more active that alkyl chlorides, this was due to the C-Br bond being much weaker than the C-Cl bond allowing atom transfer to take place more easily. It was thought that synthesising the macroinitiator using a CuBr catalyst, which would ensure all the macroinitiator chains were terminated by a bromine, would increase

the K_{act} allowing all the initiator chains to activate, and therefore a more controlled ATRP of PODMA would take place.

After the product had been dried in the vacuum oven it was characterised using GPC and ^{1}H-NMR. The P(tBMA) was dissolved in THF, filtered and analysed using GPC. This was to determine the molecular weight parameters and the dispersity index of the polymer. The M_n of the polymer was also calculated using ^{1}H-NMR, these values can be seen in Table 5.4.

All macroinitiators were synthesised using EBIB as the initiator, the other conditions varied. Both I6 and I7 PtBMA macroinitiators were synthesised under the same conditions (PMDETA/Cu(I)Cl in THF at 90°C) with the only difference being the reaction time, I6 was left for 3.5 hours and I7 was left for 4 hours. I6 was the most successful, it produced a polymer with the smallest distribution in molecular weight (Đ=1.25) while reaching its target DP, when compared to I7 that was left for longer and produced a polymer with a DP above the targeted value. I8 was synthesised with a BPy/Cu(I)Br catalyst system in THF at 90°C to see whether the initiator efficiency could be improved compared to I6f. It produced a polymer with a DP close to the target value, however it had a dispersity value higher (1.38) than the recommended 1.3 for a controlled ATRP. I9 was synthesised with PMDETA/Cu(I)Br, Cu(II)Br catalyst system in THF at 90°C. It produced the polymer with the lowest Đ of 1.22 indicating a controlled reaction and a narrow distribution in molecular weight, however the achieved DP was above the targeted DP so the reaction could have been more controlled. I10-I13 were synthesised under the similar conditions as I9 with the same target DP, however I10-12 were synthesised at 75°C in xylene and I13 was synthesised in toluene at 75°C. Both I10 and I11 reactions produced a polymer with a dispersity of <1.3 however the DP for both was above the targeted DP of 9. I12 and I13 produced polymers that achieved the target DP of 9, however their dispersity was slightly >1.3 indicating a slight lose in control. I6 was the most successful synthesis using Cu(I)Cl as the catalyst, it produced a polymer with the smallest distribution in molecular weight while achieving the target DP.

Table 5.4: Molecular weight parameters and DP value of PtBMA macroinitiator calculated using ^{1}H-NMR and GPC.

Code	DP Aim	M_n[a] (Da)	M_w[a] (Da)	Đ[a]	DP[b]	M_n[b] (Da)
I6	45	10900	13700	1.25	45	6580
I7	50	18900	24300	1.28	62	8998
I8	45	6815	9425	1.38	41	6016
I9	9	2890	3520	1.22	15	2248
I10	9	2340	3030	1.29	13	2040
I11	9	3520	3250	1.29	10	1614
I12	9	2500	3260	1.31	9	1472
I13	9	2100	2780	1.32	9	1472

[a]Calculations from GPC using PMMA standards.
[b] Calculations from ^{1}H-NMR comparing the integrals peak D (CH_2) to peak B (-$C(CH_3)_3$).

Figure 5.1 is a comparison of the ^{1}H-NMR spectrum collected for I6 (PtBMA) and the monomer tBMA. It is evident from the ^{1}H-NMR spectra below that the polymerisation was successful. This is clear from the absence of the two peaks at 5.58 ppm and 6.15 ppm that represent the protons (protons 1 and 2) adjacent to the double bond. The successful polymerisation is further illustrated by the appearance of new peaks attributable to the polymer backbone on the spectrum of P(tBMA) which have been assigned as shown and agree with previous literature.[12] This ^{1}H-NMR should be taken to represent all PtBMA macroinitiators synthesised. The singlet at 1.56 ppm is due to water from the precipitation process and the multiplet at 3.76 ppm is due to the THF used in the synthesis.

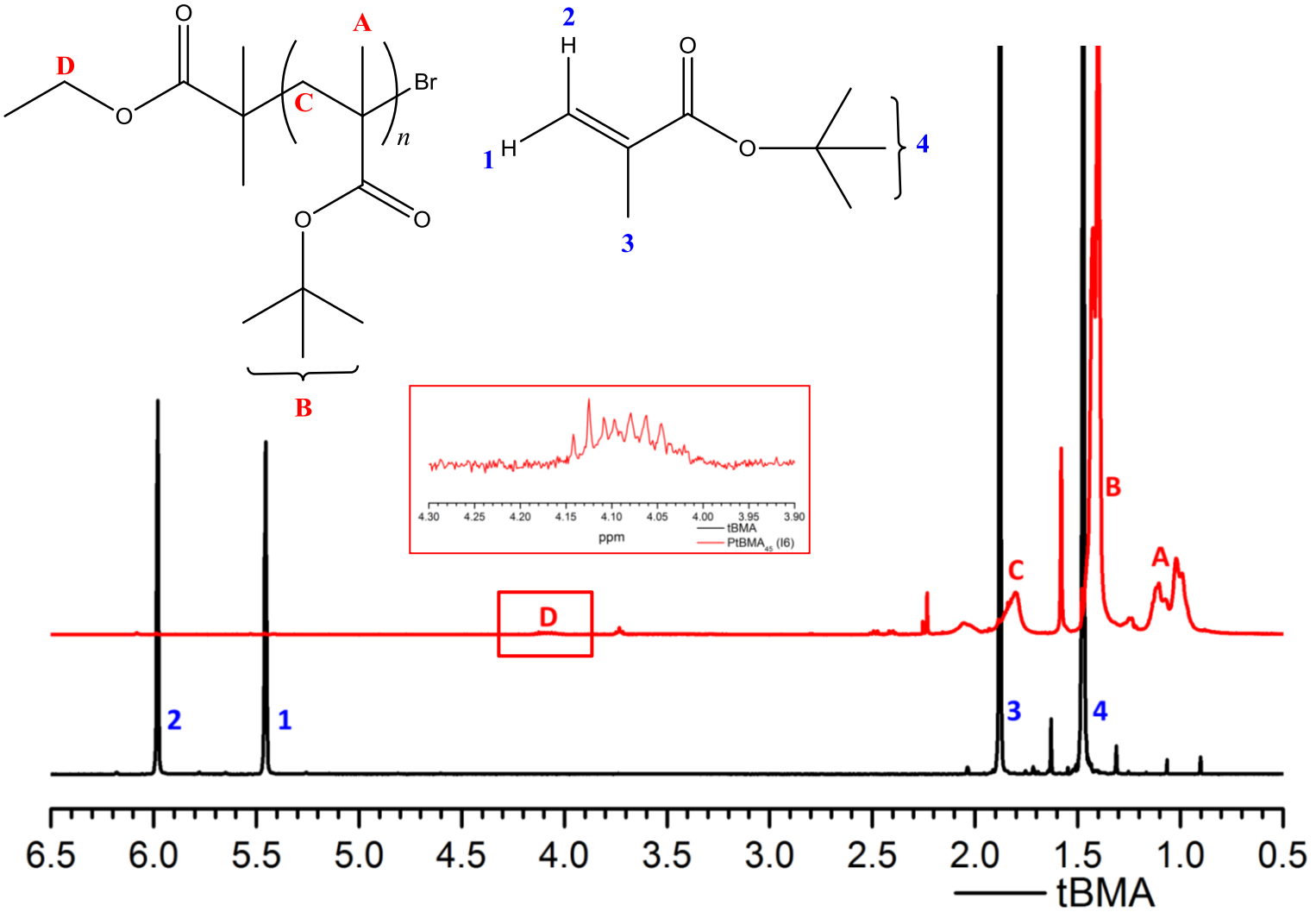

Figure 5.1: ^{1}H-NMR spectra of I6 (PtBMA) macroinitiator overlaid with tert-butyl methacrylate. The peak at 1.53 in the spectrum of I6 is present due to water.

5.4.2 Characterisation of Poly(methacrylic acid)-*block*-Poly(octadecyl methacrylate)

The block copolymers P(tBMA)-*b*-PODMA were synthesised following the same method used for the synthesis of PEO-*b*-PODMA, using macroinitiators I6-I13. The reaction was an ATRP synthesis using a number of different ligand/catalyst systems and two different solvents (toluene and xylene:IPA). The amount of solvent has an effect on the rate of reaction, the choice of solvent is dictated by the potential chain transfer, when a low molecular weight is desired (M_n < 20,000) toluene and xylene are ideal.[38] P(tBMA)-*b*-PODMA was characterised with GPC and ^{1}H-NMR to determine the purity and the molecular weight parameters. A number of PtBMA-*b*-PODMA BCPs exhibited bimodal molecular weight distributions when analysed with GPC. The M_w (x_c) and the relative peak %, calculated from the peak area, were obtained for peak 1 (left) and peak 2 (right) for all bimodal BCP distributions using the multiple peak fit function on Origin Lab. A number of different functions were tested and the best fit was used to determine the parameters displayed in Table 5.5. Some BCP distributions could be fitted more effectively than others regardless of the choice of function, an example of this is displayed in Figure 5.2.

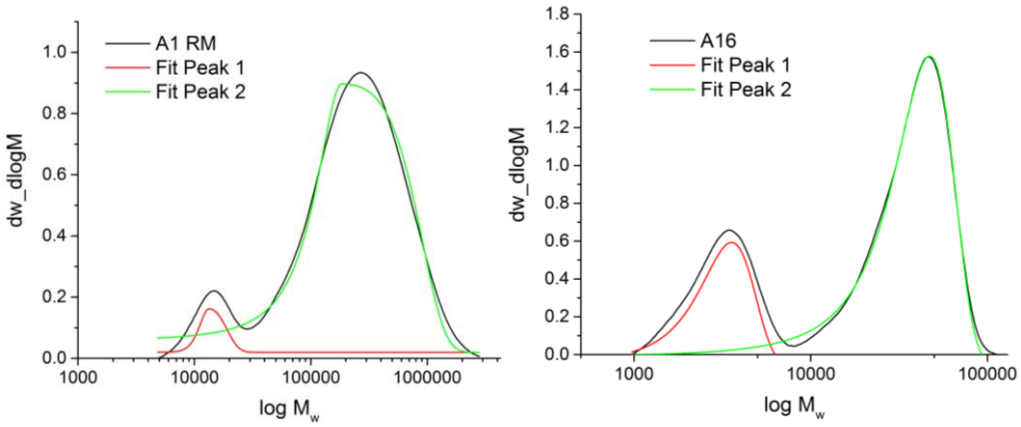

Figure 5.2: GPC traces showing a bad fit of A1 fitted with multiple peak fit function bigaussian, and a good fit of A16 fitted with multiple peak fit function gauss. Both were the best performing functions for the individual BCP distributions respectively.

The bimodal distributions of the BCPs showed that two M_w distributions were present in the BCP samples, with the first distribution being close to that of the relevant macroinitiator. This is confirmed by looking at the M_w results of the two peaks calculated using the multiple peak fit, these values are given in Table 5.5.

The table shows that the overall trend for peak 1, for all bimodal BCPs, is a slight increase in M_w when compared to the relevant macroinitiator. This suggests that a proportion of the macroinitiator has either not initiated to grow the PODMA block or slow initiation has occurred where some ODMA units have been incorporated but not at the same rate as the other macroinitiator chains. The M_w values for Peak 2, for all bimodal BCPs, suggest that a proportion of the PtBMA macroinitiator chains have had fast initiation allowing the controlled growth of the PODMA block. The peak percentages for peak 1 and 2, for all bimodal BCPs, were calculated from the relevant peak areas.

Table 5.5: GPC M_w and peak % results for all PtBMA-*b*-PODMA polymers that showed a bimodal distribution in molecular weight.

Code	Fit	Peak 1 M_w (Da)	Peak 2 M_w (Da)	Peak 1 %	Peak 2 %	Đ
I6	**-**	***10900***	**-**	**-**	**-**	***1.25***
A1	Bigaussian	13400	184100	0.2	99.8	4.00
A3	Giddings	15100	113900	5	95	2.88
A6	Bigaussian	14100	50600	20	80	2.28
I7	**-**	***18900***	**-**	**-**	**-**	***1.28***
A2	Bigaussian	14600	32100	15	85	2.00
I8	**-**	***6815***	**-**	**-**	**-**	***1.38***
A7	Gauss	11200	41700	11	89	2.47
I9	**-**	***2890***	**-**	**-**	**-**	***1.22***
A9	Bigaussian	3490	15700	20	80	1.75
A10	Gauss	3590	20000	12	88	2.19
I10	**-**	***2340***	**-**	**-**	**-**	***1.29***
A11						
A12	Bigaussian	3680	10000	30	70	1.50
A13	Gauss	3620	17500	6	94	1.95
I11	**-**	***3520***	**-**	**-**	**-**	***1.29***
A16	Gauss	3560	47000	3	97	3.66
I12	**-**	***2500***	**-**	**-**	**-**	***1.31***
A17	Gauss	3780	16400	17	83	1.97

A number of the syntheses did not produce PtBMA-b-PODMA BCPs resulting in unreacted macroinitiator and therefore monomodal GPC distributions, the GPC results for these polymers are given in Table 5.6 and will be discussed shortly.

Table 5.6: Parameters for the synthesis of block copolymers PtBMA-*b*-PODMA which exhibited monomodal molecular weight distributions observed using GPC.

Code	GPC peaks	Macroinitiator	M_n[a] (Da)	M_w[a] (Da)	Đ
I6	-	-	*10900*	*13700*	*1.25*
A4	Monomodal	I6	13100	15500	1.18
A5	Monomodal	I6	11600	14400	1.24
I8	-	-	*6815*	*9425*	*1.38*
A8	Monomodal	I8	4600	8800	1.90
I10	-	-	*2340*	*3030*	*1.29*
A14	Monomodal	I10	3500	4600	1.33
I11	-	-	*2520*	*3250*	*1.29*
A15	Monomodal	I11	3455	4608	1.33
I13	-	-	*2100*	*2780*	*1.32*
A18	Monomodal	I13	2800	3300	1.18
A19	Monomodal	I13	2700	3200	1.17

As already established PtBMA macroinitiators were synthesised under varying conditions, the catalyst, ligand and solvent were changed for each initiator. A series of BCPs of PtBMA-*b*-PODMA were synthesised with macroinitiator I6 (Cu(I)Cl/PMDETA in THF) which was the most successful synthesis of PtBMA as already mentioned. A1 was synthesised using I6 macroinitiator, a Cu(I)Br/PMDETA catalytic system in Xylene:IPA (9:1). Analysis with GPC revealed a bimodal molecular weight distribution. The bimodal distribution was fitted to establish the relative peak percentages of uninitiated I6 macroinitiator (peak 1) and the BCP PtBMA-*b*-PODMA (peak 2). They were calculated to be 0.2 % and 99.8 % respectively.

Having established from the multiple peak fit data of the GPC bimodal M_w distribution of A1 that it was the BCP with the lowest % of unreacted macroinitiator (0.2 %), the BCP A1 was back precipitated into methanol in order to obtain a monomodal distribution in molecular weight, characterised by GPC. The BCP was

then deprotected with TFA to remove the tert-butyl group. Yang *et al.*[11] removed the tert-butyl protecting group from a PtBMA-*b*-PEG-*b*-PtBMA BCP by dissolving the polymer in dioxane, adding HCl (36 %) and heating under reflux. This method was used to remove the tert-butyl protecting group, however it was established that HCl was not a strong enough acid and the BCP was not fully soluble in dioxane. Tam *et al.*[12] used DCM to dissolve the polymer followed by the addition of TFA, the solution was then left to stir at room temperature for 24 hours. We found that this method was successful in removing the tert-butyl protecting group when THF was used in place of DCM to ensure complete dissolution of the BCP. The BCP was characterised with both GPC (to confirm the change in molecular weight) and ^{1}H-NMR to confirm the removal of the t-butyl protecting group. The dispersity, Đ, (Table 5.7) for both the PtBMA-*b*-PODMA and the deprotected PMAA-*b*-PODMA was high indicating the reaction was not well controlled, as for controlled ATRP reaction a Đ of ≤ 1.3 is expected.[27, 39, 40] The lack of control was already clear when looking at the GPC traces where the reaction mix gave a bimodal distribution (Figure 5.3) indicating that some of the PtBMA macroinitiator was left unreacted. There is a decrease in M_n and M_w, calculated from both GPC and ^{1}H-NMR, between the PtBMA-b-PODMA and the deprotected PMAA-b-PODMA BCPs, this was expected as the large tBMA group has been lost to be replaced with a hydrogen.

Table 5.7: Parameters for block copolymer PtBMA-*b*-PODMA and the deprotected PMAA-*b*-PODMA alongside the relevant PtBMA macroinitiator results, obtained using ^{1}H-NMR and GPC.

Code	Structure	M_n[a] (Da)	M_w[a] (Da)	Đ[a]	DP[b]	M_n[b] (Da)	PtBMA/ PMAA wt %
I6	*P(tBMA)$_{45}$*	*10900*	*13700*	*1.25*	*45*	*6584*	*N/A*
A1	P(tBMA)$_{45}$-*b*-PODMA$_{51}$	197000	386900	1.96	51	23822	28
A1(DP)	PMAA$_{45}$-*b*-PODMA$_{51}$	133300	287900	1.78	51	21223	19

[a]Calculations from GPC in THF (PMMA Standards).
[b] Calculations from ^{1}H-NMR in $CDCl_3$ by comparing the integrals of **peak a to peak e.**

The GPC traces of I6 PtBMA macroinitiator, A1 reaction mix, A1 post back precipitation and A1 deprotected were overlaid (Figure 5.3). The reaction mix trace was bimodal, the larger peak being due to the block copolymer PtBMA-*b*-PODMA growth and the smaller peak due to unreacted I6 macroinitiator, this was clear as the smaller peak had the same M_w as the I6 initiator peak. The block copolymer was back-precipitated with a methanol/water mix to remove the unreacted macroinitiator. This was successful as Figure shows the trace for A1 (PtBMA-*b*-PODMA) was monomodal with <10 % overlap with the I6 peak. The trace for A1 deprotected (PMAA-*b*-PODMA) is also monomodal with a reduction seen in molecular weight when compared to the trace of A1 (PtBMA-*b*-PODMA). These results suggest that the t-butyl group was removed successfully.

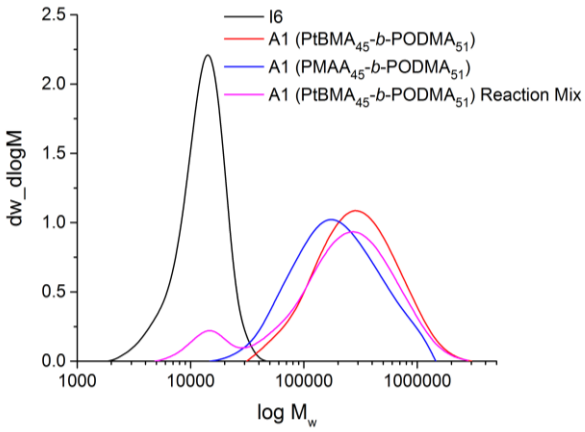

Figure 5.3: GPC traces of I6 ($PtBMA_{45}$) overlaid with A1 ($PtBMA_{45}$-b-$PODMA_{51}$) and A1 deprotected ($PMAA_{45}$-b-$PODMA_{51}$)

To confirm the removal of the tert-butyl protecting group via acid hydrolysis, the ^{1}H-NMR spectra of A1 protected and deprotected were overlaid (Figure 5.4). Both spectra are free from impurities and have no unreacted ODMA monomer present, this is evident from the absence of peaks at 5.58ppm and 6.15ppm which are due to the vinyl protons in ODMA. The deprotection of PtBMA-*b*-PODMA was successful, this is evident from the absence of the t-butyl peak (A) in the spectrum of PMAA-*b*-PODMA.The integral ratio for $COOCH_2$- (peak F) and CH_2C- (peak C) for A1 was calculated to be roughly 1:1, the integral ratio for the post-deprotection sample of A1 (PMAA-b-PODMA) was calculated to be 1:1.5 this suggests that a small proportion of ODMA chains have undergone acid hydrolysis due to the whole BCP being treated with TFA.

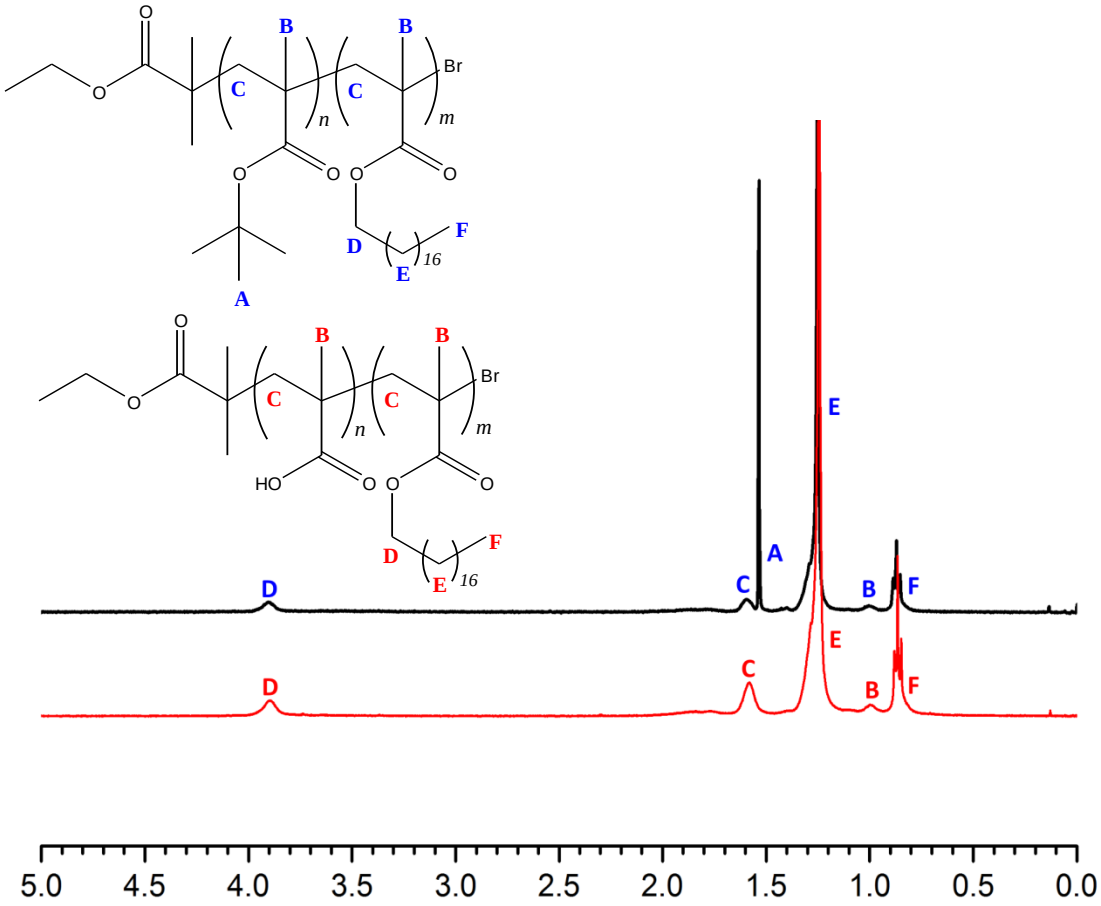

Figure 5.4: ^{1}H-NMR spectra of A1 (PtBMA-b-PODMA) (BLACK) overlaid with A1 deprotected (PMAA-b-PODMA) (RED).

The use of Cu(I)Cl in place of Cu(I)Br slows down the propagation of ODMA chains allowing more macroinitiator to be activated before the ODMA starts to grow. A3 was synthesised under the same conditions as A1 except the catalyst Cu(I)Br was replaced with Cu(I)Cl. A bimodal GPC distribution was observed (Figure 5.5B) with 5 % initiator (peak 1- Table 5.5) left unreacted. This shows that slowing the reaction down produced more BCP when compared to A2. A4 was synthesised under the same conditions as A3 with the inclusion of the deactivator Cu(II)Cl to further reduce the rate of propagation to improve the initiation step. As evident in Figure 5.5C there was little to no propagation of ODMA with only the macroinitiator peak being present on the GPC distribution plot. The same result was seen for A5 (Figure 5.5C) where the catalyst system was changed from Cu(I)Cl/PMDETA to Cu(I)Cl/Bipyridine. Bipyridine has been found to produce a slower rate of polymer propagation in comparison to PMDETA. A6 was synhtesied using Cu(I)Cl/PMDETA catalyst system and toluene in place of Xylene:IPA with the idea being that toluene may better solubilise the macroinitiator allowing a more efficient initiation. This was not the case as 20 % of the initiator was left unreacted giving a bimodal GPC distribution (Figure 5.5B).

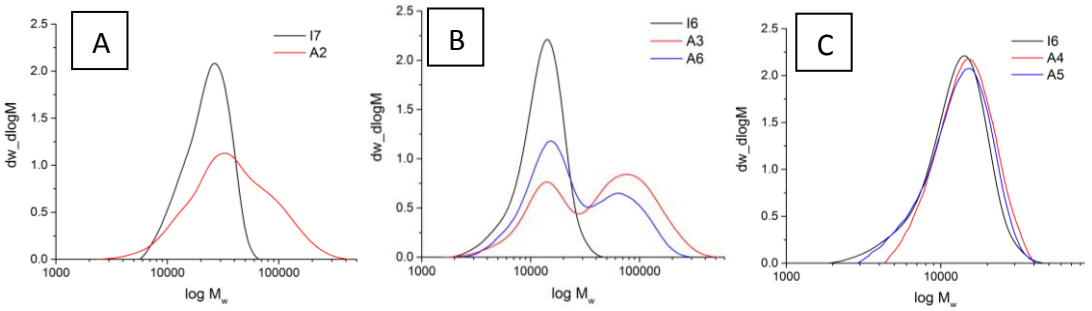

Figure 5.5: GPC traces of PtBMA-*b*-PODMA BCPs synthesised with I6.

As attempts to reproduce A1 along with improving the initiation of I6 were unsuccessful it was thought that the problem may lie with the initiator. The synthesis of PtBMA was therefore carried out using Cu(I)Br under a varying range of conditions to produce initiators I8-I13 (see previous section) whose active end groups would all be terminated by Br.

I8 was used in the synthesis of A7 and A8. A7 and A8 were synthesised under the same conditions using a Cu(I)Br/PMDETA catalyst system in Xylene:IPA (9:1). A7 produced a polymer with a bimodal GPC distribution (Figure 5.6A) and 11 %

macroinitiator left unreacted. A8 gave a monomodal GPC distribution, however when comparing the distribution plot of I8 (Figure 5.6B) it shows that little to no initiation and propagation occurred.

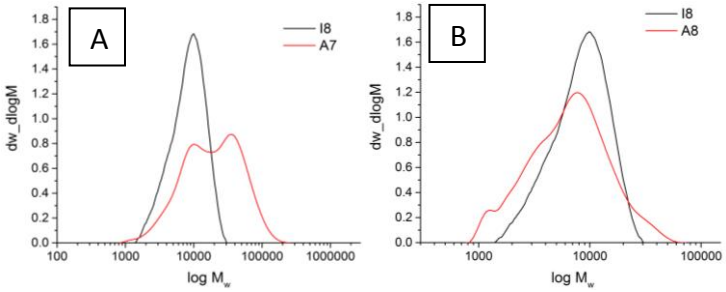

Figure 5.6: GPC traces of PtBMA-*b*-PODMA BCPs synthesised with I8.

I9 was synthesised with Cu(I)Br to ensure that all the macroinitiator end groups were terminated with Br allowing equal initiation during polymerisation. A9 and A10 were synthesised with I9 in Xylene:IPA (9:1) with a Cu(I)Br/PMDETA and a Cu(I)Cl/PMDETA catalyst system respectively. Both syntheses produced BCPs with a bimodal GPC distribution (Figure 5.7). A10 was synthesised with Cu(I)Cl which reduces the rate of propagation, had 12 % macroinitiator left unreacted in comparisons to A9's 20 %. This means the use of Cu(I)Cl gave more control to the reaction.

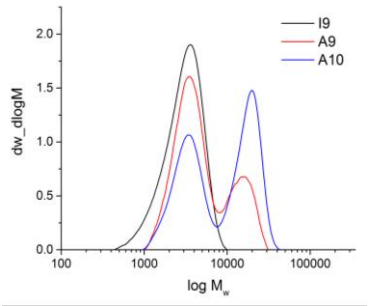

Figure 5.7: GPC traces of PtBMA-*b*-PODMA BCPs synthesised with I9.

I10-I12 were synthesised under the same conditions producing polymers with a dispersity of < 1.31 and a DP of 13, 10 and 9 respectively. A11 and A12 were synthesised with I10 and a Cu(I)Br/PMDETA catalyst system in Xylene:IPA (9:1). A11 produced a BCP with a bimodal GPC distribution. The bimodal distribution could not be fitted so the percentage of initiator left unreacted could not be determined, however a small initiator peak is evident form the distribution plot (Figure 5.8A). A12 was synthesised to see if the result seen for A11 was reproducible. A bimodal GPC

peak was observed with a much larger initiator peak (Figure 5.8A) with a peak percentage of 30 %. To reduce the amount of initiator peak left unreacted Cu(I)Cl was used as the catalyst in the synthesis of A13, this significantly reduced the amount of initiator left unreacted to 6 %. A14 was synthesised under the same conditions as A13 to see if the reaction was reproducible, the GPC traces show a monomodal distribution with the M_n being similar as that of I10 indicating that no polymer has grown (Figure 5.8B).

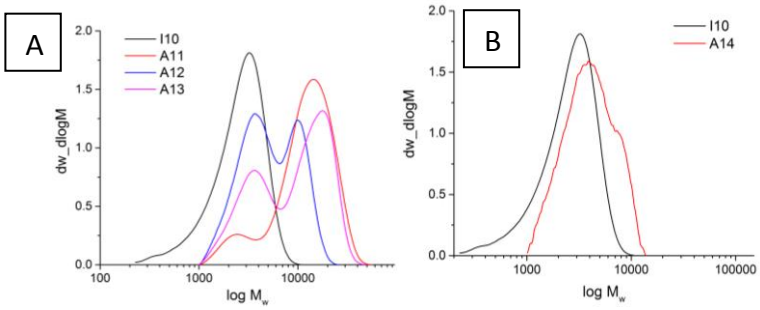

Figure 5.8: GPC traces of PtBMA-*b*-PODMA BCPs synthesised with I10.

A15 and A16 were synthesised under the same conditions (Cu(I)Cl/PMDETA catalyst system) using I11. The only difference was the choice of solvent with xylene:IPA used for A15 and toluene for A16. In the synthesis of A15 propagation did not occur this is evident as A15 has a similar M_n to that of the initiator used I11 (Table 5.6).

A16 was analysed with GPC and produced a bimodal molecular weight distribution (Figure 5.9A) with 3 % initiator left unreacted. This was promising as it is the lowest percentage of initiator left unreacted except for the synthesis of A1. A17 was a repeat of A15 and also resulted in no ODMA propagation as seen in Figure 5.9B.

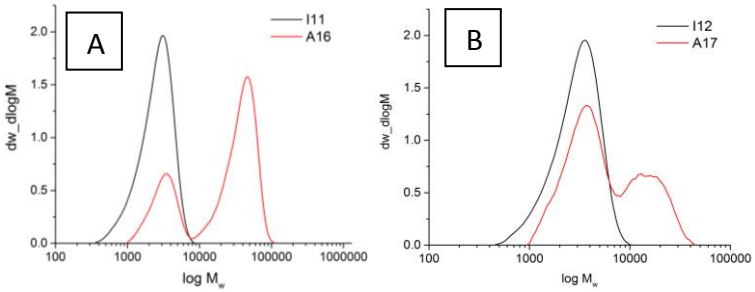

Figure 5.9: GPC traces of PtBMA-*b*-PODMA BCPs synthesised with I11.

I13 was synthesised with Cu(I)Br in toluene to ensure the active end groups were all terminated with bromine. I13 was used in the synthesis of A18 and A19 which were

synthesised under the same conditions of a Cu(I)Cl/PMDETA catalyst system in toluene, to assess whether the change in solvent was the contributing factor in the almost successful synthesis of A16.

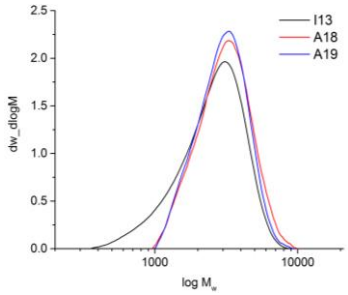

Figure 5.10: GPC traces of PtBMA-*b*-PODMA BCPs synthesised with I13.

5.4.3 Self-Assembly of PMAA-*b*-PODMA A1

The PMAA acts as the hydrophilic block[21] with the PODMA block being hydrophobic. In the self-assembly of PEO-b-PODMA via the dialysis method, THF acts as a non-selective solvent, this means it is able to solvate both the PEO and PODMA blocks. This minimises non-equilibrium structures from being kinetically trapped as water is added. It also allows the block copolymer better mobility to form these ordered assemblies.[2] PEO and PODMA are better solubilised in THF than water this is evident when their solubility parameters are taken into consideration with PEO and PODMA's solubility parameters (10.5 and 7.8 (cal $cm^{-3})^{1/2}$) being closer to that of THF (9.1 (cal $cm^{-3})^{1/2}$) than water (23 (cal $cm^{-3})^{1/2}$). It was thought that for PMAA-*b*-PODMA to self-assemble into these ordered bicontinuous nanospheres, the same method and solvent should be used to give the mobility needed to the high-molecular weight polymer. The solubility parameter of PMAA is 7.2 (cal $cm^{-3})^{1/2}$ which again is closer to that of THF than water so should act in a similar way to the PEO hydrophilic block, indicating that bicontinuous nanospheres may form.

A1 was self-assembled at 0.1 wt % in aqueous solution to produce bicontinuous nanospheres. It was self-assembled using 4 mL of THF and 6 mL of deionised water followed by dialysis at 35˚C to remove the THF. The 0.1 wt % solution produced a number average particle size of 482 nm at 15˚C and a small increase to 525 nm with an increase in measurement temperature (35˚C). This clearly shows that large particles were produced and the temperature responsive nature of the PODMA block preserved. McKenzie at al. (2010)[1] established that when a BCP bicontinuous nanospheres of PEO-*b*-PODMA was heated above the PODMA alkyl-side chains melting transition, the internal ordered bicontinuous structure was lost but that the external spherical structure was preserved. This explains the increase in particle size upon an increase in DLS measurement temperature. As the PODMA alkyl side-chains are heated above their T_m the internal structure is lost with the external structure maintained with some expansion in size expected as the chains start to disperse. As seen previously with P3 (PEO-*b*-PODMA), when A1 was heated above PODMAs T_m an increase in particle size was observed via DLS. The PEO-*b*-PODMA nanospheres at the

same concentration gave an N_{ave} of around 450 nm at 15°C, close to that observed for A1.

Table 5.8: Particle sizes for self–assembled block copolymer A1 ($PMAA_{45}$-*b*-$PODMA_{51}$) determined using dynamic light scattering.

wt %	T (°C)	N_{Ave} (nm)	SD	Z_{Ave} (nm)	SD	CONTIN	Đ
0.1	15	482	21	765	38	1180/397	0.43
0.1	35	525	69	1280	46	617/287	0.81

Analysis of the size distribution plots for A1 0.1 wt % revealed a bimodal distribution at 15˚C with the major peak having a number average of 350 nm, this matches the CONTIN analysis data calculated for this sample. The increase N_{ave} given in Table 5.8 is most likely due to the second peak, with a larger N_{ave}, being taken into account. The size distribution plot at 35˚C was monomodal with a N_{ave} of around 600 nm, upon heating the larger particles appear to have dispersed and the smaller particles might well have aggregated..

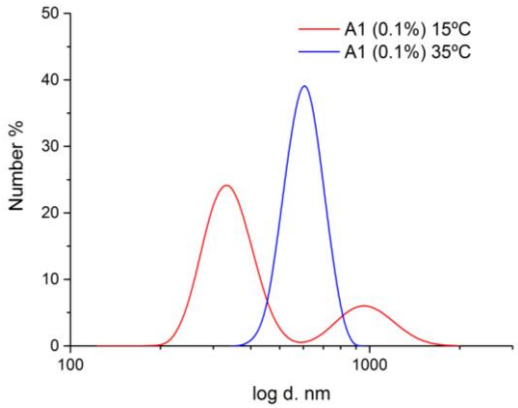

Figure 5.11: Size distribution plots for A1 0.1 wt % in solution at 15 and 35°C.

The A1 0.1 wt % solution was further analysed with TEM to confirm the N_{ave} and determine a possible particle morphology. The expected morphology was bicontinuous nanospheres as the hydrophilic block was between 15-25 wt %[2] and the same procedure was followed as for the production of bicontinuous nanospheres from P3 (chapter 2). Figure 5.12 shows the 0.1 wt % solutions particles with possible bicontinuous morphology and a N_{ave} of 114 nm (measured from 26 particles). This

was significantly lower than the N_{ave} observed via DLS, however the DLS distributions plots show two size ranges, with the lower being around 200 nm. Another reason for the difference in particle size between the TEM and DLS measurements could be due to a small field of particles being analysed in TEM compared to DLS.

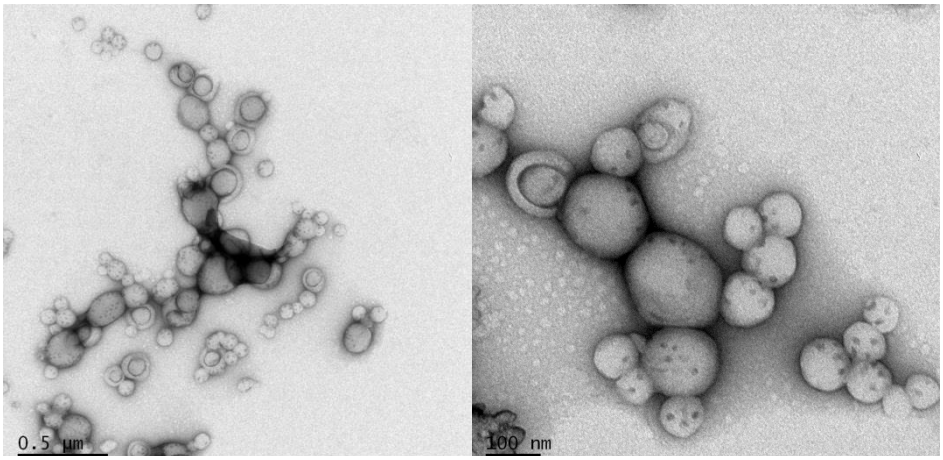

Figure 5.12: Negative stained TEM images of 0.1 wt % solution of A1 ($PMAA_{45}$-*b*-$PODMA_{51}$) with possible bicontinuous internal morphology (Stained with 5 % uranyl acetate and 1 % acetic acid).

The 0.1 wt % solution was further analysed with cryo-TEM following the same vitrification process as used with PEO-*b*-PODMA, PEO-*b*-PDSMA and PEO-*b*-(PODMA-*co*-PDSMA) in chapter 2 and 3. The images show that bicontinuous nanospheres (as shown by the red arrows in Figure 5.13A-B) were formed within the size range of 100-150 nm which is consistent with the N_{ave} calculated from negatively stained TEM. Vesicles (as shown by the green arrows in Figure 5.13B) and micelles (as shown by the blue arrows in Figure 5.13B) were also present in the sample. A larger proportion of bicontinuous nanospheres was desired if these nanospheres were to be used for biomineralisation.

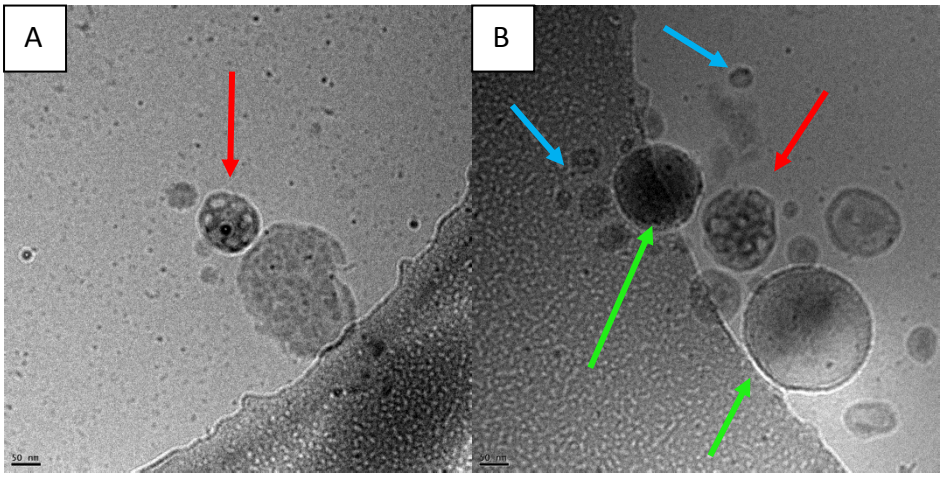

Figure 5.13: Cryo-TEM images of A1 ($PMAA_{45}$-*b*-($PODMA_{51}$)(0.1 wt %) nanospheres with internal bicontinuous morphology and vesicles. Red arrows highlight bicontinuous nanospheres. Green arrows highlight vesicles. Blue arrows highlight micelles.

The results were promising as to the best of our knowledge this is the first time bicontinuous aggregates were formed from a BCP that has a functional acid group without the use of an additive to aid the self-assembly. Wooley *et al.*[41] formed bicontinuous nanospheres from a PAA_{99}-*b*-PMA_{73}-*b*-PS_{203} in a THF: water solvent mix with a volume ratio of 1:0.2, however the polymer was complexed with 2,2'-(ethylenedioxy)diethylamine in order for the bicontinuous structure to form.

Due to the low solubility of the PMAA block in water, obtaining higher concentrations of A1 aggregates proved difficult. A1 was self-assembled at 1 wt % in solution with no precipitation upon addition of water. The solution was analysed with TEM, which showed spherical aggregates around 300-400 nm (Figure 5.14). Unfortunately the polymer precipitated out over time and DLS results therefore could not be obtained along with clearer TEM images. This shows that at increased concentrations the assembly was not stable. The self-assembly of a 5 wt % solution of A1 was attempted, however the polymer precipitated upon addition of water.

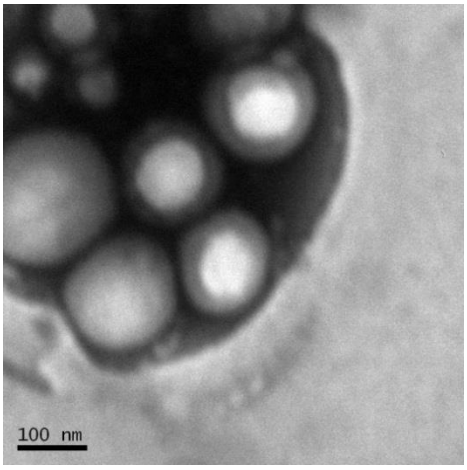

Figure 5.14: Negative stained TEM images of 1 wt % solution of A1 ($PMAA_{45}$-*b*-$PODMA_{51}$) spherical aggregates (Stained with 5 % uranyl acetate and 1 % acetic acid).

5.4.4 Characterisation of Poly(ethylene oxide)-*block*-Poly(styrene)

PEO-*b*-PS was synthesised via ATRP using a PEO macroinitiator. PEO-*b*-PS was characterised using GPC and ^{1}H-NMR to determine the purity and molecular weight parameters. These results can be seen in Table 5.9. A range of PEO wt % were synthesised to assess the affect this has on the morphology and size of the particles upon self-assembly. The M_n calculated from GPC was different from that of ^{1}H-NMR, due to the difference in hydrodynamic volume of the PEO-*b*-PS BCP and the PMMA GPC standard used,[42, 43] therefore to ensure consistency in the results the ^{1}H-NMR value was used for all calculations. The M_n[b] was calculated by comparing the integrals of CH_3O of PEO (peak A) and the aromatic ring of PS (peak F Figure 5.16). The dispersity for all the BCPs was below 1.22.

Table 5.9: Parameters for block copolymers PEO-b-PS obtained using ^{1}H-NMR and GPC.

Code	Structure	PEO wt %	DP[b]	M_n[b] (Da)	M_n[a] (Da)	M_w[a] (Da)	Đ[a]
I2	PEO_{44}	-	44	2160	3600	3900	1.07
S1(55)	PEO_{44}-*b*-PS_{114}	15	114	14020	31600	38600	1.22
S2(54)	PEO_{44}-*b*-PS_{88}	19	88	11320	20700	25200	1.22
S3(56)	PEO_{44}-*b*-PS_{69}	23	69	9350	13500	15300	1.13

[a] Calculations from GPC using PMMA standards.
[b] Calculations from ^{1}H-NMR comparing the integrals peak A (CH_3) to peak F (C_6H_5).

The GPC traces of I2 macroinitiator and S1 are shown in Figure 5.15 the BCP peak was monomodal with <10 % overlap with the PEO peak; this suggested that there was a small proportion of PEO macroinitiator in the BCP sample left unreacted. The GPC traces for S2 and S3 gave the same result.

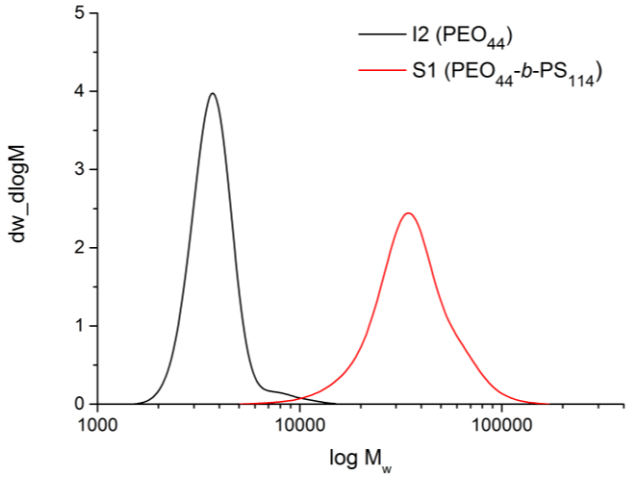

Figure 5.15: GPC traces of S1 (PEO_{44}-b-$PODMA_{114}$) overlaid against macroinitiator I2 (PEO_{44}).

To confirm the absence of macroinitiator and monomer within the BCP sample, ^{1}H-NMR was carried out on all PEO-*b*-PS samples (Figure 5.16). The two vinyl protons in styrene are normally present at 5.5 and 6.1ppm, these are absent from the ^{1}H-NMR spectrum confirming that all the monomer has been removed in the precipitation stage. Peaks 1 and 2 for the PEO macroinitiator are also not present on the BCP spectrum confirming the absence of unreacted PEO (see inset in red and blue).

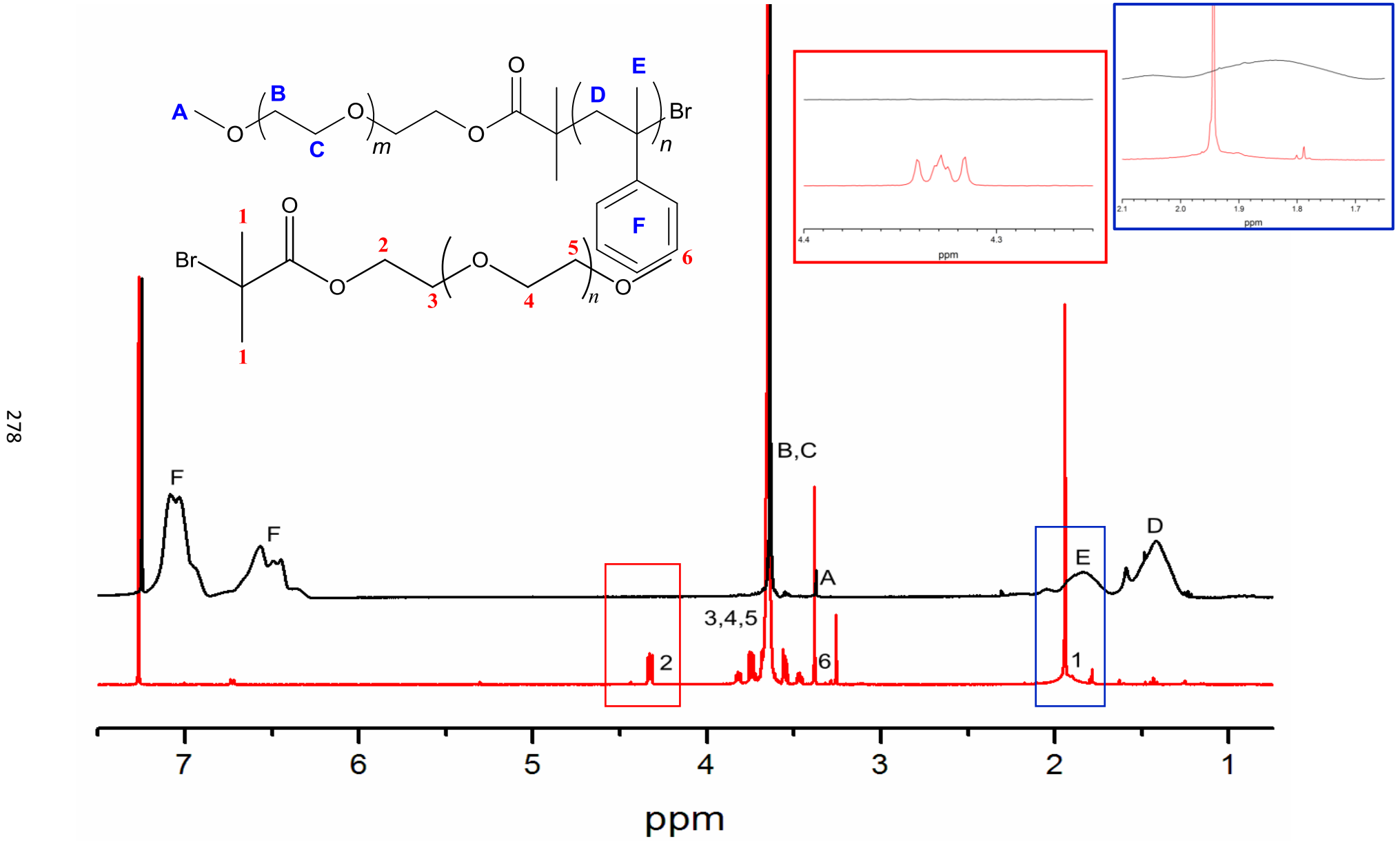

Figure 5.16: ^{1}H-NMR spectra of S1 (PEO_{44}-*b*-PS_{114}) (top) overlaid with macroinitiator I2 (PEO_{44}) (bottom). Red inset: zoomed image of peak 2. Blue inset: Zoomed images of peak 1.

5.4.5 Self-Assembly of Poly(ethylene oxide)-*block*-Poly(styrene)

The BCP PEO-*b*-PS was successfully synthesised at varying wt % of PEO with well-defined molecular weights and low dispersities. The BCPs were then self-assembled with the aim to produce bicontinuous nanospheres with the PEO acting as the hydrophilic block and the hydrophobic block being a high molecular weight glassy segment. The aim was to functionalise the nanospheres post self-assembly to produce an acid end group, following the procedure seen in Scheme 5.5. This acid functionality, as discussed previously in this chapter, would aid a number of applications, and the high glass transition temperature of the PS block would contribute massively to the stability of these nanospheres.

5.4.5.1 S2 and S3 (PEO 19 and 23 wt %)

Block copolymers S2 and S3 were self-assembled using 6 mL THF and 4 mL water at 0.1 and 1 wt % in solution. They all produced particles with a number average between 96-216 nm (Table 5.10) with the Z-average being higher due to the measurement being biased towards the larger particles as discussed in chapter 3. The Đ which measures the distribution of the particles in solution was lowest for S3 1 wt % solution at 0.05 but all aggregate solutions exhibited relatively low Đ (<0.24) indicating a narrow size distribution.

Table 5.10: Number mean values for self–assembled block copolymer S2 (PEO_{44}-*b*-PS_{88}) and S3 (PEO_{44}-*b*-PS_{69}) calculated from the Z-average using Dynamic Light Scattering.

Sample	PEO wt %	wt %	N_{Ave} (d.nm)	SD (± nm)	Z_{Ave}(d.nm)	SD (± nm)	CONTIN	Đ
S2	19	0.1	216	22	328	4	201/566	0.24
S2	19	1	122	22	308	4	108/412	0.24
S3	23	0.1	96	9	123	1	130	0.09
S3	23	1	114	5	128	1	132	0.05

Figure 5.17 represents the number distribution plot for S2 at both 0.1 and 1 wt % in solution. The 1 wt % plot is bimodal, with the major peak having a number average particle size of approximately 120 nm and the smaller peak being approximately 400 nm, these number average particle sizes are consistent with the CONTIN analysis data (Table 5.10). The 0.1 wt % distribution plot is monomodal and has a large particle size range which also explains two average particle sizes seen from the CONTIN analysis.

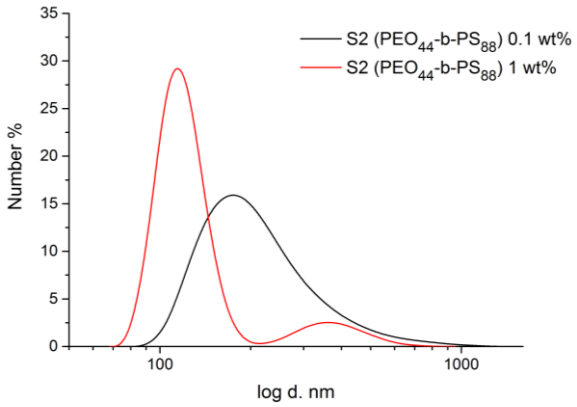

Figure 5.17: DLS distribution plot of number average particle sizes for S2 0.1 and 1 wt % solutions analysed at 25°C.

The number distribution curves for S3 0.1 and 1 wt % can be seen in Figure 5.18. Both plots are monomodal which correlates with the low Đ's of 0.09 and 0.05, with relatively similar particle sizes of around 100 nm, only one average particle size was seen in the CONTIN analysis for each concentration as seen here in the distributions.

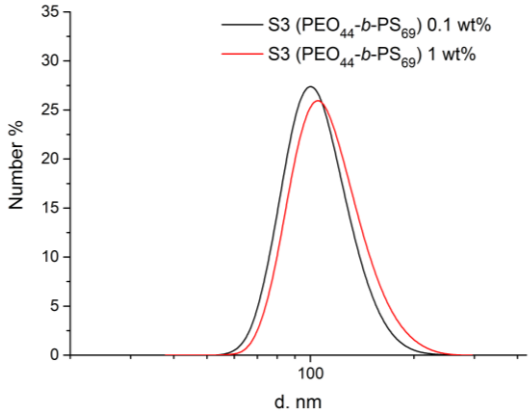

Figure 5.18: DLS distribution plot of number average particle sizes for S3 0.1 and 1 wt % solutions analysed at 25°C.

The polymers S2 and S3 were further analysed with TEM to confirm their particle sizes and morphologies. The proposed morphology was bicontinuous nanospheres

as the PEO wt % was below 25 % and the same procedure was used as for PEO_{49}-*b*-$PODMA_{21}$ (Chapter 3) which produced bicontinuous nanospheres. However, on analysis of the TEM images (Figure 5.19) S2 at 0.1 and 1 wt % in solution produced stomatocytes ("bowl" shaped vesicle with a "mouth")[44, 45] with a N_{ave} of 237 nm and 100 nm respectively (calculated from 60 and 30 particles respectively). These particle sizes agree with those observed from DLS (Figure 5.17). The controlled loss in polymer vesicles shape, by the rapid displacement of the solvent, via dialysis in water, results in a bowl shaped structure with a "mouth" that is tuneable by modification of the solvents volume.[46]

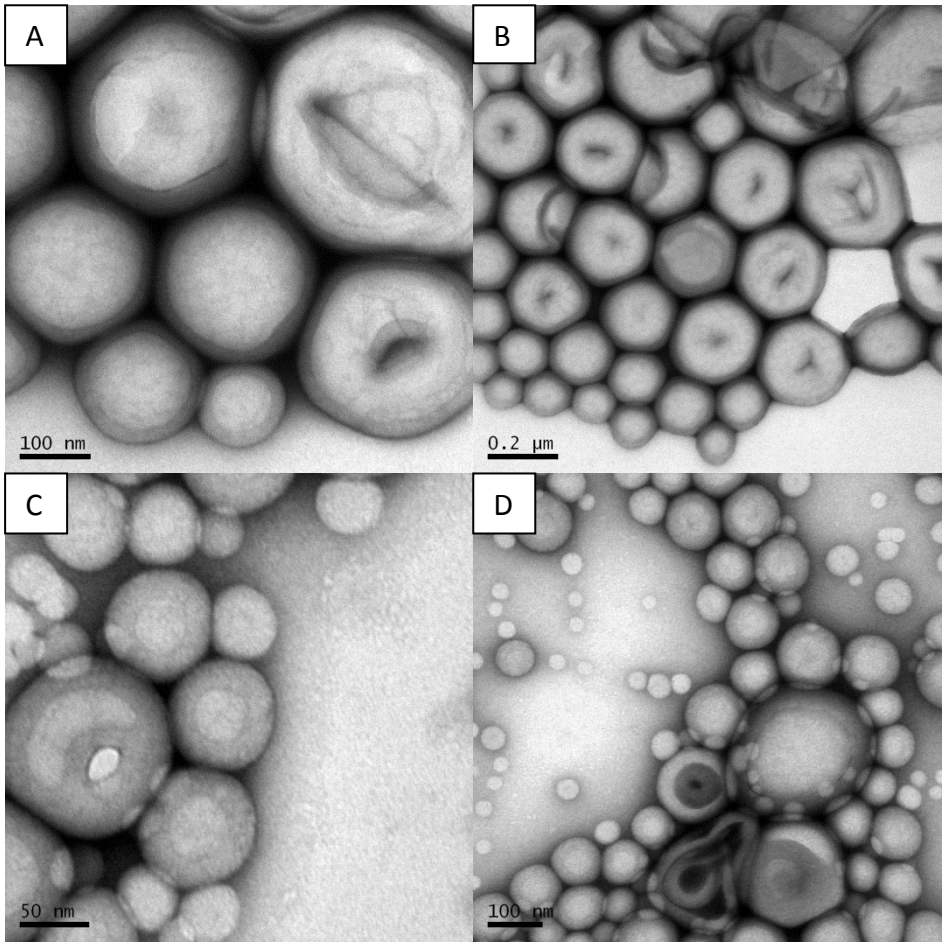

Figure 5.19: A-B) Negative stained TEM images of 0.1 wt % solution and **C-D)** 1 wt % solution of **S2** (PEO_{44}-*b*-PS_{88}) stomatocytes (Stained with 5 % uranyl acetate and 1 % acetic acid).

S3 at 0.1 and 1 wt % also produced stomatocytes (Figure 5.20) with number average particles sizes of 170 nm and 104 nm respectively (calculated from 30 particles). These particle sizes are slightly larger than observed with DLS.

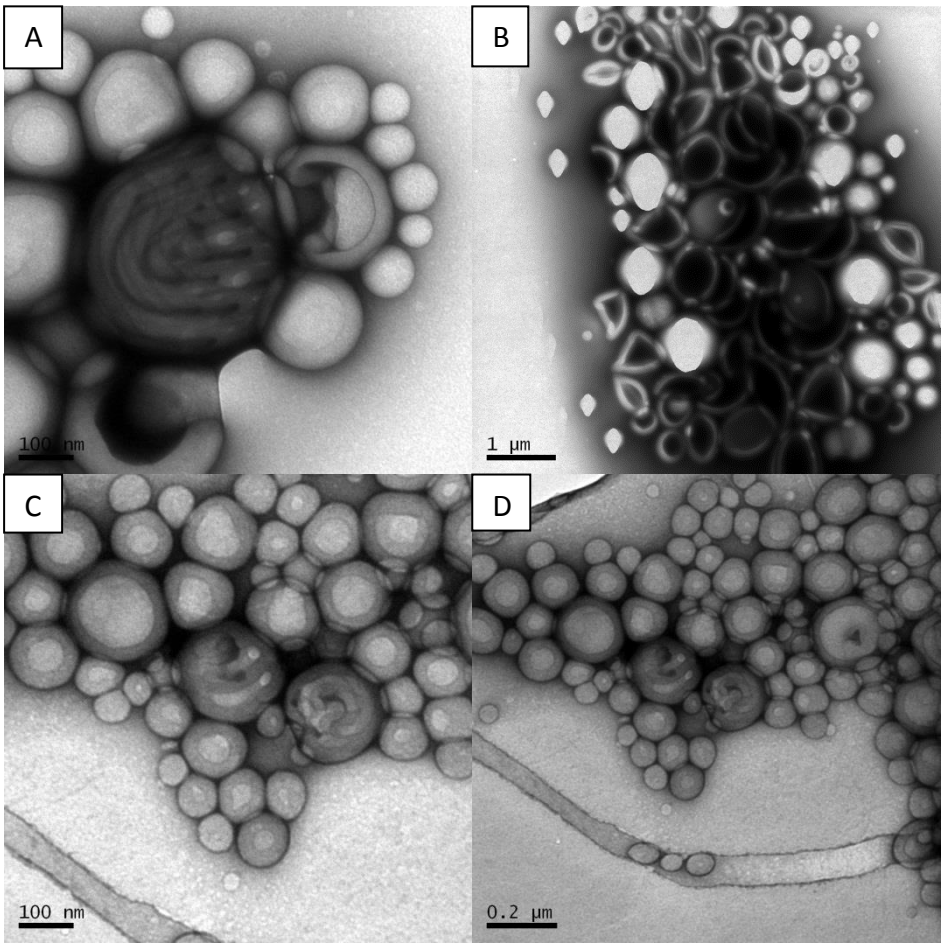

Figure 5.20: A-B) Negative stained TEM images of 0.1 wt% solution and **C-D)** 1 wt% solution of **S3** (PEO_{44}-*b*-PS_{69}) stomatocytes (Stained with 5% uranyl acetate and 1% acetic acid).

The formation of a bicontinuous structure from PEO-*b*-PS BCPs has been observed by Eisenberg *et al*.[47] with the polymer being self-assembled in a DMF-water mix. This suggests that the solvent plays a large role in subsequent morphology. The reason why these BCPs form stomatocytes has been well documented by Jan C. M. van Hest *et al.*[44, 48]. They synthesised block copolymer PEG-*b*-PS with the DP of the PS block within the range 102-312. The difference was that they used a cosolvent method of dioxane:THF (1:1) to dissolve the polymer before the addition of water. They observed vesicles, which were expected, when the aggregates solution of PEG_{45}-*b*-PS_{230} was added to a small amount of pure water to rapidly freeze the morphology, however when the solution was dialysed to remove the dioxane/THF stomatocytes were observed. This change in morphology was due to a rapid decrease in the volume of the solvent molecules within the inner compartment of the polymersomes

through the swollen fluidic PS membrane. The reason for the stomatocytes morphology is due to the fact that the rate of diffusion of the THF/dioxane through the membrane is far greater than the water molecules moving into the inner compartment due to the difference in Hildebrand solubility parameters of the solvents where there is an unfavourable energy barrier between the PS membrane and the water. This means that the water cannot fill up the space left by the leaving solvent molecules quickly enough causing the polymersomes to collapse. This continued until the membrane lost its permeability due to the decrease in solvent molecules and the PS collapses into its rigid glassy state trapping the morphology. However Jan C. M. van Hest *et al.*[48] observed that the stomatocytes formed when the DP of the PS block was 175 or greater. However we observed stomatocytes at DPs as low as 66.

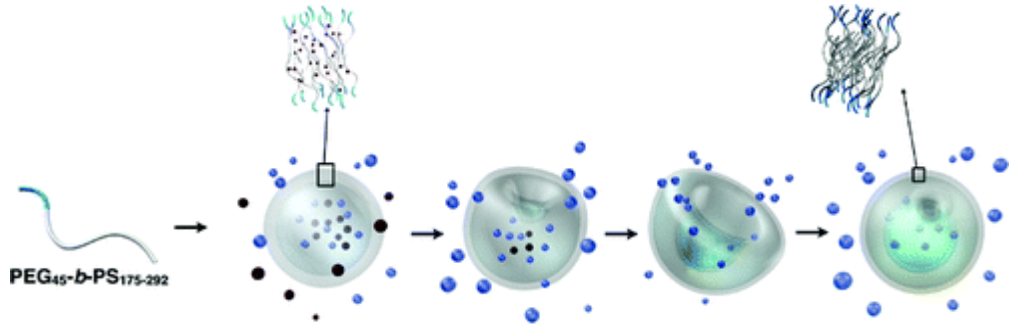

Figure 5.21: Shape transformation of polymersomes to stomatocytes during dialysis of organic solvents (dark red spheres) against water (blue spheres) through a solvent-swollen bilayer membrane. Reproduced from ref.[44]

5.4.5.2 S1 (PEO 15 wt %)

Block copolymer PEO_{44}-*b*-PS_{114} (S1) was self-assembled at 0.1 wt % using various volumes of THF (Table 5.11) and at 1 wt % using 6 mL of THF and 4 mL of water. For the 0.1 wt % in solution, as the volume of THF was increased the number average particle size decreased from 549 to 136 nm as measured by DLS. When the self-assembly was performed at room temperature rather than at 40°C, which was the case for all other aggregate solutions, with 6 mL of THF the number average particle size increased from 444 to 744 nm. The particle size seemed to stay roughly the same as the wt % in solution was increased to 1 %. The Đ for all of the aggregate solutions was relatively low (< 0.25) indicating a narrow size distribution except for the 0.1 wt % (8 mL THF) solution which had a high Đ of 0.74.

Table 5.11: Particle diameters for block copolymer S1 (PEO_{44}-*b*-PS_{114}) (25 wt % PEO) obtained by DLS.

THF (mL)	wt %	N_{ave} (d. nm)	SD (± nm)	Z_{ave} (d.nm)	SD (± nm)	CONTIN	Đ
4	0.1	549	72	577	6	628/220	0.14
6	0.1	444	24	475	5	508	0.08
8	0.1	136	12	446	48	116/1507	0.74
6 (R.T.)	0.1	744	55	758	7	919/463	0.16
6	1	490	63	537	8	599/224	0.11

The size distribution plots for S1 can be seen in

Figure **5.22**. All plots are monomodal except for the 0.1 wt % (8 mL) solution, this is consistent with the dispersity results with the 0.1 wt % (8 mL) in solution having a high Đ in comparison to all other solutions. The distribution plots confirm that as the volume of THF was increased the size of the particles decreased. This is consistent with previous studies performed by Holder *et al.* where they self-assembled PEO_{47}-*b*-$PODMA_{20}$ using varying volume ratios of THF:water to produce bicontinuous nanopsheres. They showed that the volume of THF plays a role in the resultant particle size of the nanopsheres produced, as the THF volume is increased the particle size decreases (Figure 5.23).[2]

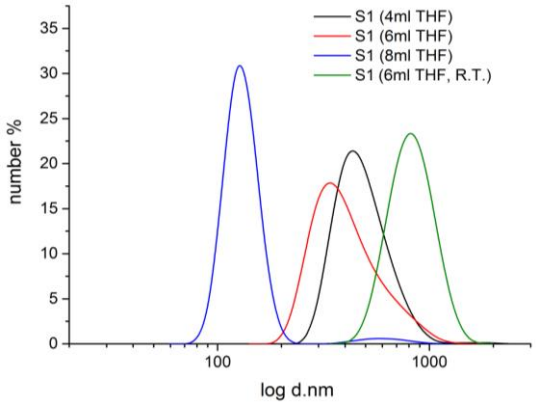

Figure 5.22: DLS distribution plot of S1 0.1 (4-8 mL) and 1 wt % (6 mL) solutions analysed at 25°C.

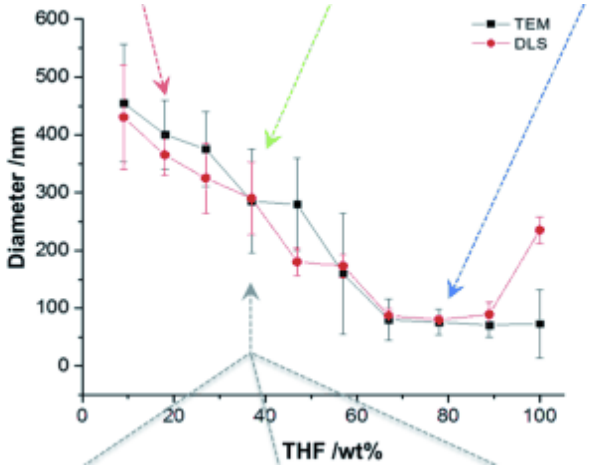

Figure 5.23: Graph showing the variation in particle diameter (as measured by TEM and DLS) with changing THF wt % content of the starting solution for dispersions formed from a single block copolymer that forms BPNs (PEO_{47}-*b*-$PODMA_{20}$; *f*=0.25). Reproduced from ref.[2]

The block copolymer aggregate solutions of S1 were further analysed with TEM to determine the particle morphology and confirm the size of the particles. The TEM images for the S1 0.1 wt % (4 mL THF) are shown in Figure 5.24. The number average particle size determined from TEM was 382 nm (calculated from 30 particles). Figure 5.24 A shows the possible presence of stomatocytes (as shown by the red arrow) and/or large vesicles (as shown by the green arrow). Some particles exhibited a bicontinuous internal morphology as displayed in Figure 5.24 B and Figure 5.24 C. Figure 5.24 D indicates multi-lamellar internal morphology. This was promising, however a higher proportion of bicontinuous nanospheres was desired with an average % of more complex morphologies being around 44 %.

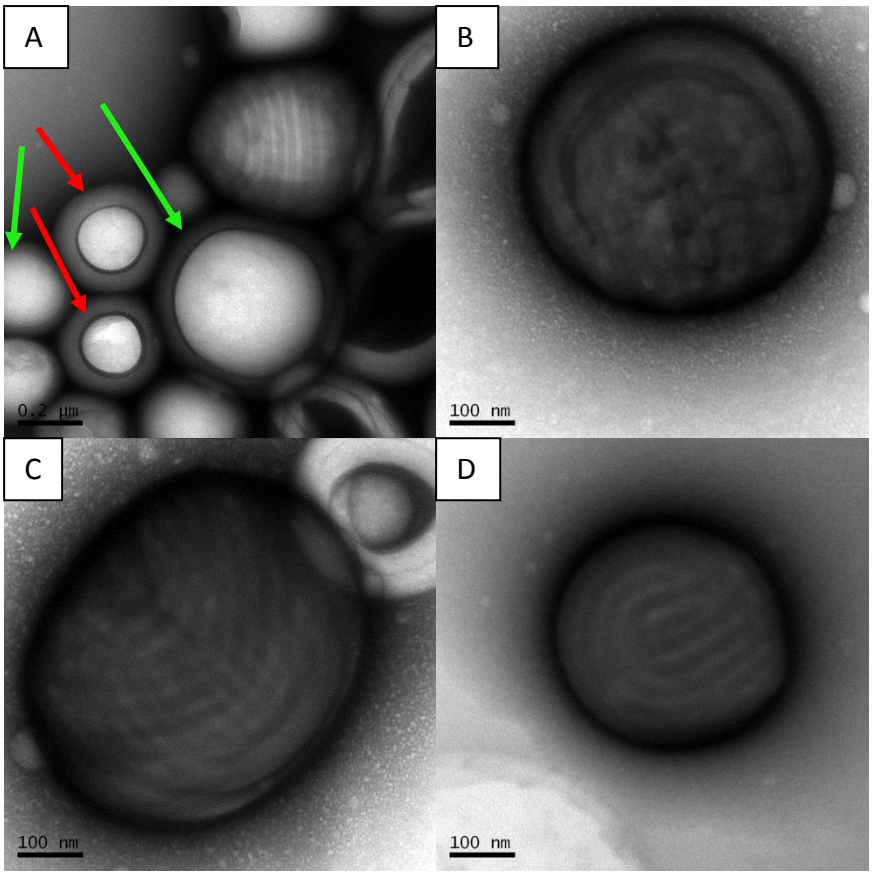

Figure 5.24: A-D) Negative stained TEM images of 0.1 wt % solution (4 mL THF) of **S1** stomatocytes (A) (red arrow) and/or vesicles (green arrows), possible bicontinuous internal morphology (B and C) and possible multi-lamellar internal morphology (D) (Stained with 5 % uranyl acetate and 1 % acetic acid).

The aggregates produced in the S1 0.1 wt % (8 mL THF) solution were large spherical vesicles with nondescript internal morphology (Figure 5.25). The number average particle size was determined from TEM, to be 154 nm (calculated from 60 particles), this is consistent with the DLS results.

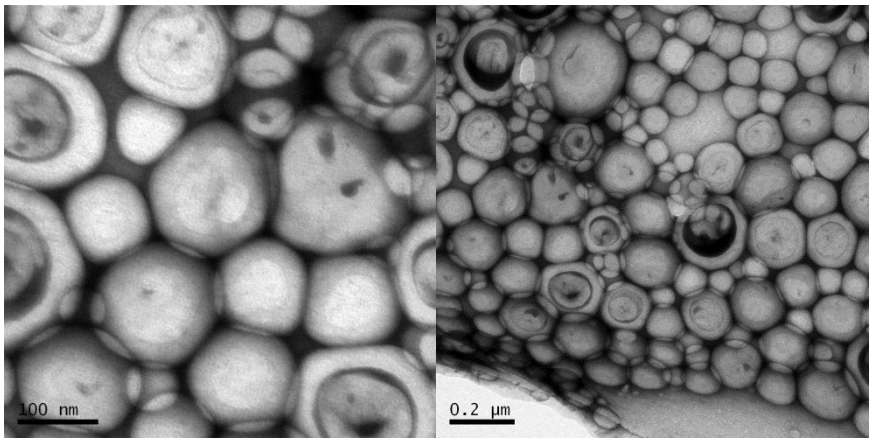

Figure 5.25: Negative stained TEM images of 0.1 wt % solution (8 mL THF) of **S1** vesicles (Stained with 5 % uranyl acetate and 1 % acetic acid).

The S1 particles self-assembled using 6 mL of THF to produce a S1 0.1 wt % (6 mL THF) solution were the most promising. The number average particle size determined from TEM was 526 nm (calculated from 60 particles), this was close to that observed by DLS. Figure 5.26 A, B, D and E illustrate the achieved bicontinuous internal morphology with some exhibiting part bicontinuous part multi-lamellar. However some stomatocytes were still present (Figure 5.26 C and F) alongside the more complex morphologies whose total presence being estimated to be around 50 %. The bicontinuous structures were expected as they have previously been observed by Eisenberg *et al.*[47] when PEO-*b*-PS was self-assembled in DMF-water mix.

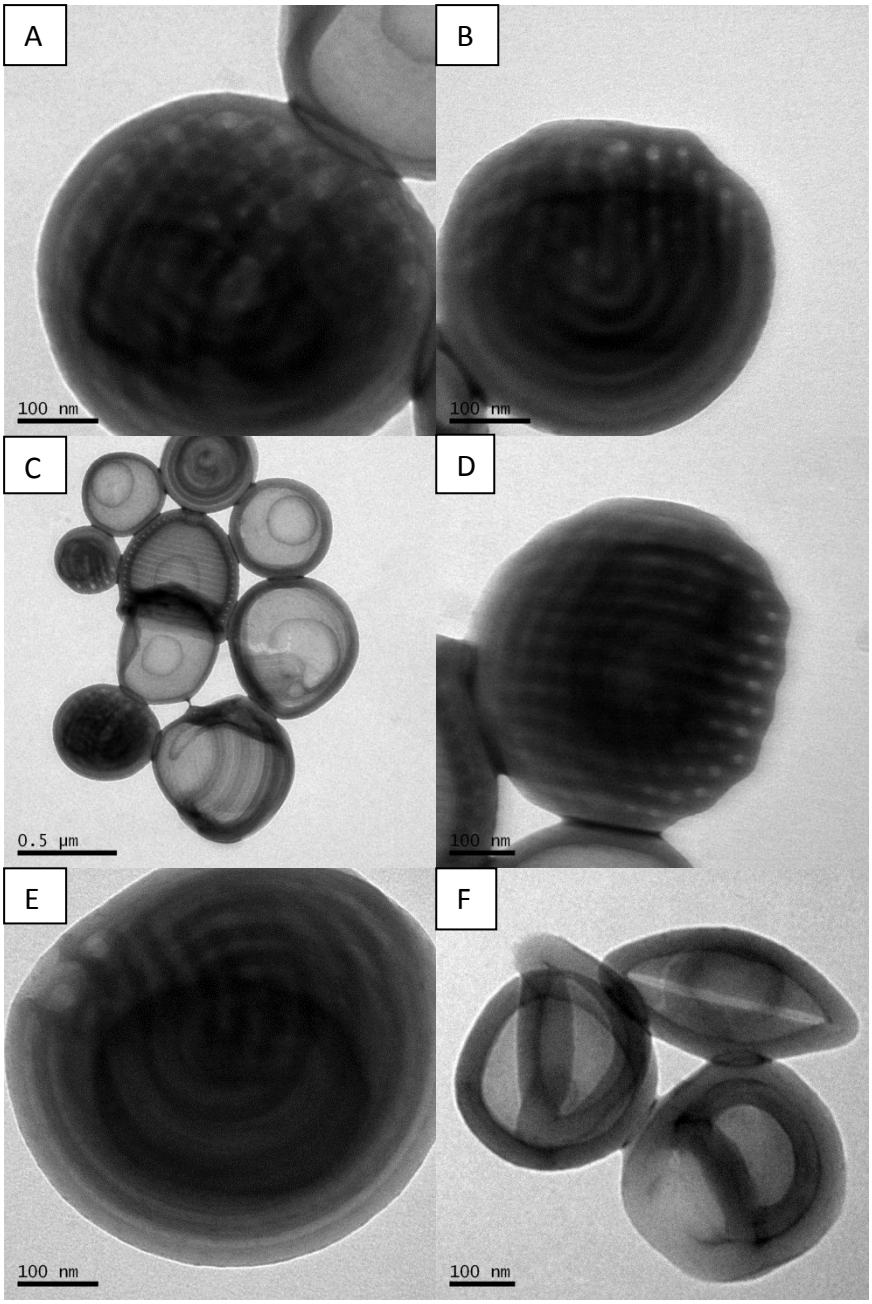

Figure 5.26: Negative stained TEM images of 0.1 wt % solution (6 mL THF) of **S1** bincontinuous internal morphology (A, B, D and E), and stomatocytes (C and F) (Stained with 5 % uranyl acetate and 1 % acetic acid).

The 1 wt % solution of S1 (6 mL THF) produced solely stomatocytes (Figure 5.27) as seen by TEM with a number average particle size of 514 nm (calculated from 25 particles).

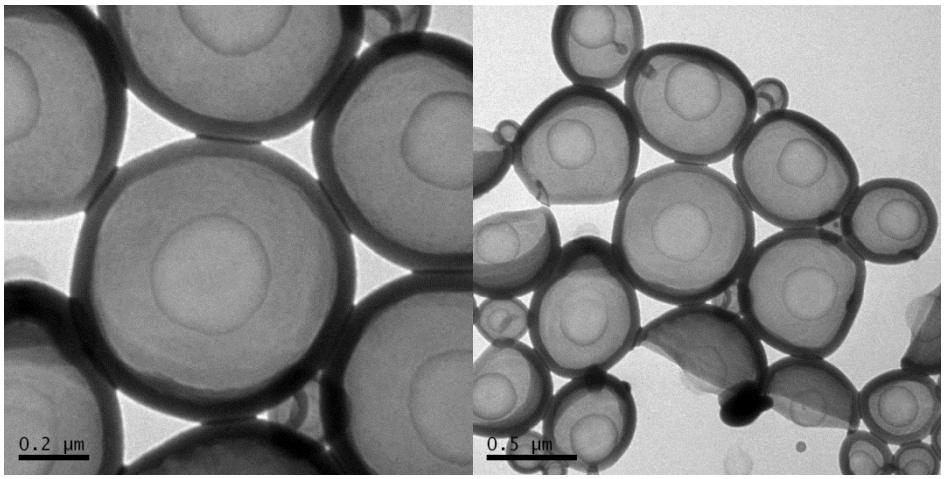

Figure 5.27: Negative stained TEM images of 1 wt % solution (6 mL THF) **S1** stomatocytes (Stained with 5 % uranyl acetate and 1 % acetic acid).

From these results it is evident that the volume of THF used in the preparation of the PEO-*b*-PS particles not only has an effect on the particle size but also the morphology. When 4 mL and 8 mL of THF were used in the preparation of PEO-*b*-PS aggregates, stomatocytes and vesicles were observed with a small amount demonstrating a bicontinuous internal morphology. As we want to use these for inorganic templating a high concentration of bicontinuous nanospheres was desired, and this was observed when 6 mL of THF was used to self-assemble S1 at 0.1 wt % in solution. When the concentration was increased to 1 wt % this bicontinuous morphology was lost and instead stomatocytes were observed.

We have observed that the volume of THF used and the temperature used for self-assembly has a significant effect on the resultant aggregate size and morphology, along with the polymer composition. This has been observed previously by Eisenberg *et al.*[49] where they self-assembled PS_{240}-*b*-PEO_{15}, PS_{240}-*b*-PEO_{45} and PS_{240}-*b*-PEO_{80} using two different methods. The first was dissolution of the BCP in DMF at varying polymer wt % followed by the addition of deionised water and then dialysis against water to remove the DMF. The second method replaces the DMF for a DMF-water mix (4-6.5 wt % water).

When self-assembled in DMF the PS_{240}-*b*-PEO_{15} produced tubules and vesicles that coexist at both 1.5 and 2 polymer wt %. However decreasing the polymer concentration to 0.2-1 wt % large compound vesicles were observed. We also saw this difference in morphology on change in concentration, S1 (PEO_{45}-b-PS_{114})

produced spherical aggregates with bicontinuous and multi-lamellar morphology and stomatocytes when self-assembled at 0.1 wt % using 6 mL of THF, interestingly when the same method was used to produce a 1 wt % solution, solely stomatocytes were observed.

Lamellae were observed for PS_{240}-*b*-PEO_{45} BCP at 1.5 wt % when self-assembled in DMF, with a minority of vesicles also present, showing a change in polymer composition results in a new morphology. This however was not the case when the DMF was replaced with a DMF-water mix. When a DMF-water mix was used all the morphologies (tubules, LCV, vesicles and lamellae) were observed for all three polymer compositions. Changing the solvent to include water meant that tubules could self-assembled as an isolated morphology from PS_{240}-*b*-PEO_{15} at 1.5-2 wt % using 4.5 wt % of water and at 1.5 wt % only, using 4 wt % if water.

It is clear that it is not only the polymer composition and concentrations that has an effect on the resultant aggregate morphology but also the solvent used to dissolve the BCP. This would explain why we see a mixture of stomatocytes and more complex bicontinuous and multi-lamellar morphologies upon a change in THF volume. Also stomatocytes were observed at a PS DP of below 175 even though Jan C. M. van Hest *et al.* observed them for PEO-*b*-PS only when the PS blocks DP exceeded 175 with a PEO DP of 45.

The TEM images of the 1 wt % solution of S1 revealed solely stomatocytes which was in contrast to the 0.1 wt % solution prepared with the same volume of THF which exhibited possible bicontinuous morphology along with multi-lamellar and stomatocytes. This result demonstrated that the polymer concentration can have an effect on the resultant morphology, this has been observed many time in the literature. Feng *et al*.[50] investigated the self-assembly of ferrocene and carboxyl containing homopolymers, and found that upon increase in homopolymer concentration the morphology of the resultant aggregates changed from micelles to spindle like micelles to connected spindle micelles. Eisenberg *et al.* found a similar effect when investigating the self-assembly of PS_{190}-b-PAA_{20} in DMF/water where an increase in polymer concentration resulted in a morphological change from sphere

to rod-like micelles, then interconnected rods, with the highest polymer concentration forming bilayers.[51]

5.4.6 Removal of PEO from PEO-*b*-PS Bicontinuous Nanospheres *via* Hydrolysis

The PEO block was cleaved from the PEO-*b*-PS BCP via alkaline hydrolysis resulting in an acid functional end group. To confirm the absence of PEO the resultant solution was dried and then a ^{1}H-NMR was ran. The ^{1}H-NMR shows that not all of the PEO has been removed with the PEO peaks still present at 3.4 and 3.5 ppm.

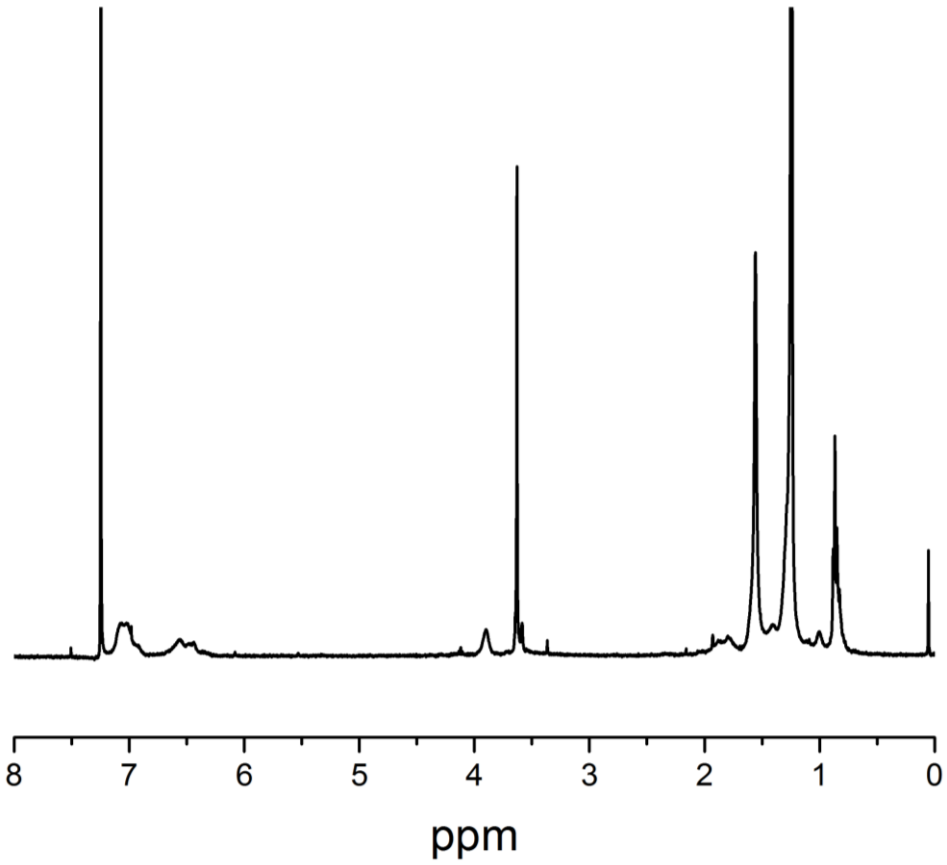

Figure 5.287: ^{1}H-NMR of S1 0.1 wt % (6 mL) post hydrolysis.

The solution was then analysed with DLS to confirm the particles had been preserved post-hydrolysis. The number average particle size increased, upon the removal of PEO, by 145 nm (Table 5.12). The DLS size distribution plots (Figure 5.29) supports this with both samples having bimodal distribution, S1 0.1 % post-hydrolysis has a narrower size distribution.

Table 5.12: N_{ave} and Z_{ave} values for self-assembled block copolymer S1 0.1 % (THF 6 mL) (PEO_{44}-*b*-PS_{114}) and S1 0.1 % post-hydrolysis to remove the PEO block (PS_{114}) calculated using Dynamic Light Scattering at 25°C.

Sample	wt %	N_{Ave} (d.nm)	SD (± nm)	Z_{Ave}(d.nm)	SD (± nm)	Đ
S1	0.1	444	24	475	5	0.08
S1 (NO PEO)	0.1	590	33	595	40	0.19

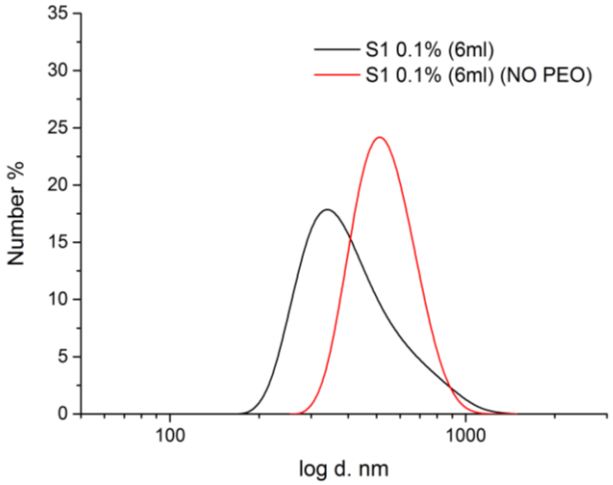

Figure 5.29: DLS distribution plots of number average particle sizes for S1 0.1 % (6 mL THF) and S1 0.1 % (6 mL THF) post-hydrolysis.

The post-hydrolysis sample of S1 0.1 wt % was further analysed with TEM to confirm the number average particle size and establish whether the internal bicontinuous morphology had been preserved. The TEM images (Figure 5.30) revealed that the majority of aggregates exhibited bicontinuous internal morphology although not highly ordered with some regions showing multi-lamellar, with some stomatocytes remaining.

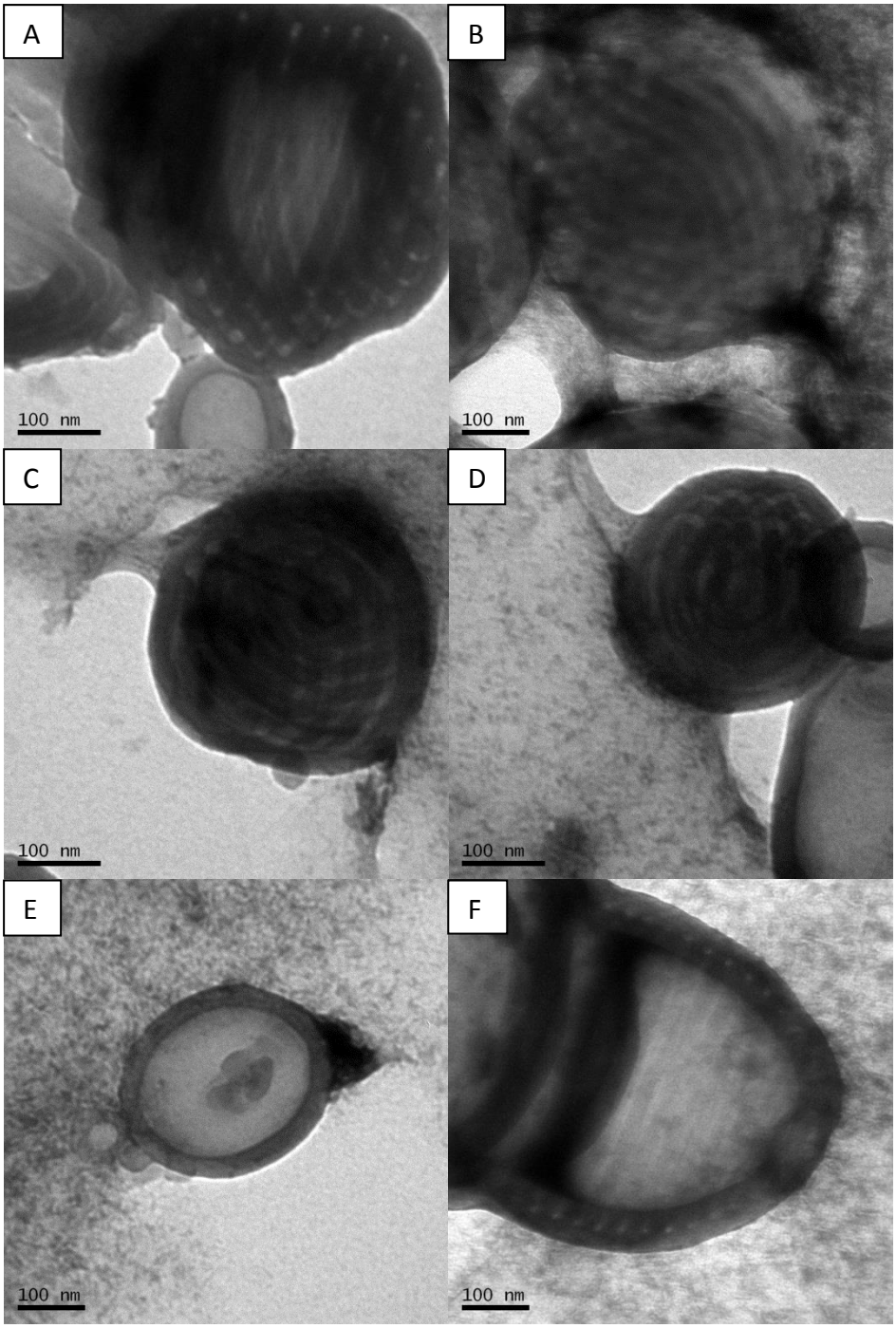

Figure 5.30: Negative stained TEM images of 0.1 wt % solution (6 ml THF) of **S1** deprotected (HOOC-PS) with bicontinuous internal morphology (A, B, D and E), stomatocytes (E) and possible inverted hexagonal phase aggregates (Stained with 5 % uranyl acetate and 1 % acetic acid).

5.4.7 Removal of PEO from PEO_{44}-*b*-$PODMA_{19}$ (P4) Bicontinuous Nanospheres via Alkaline Hydrolysis

As the self-assembly of PEO-*b*-PS did not produce an aggregate solution of solely bicontinuous nanospheres, the removal of PEO from PEO-*b*-PODMA nanospheres was attempted. It was already established that PEO-*b*-PODMA self-assembles to form a solution of solely bicontinuous nanospheres when the PEO wt % is 25 %. Therefore P4 (PEO_{44}-*b*-$PODMA_{19}$), which was synthesized via ATRP and characterised in chapter 2, was self-assembled at 1 wt % following the dialysis method using 4 mL of THF and 6 mL of water. To cleave the PEO block KOH was added to the PEO-b-PODMA solution to form a 1.5 mol dm^{-3} solution of KOH. It was thought that as the ester groups within the side chain of the PODMA block were not solvated by the water, due to PODMA acting as the hydrophobic block, that the ester groups would be protected and the KOH molecule would not be able to reach these bonds to cause hydrolysis. Therefore the idea was that only the ester bond connecting the PEO block to the PODMA block would be cleaved leaving an acid functional end group in contrast to the PMAA-*b*-PODMA where a whole block was acid functionalised.

The solution of P4 at 1 wt % was analysed using DLS pre and post hydrolysis at 15°C. Post hydrolysis the aggregates N_{ave} decreased in size from 450 nm to 400 nm (Table 5.13). This indicates a loss in polymer, however it cannot be confirmed from DLS if this loss in size was due to the removal of PEO or a loss in side-chains from the PODMA block. The N_{ave} DLS distribution plots also show this loss in particle size (Figure 5.31).

Table 5.13: N_{ave} and Z_{ave} values for self-assembled block copolymer P4 (PEO_{44}-*b*-$PODMA_{19}$) at 1 wt % pre and post hydrolysis, calculated using dynamic light scattering at 15°C.

Sample	Wt %	N_{ave} (d.nm)	SD (± nm)	Z_{ave} (d.nm)	SD (± nm)	Đ
PEO_{44}-*b*-$PODMA_{19}$	1	452	77	844	28	0.55
PEO_{44}-*b*-$PODMA_{19}$ (Post hydrolysis)	1	399	62	680	14	0.62

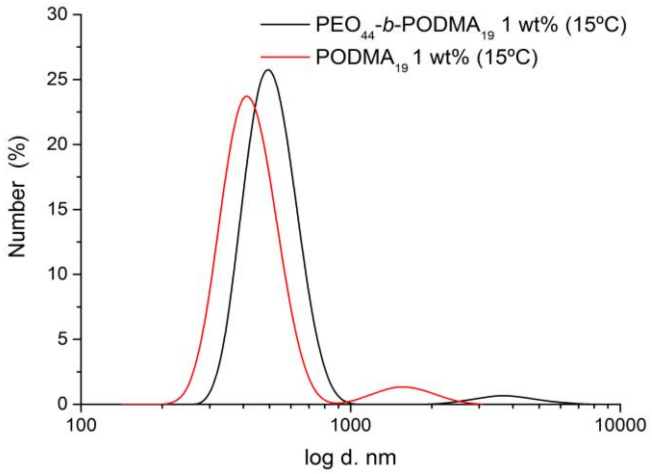

Figure 5.31: DLS distribution plots of number average particle sizes for PEO_{44}-*b*-$PODMA_{19}$ (P4) 1 wt % and PEO_{44}-*b*-$PODMA_{19}$ (P4) 1 wt % post-hydrolysis.

Figure 5.32 displays the TEM images of P4 pre and post-hydrolysis, they show that spherical aggregates were observed still post hydrolysis with an insignificant difference in particle size between the pre and post hydrolysis samples (around 400 nm).

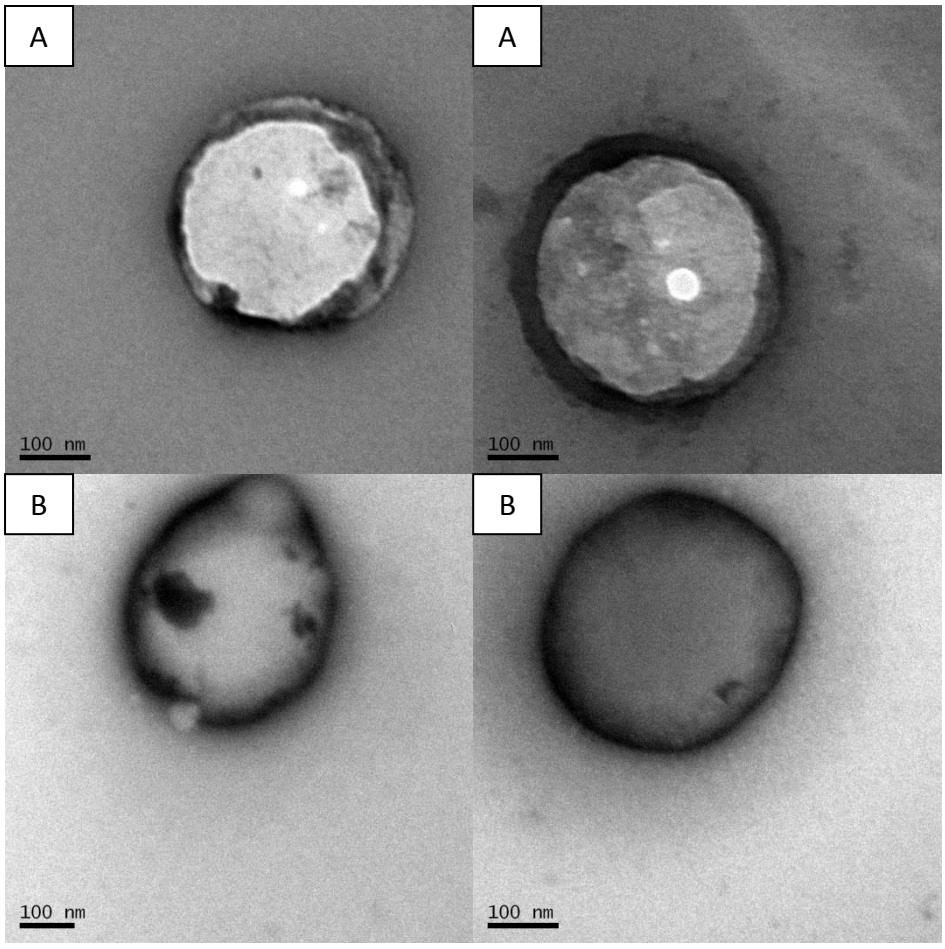

Figure 5.32: TEM images of PEO_{44}-*b*-$PODMA_{19}$ (P4) pre hydrolysis (A) and post hydrolysis (B). Negatively stained with uranyl acetate (5 %)

To establish whether the PEO had been removed successfully via alkaline hydrolysis, the post hydrolysis aggregate solution was left to dry to remove the water before the resultant solid was dissolved in $CDCl_3$ and analysed with ^{1}H-NMR. The ^{1}H-NMR showed that not all the PEO had been removed and that some of the ODMA chains had been cleaved by the KOH.

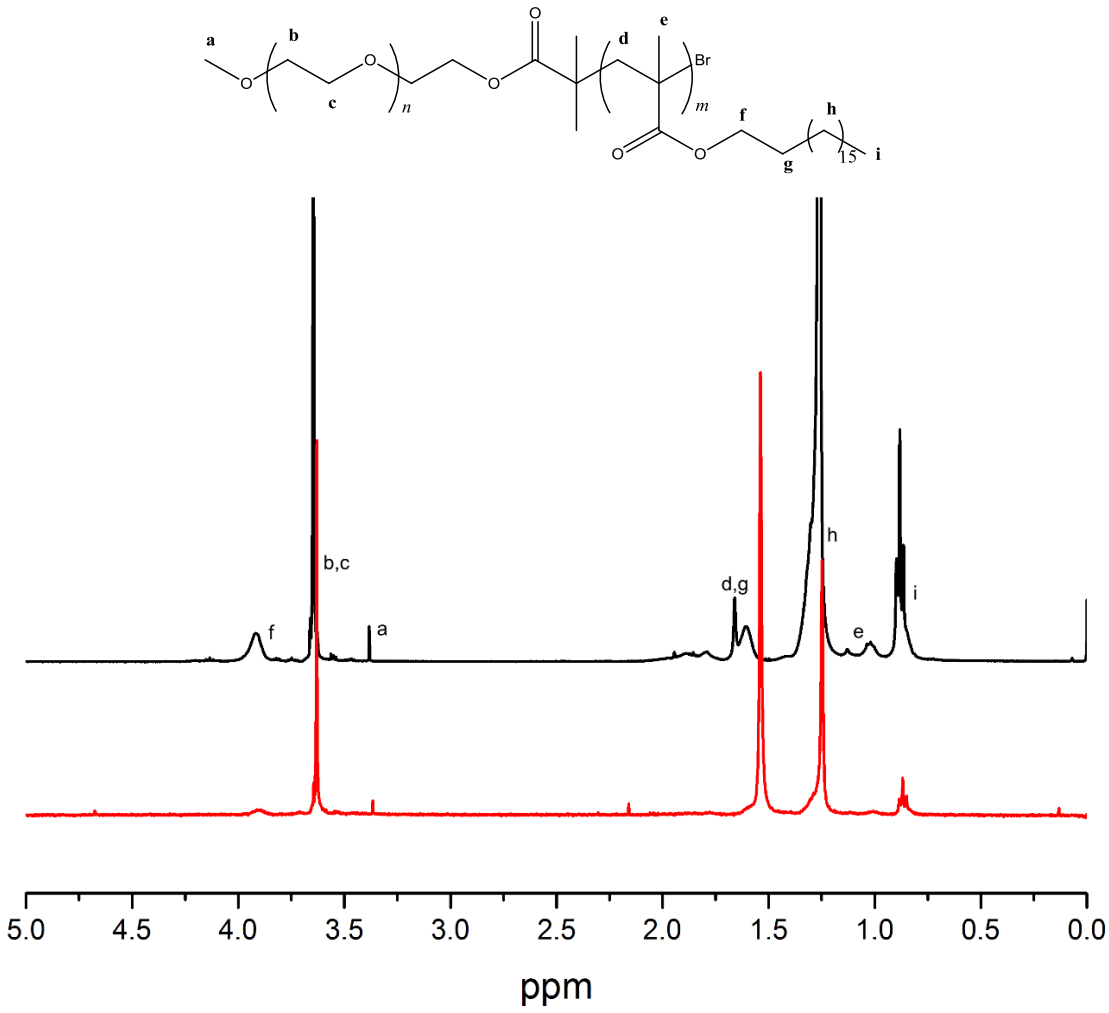

Figure 5.33: ^{1}H-NMR of P4 (PEO_{44}-*b*-$PODMA_{19}$) pre-hydrolysis (black) and post hydrolysis (red).

5.5 Conclusion

The synthesis of PtBMA-*b*-PODMA via ATRP proved difficult due to the use of PtBMA as the macroinitiator. A number of different synthesis conditions were used for PMAA-*b*-PODMA with a back precipitation being required to obtain a monomodal peak on GPC with the dispersity around 1.7, too high to say the reaction was controlled. A BCP of PMAA-*b*-PODMA was achieved by deprotection of PtBMA-*b*-PODMA with TFA to produce a BCP with a PMAA wt % of 19 %. However the PMAA wt % and the DP could not be predicted due to the lack of control over the reaction. This BCP was then self-assembled following the dialysis method and produced spherical particles with a bicontinuous internal morphology alongside micelles and vesicles. This shows that even though the hydrophilic block was changed from PEO to PMAA, the bicontinuous morphology was still maintained. The weight percent of the PMAA block was 19 % which was within the range required for bicontinuous nanospheres to form (15-25 wt %) this indicates that PMAA-*b*-PODMA follows the same rules as for the PEO-*b*-PODMA BCP. The development of this acid functionalised bicontinuous nanospheres is promising for use in not only biomimetic mineralisation but also as a pH and thermo-responsive drug carrier, with the PMAA contributing the pH responsive nature and the PODMA contributing, as seen previously, the thermo-responsive nature with use of its T_m.

PEO-*b*-PS was synthesised with a PEO wt % of 15 (S1), 19 (S2) and 23 (S3) %. It was expected that all three would self-assemble to form bicontinuous nanospheres, however this was not the case, S2 and S3 (0.1 wt % in solution, 6 mL THF, 4 mL H_2O) self-assembled to form stomatocytes. As discussed previously in this chapter this morphology has been seen to be produced before from PEG-*b*-PS, however with a much higher DP of PS. [44, 48] Interestingly when S1 was self-assembled at 0.1 wt % in solution the preparation procedure seemed to play a significant role in the resultant morphology. A range of volumes of the THF used to dissolve the polymer pre-dialysis were used. When 4 mL of THF was used a range of morphologies were seen including stomatocytes and some with possible bicontinuous morphology. When 8 mL of THF was used only stomatocytes and vesicles were observed. The most interesting was when 6 mL of THF was used, spherical aggregates with bicontinuous internal

morphology were observed with a small proportion of stomatocytes. However when S1 was self-assembled at 1 wt % in solution using 6 mL of THF, solely stomatocytes were observed. The solution of S1 0.1 wt % solution (6 mL THF) exhibited the highest proportion of bicontinuous nanospheres and therefore was chosen for further studies. This solution underwent alkaline hydrolysis in order to remove the PEO block to leave an acid functionalised end group within the bicontinuous nanospheres. The DLS and TEM results showed that the size and morphology of these aggregates did not alter significantly post hydrolysis.

The formation of bicontinuous nanospheres from PMAA-*b*-PODMA was promising, however isolation of the bicontinuous nanospheres is desired. Investigation into the effect the wt % of PMAA has upon forming bicontinuous nanospheres will be investigated in the future to establish if bicontinuous nanospheres can be formed as an isolated morphology. Once the self-assembly of PMAA-*b*-PODMA BNs has been refined then further research into their use in biomineralisation is needed. The effect the combined stimuli-responses of pH and temperature has upon the BNs would be interesting to investigate. Primarily however, further work on the synthesis of PMAA-*b*-PODMA is necessary to be able to synthesise the BCP with a pre-determined molecular weight and therefore DP. The synthesis of PtBMA via RAFT has seen to be successful in the literature, therefore investigation of the use of RAFT dispersion polymerisation to form PMAA-*b*-PODMA bicontinuous nanospheres would be interesting.

As with PMAA-*b*-PODMA aggregate solutions PEO-*b*-PS self-assembled to form bicontinuous nanospheres alongside other morphologies. Not all the PEO was removed during alkaline hydrolysis to leave an acid functional end group so further experimental research is needed into determining the appropriate concentration of KOH to achieve total removal of PEO. The same issue was seen for the removal of PEO from PEO-b-PODMA and further research is needed into the removal of PEO without cleaving any of the long octadecyl side chains upon the methacrylate backbone. Once the self-assembly and hydrolysis of these two polymer systems has been fine-tuned, experiments can be carried out for their use in biomineralisation.

5.6 References

1. McKenzie, B. E.; Nudelman, F.; Bomans, P. H. H.; Holder, S. J.; Sommerdijk, N., Temperature-Responsive Nanospheres with Bicontinuous Internal Structures from a Semicrystalline Amphiphilic Block Copolymer. *Journal of the American Chemical Society* **2010,** *132* (30), 10256-10259.

2. McKenzie, B. E.; Friedrich, H.; Wirix, M. J. M.; de Visser, J. F.; Monaghan, O. R.; Bomans, P. H. H.; Nudelman, F.; Holder, S. J.; Sommerdijk, N. A. J. M., Controlling Internal Pore Sizes in Bicontinuous Polymeric Nanospheres. *Angewandte Chemie International Edition* **2015,** *54* (8), 2457-2461.

3. Holder, S. J.; Woodward, G.; McKenzie, B.; Sommerdijk, N. A. J. M., Semi-crystalline block copolymer bicontinuous nanospheres for thermoresponsive controlled release. *RSC Advances* **2014,** *4* (50), 26354-26358.

4. McKenzie, B. E.; Holder, S. J.; Sommerdijk, N., Assessing internal structure of polymer assemblies from 2D to 3D CryoTEM: Bicontinuous micelles. *Current Opinion in Colloid & Interface Science* **2012,** *17* (6), 343-349.

5. Bronstein, L.; Krämer, E.; Berton, B.; Burger, C.; Förster, S.; Antonietti, M., Successive Use of Amphiphilic Block Copolymers as Nanoreactors and Templates: Preparation of Porous Silica with Metal Nanoparticles. *Chemistry of Materials* **1999,** *11* (6), 1402-1405.

6. Xu, A.-W.; Ma, Y.; Colfen, H., Biomimetic mineralization. *Journal of Materials Chemistry* **2007,** *17* (5), 415-449.

7. Coessens, V.; Pintauer, T.; Matyjaszewski, K., Functional polymers by atom transfer radical polymerization. *Progress in Polymer Science* **2001,** *26* (3), 337-377.

8. Matyjaszewski, K.; Nakagawa, Y.; Gaynor, S. G., Synthesis of well-defined azido and amino end-functionalized polystyrene by atom transfer radical polymerization. *Macromolecular Rapid Communications* **1997,** *18* (12), 1057-1066.

9. Matyjaszewski, K.; Davis, K.; Patten, T. E.; Wei, M., Observation and analysis of a slow termination process in the atom transfer radical polymerization of styrene. *Tetrahedron* **1997,** *53* (45), 15321-15329.

10. Mori, H.; Müller, A. H. E., New polymeric architectures with (meth)acrylic acid segments. *Progress in Polymer Science* **2003,** *28* (10), 1403-1439.

11. Liu, R.; Tao, Y.; Zhu, Y.; Chen, M.; Yang, C.; Liu, X., Synthesis of double-hydrophilic poly(methylacrylic acid)–poly(ethylene glycol)–poly(methylacrylic acid) triblock copolymers and their micelle formation. *Polymer International* **2011,** *60* (2), 327-332.

12. He, E.; Yue, C. Y.; Tam, K. C., Association Behavior of Star-Shaped pH-Responsive Block Copolymer: Four-Arm Poly(ethylene oxide)-b-Poly(methacrylic acid) in Aqueous Medium. *Langmuir* **2009,** *25* (9), 4892-4899.

13. Zhang, X.; Xia, J.; Matyjaszewski, K., Atom transfer radical polymerization of protected methacrylic acids. *Polymer Preprints (American Chemical Society, Division Polymer Chem)* **1999,** *40* (2), 440-441.

14. Wim Van, C.; Filip, E. D. P., Controlled Radical Polymerization of 1-Ethoxyethyl (Meth)acrylate: Novel Route for the Synthesis of Poly((meth)acrylic acid) Containing Polymer Structures. In *Controlled/Living Radical Polymerization*, American Chemical Society: 2006; Vol. 944, pp 171-184.

15. Davis, K. A.; Matyjaszewski, K., Atom Transfer Radical Polymerization of tert-Butyl Acrylate and Preparation of Block Copolymers. *Macromolecules* **2000,** *33* (11), 4039-4047.

16. Davis, K. A.; Charleux, B.; Matyjaszewski, K., Preparation of block copolymers of polystyrene and poly (t-butyl acrylate) of various molecular weights and architectures by atom transfer radical polymerization. *Journal of Polymer Science Part A: Polymer Chemistry* **2000,** *38* (12), 2274-2283.

17. Wang, G.; Yan, D., Preparation of amphiphilic PS-b-PMAA diblock copolymer by means of atom transfer radical polymerization. *Journal of Applied Polymer Science* **2001,** *82* (10), 2381-2386.

18. Robinson, D. N.; Peppas, N. A., Preparation and Characterization of pH-Responsive Poly(methacrylic acid-g-ethylene glycol) Nanospheres. *Macromolecules* **2002,** *35* (9), 3668-3674.

19. Li, G.; Song, S.; Guo, L.; Ma, S., Self-assembly of thermo- and pH-responsive poly(acrylic acid)-b-poly(N-isopropylacrylamide) micelles for drug delivery. *Journal of Polymer Science Part A: Polymer Chemistry* **2008,** *46* (15), 5028-5035.

20. Tugulu, S.; Barbey, R.; Harms, M.; Fricke, M.; Volkmer, D.; Rossi, A.; Klok, H.-A., Synthesis of Poly(methacrylic acid) Brushes via Surface-Initiated Atom Transfer Radical Polymerization of Sodium Methacrylate and Their Use as Substrates for the Mineralization of Calcium Carbonate. *Macromolecules* **2007,** *40* (2), 168-177.

21. Qin, A.; Tian, M.; Ramireddy, C.; Webber, S. E.; Munk, P.; Tuzar, Z., Polystyrene-poly(methacrylic acid) block copolymer micelles. *Macromolecules* **1994,** *27* (1), 120-126.

22. Chen, G.; Liu, J.; Yang, Y.; Zhang, L.; Wu, M.; Ni, H., Preparation of pH-sensitive nanoparticles of poly (methacrylic acid) (PMAA)/poly (vinyl pyrrolidone) (PVP) by ATRP-template miniemulsion polymerization in the aqueous solution. *Colloid and Polymer Science* **2015,** *293* (7), 2035-2044.

23. Sommerdijk, N. A. J. M.; With, G. d., Biomimetic CaCO3 Mineralization using Designer Molecules and Interfaces. *Chemical Reviews* **2008,** *108* (11), 4499-4550.

24. Addadi, L.; Moradian, J.; Shay, E.; Maroudas, N. G.; Weiner, S., A chemical model for the cooperation of sulfates and carboxylates in calcite crystal nucleation: Relevance to biomineralization. *Proceedings of the National Academy of Sciences of the United States of America* **1987,** *84* (9), 2732-2736.

25. Mann, S.; Heywood, B. R.; Rajam, S.; Birchall, J. D., Controlled crystallization of CaCO3 under stearic acid monolayers. *Nature* **1988,** *334* (6184), 692-695.

26. Addadi, L.; Weiner, S., Interactions between acidic proteins and crystals: stereochemical requirements in biomineralization. *Proceedings of the National Academy of Sciences* **1985,** *82* (12), 4110-4114.

27. Wang, J. S.; Matyjaszewski, K., Controlled Living Radical Polymerization - Atom-Transfer Radical Polymerization in the Presence of Transition-Metal Complexes. *Journal of the American Chemical Society* **1995,** *117* (20), 5614-5615.

28. Kwak, Y.; Nicolaÿ, R.; Matyjaszewski, K., Concurrent ATRP/RAFT of Styrene and Methyl Methacrylate with Dithioesters Catalyzed by Copper(I) Complexes. *Macromolecules* **2008,** *41* (18), 6602-6604.

29. Xu, D.-M.; Zhang, K.-D.; Wu, J.-F., Synthesis and properties of polystyrene-b-poly(ethylene oxide)-b-polystyrene triblock copolymers. *Journal of Applied Polymer Science* **2006,** *101* (1), 727-730.

30. Kim, K. T.; Cornelissen, J. J. L. M.; Nolte, R. J. M.; van Hest, J. C. M., A Polymersome Nanoreactor with Controllable Permeability Induced by Stimuli-Responsive Block Copolymers. *Advanced Materials* **2009,** *21* (27), 2787-2791.

31. Ritz, P.; Látalová, P.; Janata, M.; Toman, L.; Kříž, J.; Genzer, J.; Vlček, P., Synthesis of amphiphilic copolymers by ATRP initiated with a bifunctional initiator containing trichloromethyl groups. *Reactive and Functional Polymers* **2007,** *67* (10), 1027-1039.

32. Wang, J.-S.; Matyjaszewski, K., Controlled/"Living" Radical Polymerization. Halogen Atom Transfer Radical Polymerization Promoted by a Cu(I)/Cu(II) Redox Process. *Macromolecules* **1995,** *28* (23), 7901-7910.

33. Matyjaszewski, K., Atom Transfer Radical Polymerization (ATRP): Current Status and Future Perspectives. *Macromolecules* **2012,** *45* (10), 4015-4039.

34. Matyjaszewski, K., Atom Transfer Radical Polymerization: From Mechanisms to Applications. *Israel Journal of Chemistry* **2012,** *52* (3-4), 206-220.

35. Tang, W.; Tsarevsky, N. V.; Matyjaszewski, K., Determination of Equilibrium Constants for Atom Transfer Radical Polymerization. *Journal of the American Chemical Society.* **2006,** *128* (5), 1598-1604.

36. Tang, W.; Matyjaszewski, K., Effects of Initiator Structure on Activation Rate Constants in ATRP. *Macromolecules* **2007,** *40* (6), 1858-1863.

37. Matyjaszewski, K.; Xia, J., Atom Transfer Radical Polymerization. *Chemical Reviews* **2001,** *101* (9), 2921-2990.

38. Matyjaszewski, K., Mechanistic and synthetic aspects of atom transfer radical polymerization. *Journal of Macromolecular Science-Pure and Applied Chemistry* **1997,** *A34* (10), 1785-1801.

39. Matyjaszewski, K., Controlled radical polymerization. *Current Opinion in Solid State & Materials Science* **1996,** *1* (6), 769-776.

40. Gaynor, S. G.; Wang, J. S.; Matyjaszewski, K., Controlled Radical Polymerization by Degenerative Transfer - Effect of the Structure of the Transfer Agent. *Macromolecules* **1995,** *28* (24), 8051-8056.

41. Hales, K.; Chen, Z.; Wooley, K. L.; Pochan, D. J., Nanoparticles with Tunable Internal Structure from Triblock Copolymers of PAA-b-PMA-b-PS. *Nano Letters* **2008,** *8* (7), 2023-2026.

42. Rudin, A.; Hoegy, H. L. W., Universal calibration in GPC. *Journal of Polymer Science Part A-1: Polymer Chemistry* **1972,** *10* (1), 217-235.

43. Gaborieau, M.; Castignolles, P., Size-exclusion chromatography (SEC) of branched polymers and polysaccharides. *Analytical and Bioanalytical Chemistry* **2011,** *399* (4), 1413-1423.

44. Kim, K. T.; Zhu, J.; Meeuwissen, S. A.; Cornelissen, J. J. L. M.; Pochan, D. J.; Nolte, R. J. M.; van Hest, J. C. M., Polymersome Stomatocytes: Controlled Shape Transformation in Polymer Vesicles. *Journal of the American Chemical Society* **2010,** *132* (Copyright (C) 2015 American Chemical Society (ACS). All Rights Reserved.), 12522-12524.

45. Wilson, D. A.; Nolte, R. J. M.; van Hest, J. C. M., Entrapment of Metal Nanoparticles in Polymer Stomatocytes. *Journal of the American Chemical Society* **2012,** *134* (24), 9894-9897.

46. Wilson, D. A.; Nolte, R. J. M.; van Hest, J. C. M., Autonomous movement of platinum-loaded stomatocytes. *Nature Chemistry* **2012,** *4* (4), 268-274.

47. Yu, K.; Zhang, L.; Eisenberg, A., Novel Morphologies of “Crew-Cut” Aggregates of Amphiphilic Diblock Copolymers in Dilute Solution. *Langmuir* **1996,** *12* (25), 5980-5984.

48. Meeuwissen, S. A.; Kim, K.-T.; Chen, Y.-C.; Pochan, D. J.; van Hest, J. C. M., Controlled Shape Transformation of Polymersome Stomatocytes. *Angewandte Chemie, International Edition* **2011,** *50* (Copyright (C) 2015 American Chemical Society (ACS). All Rights Reserved.), 7070-7073, S7070/1-S7070/14.

49. Yu, K.; Eisenberg, A., Bilayer Morphologies of Self-Assembled Crew-Cut Aggregates of Amphiphilic PS-b-PEO Diblock Copolymers in Solution. *Macromolecules* **1998,** *31* (11), 3509-3518.

50. Feng, C.; Lu, G.; Li, Y.; Huang, X., Self-Assembly of Amphiphilic Homopolymers Bearing Ferrocene and Carboxyl Functionalities: Effect of Polymer Concentration, β-Cyclodextrin, and Length of Alkyl Linker. *Langmuir* **2013,** *29* (34), 10922-10931.

51. Zhang, L.; Eisenberg, A., Multiple Morphologies of "Crew-Cut" Aggregates of Polystyrene-b-poly(acrylic acid) Block Copolymers. *Science* **1995,** *268* (5218), 1728-1731.

Chapter 6. Conclusion and Future Work

6.1 Conclusion

The synthesis of PEO-*b*-PODMA via ATRP was followed from a previously successful method. First a series of PEO macroinitiators were synthesised from poly(ethylene glycol) methyl ether, with varying DPs, to incorporate a functional bromine end group. The macroinitiators were then characterised with GPC which showed that the macroinitiators had a narrow dispersity. The DPs were determined using ^{1}H-NMR. These PEO macroinitiators were then used in the synthesis of PEO-*b*-PODMA, PEO-*b*-PDSMA, PEO-*b*-(PODMA-*co*-PDSMA) and PEO-*b*-PS.

The self-assembly of PEO-*b*-PODMA was self assembled following the dialysis method at various weight fractions of PEO and at polymer concentrations of 0.1-5 wt %. The cryo-TEM images confirmed that BNs can be obtained at polymer concentrations as high as 4 wt % when the PEO weight fraction is 25 %. With a PEO weight fraction of 30 % cylindrical micelles were observed at low concentration, this morphology was not observed as the concentration of polymer was increased, this was not suprising as cylindrical micelles are often observed alongside another morphology.

The self-assembly of PEO-*b*-PODMA was carried out using a number of methods, as discussed the dialysis method has already been extensively reviewed for the formation of BNs. To reduce the experimental time three other methods were employed, the BCP was dissolved in THF followed by the fast addition of water, the THF was removed via rotary evaporation. This method produced particles that had a number average of around 70 nm indicating micelles, however BNs have been observed at similar sizes from the same polymer system. The next method involved the dissolution of the BCP in THF with the water added drop wise. The THF was again removed via rotary evaporation. This method produced particles with largest number average with the exception of the dialysis method. The last method was emulsification of the polymer in water at temperatures above the T_m of the PODMA block. Particles were produced from this method however the internal morphology for all three methods could not be obtained due to low polymer concentrations.

PEO-*b*-PDSMA and PEO-*b*-(PODMA-*b*-PDSMA) block copolymers were successfully synthesised via ATRP. All the BCPS had narrow dispersities in molecular weight, as

characterised by GPC and the overall DP of the hydrophilic block was established by analysis with ^{1}H-NMR. These BCP were self-assembled at 0.1-5 wt % polymer in solution with the aim of forming BNs. The particles produced from PEO-*b*-PDSMA at PEO 25 wt % exhibited internal bicontinuous morphology at 0.1 and 1 wt %. It was established that self-assembly of the copolymers at each concentration produced BNs alongside multi–lamellar aggregates with an increase in multi–lamellar aggregates as the DSMA wt % increased.

DSC analysis was carried out for all BCPs with a PEO weight fraction of 25 %. For the bulk samples DSC revealed that upon an increase in DSMA wt %, and therefore an increase in the average side – chain length upon the methacrylate backbone, there was an increase the in the T_m. An increase in the D_c of the hydrophobic block was also observed upon an increase in DSMA wt % with PEO-*b*-PODMA as an anomaly. The same trends were also observed for the aggregate solutions, the aggregate solutions had a lower D_c than the corresponding bulk BCP, but as already stated this may not have been as reliable due to the small transits observed because of the low polymer concentration and the water transition.

The encapsulation and controlled release of ibuprofen was carried out with PEO-*b*-PODMA, PEO-*b*-PODMA and a series of copolymers of PEO-*b*-(PODMA-*co*-PDSMA). PEO-*b*-PODMA with ibuprofen exhibited the same thermo-response as was seen with the encapsulation and release of pyrene. Above the calculated melting transition the rate of release increased. As the wt % of DSMA was increased the rate of release at each corresponding temperature decreased, demonstrating that the increasing T_m for the hydrophobic block effects the release of ibuprofen. The amount of ibuprofen encapsulated within the nanospheres also increased with an increase in DSMA wt % indicting the Ibuprofen is interacting with the hydrophobic block.

The synthesis of PtBMA macroinitiators was carried out via ATRP, a macro initiator was successfully synthesised using Cu(I)Cl, however due to the strong affinity Cl has to carbon the majority of the chains were terminated with chlorine which caused slow initiator when used for the synthesis of PMAA-*b*-PODMA. Therefore a number of initiators were synthesised with Cu bromide species to ty and overcome the slow initiation. Slow initiation was however observed for all synthesise of PMAA-*b*–

PODMA with one BCP being successfully isolated by back precipitation. This BCP had a PMAA wt % of 20 %. The BCP was successfully self-assembly via the dialysis method to form BNs, however a number of other morphologies were also observed. These results demonstrate that acid functionality can be obtained within these BNS, however further work is needed to isolate the morphology.

Another example of obtaining acid functionality within these BNs was attempted with the synthesis and self-assembly of PEO-*b*-PS. A number of BCPS of PEO-*b*-PS were successfully synthesised via ATRP using a PEO macroinitiator. All the BCPS had low dispersities in molecular weight and achieved the predicted DP. Self-assembly of the BCPs was carried out via the dialysis method with a BCP with a PEO weight fraction of 15 % producing BNs and stomatocytes when various volumes of THF were used initially. The removal of PEO was then attempted via alkaline hydrolysis to leave an acid functional end group, however ^{1}H-NMR showed that not all the PEO was removed.

6.1 Future Work

A more in depth study of the formation of BNS from the copolymers PEO-*b*-(PODMA-*co*-PDSMA) is needed to establish whether these copolymers self-assembly following the phase diagram outlined for PEO-*b*-PODMA. Self-assembly of the copolymers at different PEO wt fractions and under different preparation conditions may reveal the optimum conditions for an aggregate solution of solely BNS.

The preliminary results for the encapsulation and release of ibuprofen were promising and demonstrated that an increase in DSMA wt % affected not only the rate of release but also the amount of drug encapsulated within the BNS. Further investigation into the affect of DSMA wt % upon the encapsulation and release of ibuprofen is needed at a wider variety of DSMA wt % content. Analysis of the BN in the presence of ibuprofen with NMR would be interesting to establish if the Ibuprofen is interacting with the polymer chains via hydrogen bonding, as this may affect he rate of release. Also encapsulation of a number of different drugs both hydrophilic and hydrophobic would be shed light on the affect the drugs interaction with the polymer and also the drugs solubility has upon the rate of release.

The synthesis of PMAA-*b*-PODMA needs to be optimised so that a BCP can be synthesised with a pre-determined DP and M_n. RAFT has been used with great success for the synthesis of PMAA and therefore may be a good technique to use for the controlled polymerisation of PMAA-*b*-PODMA. More interestingly with growing interest and literature on RAFT dispersion polymerisation, the BNs could be formed during the synthesis.

The self-assembly of PEO-*b*-PS was carried out using THF as the common solvent. Changes in the solvent volume produced aggregates with different morphologies. It would be interesting to carry out a series of self-assembly establish using a variety of solvents and cosolvents to establish the optimum conditions for producing solely BNs. Once a solution is obtained where the BNs morphology has been isolated the removal of PEO can be carried out to produce and acid functional end group. Establishing the appropriate concentrator of KOH is needed to completely remove the PEO block. The same needs to be done for the removal of PEO from PEO-*b*-PODMA BNs to ensure the octadecyl side chains upon the methacrylate backbone are not cleaved.